

Diese Dissertation wurde begutachtet von:

Prof. Dr. Robert Liska Prof. Dr. Heinz Redl



TECHNISCHE  
UNIVERSITÄT  
WIEN

Vienna University of Technology

DISSERTATION

# **3D Construction of Artificial Extracellular Matrix Hydrogels by Two-Photon-Induced Polymerization**

ausgeführt zum Zwecke der Erlangung des akademischen Grades eines  
Doktors der technischen Wissenschaften unter der Leitung von

**Ao.Univ.Prof. Dr. Robert Liska**

E163

Institut für Angewandte Synthesechemie

eingereicht an der Technischen Universität Wien

Fakultät für Technische Chemie

Von

**M.Eng. Xiao-Hua Qin**

0928755

Breitenfurter straÙe 374/13/43, 1230 WIEN

Wien, 08.05.2014

M.Eng. Xiao-Hua Qin



To Jie & my parents.

*"Talent is enduring patience."* --- François-Marie Arouet (1694-1778)

"天分是持久的毅力和坚忍."--- 王强

# Acknowledgement

To begin with, I like to thank my advisor, Prof. Robert Liska, for his insightful direction and full support during my PhD thesis. Without his guidance, I am not able to keep myself away from the scientific ‘dead-alleys’ and complement my thesis with a balance between novelty and systematicity. His patience provided me the possibility to cross over research bottlenecks, learn from experimental failures and improve myself step-by-step in the last four years. His expertise in photopolymer science will benefit my future career. I also like to thank my co-advisor, Prof. Jürgen Stampfl in the Institute of Materials Science and Technology (IMST), for his invaluable co-supervision and input into my thesis research. His expertise in AMT-techniques and biomaterials offered essential values into my thesis research. In addition, I am grateful for his advices on my career development.

I like to thank Prof. Aleksandr Ovsianikov (IMST) for enriching me the knowledge on laser fabrication of biomaterial scaffolds as well as the general support by his sub-team (Peter, Marica, Franz, Evaldas). Dr. Jan Torgersen and Peter Gruber (IMST) are gratefully acknowledged for their creative input on scaffold design and 2PP-processing. Furthermore, Severin Mühleder, Dr. Wolfgang Holnthoner and Prof. Heinz Redl in the Ludwig Boltzmann Institute for Experimental and Clinical Traumatology are particularly acknowledged for their essential input on the biocompatibility analysis as well as scientific interactions on ‘‘Tissue Regeneration’’. Prof. Robert Saf (TU Graz) is thanked for his efforts on the MALDI-TOF study. Drs. Birgit Plochberger and Enrico Klotsch in the Institute of Applied Physics (TU Vienna) are gratefully acknowledged for their Biophysics input on AFM-Indentation.

I appreciate the synthesis training given by Christian Heller when I firstly got Vienna. Without this fundamental but critical training, I was not able to adapt myself from a material scientist to a synthetic chemist. Furthermore, I would like to thank Niklas Pucher and Zhiquan Li for developing their highly efficient 2PIs. In addition, thanks are given to the great ‘‘Macromolecular’’ colleagues: Andi, Brani, Christian, Claudia, Clark, Daniel, Harald, Kati, Konstanze, Kirstin, Markus, Max, Mia, Nele, Patrick, Paul, Sepp, Stephan, Zuzanna, and .... In addition, the generous support by Walter, Florian, Isolda, Franze, Dagmar, Daniel, Prof. Gruber, Prof. Knaus and other institute

colleagues are also unforgettable. Besides, Prof. Marko Mihovilovic's Journal-Club team (Drs. M. Schnürch and F. Rudroff) is thanked for training on scientific presentations.

The financial support by China Education Ministry is highly appreciated. Without the PhD fellowship, I could not imagine studying abroad. In addition, I thank Prof. NIE Jun at Beijing University of Chemical Technology, for introducing me to the field of photopolymer science and for kindly recommending me to Prof. Liska.

Finally, I show my special thanks to my wife, Jie, for her endless love and support, for taking every care of me in the last four years. I also like to show my gratitude to my beloved parents and my brother for their long-term support during my study.

# Abstract

Hydrogels are extensively explored as soft biomaterials for cell culture and tissue regeneration. In particular, designing 3D hydrogels that closely mimic extracellular matrix (ECM) functions has become increasingly important. One approach to create ECM-mimetic hydrogels is two-photon polymerization (2PP), which allows 3D construction of hydrogels with user-dictated  $\mu\text{m}$ -scale architectures. However, biological application of this method is limited by the lack of appropriate hydrogel precursors that are biocompatible and highly reactive for 2PP. This thesis aimed to develop novel hydrogel precursors that are biocompatible, biodegradable and photopolymerizable for fast 3D fabrication of artificial ECM hydrogels via 2PP.

Specifically, both naturally-derived (gelatin and hyaluronic acid) and synthetic materials (polyethylene glycol, PEG) were functionalized with low toxic vinyl ester groups. Biocompatibility assay revealed that these precursors exhibited significantly lower cytotoxicity than their (meth)acrylates references. Although their reactivities were not sufficient for 2PP, it was proved that thiol-ene chemistry could effectively improve their reactivity. Hydrogels with tunable properties were accessible by either changing the thiol to ene ratio or macromer content. These optimized formulations enabled 2PP-fabrication of 3D biomimetic hydrogels at a writing speed up to 50 mm/s.

To further improve the reactivity, polyvinyl alcohol with pendant norbornene groups was developed as a novel hydrogel precursor. Cytotoxicity of this material on fibroblasts was found to be negligible while its reactivity towards thiol-ene polymerization was even higher than that of a PEG diacrylates control. Mechanical properties of these hydrogels (elastic moduli: 0.5-400 kPa) could match various soft tissues. The robust thiol-norbornene chemistry enabled 2PP-fabrication of complex hydrogel constructs at a writing speed up to 100 mm/s.

A novel concept ‘‘Two-photon Cell-Encapsulation’’ was finally explored to test the feasibility of encapsulating living cells within 3D hydrogels via 2PP. It was found that most cells exposed to laser irradiation were dead after encapsulation. Control experiments revealed that laser irradiation alone (no photoinitiator) did not induce cell death. Molecular mechanisms to cell damage during 2PP-encapsulation were proposed from two aspects: photoinitiator-derived radicals and reactive oxygen species.

Collectively, this thesis developed novel hydrogel precursors for fast 2PP-fabrication of biocompatible hydrogel constructs. These hydrogels may help to better understand how cells receive information from and interact with the ECM microenvironment. The knowledge can be exploited for engineering complex tissues and designing novel strategies for tissue regeneration.





# Kurzfassung

Hydrogele werden zurzeit intensiv für den Einsatz als weiche Biomaterialien für Zellkulturen und Geweberegeneration untersucht. Besonderes Interesse hat das Designen von 3D Hydrogelen, welche die essentiellen Eigenschaften der extrazellulären Matrix (ECM) widerspiegeln, geweckt. Eine Methode, um solche biomimetischen Hydrogele herzustellen, ist die Zwei-Photonen-Polymerisation (2PP), welche es erlaubt, 3D Konstruktionen von Hydrogelen mit benutzerdefinierten Architekturen im  $\mu\text{m}$ -Bereich zu generieren. Jedoch ist die biologische Anwendung dieser Methode noch limitiert aufgrund des Fehlens geeigneter Hydrogel-Precursor, die sowohl biokompatibel als auch hochreaktiv im Hinblick auf die 2PP sind. Die vorliegende Arbeit zielt darauf ab, neue Hydrogel-Precursor zu entwickeln, welche zugleich biokompatibel, bioabbaubar und photopolymerisierbar sind und welche sich zur 3D Strukturierung von künstlichen ECM Hydrogelen mittels 2PP eignen.

In dieser Arbeit wurden sowohl natürliche (Gelatine und Hyaluronsäure) als auch synthetische Materialien (Polyethylenglykol, PEG) mit wenig toxischen Vinylestergruppen funktionalisiert. Die Untersuchung auf Biokompatibilität zeigte, dass diese Precursor eine signifikant geringere Zytotoxizität aufweisen, als ihre (Meth)acrylat-Analoga. Obwohl sich ihre Reaktivität als nicht hoch genug für 2PP herausstellte, konnte gezeigt werden, dass die Thiol-En-Chemie die Reaktivität effektiv erhöhen kann. Durch verschiedene Thiol/En-Verhältnisse bzw. durch Variation des Makromer-Gehalts sind Hydrogele mit variablen Eigenschaften zugänglich. Diese optimierten Formulierungen erlaubten die 2PP-Herstellung von 3D biomimetischen Hydrogelen bei einer Schreibgeschwindigkeit von bis zu 50 mm/s.

Um die Reaktivität weiter zu erhöhen, wurde Polyvinylalkohol als Polymerrückgrad mit Norbornen-Gruppen modifiziert und so ein neuer Hydrogel-Precursor entwickelt. Die Zytotoxizität dieses Materials stellte sich als vernachlässigbar heraus, während die Reaktivität hinsichtlich Thiol-En-Polymerisation höher war als beim Kontrollmaterial (PEG-Diacrylat). Mechanische Eigenschaften dieser Hydrogele (Elastizitätsmodul: 0,5-400 kPa) lagen im Bereich verschiedener weicher Gewebe. Diese stabile Thiol-Norbornen-Chemie erlaubte die 2PP-Herstellung von komplexen Hydrogel-Konstrukten mit einer Schreibgeschwindigkeit von bis zu 100 mm/s.

Als neues Konzept wurde letztendlich die „Zwei-Photonen Zell-Einkapselung“ untersucht, um zu testen, ob sich lebende Zellen in 3D Hydrogelen mittels 2PP einschließen lassen. Es stellte sich heraus, dass die meisten Zellen, welche der Laserbestrahlung ausgesetzt wurden, nach der Einkapselung abgestorben waren. Kontrollexperimente zeigten, dass Laserbestrahlung alleine (ohne Photoinitiator) keinen Zelltod induzierte. Zwei molekulare Mechanismen für die Zellschädigung während 2PP-Einkapselung wurden vorgeschlagen: vom Photoinitiator stammende Radikale und reaktive Sauerstoff-Spezies.

Zusammenfassend wurden in der vorliegenden Arbeit neue Hydrogel-Precursor für die rasche 2PP-Fabrikation von biokompatiblen Hydrogel-Konstrukten entwickelt. Diese Hydrogele könnten dabei helfen, besser zu verstehen, wie Zellen Information von der ECM-Mikroumgebung erhalten und mit dieser interagieren können. Dieses Wissen kann zur Entwicklung komplexer Gewebe und dem Designen neuer Strategien für Geweberegeneration genutzt werden.

# Table of content

			Exp.
<b>Introduction</b>		<b>1</b>	
<b>1. Tissue Engineering</b>		<b>1</b>	
<b>2. Artificial ECM Hydrogels</b>		<b>7</b>	
<b>3. Additive Manufacturing of 3D Hydrogels</b>		<b>25</b>	
<b>Objective</b>		<b>31</b>	
<b>State of the art</b>		<b>37</b>	
<b>Results and Discussion</b>		<b>43</b>	
<b>1 Gelatin-based Hydrogels</b>		<b>43</b>	<b>181</b>
1.1 Synthesis of Gelatin Derivatives		45	182
1.1.1 Synthesis of Gelatin Methacrylates (GH-MA)		45	182
1.1.2 Synthesis of High MW Gelatin Methacrylates (gelMOD)		46	183
1.1.3 Synthesis of Gelatin Acrylates (GH-AC)		48	185
1.1.4 Synthesis of Gelatin Vinylesters (GH-VE)		51	187
1.2 Characterization of Gelatin Derivatives		55	190
1.2.1 Photo-Rheometry		55	190
1.2.2 Cytotoxicity		57	190
1.3 Preparation of Albumin Macrothiols (BSA-SH)		58	190
1.3.1 Selection of Reducing Agent		59	
1.3.2 Ellman's Test		61	191
1.4 Characterization of GH-VE/BSA-SH Hydrogels		63	193
1.4.1 Photo-Rheometry		64	193
1.4.2 Swelling Test		65	194
1.4.3 Hydrogel Toxicity		66	194
1.4.4 Cell Adhesion		67	194
1.5 2PP Microfabrication		67	194
1.5.1 Selection of Two-photon Initiator		67	

1.5.2	Scaffold Design	69	
1.5.3	Microfabrication	70	
1.6	Attempts to Increase Crosslinking Density	71	195
1.6.1	Synthesis of GH-Epo	72	195
1.6.2	Synthesis of GH-Epo-PEI	74	197
1.6.3	Synthesis of GH-Epo-PEI-VE	75	198
<b>2</b>	<b>Hyaluronan-based Hydrogels</b>	<b>79</b>	<b>201</b>
2.1	Background	79	
2.2	Synthesis of HA-derivatives	82	201
2.2.1	Preparation of Low MW HA	82	201
2.2.2	Synthesis of Hyaluronate Methacrylates (HA-MA)	83	202
2.2.3	Synthesis of Hyaluronate Acrylates (HA-AC)	85	203
2.2.4	Synthesis of Hyaluronate Vinyl Esters (HA-VE)	86	204
2.2.4.1	Preparation of Tetrabutylammonium Salt of HA (HA-TBA)	88	204
2.2.4.2	Synthesis of HA-VE	90	205
2.2.5	Synthesis of Thiolated Hyaluronan (HA-SH)	92	207
2.3	Characterization of HA Derivatives	95	208
2.3.1	HA-VE Hydrogels	95	208
2.3.1.1	Photopolymerization	96	208
2.3.1.2	Influence of DS on Photoreactivity	96	208
2.3.1.3	Influence of Macromer Content on Gel Stiffness	97	208
2.3.1.4	Temporal Control	98	208
2.3.1.5	Degradation	99	208
2.3.2	Comparative Characterization	100	209
2.3.2.1	Cytotoxicity	101	209
2.3.2.2	Photoreactivity	102	210
2.3.2.3	Influence of Thiol-ene Chemistry	103	210
2.3.2.4	Swelling Test	105	210
2.3.2.5	AFM Modulus Test	106	220
2.4	2PP Microfabrication	107	211
2.5	Engineering Cell Adhesion	109	212

2.5.1	Preliminary Cell Top-seeding	109	212
2.5.2	A Photopatterning Approach	110	212
2.5.3	Model One-photon Patterning	111	212
2.5.4	Model Two-photon Patterning	112	213
<b>3</b>	<b>Synthetic Hydrogels</b>	<b>115</b>	<b>215</b>
<b>3.1</b>	<b>Vinyl Carbonates/Carbamates-based Hydrogels</b>	<b>115</b>	<b>215</b>
3.1.1	Synthesis	117	215
3.1.1.1	Synthesis of Hydroxyethyl Vinyl Carbonate	117	215
3.1.1.2	Synthesis of Glycerol Trivinyl Carbonate	117	216
3.1.1.3	Synthesis of Hydroxyethyl Vinyl Carbamate	118	217
3.1.2	Characterization	118	219
3.1.2.1	Cytotoxicity	118	219
3.1.2.2	Photo-Differential Scanning Calorimetry	121	219
3.1.2.3	Proof-of-Concept 2PP	122	219
<b>3.2</b>	<b>PEG-based Hydrogels</b>	<b>125</b>	<b>220</b>
3.2.1	Synthesis	125	220
3.2.1.1	Synthesis of PEG-600-Divinyl Esters	125	220
3.2.1.2	Synthesis of PEG-10k-Diacrylates	126	221
3.2.1.3	Synthesis of Water-soluble Thiols	127	
3.2.1.4	Preparation of Macrothiols by Inclusion Complexation	128	221
3.2.2	Characterization	130	222
3.2.2.1	Cytotoxicity	130	222
3.2.2.2	Photo-DSC	133	222
3.2.3	2PP Microfabrication	136	222
3.2.3.1	PEG Diacrylates	137	222
3.2.3.1.1	PEGDA-700	137	222
3.2.3.1.2	PEGDA-10k	140	223
3.2.3.2	PEG Dimethacrylates	142	223
3.2.3.2.1	PEG-1000-DMA	142	223
3.2.3.2.2	PEG-600-DMA	143	223
3.2.3.2.3	Formulation-3	143	223
3.2.3.3	PEG Divinyl Esters	144	224

3.2.3.3.1	PEG-600-DVE	144	224
3.2.3.3.2	PEG-250-DVE	145	225
3.2.3.3.3	DVA	146	225
<b>3.3</b>	<b>PVA-based Hydrogels</b>	<b>149</b>	<b>226</b>
3.3.1	Background	149	
3.3.2	Synthesis of PVA-Norbornene	153	227
3.3.3	Characterization	156	228
3.3.3.1	Cytotoxicity	156	228
3.3.3.2	Photo-Rheometry	158	228
3.3.4	2PP Microfabrication	165	229
<b>4</b>	<b>Two-photon Cell-Encapsulation</b>	<b>169</b>	<b>229</b>
4.1	Background	169	
4.2	Two-photon Photo-encapsulation	171	229
4.2.1	Material Selection	172	229
4.2.2	2PP Processing	174	229
4.2.3	Molecular Pathways to Cell Damage	176	229
4.2.4	Cell Proliferation	178	229
	<b>Conclusion</b>	<b>231</b>	
	<b>Outlook</b>	<b>238</b>	
	<b>Abbreviations</b>	<b>240</b>	
	<b>Materials &amp; Methods</b>	<b>243</b>	
	<b>References</b>	<b>259</b>	

# Introduction

## 1. Tissue Engineering

Nowadays, human beings are living in an aging society while suffering a variety of life-threatening diseases such as severe trauma, cancer, diabetes and Parkinson's diseases. Organ shortage and lack of effective methods to repair damaged or diseased human organs and tissues are the major causes for disability and mortality. Although transplantation of organs like heart and liver has been successful, the donor supply is far less than the clinical need.<sup>1</sup> Every year there is an increasing number of patients on the waiting list for organ donation. While patients can be treated with alternative organs from other species (e.g., pig), the associated issues in terms of immunocompatibility and microbiological safety remain speculative.<sup>2</sup>

Tissue engineering holds the most promise to tackle the organ shortage crisis. In this burgeoning field, researchers from multidisciplinary area aim to engineer artificial tissues with the abilities to function, grow, repair and remodel. The tissue engineering concept is established on the seminal work of Vacanti, a surgeon-scientist, in the early 1980s. The concept is defined as the application involving interdisciplinary sciences of medicine, chemistry and engineering to repair, restore and regeneration of tissue function or a whole organ. Detailed milestones in tissue engineering could be found in a review article of Vacanti.<sup>3</sup>

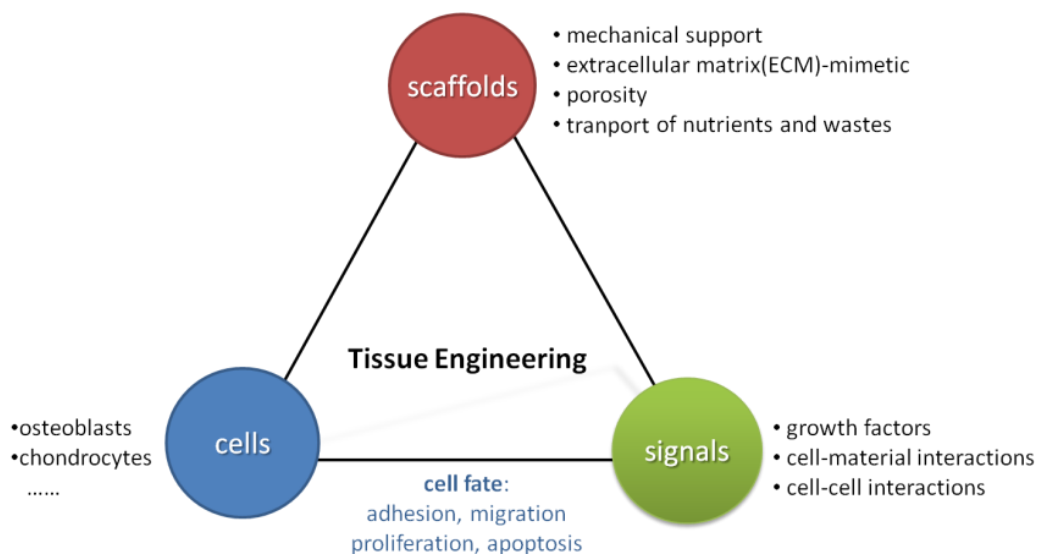


**Figure 1.** Principle of tissue engineering<sup>3</sup>

The basic principle in tissue engineering (Figure 1) is to use cells, scaffolds or cell-seeded scaffolds. In particular, the most common approach is to use a biodegradable scaffold that mimics the strength, shape and biological function of the tissue to be repaired. The scaffold can provide mechanical support and space for seeding cells of interests. Over time the seeded cells can proliferate and reproduce the extracellular matrix (ECM) while the scaffolding material is degraded or metabolized (Figure 2) until a new tissue with full functions is formed.

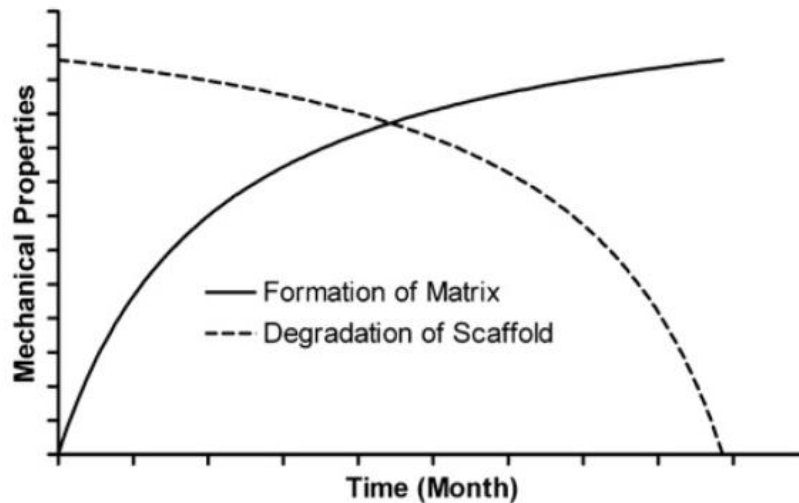


**Figure 2.** Schematic showing the evolution of biodegradable scaffolds<sup>4</sup>

### Biodegradable Polymers

For most clinical applications, implants are required to serve a temporary rather than a permanent purpose. To this goal, biodegradable polymers have gained wide interests since biodegradable implants can avoid a second surgery and associated surgical complication. The time-scale of degradation process can be carefully designed to match a specific application.<sup>5,6</sup>

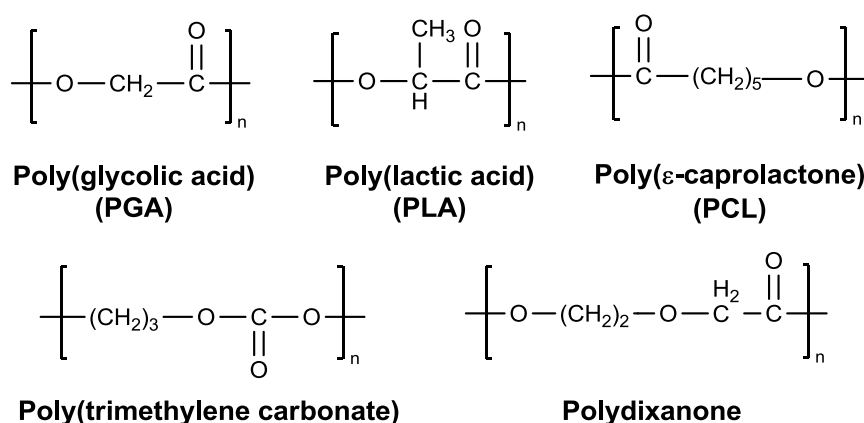
Over the last decades a wide range of biodegradable polymers have been developed as scaffolding materials in tissue engineering. Table 1 gives an overview of scaffolding materials. They can be classified into two groups: synthetic origin and natural origin. Hydrolytically degradable materials are mostly synthetic polymers with multiple ester linkages such as poly (glycolic acid) (PGA) and poly (lactic acid) (PLA). In contrast, protease-induced enzymatic degradation is often related to naturally-derived materials such as collagen and fibrin.



**Table 1.** Biodegradable scaffolding materials in tissue engineering

	Synthetic origin	Natural origin
1 <sup>st</sup> generation	Polyglycolic acid (PGA)	decellularized tissue
	Poly(lactic acid) (PLA)	Collagen
	Polycaprolactone (PCL)	Fibrin
2 <sup>nd</sup> generation	Hydrogels...	

Notably, in 2006 the USA Food and Drug Administration (FDA) has approved seven distinct synthetic polymers (Figure 3) for their use in clinical applications. They are polyesters containing glycolic acid, lactic acid, caprolactone or dioxanone, polyanhydrides containing sebacic acid, poly(trimethylene carbonate)s, and tyrosine-derived polyarylates.<sup>7</sup> Among these materials, PGA, PLA, and PCL are the major representatives.

**Figure 3.** Chemical structures of FDA-approved hydrolytically degradable polymers

PGA, PLA, and their copolymers are widely used as biodegradable synthetic implants. PGA is the simplest aliphatic polyester and the first developed for use as bioabsorbable sutures.<sup>8</sup> PGA sutures are commercially available under the trade name “Dexon<sup>TM</sup>”. A major problem related to PGA-based implants is the rapid loss of mechanical strength as a result of fast degradation (2-4 weeks). Therefore, researchers have intensively attempted to copolymerize glycolic acid with the more hydrophobic lactic acid to decrease the hydrolysis rate.<sup>9</sup> Copolymers of glycolic acid and lactic acid (PLGA) can provide tunable degradation rates by carefully controlling the relative ratio of glycolic acid to lactic acid. For instance, PLGA sutures are distributed under the trade names “Vicryl<sup>TM</sup>” while the 90:10 PLGA copolymer are traded as “Polyglactin 910<sup>TM</sup>”.

While many clinical successes have been achieved using PGA, PLA, and PLGA, there are still remaining problems: 1) most cells do not attach on the surface of these materials due to the lack of specific binding sites, making them poor substrates for cell culture *in vitro*; 2) the degradation products (either lactic acid or glycolic acid) are relatively strong acids. The accumulation of these acids at the implant site can evoke inflammatory responses after implantation.<sup>10</sup>

In 2006, Ikata et al. reported a comprehensive review of structure-property relationship of poly( $\alpha$ -hydroxy acid)s.<sup>11</sup> The degradation rate of poly( $\alpha$ -hydroxy acid)s may vary from two weeks to five years (Figure 4). The difference lies in the hydrophobicity of the polymer backbone. For instance, upon hydrolysis PCL degrades about 100 times slower than PGA since caprolactone are more hydrophobic than glycolic acid. It is accepted that whether water molecules could reach and ‘interact with’ the chemical groups (i.e., ester linkages) plays a critical role in the degradation process.

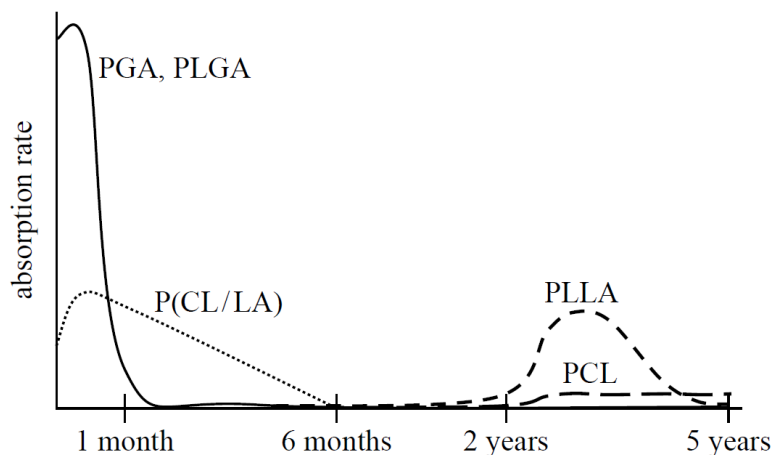


**Figure 4.** Comparative illustration of degradation rates of poly( $\alpha$ -hydroxy acid)s<sup>11</sup>

While a series of poly( $\alpha$ -hydroxy acid)s are on the market, they are limited to regenerate hard tissues with high modulus ( $> 10$  GPa). For instance, the elastic modulus of cortical bone at the longitudinal direction is about 17.7 GPa (Table 2). In comparison, however, the elastic modulus of articular cartilage is 10.5 MPa, making poly( $\alpha$ -hydroxy acid)s undesirable for soft tissue engineering. Furthermore, hydrophobicity of these materials cannot recapitulate the native environment of soft tissues that often contain high water content. For soft tissue engineering applications, hydrogels are the material of choice.

**Table 2.** Mechanical properties of hard and soft tissues<sup>12</sup>

<b>Hard Tissue</b>	<b>Modulus (GPa)</b>	<b>Soft Tissue</b>	<b>Modulus (MPa)</b>
Cortical bone (longitudinal)	17.7	Articular cartilage	10.5
Cortical bone (transverse)	12.8	Ligament	303.0
Enamel	84.3	Intraocular lense	5.6
Dentine	11.0	Skin	0.1



## 2. Artificial ECM Hydrogels

Hydrogels are crosslinked, three-dimensional polymer networks formed by hydrophilic monomers or macromers (Figure 5). In the voids area, significant amounts of water are present in the surroundings of polymer chains. The crosslinking feature renders hydrogels water-insoluble, yet they could hold up to 1000 times of water to their dry weight. The macromolecular pores inside the networks allow high permeability for nutrients, oxygen and cellular wastes.<sup>13</sup> Owing to these features, hydrogels exhibit superior biocompatibility and cause minimal cellular damage when used for cell culture.<sup>14</sup>

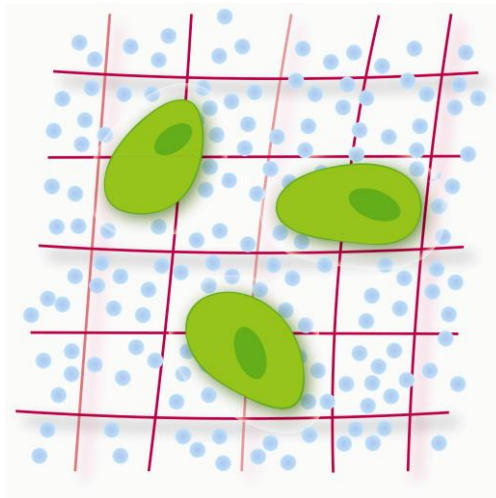


**Figure 5.** Schematics of hydrogel networks for cell culture

Importantly, the structural and biochemical features of hydrogels are highly similar to those of soft tissues. By changing the crosslinking density, physical properties of hydrogels could be tuned to match the mechanical properties of various soft tissues.<sup>15, 16</sup> As such, hydrogels are increasingly important materials for a variety of applications in tissue engineering and regenerative medicine.

In tissues, cells are generally growing within the extracellular matrix (ECM). The native ECM (Figure 6A) is a crosslinked hydrogel that includes polysaccharide as well as structural, cell-adhesive, and cell-signaling proteins. Each of these components plays distinctive functions. For instance, collagen fibers are major components for providing structural support to cells, while hyaluronic acid plays an important role in maintaining water content. Besides, there are thousands of hundreds of cell-signaling pathways that are governed by the local characteristics (biochemical, physical, geometrical...) of the

ECM. Moreover, there are numerous cell-cell and/or cell-matrix interactions that are orchestrated in a dynamic manner. Integrated signals from these interactions would intracellularly determine the cell fate. Such a highly complex environment makes it hard to recapitulate the physiological aspects of the native ECM *in vitro*.

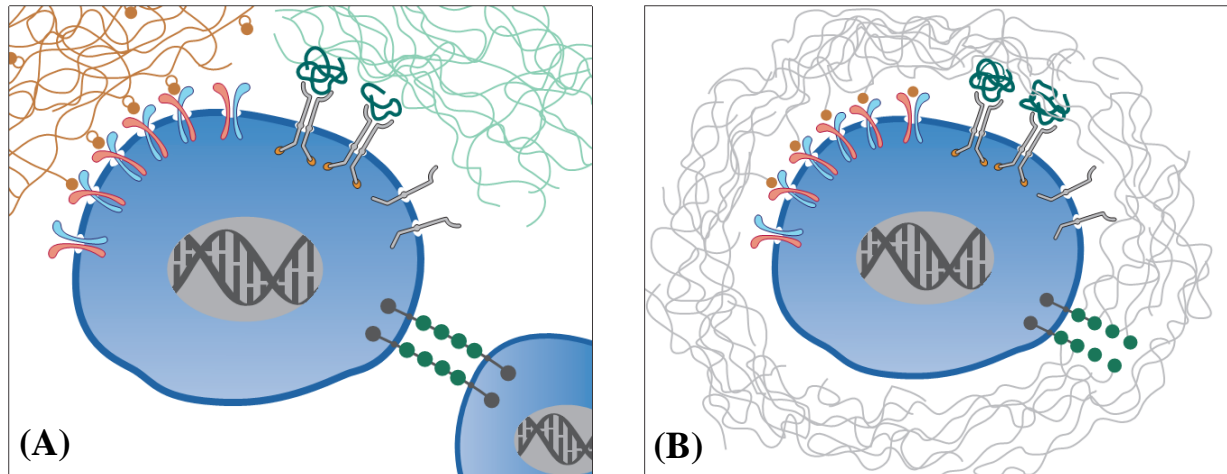


**Figure 6.** The concept of artificial ECM hydrogels: (A) the native ECM environment and (B) the use of artificial ECM hydrogels (e.g., synthetic PEG gels) with micropatterned bioactive ligands for mimicking the native ECM (reprinted with permission from Nature Publishing Group<sup>17</sup>)

To dissect the complexities in native ECM, a variety of biomimetic hydrogels with highly defined properties have been explored. For instance, synthetic PEG gels were micropatterned with bioactive ligands to mimic the cell attachment via integrin-binding (Figure 6B).<sup>18</sup> According to the methods of crosslinking, these hydrogel networks could be formed by: 1) enzymatic crosslinking, 2) physical crosslinking, or 3) chemical crosslinking. For instance, fibrin is a typical example of enzymatic hydrogels, that are formed after the cleavage of fibrinogen by thrombin (protease) and subsequent self-assembly of protofibrils with the help of factor XIII enzyme.<sup>19</sup> Besides, amphiphilic block copolymers such as Pluronic form physically-crosslinked hydrogels via non-covalent (hydrophobic or ionic) interactions.<sup>20</sup> These materials typically present thermo-responsive characteristics. Additionally, chemically-crosslinked hydrogels are typically formed by thermo- or photo-induced polymerization of water-soluble precursor molecules that have multiple reactive sites.

Notably, photopolymerization has drawn the most interests because the use of light allows facile preparation of hydrogels with controlled geometry and properties.<sup>21, 22</sup> Compared to conventional methods, photopolymerization presents numerous advantages,

including fast reaction kinetics (below several minutes), spatiotemporal control over the polymerization process and processability at room temperature and physiological conditions.<sup>23</sup> All these attributes have enabled a wide range of photopatterning and stereolithography-based additive manufacturing techniques (AMT).<sup>24-26</sup> Integration of these techniques with hydrogels have facilitated further tissue engineering applications, such as *in situ* cell encapsulation,<sup>27</sup> and spatiotemporal distribution of bioactive ligands.<sup>28</sup> Certain types of hydrogels could be *in situ* photopolymerized in the presence of light-sensitive compounds (photoinitiators, PIs) and light. When UV or visible light interacts with PIs, free radicals are generated to initiate polymerization of monomers/macromers and finally form crosslinked hydrogel networks. Given the importance of these materials, both water-soluble PIs and hydrogel precursors will be reviewed in the following sections. Specifically, the selection principle for water-soluble PIs will be described with a focus on initiating mechanism, efficiency, and cytocompatibility. Next, photopolymerizable hydrogel precursors are further illustrated in details from design criteria to gel-formation chemistry. In the end, both synthetic and naturally-derived precursors will be briefly overviewed with a focus on substrate chemistry.

### Water-soluble Photoinitiators (PIs)

When one designs a photopolymerization system, PI is the primary component to be considered since the selection of PI is critical to the polymerization efficiency. First, the absorption spectrum of selected PI should overlap to a large extent with the irradiation profile of light source. Second, the selected PI should have high efficiency in generating free radicals.

According to the radical generation mechanisms, radical PIs can be divided into two categories: cleavable PIs (Type-I) and bimolecular photoinitiating system (Type-II). Upon irradiation, Type-I PIs such as Irgacure 2959 (I2959) undergo cleavage from the excited triplet state and generate two radicals for initiating polymerization (Figure 7A). In contrast, the initiating mechanism of Type-II systems (e.g., benzophenone/tertiary amine) is more complex. The excited benzophenone initiates a fast electron transfer from the lone pair of tertiary amine followed by a slow proton transfer process, providing the H-donor radical for initiating polymerization (Figure 7B). Notably, compared to Type-I PIs, Type-

II systems are much less efficient due to the bimolecular process, back electron transfer and especially the solvent cage effect in aqueous solutions.<sup>29</sup>

Besides, it is noteworthy to mention the initiation mechanism of two-photon active initiators (Figure 7C). These PIs essentially have highly conjugated  $\pi$ -systems, good coplanarity and strong donor/acceptor groups. In the simplest case (i.e., radical polymerization), the initiation mechanism is currently accepted as: after intra- and inter-molecular charge transfer interactions between the two-photon excited PI and monomer, radicals are formed by electron transfer to initiate polymerization.<sup>30</sup> However, two-photon initiating mechanism for more complex systems (e.g., thiol-ene polymerization) remains largely unexplored.

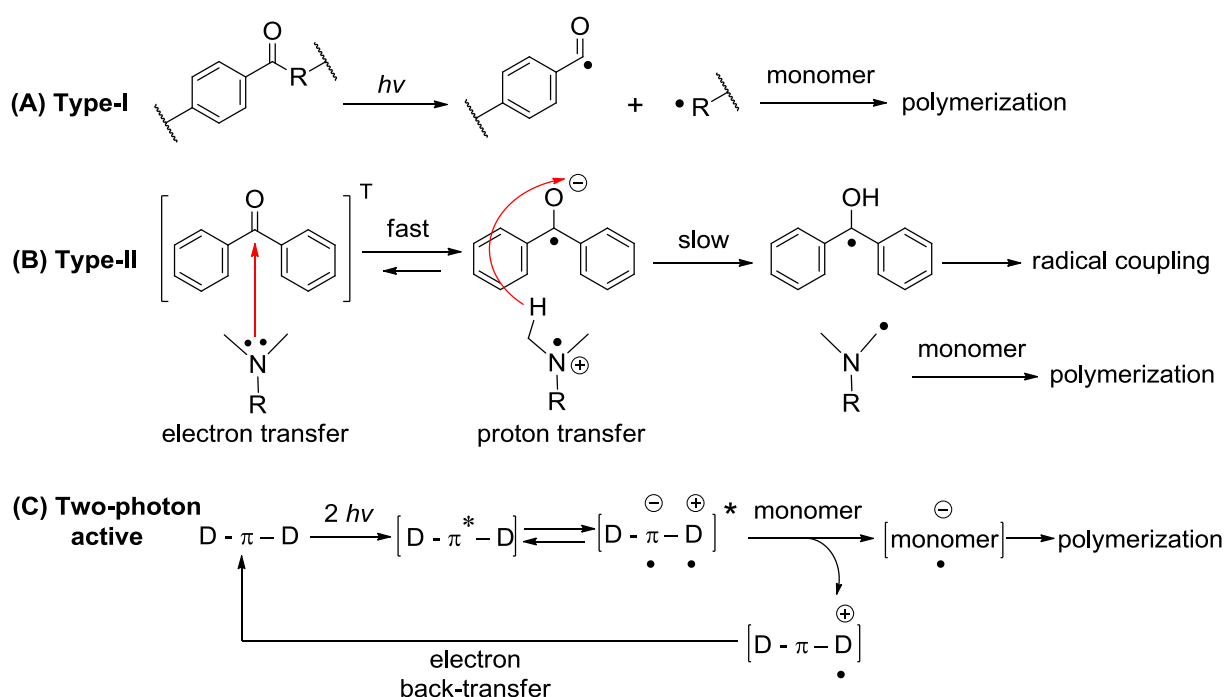


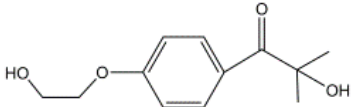
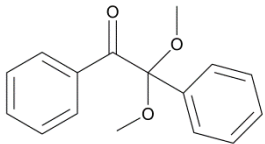
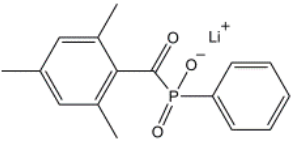
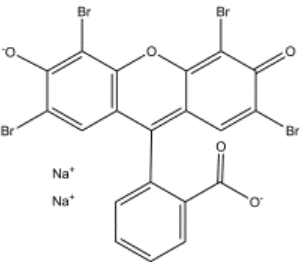
**Figure 7.** Photoinitiating mechanisms of Type-I (A), Type-II (B) and two-photon active (C) initiators

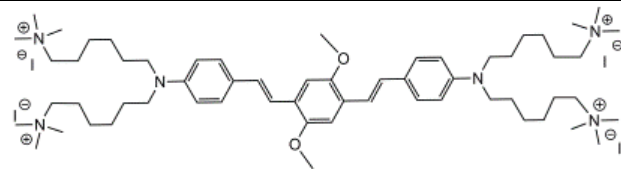
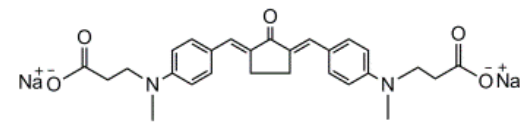
To prepare hydrogels, more factors should be considered, particularly the water-solubility and cytocompatibility of PIs. For *in situ* cell encapsulation studies, PIs are used to polymerize gel precursor solutions containing cell suspension. After polymerization, ideally viable cells are encapsulated in hydrogel matrices. Table 3 presents an overview of state-of-the-art PIs that have been used in preparing hydrogels. From the illustrated examples, it is important to note that each PI has different characteristics in terms of absorption profile, cytocompatibility, water-solubility and initiation mechanism.



For UV photopolymerization, classical type-I PIs with low cytotoxicity such as I2959 have been used for *in situ* cell-encapsulation studies.<sup>31, 32</sup> However I2959 suffers from low efficiency for cell-encapsulation purposes due to its limited absorption at UV-A range. The important  $n-\pi^*$  transition of I2959 at  $\sim 330$  nm has very low extinction coefficient. Combined with low initiator concentration due to limited solubility, its contribution to the initiation process is rather limited. While alternative cleavable initiators such as I651 possess much higher initiating efficiency at UV-A range, poor water-solubility often necessitates the use of organic solvents. Eosin Y has been used as visible light initiator in combination with triethanolamine (TEA).<sup>33</sup> While Eosin Y has strong absorption in the visible light range, it is less efficient than cleavable initiators due to intrinsic limitations of type-II systems. Previous work by West and co-workers has explored the non-cytotoxic conditions of this three-component system.<sup>34</sup> It was found that the ‘optimum’ condition ( $\sim 88\%$  cell viability) was achieved using 0.01 mM Eosin Y and 0.1% TEA beyond which significant toxicity effects were observed.

**Table 3.** Water-soluble photoinitiators (PIs) for photopolymerization of hydrogels

	PIs	Chemical structures	Water soluble ?	$\lambda_{\text{abs}}$ (nm)	Ref
Type-I	I2959		Y	276 <sup>a</sup> 330 <sup>b</sup>	32
	I651 <sup>*</sup>		N	335 <sup>b</sup>	32
	LAP		Y	375 <sup>b</sup>	35
Type-II	Eosin Y		Y	514 <sup>a</sup>	34

<b>Two-photon active</b>	WSPI 	Y	423 <sup>a</sup>	36
	P2CK 	Y	470 <sup>a</sup>	37

<sup>a</sup>  $\pi$ - $\pi$ \* absorption, <sup>b</sup> n- $\pi$ \* absorption;

\* ethanol has been used to increase the solubility of I651.

In a recent study by Anseth and Bowman research groups, a type-I visible light PI (lithium phenyl-2,4,6-trimethylbenzoylphosphinates, LAP,  $\lambda_{\max}$ ~375 nm) has proven to be much more efficient and less cytotoxic than I2959, thus making it a better PI for *in situ* cell encapsulation studies.<sup>38</sup> Very recently, a series of water-soluble, two-photon active initiators have been developed for laser-induced microfabrication of hydrogels at TU Vienna.<sup>37, 39</sup> For instance, a highly efficient initiator, WSPI, has been exploited to fabricate PEG hydrogels in the presence of living organisms.<sup>39</sup> Since the synthesis of WSPI is rather sophisticated (> 5 steps), a novel synthetic approach was established by Zhiqian Li (IAS) for facile synthesis (2 steps) of carboxylate sodium salts of cyclic benzylidene ketone-based PIs (e.g., P2CK).<sup>37</sup> Importantly, these initiators exhibited large two-photon cross-section values (>150 GM) and high initiating efficiency. Moreover, it was found that the exposure-toxicity of P2CK against MG63 cells is as low as that of the well-proven biocompatible PI I2959.<sup>37</sup>

### Photopolymerizable Hydrogel Precursors

Although the access to efficient PIs is a prerequisite for additive manufacturing of hydrogels, design and synthesis of photopolymerizable monomers/macromers as hydrogel precursors are even more important. The up-to-date hydrogel platforms can be broadly divided into two classes associated with their origin:

- 1) synthetic polymeric hydrogels that allow flexible tuning of chemical and mechanical properties;
- 2) naturally-derived hydrogels that generally have superior biocompatibility and similar biological functions as their biomacromolecule origins.

### Design Considerations

To design hydrogel precursors for potential AMT applications in tissue engineering, several considerations should be addressed, including water-solubility, photoreactivity, cytotoxicity, bioactivity, and biodegradability. First, from a chemical point of view, hydrogel precursors should possess sufficient water solubility. To achieve this goal, polyethylene glycol (PEG) based synthetic polymers as well as certain naturally-derived polymers (e.g., gelatin, hyaluronan or HA) have drawn much attention due to their superior hydrophilicity. On the other hand, the photoreactivity of hydrogel precursors plays an important role in the feasibility to AMT. To fabricate an object with size scales that are clinically relevant (mm to cm scale), the photoreactivity of monomers/macromers directly determines both the writing speed and time costs of the manufacturing process.

Second, from a biological point of view, hydrogel precursors must meet further requirements.

- **Cytocompatibility:** For *in situ* cell encapsulation, cells are directly exposed to a series of materials at varying stages: initially hydrogel precursors, then radical-mediated polymerization process, subsequent crosslinked networks, photoinduced byproducts and finally degradation products. Therefore, all of these involved chemicals and related polymer chemistry must be cytocompatible or at least of very low cytotoxicity.
- **Bioactivity:** Besides cytocompatibility, printed hydrogel scaffolds should provide cells a physiologically-relevant environment and thus maintain all cell functions that are happening *in vivo* (adhesion, movement, division, death). In natural situations, cell attachment is regulated by the crosstalk between integrin receptors on cell membranes and integrin binding motifs (e.g., RGD motif peptides). To this end, researchers have utilized either synthetic materials in combination with RGD motifs or naturally-derived proteins containing RGD motifs (e.g., gelatin, fibrin, fibrinogen).<sup>40</sup>
- **Biodegradability:** Since the ultimate goal of implantable hydrogels is to replace or repair damaged tissues, the degradation kinetics of printed hydrogels should be tunable to match the growth rate of new tissues.

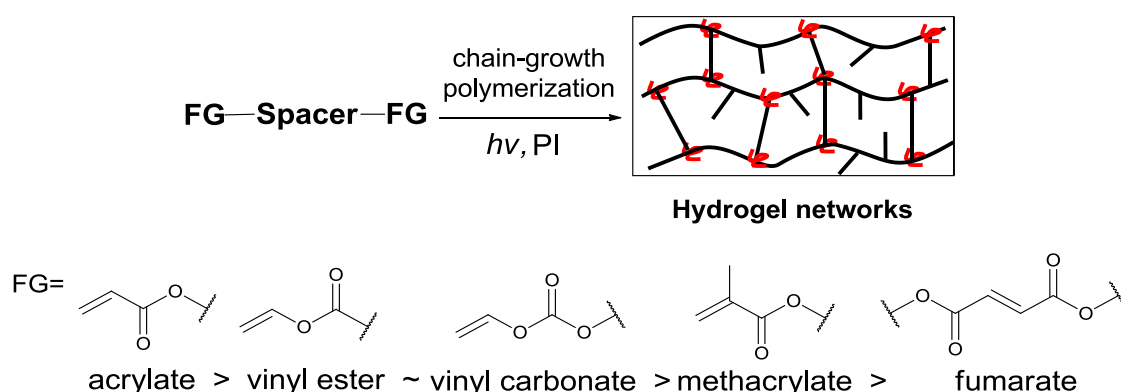
In the following text, photopolymerizable hydrogel precursors that have been used in tissue engineering will be reviewed, proceeding from the chemistry of hydrogel

formation, to synthetic hydrogels and naturally-derived hydrogels while discussing structure-property relationships and their applications in AMT.

### Chemistry of Hydrogel Formation

The formation of hydrogel networks is based on the presence of multifunctional crosslinker during network formation. Thus, synthetic approaches to light-induced network formation are not only limited to classical free-radical chain polymerization, but also alternative approaches based on click chemistry.

*Chain-growth polymerization:* Free-radical chain polymerization is a facile approach to prepare hydrogels where a chain reaction propagates through vinyl-group containing monomers. The reactivity of vinyl monomers towards chain polymerization is dependent on the electronic environment of vinyl groups. Generally, it is accepted that the reactivity of vinyl monomers towards free-radical chain polymerization follows this sequence (Scheme 1): **acrylate > vinyl ester ~ vinyl carbonate > methacrylate > fumarate.**<sup>41</sup>



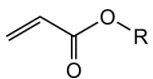
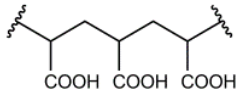
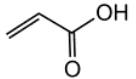
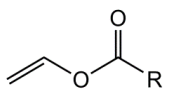
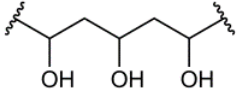
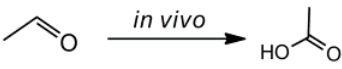
**Scheme 1.** Schematic showing the formation of hydrogel networks via free-radical chain-growth polymerization and reactivity sequence of vinyl groups

Up to date, acrylated monomers are the state-of-the-art materials for AMT applications due to their high reactivity. A general method to synthesize acrylated macromers is based on esterification reaction between acryloyl chloride and hydroxyl groups of several synthetic building blocks (PEG, polyvinyl alcohol or PVA, etc.). Although acrylates have superior reactivity, irritancy and potential cytotoxicity of unreacted acrylate groups is posing a challenge for their potential clinical-relevant applications. In contrast, methacrylates are much less cytotoxic as evidenced by their wide use as dental filling materials.<sup>42</sup> But the moderate photoreactivity of methacrylates raises many practical problems in most photolithography-based AMT. To address this challenge, alternative

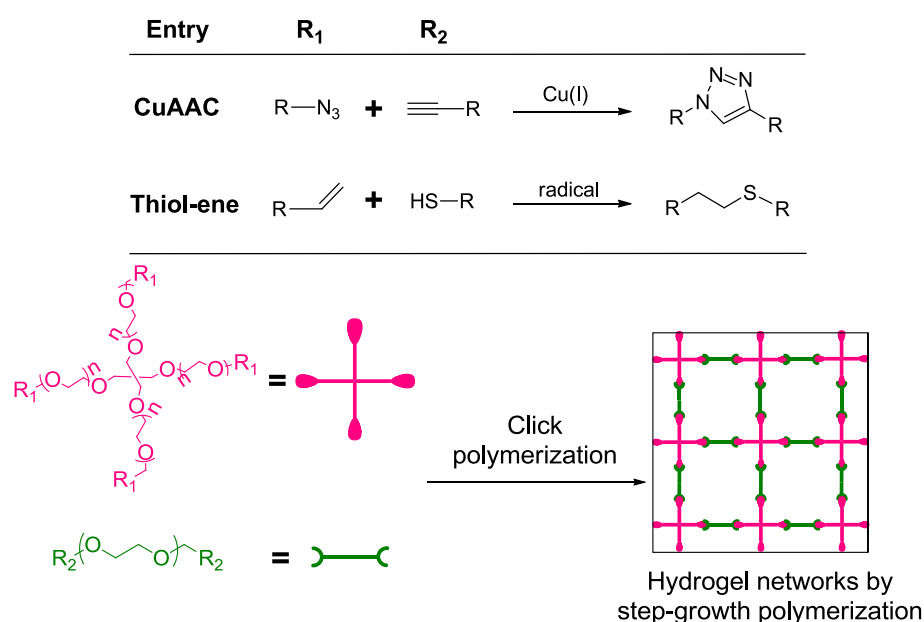
photopolymers such as vinyl esters have been developed by Liska and co-workers at TU Wien in order to reach a good trade-off between high reactivity and low toxicity.<sup>43</sup> Interestingly, there are very few monofunctional vinyl ester derivatives and only one hydrophobic difunctional vinyl esters (divinyl adipate) commercially available and a very limited number of photopolymerization studies related to vinyl esters have been reported so far.<sup>44</sup> Furthermore, hydrogels formed by vinyl ester chemistry remains unknown.

Table 4 presents a comparative analysis concerning the biocompatibility of acrylates and vinyl esters. Importantly, upon hydrolytic degradation, the major degradation products out of poly (vinyl esters) are FDA-approved poly (vinyl alcohol) (PVA) while polyacrylates provide high molecular weight poly (acrylic acids) which have proven very difficult to be excreted from the human body.<sup>43</sup> On the other hand, since it is unlikely to reach complete conversion of vinyl groups in radical photopolymerization, careful attention should be paid to the remaining unpolymerized vinyl groups (at least 10-20 %). It is noteworthy that the remaining acrylate groups would form acrylic acids as degradation products that are highly cytotoxic and irritant whereas the left vinyl ester groups can be easily hydrolyzed into acetaldehyde that could be metabolized into acetic acid *in vivo* under the catalysis of acetaldehyde dehydrogenase. Moreover, it is important to note that the poor storage stability related to thiol-ene systems have recently been solved by Liska and co-workers using a combination of radical and acidic stabilizing system.<sup>45</sup> All these aspects show that water-soluble vinyl esters are promising hydrogel precursors for photolithography-based AMT.

**Table 4.** Comparative analysis of biocompatibility: acrylates versus vinyl esters

Monomers	Major degradation products	Hydrolyzed product of residual group
Acrylates 	 <b>high M<sub>w</sub> poly(acrylic acid)</b>	 <b>acrylic acid</b> Highly irritant
Vinyl esters 	 <b>low M<sub>w</sub> poly(vinyl alcohol)</b>	 <b>acetaldehyde</b> $\xrightarrow{\text{in vivo}}$ <b>acetic acid</b>

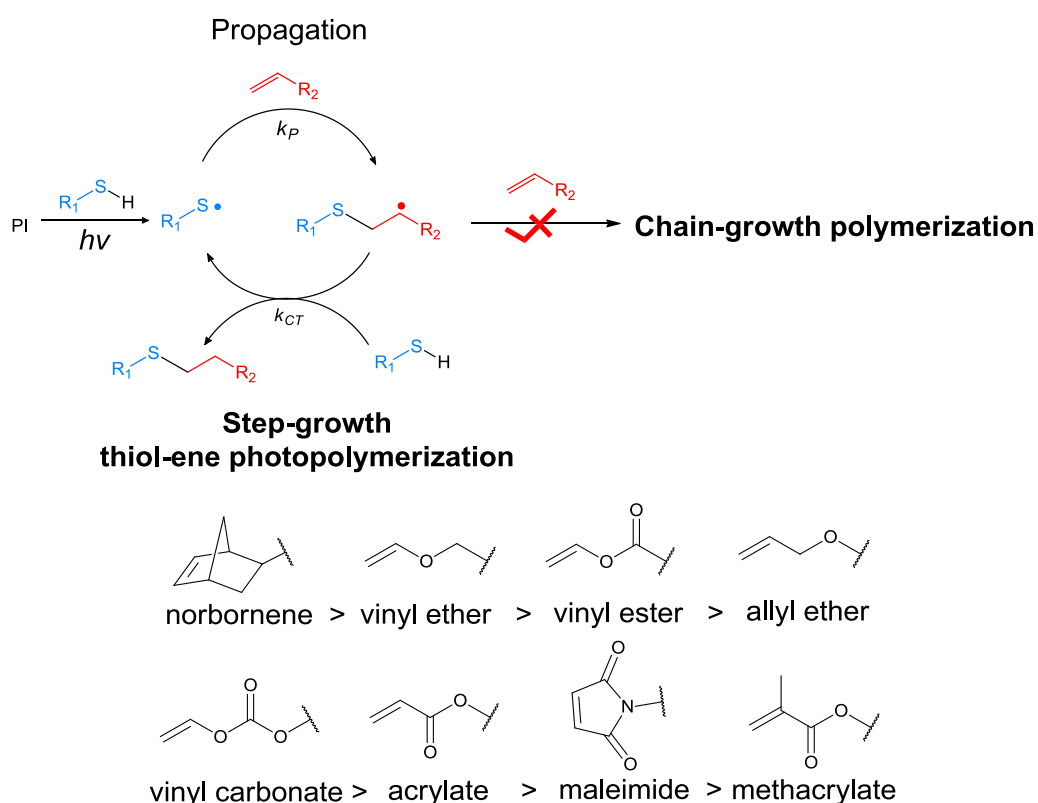
*Click-chemistry based polymerization:* Apart from chain-growth polymerization, click chemistry is an emerging methodology to prepare chemically-crosslinked hydrogels (Scheme 2). According to the initial concept proposed by Barry Sharpless,<sup>46</sup> click chemistry refers to unique chemical reactions between orthogonal groups that react with high selectivity under mild conditions.<sup>47</sup> For instance, copper(I)-catalyzed azide-alkyne cycloaddition (CuAAC) is highly specific and occurs in the presence of competing functional groups (Scheme 2). Researchers have successfully used CuAAC chemistry in combination with a series of hydrophilic macromers (PEG, PVA, HA) to prepare hydrogels.<sup>48-50</sup> However, spatiotemporal control was not readily accessible in these hydrogel systems. Interestingly, a collaborative study from Anseth and Bowman groups explored photoinitiated CuAAC reaction to create hydrogels with spatiotemporal control.<sup>51</sup> In this work, the CuAAC reaction was catalyzed by the photoreduction of Cu(II) to Cu(I) whereby the reduction was initiated by free radicals from activated PIs. This method demonstrated comprehensive spatiotemporal control over the process of hydrogel formation, thus showing great promise for photopatterning of hydrogels. But utilization of this method in AMT remains unexplored. Although hydrogels could also be formed via other click approaches such as tetrazine–norbornene Diels–Alder reaction and oxime-ligation,<sup>52, 53</sup> these approaches generally lack of spatiotemporal control and thus not suitable for direct utilization in AMT applications.



**Scheme 2.** Schematic showing the formation of hydrogel networks via click- polymerization

Radical-mediated thiol-ene photopolymerizations are alternative click approaches to create chemically-crosslinked hydrogels with spatiotemporal control. Such reactions are chemo-selective, robust and applicable to a wide range of macromers containing multiple ene or thiol groups. For instance, the pioneering work of Anseth and co-workers demonstrated that thiol-norbornene step-growth photopolymerizations are extremely robust systems for preparing hydrogels.<sup>54</sup> In this work, 4-arm PEG norbornenes could efficiently ‘click’ with a dithiol (i.e., a peptide with 2 cysteines), forming ideal hydrogel networks in less than one minute.<sup>54</sup>

The underlying mechanism of step-growth thiol-ene photopolymerizations is proposed below (Scheme 3). Upon irradiation, free radicals are generated from PIs followed by the H-abstraction reaction from thiols. The resulting thiyl radicals propagate across the ‘ene’ functionalities, forming the carbon-centered radicals. Ideally, chain-transfer reactions are much more competitive than further chain-propagation reactions. Thus, the thiyl radicals are generated again upon highly efficient chain-transfer reactions.



**Scheme 3.** Proposed mechanism of radical-mediated thiol-ene photopolymerization and reactivity sequence of variable ‘ene’ groups towards thiol-ene conjugation

Within the scope of "ene" groups, the conjugation rate with thiol groups differ greatly from one to another according to the electron density of the "ene" groups.<sup>55</sup> For a specific thiol, electron-rich enes polymerize much faster than electron-poor enes. It is accepted that reactivity of ene groups towards radical-mediated thiol-ene polymerization follows this sequence: **norbornene > vinyl ether > vinyl ester > allyl ether > vinyl carbonate > acrylate > N-substituted maleimide > methacrylate.**

It is important to note that some of these groups (e.g., norbornene, maleimide) undergo idealized step-growth polymerization while other functional groups (e.g., vinyl ester, vinyl carbonate, acrylate, methacrylate) undergo a mixed-mode (step-growth and chain-growth) polymerization mechanism. More information related to thiol-ene photo-click chemistry could be found in comprehensive reviews by Hoyle and Bowman.<sup>55, 56</sup>

### Synthetic Hydrogels

Synthetic hydrogels are increasingly explored for tissue engineering applications due to numerous advantages, such as easy access, cost efficacy, biologically blank state, and so forth. It is feasible to molecularly tailor the mechanical properties and degradation profiles of synthetic hydrogels and to match requirements for a specific application. Precursors of synthetic hydrogels include PEG, PVA, and poly(2-hydroxyethyl methacrylate) (PHEMA) (Figure 8). Considering that very few examples of PHEMA could be found in AMT applications, this section focuses on precursors based on PEG and PVA only.

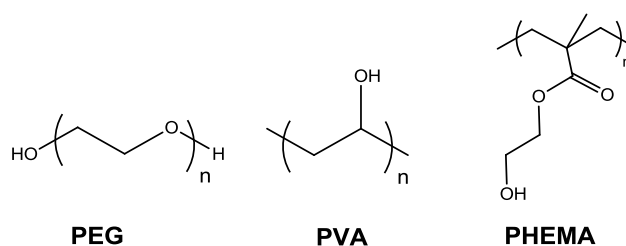


**Figure 8.** Neutrally charged synthetic hydrogels.

*Poly(ethylene glycol):* PEG and its derivatives have proved extremely versatile for tissue engineering applications, such as non-fouling coatings that are resistant to protein adsorption.<sup>57</sup> In recent years researchers have witnessed the wide use of PEG in the field of hydrogels due to its superior hydrophilicity, biocompatibility, and negligible immunogenicity.<sup>58</sup> PEG-based hydrogel precursors could be synthesized by introducing



multifunctional vinyl or clickable groups to the pendant hydroxyl groups (Fig. 4). For example, high MW (3-20 K Da) (meth)acrylated PEG (PEGDA/PEGDMA) can be synthesized in one step by reacting (meth)acryloyl chloride with pendant hydroxyl groups,<sup>59</sup> while lower MW ones (0.3-1 kDa) are commercially available. Notably, PEGDA with an average MW of 700 Da exhibited significant cytotoxicity,<sup>39</sup> whereas PEGDA with higher MW (4.6 kDa) has enabled *in situ* photo-encapsulation of living cells.<sup>60</sup> The toxicity difference could be addressed to the lower concentration of acrylate groups for the high MW macromer in comparison to PEGDA-700 analogue with equal concentration.

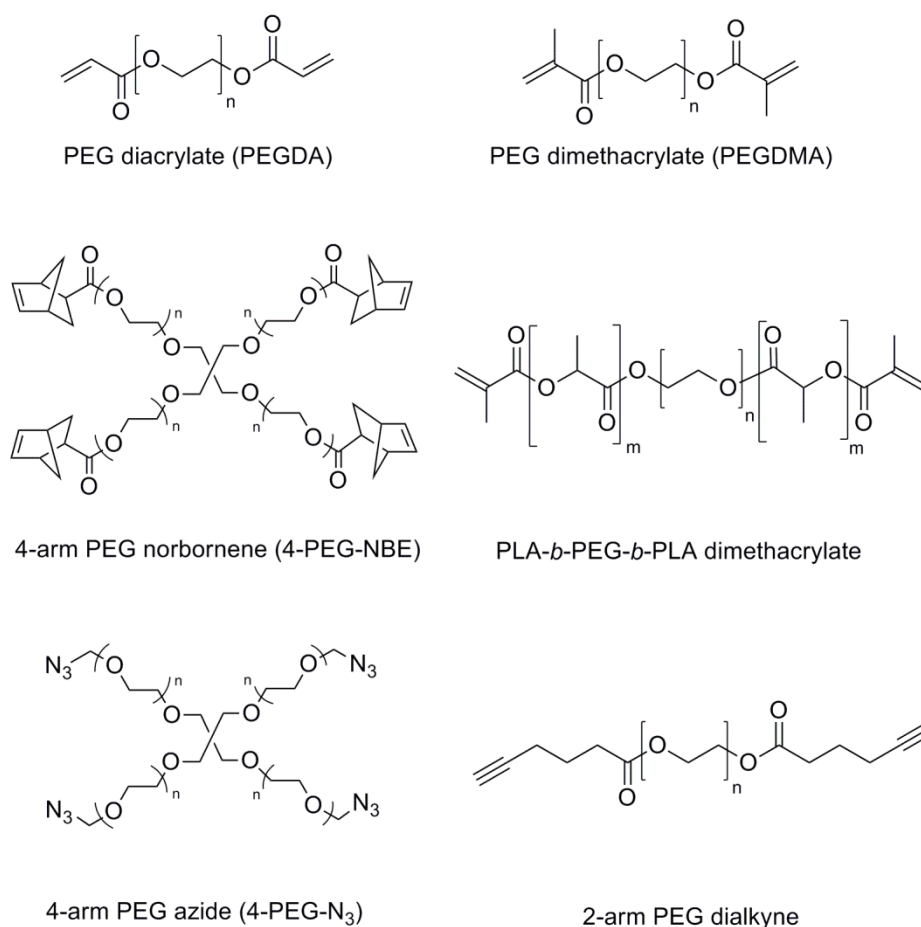


**Figure 9.** Chemical structures of PEG-based hydrogel precursors

Researchers have also developed bioerodible PEG hydrogels using photopolymerizable macromers that contain a PEG central core but terminate with oligomers of alpha-hydroxy acids such as PLA.<sup>13, 61-63</sup> Specifically, the PLA-*b*-PEG-*b*-PLA triblock copolymers were firstly synthesized via classical ring-opening polymerization. An excess of (meth)acryloyl chloride was then reacted with PLA-*b*-PEG-*b*-PLA. The degradation rate of formed hydrogels can be tailored from less than 1 day to up to 4 months by

controlling the crosslinking density of the gel or by selecting the type and amount of  $\alpha$ -hydroxy esters. It is noteworthy to mention the reactivity differences between acrylated PEG and methacrylated PEG. For instance, 2 min exposure time was required for the former while 10 min was needed for the latter.<sup>61, 62</sup>

As mentioned before, although PEGDA are the most widely used hydrogel precursor in the biomaterials community, their irritancy and potential cytotoxicity of unreacted acrylate groups might preclude them from further clinical-relevant applications.<sup>43</sup> Alternatively, PEG norbornenes are ideal hydrogel precursors in terms of high reactivity for thiol-ene step-growth photopolymerization. Fairbanks et al. demonstrated that thiol-norbornene photopolymerizations are suitable models to prepare hydrogels with CRGDS peptide in cell photo-encapsulation studies.<sup>54</sup> The robustness of thiol-norbornene click reactions even minimized the dose of PIs required for cell-encapsulation and thus to certain extent optimized cytocompatibility. A recent study by McCall et al. proved that thiol-ene photopolymerizations are promising methods to form hydrogels for protein encapsulation while maintaining most bioactivities of proteins.<sup>64</sup>

*Poly(vinyl alcohol):* PVA are FDA-approved, hydrophilic polymers that are produced from hydrolysis of poly (vinyl acetate). PVA-based hydrogels have been widely studied for tissue engineering applications due to their superior biocompatibility and unique mechanical strength.<sup>21</sup> Although aqueous PVA solutions can be physically crosslinked by crystallites formed by repeated freeze-thawing,<sup>65</sup> the resultant hydrogels lack of stability at high temperature because of the melting crystallites. To get better stability, chemically crosslinked PVA hydrogels have been synthesized by using glutaraldehyde<sup>66</sup> or succinyl chloride.<sup>67</sup> However, these crosslinking agents are highly toxic and exclude the feasibility for *in situ* cell encapsulation applications.

In the last few decades, chemical modification of PVA has been widely explored in the biomaterial community, including photocrosslinkable and clickable PVA derivatives.<sup>49, 68-71</sup> Detailed description of the synthesis routes to these derivatives is given in section 3.3.1.

### Naturally-derived Hydrogels

When it comes to biocompatibility issues, naturally-derived hydrogels are generally thought to be advantageous over synthetic hydrogels since natural gels may offer better biochemical and biological cues to surrounding cells. Most naturally derived hydrogels are either components of natural ECM or provide similar properties that mimic the natural situations. Researchers have used a variety of naturally-derived materials, including collagen, gelatin, hyaluronic acid (HA), chitosan, alginate, and so forth.<sup>72-75</sup>

Importantly, collagen is the major component of the proteins in the ECM of human tissues and takes up approx. 25% of the total protein mass. Furthermore, HA is another important ECM component and widely distributed throughout connective, epithelial, and neural tissues. Chemically, HA is a non-sulfated, anionic glycosaminoglycan consisting of repeating disaccharide units. Similar to HA, both chitosan and alginate are linear, hydrophilic polysaccharides with superior biocompatibility (Figure 10). They have been shown to present favorable *in vivo* characteristics and thus they have been widely accepted as excellent hydrogel precursors for various tissue engineering applications.<sup>76-78</sup>

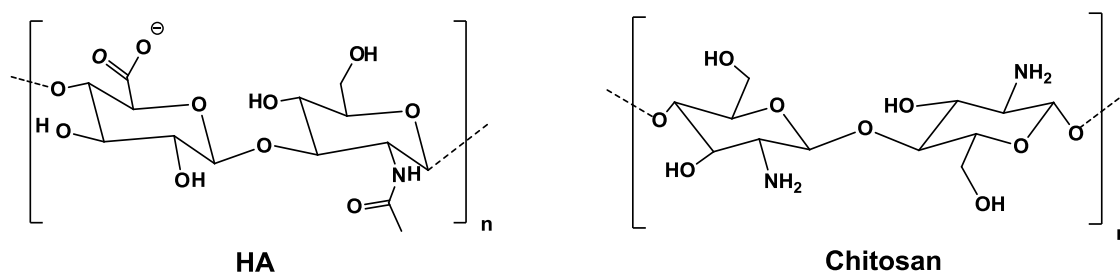


**Figure 10.** Structures of common substrates for naturally-derived hydrogels

*Collagen:* Collagen is one type of fibrous proteins and the most abundant protein in mammals. Collagen has a triple helical structure formed by polypeptide helices made of Gly-X-Y repeating units.<sup>79</sup> As a major structural protein of most ECMs, collagen type-I plays important passive roles in stress-bearing by providing skin, bone, tendon, and ligament with their characteristic tensile strengths. Since collagen type-I covers a wide range of domains that could crosstalk with integrin receptors on the cell surfaces and other matrix proteins, collagen-based hydrogels are cell adhesive and favourable for cell migration.<sup>80</sup> Hydrogels based on collagen can be formed by either physically crosslinking treatments (i.e., irradiation, freeze-drying),<sup>81, 82</sup> or chemically crosslinking agents (i.e., glutaraldehyde, carbodiimide).<sup>82, 83</sup> However, there are very few examples of

photopolymerizable collagen derivatives, probably due to the difficulty of collagen dissolution.

*Gelatin:* Compared to native collagen, gelatin is much more cost-effective and has easier access. Gelatin products with different isoelectronic points can be prepared via acidic or alkaline denaturation.<sup>84</sup> Gelatin is derived from collagen type-I via heat denaturation and has gained increasing popularity in the biomaterials community. For this point gelatin hydrogels have been widely used as drug carriers in controlled delivery systems.<sup>85</sup>

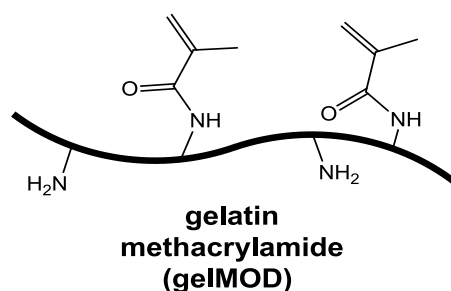


**Figure 11.** Structure of a photopolymerizable gelatin derivative (gelatin methacrylamide)

A general problem related to gelatin hydrogels is their poor mechanical properties which can be improved by physical or chemical crosslinking methods. Among them, photopolymerizable gelatin derivatives have received the most attention due to their great advantage for *in situ* photoencapsulation. To render gelatin polymerizable, target functional groups could be introduced by modifying lysine units or glutamic/aspartic acid units (Figure 11). For instance, Van den Bulcke et al. have reported a methacrylamide derivative of high MW gelatin (50-100 kDa, gelMOD).<sup>86</sup> In this work gelMOD was prepared through an amidation reaction between  $\epsilon$ -amino groups of lysine units in gelatin and methacrylic anhydride. GelMOD hydrogels have been used for *in situ* cell encapsulation providing favorable cell-viability and cell adhesion.<sup>87</sup>

*Hyaluronic acid:* HA or hyaluronan is a linear polysaccharide consisting of D-glucuronic acid and D-N-acetylglucosamine as repeating units.<sup>88</sup> As a major ECM component, HA plays important roles in wound healing, cell signaling and tissue morphogenesis. Due to its unique biological functions, HA has been widely used in biomedical applications such as for treatment of osteoarthritis and regeneration of vocal cord.<sup>89, 90</sup> Since native HA suffers from poor mechanical properties and short half-lives *in*

*in vivo* and is inappropriate for certain clinical applications, a variety of methods to chemically modify HA with polymerizable groups have been extensively explored, finally providing covalently crosslinked hydrogel networks.<sup>91-93</sup>

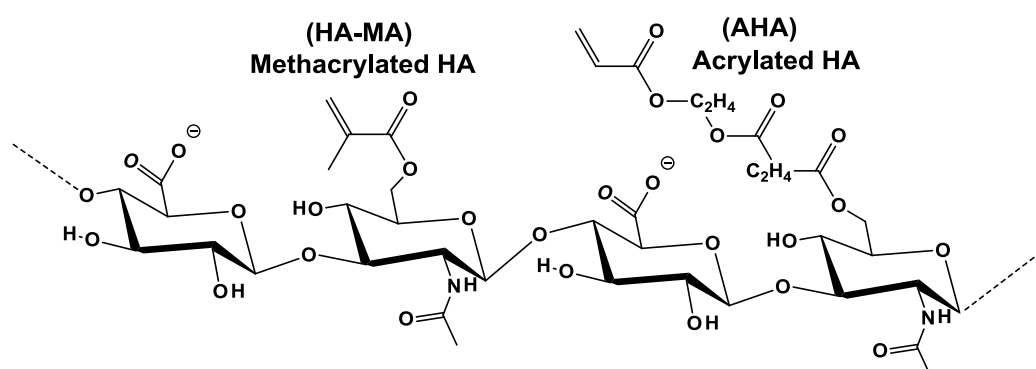


**Figure 12.** Chemical structures of HA derivatives: HA-MA and AHA

The principle targets of HA for chemical modification are carboxyl groups as well as primary and secondary hydroxyl groups (Figure 12). For instance, photopolymerizable methacrylated HA (HA-MA) were synthesized by reacting either methacrylic anhydride (or glycidyl methacrylate) with the primary hydroxyl groups in HA.<sup>94, 95</sup> Khademhosseini et al. have explored the micromolding-based photopatterning of HA-MA hydrogels for cell encapsulation applications.<sup>96</sup> In this work, the irradiation conditions were rather harsh (300 mW/cm<sup>2</sup> UV light, 3 min), presumably as a result of the limited reactivity of HA-MA. Recently, Khetan and Burdick reported bioerodible acrylated HA with ester linkages (AHA, Figure 12).<sup>97</sup> Detailed illustration of the synthetic routes to AHA is given in section 2.1. Although the photoreactivity of AHA is supposed to be higher than that of HA-MA, the use of HA-AC for AMT applications has not been reported.



### 3. Additive Manufacturing of 3D Hydrogels

Hydrogels are superior scaffolding materials to mimic the native ECM from various aspects, particularly tissue-mimetic architectures. From the engineering point of view, hydrogel scaffolds should be designed with ‘solute transport’ properties, i.e., free transport of nutrients and wastes. Although small molecules such as glucose and oxygen can freely diffuse into and out of the gel networks, the transport of most biomacromolecules may largely depend on various factors, including molecular weight and hydrodynamic radius of the solute, mesh size of the networks, and pore size of hydrogel scaffolds. The network mesh size is dictated by macromer size, macromer composition and crosslinking density of the gel network,<sup>13</sup> while the macroscopic porosity is dependant on the scaffold design and requirements for a specific application.

Importantly, researchers have proven that scaffolds with tuning porosity are critical for the assimilation of implanted scaffolds with host tissue. A milestone work of Brauker et al. has shown that engineered scaffolds with pore sizes between 0.8 and 8  $\mu\text{m}$  always permitted the complete penetration of the host cells and neovascularization, regardless of the chemical nature of scaffolding material.<sup>98</sup> As one type of scaffolds, hydrogels follow the same principle. For example, hydrogels with porosity at the same range have enabled the infiltration of host cells as evidenced in the long-term success of PHEMA hydrogels for cornea replacement.<sup>99</sup>

To fabricate porous hydrogel scaffolds, researchers have explored a variety of techniques, including particulate leaching, gas forming and so forth. Although such traditional techniques have shown the feasibility to generate porous structures, precise control over the pore geometry, size or interconnectivity are challenging to achieve, not to mention complex structures. In recent years, computer-aided-design (CAD)-based AMT have gained increasing popularity in the tissue engineering field. Importantly, the integration of clinical imaging data with AMT may allow the creation of a patient-specific construct for a specific tissue injury. Among these AMT techniques, photolithography-based AMT techniques have shown the greatest promise because of the use of light. Through various AMT devices light could be selectively delivered to targeted regions and induce local phase changes, thus providing full spatiotemporal control. For instance, digital light

processing (DLP) is a single-photon lithography technique, allowing layer-by-layer fabrication of hydrogel structures that are uniform in z-direction but vary in structure in the x-/y- directions.<sup>100</sup> Apart from creating macroscale features (porosity), fabrication of well-defined microscale features (local geometry) is also very important for basic biological research in tissue engineering. For precise 3D microfabrication, two-photon lithography appears to be an ideal solution.

### Single-photon Lithography

According to the working principle, lithography-based AMT can be further divided into single-photon and multi-photon techniques. Mask-based SP photopatterning techniques offer several benefits, mainly because they are fairly easy to use. Bhatia and co-workers have developed a method to create 3D hydrogel constructs via iterative two-dimensional (2D) photopatterning (Figure 13).<sup>101</sup> In this study, it was feasible to create PEGDA-based hydrogel microstructures made of overlaid layers with a resolution of hundreds of microns. In a later study, they have successfully translated this approach into the fabrication of a functional 3D hepatic construct with complex internal architectures.<sup>102</sup>

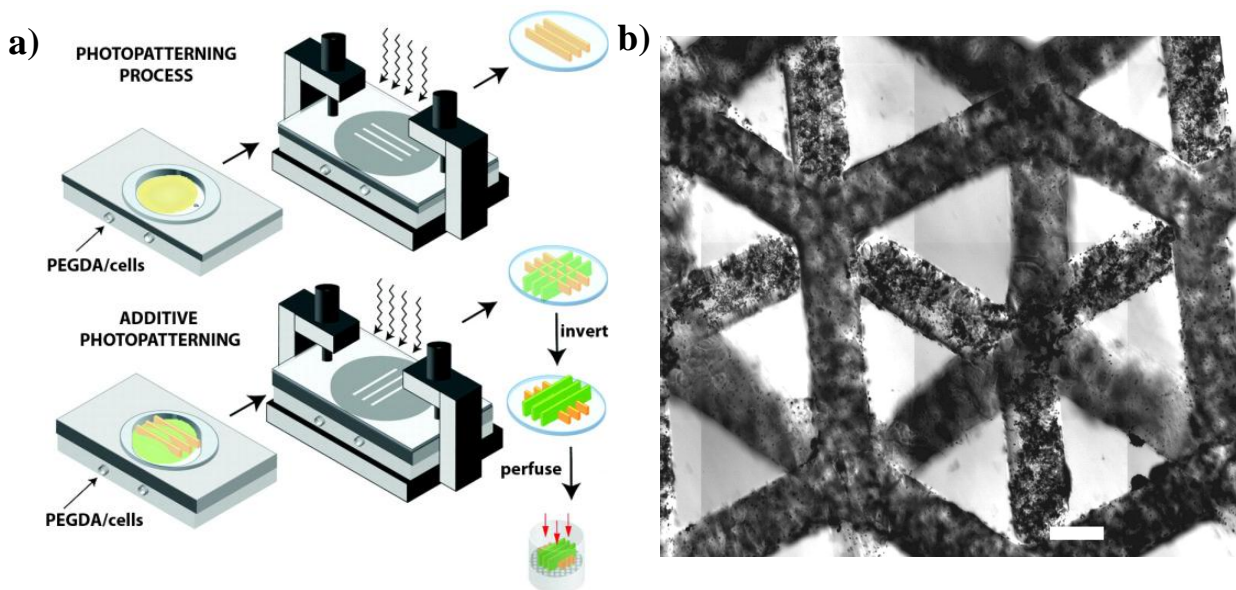


**Figure 13.** Single-photon additive photopatterning of cell-laden 3D hydrogels with interconnected porosity for mimicking a hepatic-tissue: **a)** fabrication schematics and **b)** photomicrograph of the cell-laden gel construct (scale bar: 500  $\mu\text{m}$ , reprinted with permission from FASEB-Journal<sup>102</sup>)



Since the presence of mechanical gradients within hydrogels plays an important role in regulating cell migration and other activities, researchers have explored photolithographical approaches to create 3D hydrogels with patterned stiffness.<sup>103-107</sup> West and co-workers have shown that mask-based UV patterning provided PEGDA hydrogels with spatially patterned and tunable stiffness.<sup>104</sup> In this work the stiffness gradient relied on the gradient of crosslinking density which was further dictated by PEGDA macromers of varying molecular weight and controlled mixing and photopatterning protocols.

Another single-photon AMT technique is DLP (Figure 14) where UV or visible light laser-scanning system is projected to the photopolymer solution on the top of a programmable stage. 3D hydrogel structures can be accordingly laid up in a layer-by-layer manner. Roy and co-workers have created PEGDA-based hydrogel scaffolds with open structures for stem-cell-differentiation studies.<sup>108</sup> It is important to note that the maximal resolution of DLP is around 30  $\mu\text{m}$  which is intrinsically limited by diffraction.

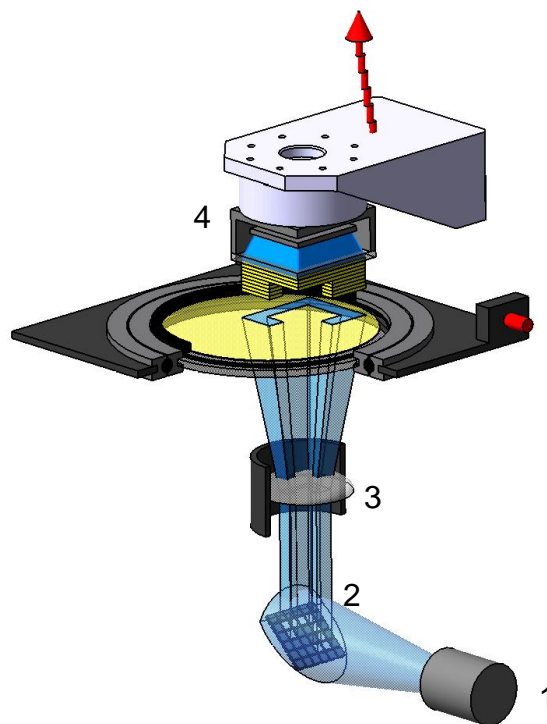


**Figure 14.** Schematic showing the DLP system: 1-light source, 2-digital mirror device, 3-optics, 4-build platform

## Two-photon Lithography

Although mask-based photopatterning (single-photon) has been extensively used for creating patterns within 3D substrates, it is challenging to achieve true 3D control over the material properties since any area exposed to light would react. As a result, most “3D” patterning based on single-photon irradiation is actually 2D in nature. For instance, cylindrical columns of cysteine groups were patterned in agarose hydrogels using single-photon laser scanning.<sup>109</sup> Using this method, however, it is not feasible to produce a discrete point within the hydrogel. While alternative AMT techniques such as DLP indeed allow 3D fabrication of complex structures, the optimal resolution is limited to  $\sim 30\ \mu\text{m}$ .

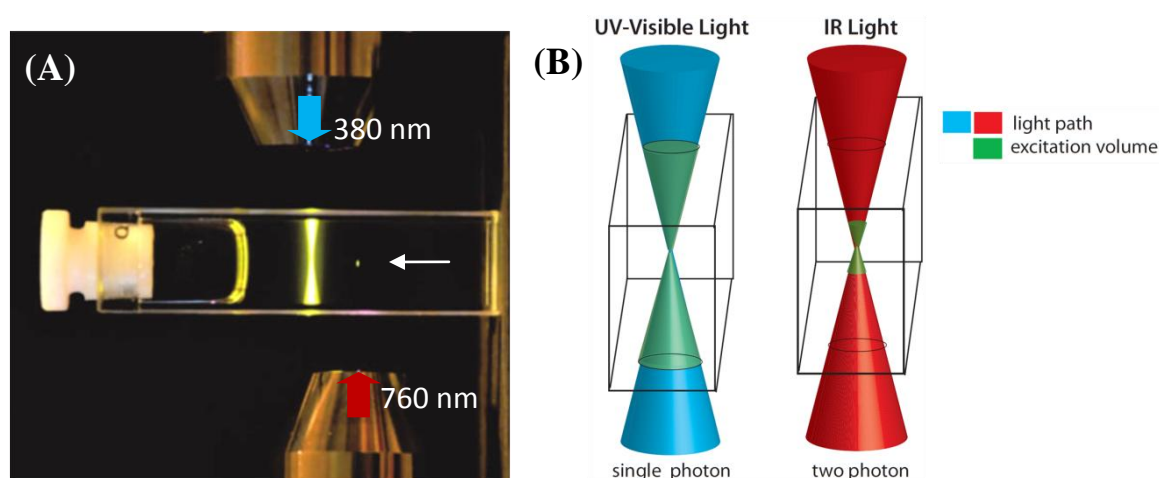


**Figure 15.** (A) Observations of single-photon (380 nm) vs. two-photon (760 nm) excitation in a solution of fluorescent dye, showing the highly localized excitation in 2PA; (B) schematics of light path and excitation volume in single-photon excitation (left) and two-photon excitation (right) (adapted with permission<sup>110-112</sup>)

For true 3D photopatterning, two-photon lithography appears to be the most suitable technique. The origin of two-photon lithography is closely relevant to the invention of multi-photon fluorescent microscope which was pioneered by Webb and co-workers at Cornell University in 1990s.<sup>113, 114</sup> The principle of this technique lies in the two-photon absorption (2PA) of a fluorophore.<sup>115</sup> Although three-photon absorption (3PA) is also known in literature,<sup>116</sup> in this thesis only 2PA and 2PA-relevant reactions are discussed to keep simplicity.

To differentiate two-photon lithography from single-photon lithography, it is reasonable to look into a direct comparison between single- and two-photon excitation (Figure 15A).

When a fluorophore solution is irradiated with a blue laser (380 nm, 200 fs), single-photon excitation occurs along the entire path of the light. In other words, any exposed area is activated. When the same solution was exposed to a near-IR laser (760 nm, 200 fs), two-photon excited area is tightly localized to the focal point of the focused laser. These different observations are due to the varying photophysical processes. In single-photon absorption, the absorption is directly proportional to the incident light-intensity; whereas in 2PA, the probability of simultaneous absorption of two photons is proportional to the square of the incident light-intensity.<sup>117</sup>

The non-linear optical processes in 2PA offer numerous advantages over conventional single-photon techniques. Since 2PA events are highly confined in the focused volume (Figure 15B), spatial resolution down to 100 nm could be achieved. By scanning a femtosecond laser within a thick subject, 3D patterns with user-dictated shapes can be produced in accordance with a CAD model. When compared to single-photon lithography (typically UV-Vis light), two-photon lithography (near-IR light) offers greater penetration depth while causing less damage to live tissues, making it promising for applications in tissue regeneration.

By replacing a fluorophore with a two-photon-active initiator (2PI), upon laser irradiation free radicals could be generated after interaction with monomers and initiate subsequent polymerization processes. These processes are termed as ‘‘two-photon polymerization’’-2PP. Detailed description on the principle and applications of 2PP technique could be found in comprehensive reviews written by LaFratta and Lee.<sup>115, 118</sup>

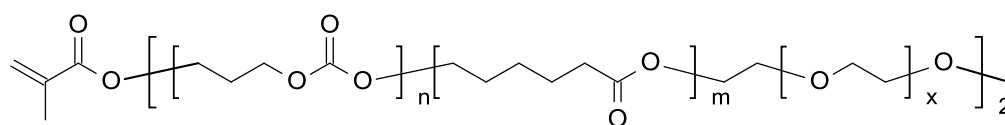


**Figure 16.** Methacrylate end-capped PEG-PCL-TMC oligomers<sup>119</sup>

Early examples of 2PP microfabrication are mostly based on highly reactive oligomers such as trimethylolpropane triacrylate (TTA). While delicate 3D structures could be produced, these materials lack of water-solubility and biocompatibility, making them inappropriate for biological applications. In 2009, Claeysens *et al.* reported the 1<sup>st</sup> example of 2PP microfabrication of biodegradable scaffolds using methacrylate end-

capped PEG-PCL-TMC oligomers (Figure 16).<sup>119</sup> In this study, 3D porous structures (Figure 17) were fabricated with a resolution of 4  $\mu\text{m}$ . Furthermore, the authors proved that proliferation of NIH-3T3 fibroblast cells that were seeded onto the scaffolds was not affected. Although well-defined structures were produced, laser scanning was repeated eight times for each layer at a speed of 50  $\mu\text{m/s}$ . These parameters imply that the reactivity of the selected oligomer is quite low.

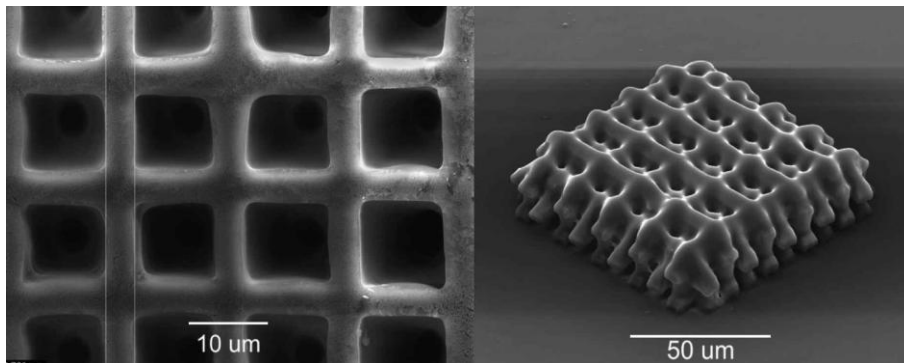


**Figure 17.** Microscope images of biodegradable scaffolds produced by 2PP<sup>119</sup>

In order to target biological applications, 2PP fabrication of hydrogel scaffolds has been extensively explored in recent years.<sup>120-123</sup> Notably, most studies utilized low MW acrylate-based monomers, including acrylamide,<sup>123</sup> acryloylacetone,<sup>123</sup> and PEG diacrylates.<sup>120, 122</sup> It has to be noted that all these materials are highly cytotoxic although they are very reactive. Another challenge in 2PP fabrication of hydrogels is that few PIs used for 2PP are water-soluble. For example, in a study by Jhaveri et al,<sup>122</sup> PEO-PPO-PEO triblock copolymer (Pluronic F127®) was used as a surfactant to enhance the solubility of the PI. Together, previous efforts suggest that there is a strong requirement for alternative biocompatible hydrogel systems that can be structured by 2PP.

## Objective

Developing 3D hydrogel scaffolds capable of promoting cell viability and *in-vivo* like cell functions has become increasingly important for tissue engineering and regenerative medicine. Lithography-based two-photon polymerization (2PP) technique provides the greatest promise to realize 3D printing of user-defined hydrogel structures according to computer-aided-design (CAD). While proof-of-concept 2PP fabrication of hydrogel constructs have been reported in literature, materials used in these examples are mostly based on acrylate chemistry or based on the di-tyrosine crosslinking of native proteins. The irritancy and cytotoxicity of acrylate chemistry pose a big challenge for 2PP in the presence of cells (i.e., 2PP cell-encapsulation) while the di-tyrosine crosslinking lacks efficiency and often necessitates high laser energy. Consequently, optimal hydrogel precursors are needed to present sufficient reactivity for 2PP under low laser dosage and expose low cytotoxicity for *in situ* cell encapsulation.

The overall goal of this thesis is to design and synthesize a series of biocompatible, biodegradable and photopolymerizable hydrogel precursors that circumvent the irritating acrylate chemistry and allow fast 2PP microfabrication of hydrogel constructs with user-defined geometry.

Furthermore, functional groups and crosslinking chemistry of these new hydrogel systems have to meet the following requirements (Figure 18).

- negligible or even no cytotoxicity of the gel precursor
- good water-solubility of the gel precursor
- high crosslinking efficiency of the functional group for radical polymerization
- sufficient photoreactivity of the gel precursor for 2PP-processing
- good storage stability of the gel formulation
- tunable crosslinking density of the network and tunable macroscopic gel modulus
- biodegradability of the network by hydrolysis and/or enzyme
- non-toxic degradation products of the hydrogel
- cytocompatibility of the hydrogel system for *in situ* cell-encapsulation

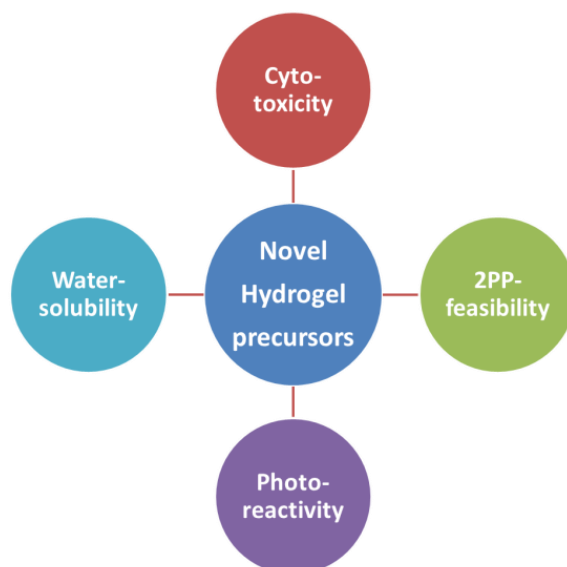


**Figure 18.** Design principles of hydrogel precursors for 2PP microfabrication

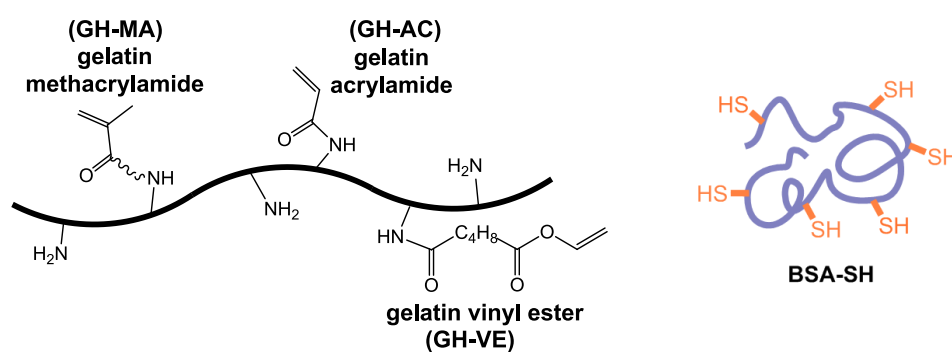
Therefore, this thesis is aiming at the development of water-soluble macromers/monomers (synthetic or natural origin) terminated with vinyl or thiol groups that are biodegradable, cytocompatible and photopolymerizable. It is hypothesized that vinyl esters/carbonates are much less cytotoxic than acrylate analogues, providing polyvinyl alcohol (PVA)-based degradation products. While homopolymerization rate of vinyl esters/carbonates is slower than the one of acrylates, it is supposed that thiol-ene polymerization can improve the reactivity of vinyl esters/carbonates to a sufficient level for 2PP. In addition, it is anticipated that the optimal hydrogel formulation with sufficient photoreactivity and cytocompatibility would provide the feasibility of 2PP processing of cell-laden hydrogel constructs.

Hence, both naturally-derived such as gelatin and hyaluronic acid (HA) and synthetic polymers like polyethylene glycol (PEG) and PVA are selected as substrates for chemical modification due to their superior biocompatibility. For naturally-derived hydrogels, major ECM components such as gelatin and HA are selected as substrates for chemical modification due to their superior biocompatibility.

### Objective I

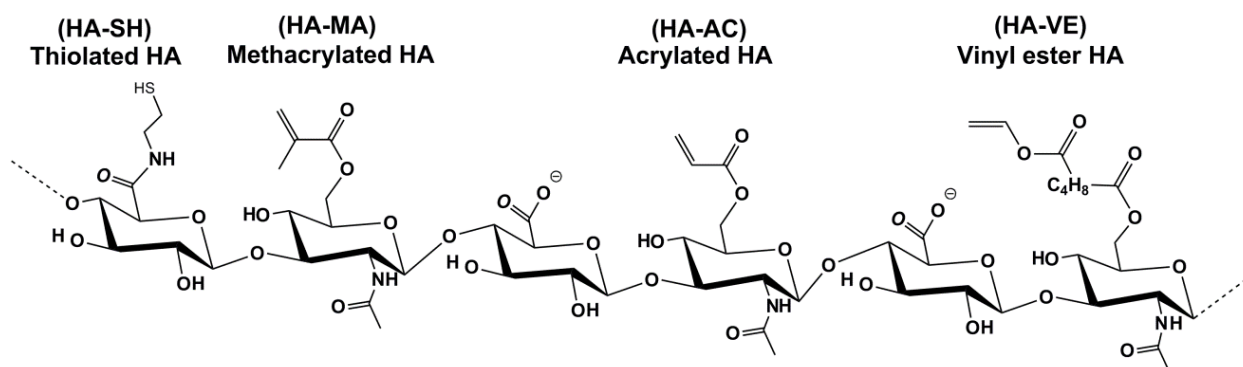
In the first chapter, a series of gelatin-based hydrogel precursors shall be prepared. Specifically, gelatin hydrolysate with low-cytotoxic vinyl ester groups (GH-VE) shall be prepared and compared to GH acrylates (GH-AC) and GH methacrylates (GH-MA).

Characterization of these macromers has to focus on their cytotoxicity and photoreactivity. To investigate thiol-ene polymerization, water-soluble protein macrothiols should be prepared by reductive cleavage of disulfide bridges in bovine serum albumin (BSA), giving BSA-SH. Hydrogels formed by thiol-ene copolymerization between GH-VE and BSA-SH shall be characterized from several aspects, including pellet toxicity, photoreactivity, water-uptake, 2PP processability, and so forth.



## Objective II

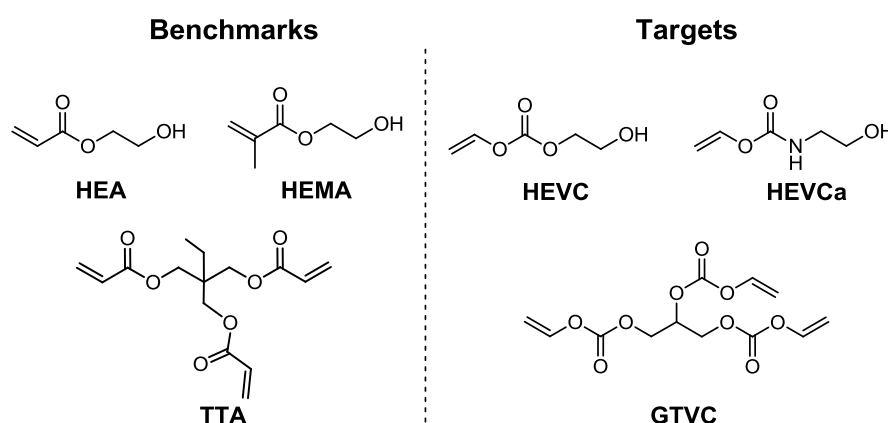
In the second chapter, a series of HA-based hydrogel precursors has to be prepared. Specifically, a novel HA derivative with pendant vinyl ester groups (HA vinyl esters, HA-VE) shall be synthesized and compared to HA acrylates (HA-AC) and HA methacrylates (HA-MA). Since HA has more reactive sites than GH, whether it is feasible to access HA-VE with tunable degree of substitution (DS) shall be explored. Physicochemical properties of HA-VE macromer and/or hydrogels shall be tested in comparison with its (meth)acrylate analogues, including cytotoxicity, photoreactivity, water uptake, gel modulus, 2PP feasibility, and so forth. Additionally, the thiolated HA (HA-SH) shall be prepared as a reference macrothiol.



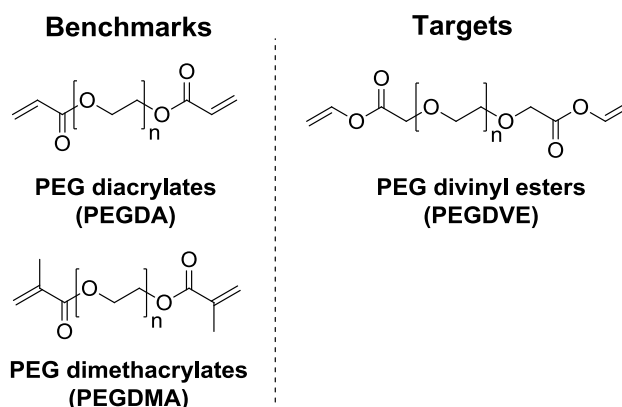
### Objective III

In the third chapter, a series of biocompatible synthetic materials has to be prepared and tested with a focus on their suitability as hydrogel precursors for 2PP microfabrication. These materials could be divided into three categories: a) vinyl carbonates/carbamates; b) PEG divinyl esters; and c) PVA norbornenes.

Given that HEMA lacks of sufficient reactivity for 2PP while its acrylate analogue (HEA) suffers from high cytotoxicity, alternative water-soluble monomers with low cytotoxicity shall be developed for 2PP microfabrication. Owing to the superior biocompatibility of vinyl carbonates/carbamates, both 2-hydroxyethyl vinyl carbonate (HEVC) and 2-hydroxyethyl vinyl carbamate (HEVCa) shall be prepared and compared to HEMA and HEA. Furthermore, a trifunctional crosslinker-glycerol trivinyl carbonates (GTVC) shall be prepared and compared to a benchmark crosslinker-trimethylolpropane triacrylate (TTA).



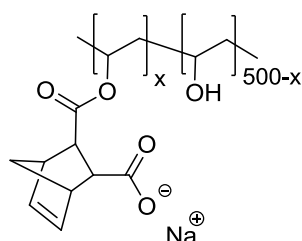
Since PEG di(meth)acrylates are the most often used hydrogel precursors in literature, biocompatible PEG macromers with alternative chemistry such as PEG divinyl ester (PEGDVE) shall be prepared and compared with the (meth)acrylate analogues: PEGDA and PEGDMA.





Apart from conventional cytotoxicity test, photoreactivity of these macromers towards either homopolymerization or thiol-ene copolymerization shall be investigated in details using photo-differential scanning calorimetry (photo-DSC). Based on one-photon reactivity test, feasibility of these macromers towards 2PP shall be tested systematically.

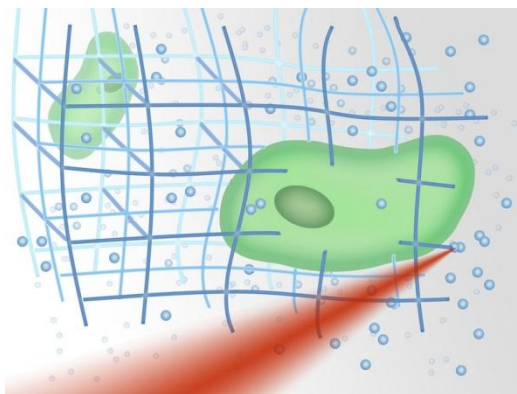
Since PEG has merely two reactive sites for modification while PVA has hundreds of sites, PVA-based macromers with novel functional groups shall be developed. Considering that thiol-norbornene reactions are highly efficient while suitable for cell encapsulation, PVA-norbornene shall be prepared and utilized as hydrogel precursor. Specifically, how thiol-ene chemistry influences photo-induced gelation process of PVA-norbornene shall be studied. Besides, cytotoxicity and 2PP-feasibility of PVA-norbornene shall also be tested.



**Sodium PVA-norbornene**

#### Objective IV

In the last chapter, laser processing of hydrogel constructs in the presence of viable cells has to be explored in order to establish a novel concept termed “two-photon cell-encapsulation”. Prior to two-photon cell-encapsulation, cytocompatibility of the selected hydrogel formulation shall be tested. Furthermore, the influence of laser irradiation on cell viability in the absence and/or presence of initiators shall be evaluated, respectively. Last, proliferative potential of encapsulated cells shall be tested in a longer culture period.



(Courtesy: Dr. Florian Aigner, TU Wien)



## State of the art

*In vivo*, tissues include 3D macroscopic architectures of repeating subunits on the length scale of 100  $\mu\text{m}$ -1000  $\mu\text{m}$ .<sup>124-126</sup> To mimic such structures, traditional AMTs have been explored to create 3D scaffolds with physiologically-relevant features.<sup>127</sup> For instance, Tsang et al. reported the fabrication of cell-laden hydrogel constructs by iterative UV-photopatterning. With the help of a perfusion bioreactor, these porous artificial matrices enabled long-term culture of hepatocytes.<sup>102</sup>

In recent years, cell biologists have gained substantial evidences on the significance of three-dimensional cell culture. Compared to petri dishes and 2D gels, 3D hydrogels could better represent the cell morphology and physiology that are happening *in vivo*.<sup>128</sup> Instead of simply creating a 3D bulk environment, it is noteworthy that cells respond to their local microenvironment at subcellular scale (1-10  $\mu\text{m}$ ).<sup>40, 129, 130</sup> The milestone work of Chen and Whitesides elegantly proved that the micro-scale geometrical control of cell morphology is effective to control cell proliferation and apoptosis.<sup>131</sup>

The success of hydrogel scaffolds is primarily dependent on the crosstalk between host cells and the gel matrix. As the understanding of matrix biology goes deeper, rapid construction of 3D hydrogels with subcellular features is increasingly necessary. Early work of Hubbell and co-workers has comprehensively highlighted the influence of matrix effects on the determination of cell fate.<sup>132</sup> It is accepted that the length scale at which cells sense and respond to their surrounding signals is on the scale of 1  $\mu\text{m}$  or less. Therefore, from an engineering point of view, creating cellular microenvironment with (sub)micron-scale resolution is critical to achieve better control over cell functions. As mentioned before, techniques related to single-photon lithography are problematic to achieve (sub)micron-scale resolution and thus not appropriate for engineering the cellular microenvironment. To cross the resolution limitation, two-photon lithography has recently proven to be a very promising technique.<sup>115, 120, 133-137</sup>

In the last few years, two-photon lithography has been extensively explored for creating customized ECM hydrogels in different ways, including **1)** two-photon-induced degradation of preformed hydrogel networks; **2)** directly assembly of 3D hydrogel

constructs via two-photon-induced polymerization (2PP); and **3**) two-photon-induced biofunctionalization of preformed 3D hydrogel networks.

### Two-photon-induced Degradation

In 2009, Anseth's group reported the 1<sup>st</sup> photodegradable hydrogel system that allows precise manipulation of hydrogel properties and chemistry by two-photon activation.<sup>138</sup> The principle of this method relies on the photolabile properties of *ortho*-nitrobenzylether (o-NB) groups that are incorporated into an acrylic PEG crosslinker. The authors firstly synthesized a photodegradable crosslinker (compound **1**, Figure 19B) by reacting a PEG diamine linker ( $M_n \sim 4$  kDa) with a base acrylic monomer containing o-NB moiety (Figure 19A).

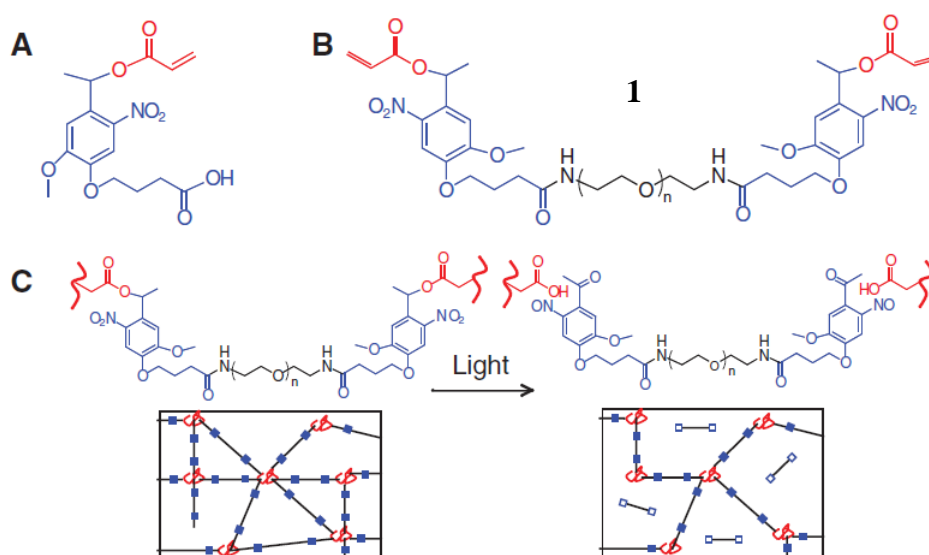
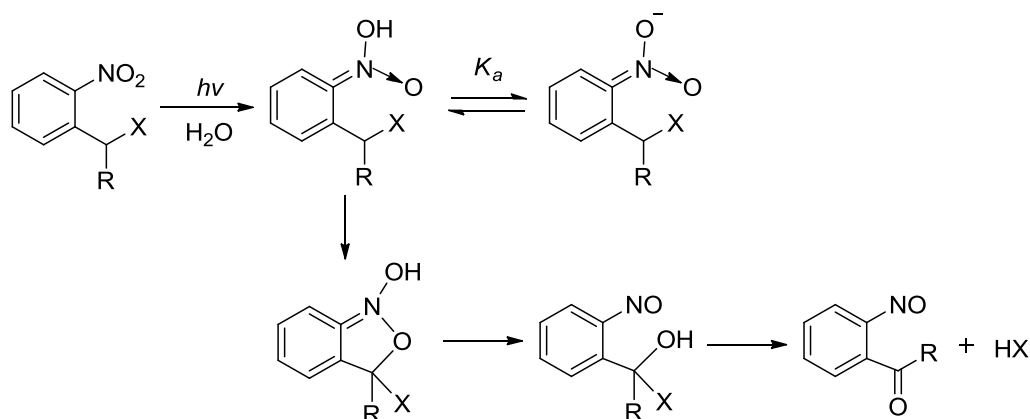


**Figure 19.** Photodegradable hydrogel synthesis and photodegradation of gel networks: (A) the base photodegradable acrylic monomer; (B) the photodegradable crosslinking macromer (Compound **1**); and (C) schematic showing the photodegradation of gel networks formed by Compound **1** and PEG monoacrylate (adapted with permission from Science<sup>138</sup>)

Second, the photodegradable crosslinker (**1**) was copolymerized with PEG monoacrylate ( $M_n \sim 375$  Da) by redox-initiated free-radical polymerization to form PEG gels. These gels consisted of polyacrylate chains (red coils) connected by PEG chains (black lines) with photolabile o-NB moieties (blue squares). Upon irradiation, o-NB moieties undergo photolysis processes (Scheme 4) in which intramolecular H-abstraction by the excited nitro group is the primary photochemical process, followed by the formation of the aci-nitro form and the rearrangement to the nitroso derivatives. Mechanistic studies over the

formation of aci-nitro intermediates and subsequent release of nitroso derivatives upon photolysis are well established and have been reviewed by Wirz and co-workers.<sup>139</sup>



**Scheme 4.** Mechanism of photolysis of o-nitrobenzyl ether compounds

For the hydrogel system described by the Anseth group,<sup>138</sup> the caged PEG linker would be released due to the cleavage of o-NB linkages. The accumulative break-down of these linkages led to a macroscopic decrease of gel crosslinking density, causing a ‘loosening’ effect of the network. Spatially erosion of preformed gels in a user-defined manner exhibits great promise for a variety of biological applications, since cells delicately sense and respond to the ECM substrate in a stiffness-dependent manner.<sup>16</sup>

### Two-photon-induced Polymerization

Although two-photon-induced polymerization (2PP) has been extensively used for fabrication of photonic crystals using commercial acrylic resin, 2PP fabrication of hydrogels is much less reported. Till now, the reported successes for 2PP processing of hydrogels are mainly based on PEG-based monomers with acrylate groups, in particular low MW PEG diacrylates ( $M_n \sim 300$  Da, 740 Da).<sup>121</sup> Although well-defined gel structures were produced, the significant toxicity of these monomers and high content of I2959 (2 %) made these materials inappropriate for biological-relevant applications where cells are directly exposed to the formulations.

Apart from PEG-based materials for 2PP, naturally-derived materials have also been explored. Notably, Ovsianikov et al. reported the two-photon polymerization of gelatin methacrylamide (gelMOD) using I2959 as PI (Figure 20).<sup>133</sup> Although proof-of-concept

structuring succeeded, it is important to note that the photoreactivity of methacrylated macromers are generally too low for most photolithography-based AMT applications.

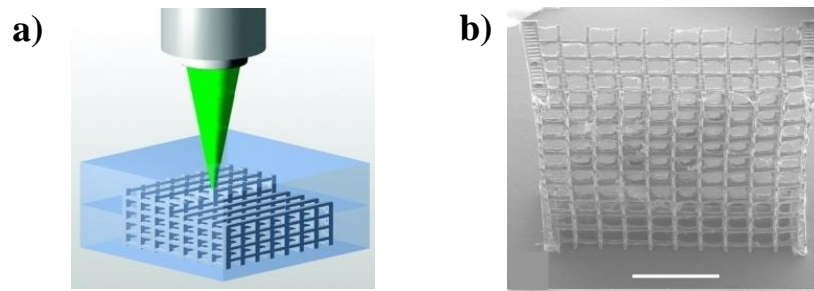


**Figure 20.** Two-photon microfabrication of porous, 3D hydrogel scaffolds made of gelatin methacrylamide (scale bar: 1 mm, adapted with permission from ACS<sup>133</sup>)

Berg et al. reported the 2PP processing of hyaluronan-based hydrogel constructs using HA methacrylates (HA-MA) as gel precursor.<sup>140</sup> In this study, however, the hydrogel formulation not only consisted of HA-MA (2 wt%), but also acrylamide (20 wt%) and N,N-ethylene bisacrylamide (1.2 wt%) as co-monomers. These information imply that the photoreactivity of HA-MA was not sufficient for 2PP. Cell-viability test showed that the gel extracts exhibited non-significant toxic effects on 3T3 fibroblasts. Nevertheless, cell attachment were rather low on the gel structures.<sup>140</sup>

### Two-photon-induced Biofunctionalization

In a natural environment, cells are embedded in the ECM which is a complex 3D gel networks containing a variety of biochemical and physical signals. Within the ECM context, spatial and temporal access of integrin ligands, morphogens and growth factors regulate a number of biological processes.<sup>124, 141-143</sup> For instance, formation of new blood vessels (neovascularization) is dictated by the spatial and temporal availability of vascular endothelial growth factor.<sup>144</sup> Thus, spatiotemporal patterning of bioactive molecules in 3D hydrogels is extremely useful for tissue engineers to precisely control cell behaviours. West and co-workers have shown that the two-photon patterning of RGD motifs in PEG-based hydrogels could effectively confine cell adhesion and cell migration in the area functionalized with RGD.<sup>28, 145</sup> In these studies hydrogel pellets were firstly formed by UV photopolymerization and then soaked in a solution of PI and acrylated RGD peptides.

Besides, researchers have also explored the two-photon uncaging concept for biofunctionalization of 3D hydrogels. In a recent study of Shoichet and co-workers, multiple growth factors were sequentially immobilized within agarose hydrogels (Figure 21).<sup>146</sup> Specifically, agarose hydrogel matrices were firstly activated with carbonyldiimidazole (CDI) and then modified with 2-nitrobenzyl-protected cysteines.<sup>109</sup> Upon two-photon irradiation, cysteine pendant groups were liberated for thiol-ene conjugation with maleimide-containing barnase/streptavidin. Finally, growth factors terminated with orthogonal counterparts (barstar/biotin) were immobilized via affinity-binding within the 3D pattern.

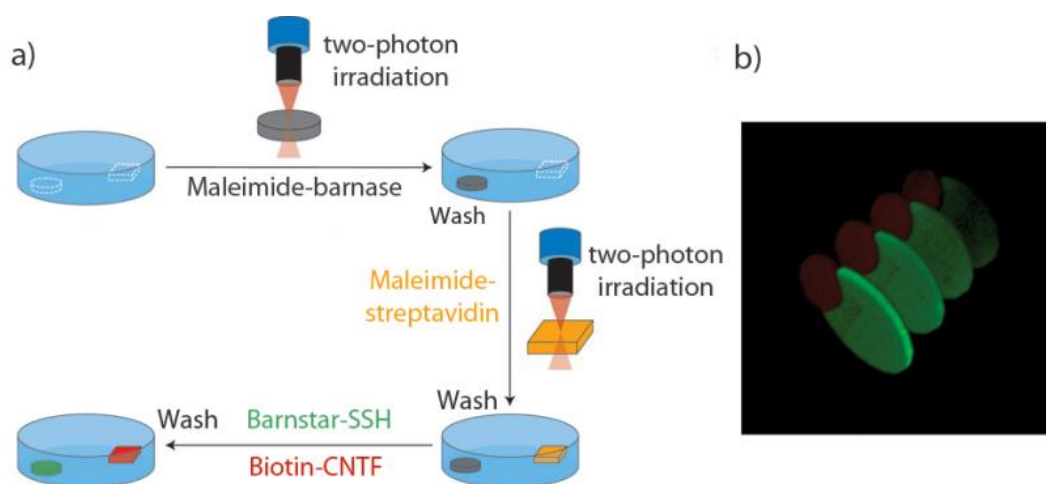


**Figure 21.** Two-photon biofunctionalization of alginate gels with various growth factors (reprinted with permission from Nature Publishing Group<sup>147</sup>)

A recent study by Liska and co-workers has established that bio-orthogonal groups such as azides can be precisely immobilized within PEG matrices via 3D photografting.<sup>148</sup> Specifically, the grafting process was based on the decomposition of a commercially available aromatic diazide under three-photon excitation and subsequent nitrene insertion, finally leaving pendant azide groups for further functionalization. However, it is noteworthy that three-photon absorption (3PA) is often less efficient and thus requires much higher laser intensity than 2PA due to the lower probability of 3PA.<sup>149</sup>

Li et al. recently developed a novel fluoroaryl azide compound (FAF-3) for efficient 2PA grafting (Figure 22a).<sup>150</sup> The rational molecular design provides FAF-3 with a large 2PA cross section (178 GM at 800 nm) while the alkyne tail facilitates further bio-orthogonal conjugation. Specifically, FAF-3 was precisely grafted within PEG matrices via 2PA-

induced photolysis and subsequent nitrene insertion. Since the grafting reactions are highly localized in a confined volume within the laser focal spot, arbitrary Yin-Yang pattern of alkyne groups (Figure 22b) was created in the PEG matrices with high spatial resolution ( $\sim 3.6 \mu\text{m}$ ).<sup>150</sup> In addition, ultrafast scanning ( $\sim 550 \text{ mm s}^{-1}$ ) was achieved due to the highly efficient grafting reactions.

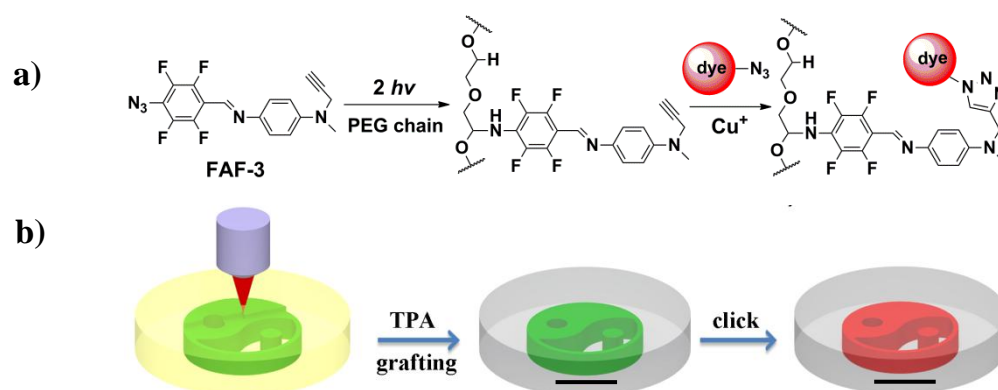


**Figure 22.** 3D site-specific functionalization of PEG matrices: **a)** chemical reactions and **b)** schematics of 3D-photografting and further bio-orthogonal conjugation (scale bar:  $50 \mu\text{m}$ )

To realize 3D site-specific functionalization, a model compound (i.e., red fluorophore terminated with azide group) was further conjugated on the “clickable” Yin-Yang pattern through CuAAC reactions. After that the Yin-Yang pattern changed from green to red, indicating the success of site-specific functionalization. This work shows great potential for further biologically-relevant studies where matrix biofunctionalization is necessary. In theory, any bioactive molecule of interest (e.g., VEGF-2) with alkyne groups could be readily incorporated through CuAAC-based click reactions.



# Results & Discussion

## 1 Gelatin-based Hydrogels

One objective of this thesis is the development of photopolymerizable gel precursors with superior reactivity and cytocompatibility for creating ECM-mimetic hydrogels via 2PP lithography. Inspired by the ECM component-collagen, gelatin was selected as one of the substrates considering the fact that gelatin is biocompatible, cell-adhesive, and biodegradable. As such, it is intriguing to synthesize gelatin derivatives with different polymerizable vinyl groups (i.e., acrylate, methacrylate, vinyl ester, Figure 23) and compare their cytotoxicity and reactivity.

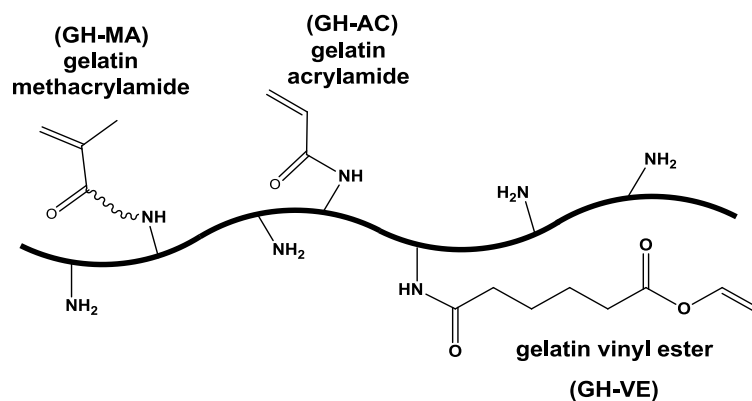


**Figure 23.** Chemical structures of targeted gelatin derivatives

To synthesize these compounds, commercial enzymatic gelatin hydrolysate (GH) was used as starting material. It is noteworthy that GH is an enzymatic degradation product of porcine collagen with molecular weight distribution between 0 and 6000 g/mol. Unlike other commercial sources of gelatin with higher molecular weight (Type A or B), GH could achieve a maximum solubility at room temperature in PBS up to 50 wt % without forming a physical gel, thus providing better processability for 2PP lithography. In order to retain sufficient number of vinyl groups per chain, dialysis (MW cutting-off: 3500) was always performed prior to use, so that only GH fragments between 3500 and 6000 were used for further modification.

Prior to synthesis, an internal standard method based on NMR was selected for further quantification of degree of substitution (DS) of gelatin derivatives. Gelatin from porcine skin has a content of 0.465 mmol/g  $-CH_3$  groups originating from valine, leucine, and

isoleucine residues.<sup>151</sup> However, enzymatic degradation or a dialysis process would presumably change the  $-\text{CH}_3$  content. To roughly determine the final concentration of  $-\text{CH}_3$  groups in dialyzed GH,  $^1\text{H-NMR}$  spectrum with phenol as internal standard was measured (Figure 24). The proton signal at 1.12 ppm corresponding to all  $-\text{CH}_3$  groups in GH could be used as reference while the exact amount of phenol is pre-determined. From this method, a concentration of  $-\text{CH}_3$  groups in GH was calculated to be 1.04 mmol/g.

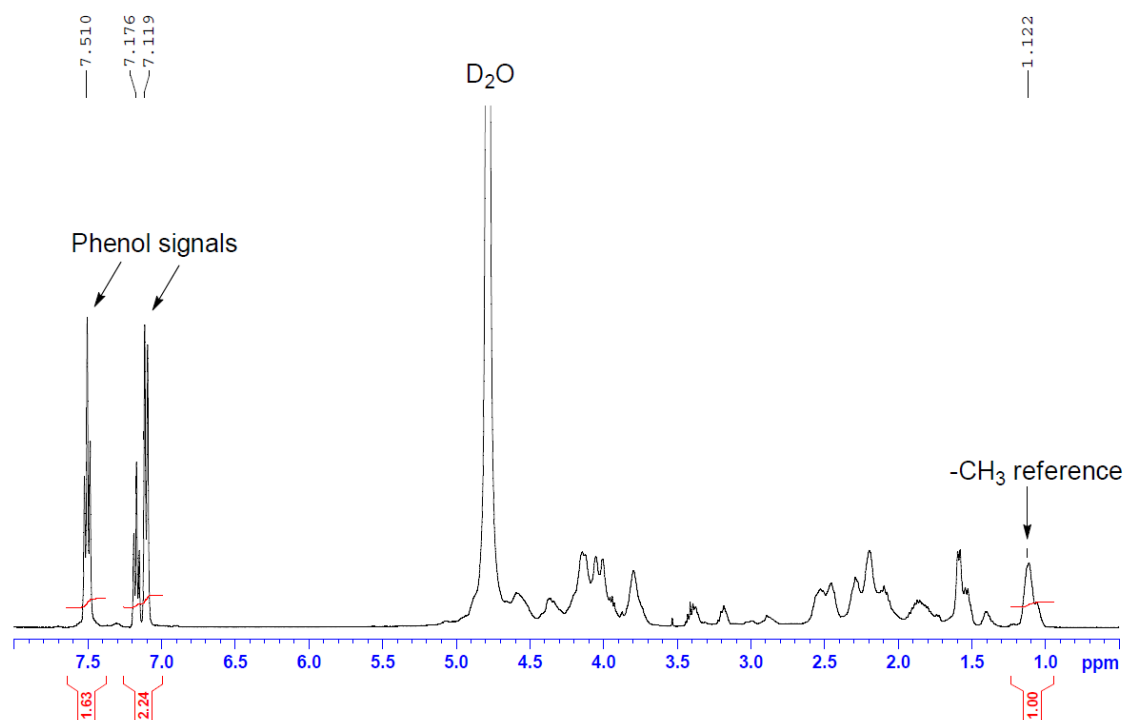


**Figure 24.**  $^1\text{H-NMR}$  spectrum of GH with phenol as internal standard ( $\text{D}_2\text{O}$ , 40 °C, 400 MHz)

There are two different targets in gelatin for chemical modification. One is the free amino groups on (hydroxy)lysine units (0.38 mmol/g,<sup>151</sup> Table 5) that offers easy access for varying synthetic approaches. For instance, photocrosslinkable gelatin methacrylamide (Gel-MA) was synthesized through amidation of lysine units with methacrylic anhydride.<sup>86</sup> Gel-MA has enabled a number of cell-encapsulation and microfluidic applications.<sup>152, 153</sup> In addition, the N-terminus of gelatin should be also taken into account. For a GH substrate with average molecular weight of 4750 g/mmol, the N-terminus concentration is 0.21 mmol/g after calculation. Together, one can expect that free amino group concentration in GH is 0.59 mmol/g.

Alternatively, free acidic groups on aspartic acid and glutamic acid can also be exploited for modification. Koepff et al. reported the modification of gelatin with glycidyl

methacrylate (GMA) which underwent ring-opening reactions with both amino (Lys) and acidic groups (Asp & Glu).<sup>151, 154</sup>

**Table 5.** Contents of alkaline and acidic amino acids in different gelatin resources <sup>151</sup>

	(hydroxy)lysine (mmol/g)	aspartic & glutamic acids (mmol/g)
Type A gelatin	0.38	0.85
Type B gelatin	0.38	1.27
GH	0.38	NA

## 1.1 Synthesis of Gelatin Derivatives

### 1.1.1 Synthesis of Gelatin Methacrylates (GH-MA)

Methacrylated gelatin (GH-MA) was synthesized (Figure 25) as described by Schuster,<sup>154</sup> except using dialyzed gelatin hydrolysate (GH) as substrate. Dialyzed GH was allowed to react with GMA in alkaline solution (pH=8.5) at 40 °C. Since both acidic and alkaline amino acid residues are supposed to undergo ring-opening reaction, a 5-fold excess of GMA relative to the total amount of these residues was used.<sup>154</sup> After overnight reaction, the mixture was washed with ethyl acetate to remove unreacted GMA and further purified by dialysis against water. After lyophilization, the product (GH-MA) was obtained as yellow solid (65% of theory).

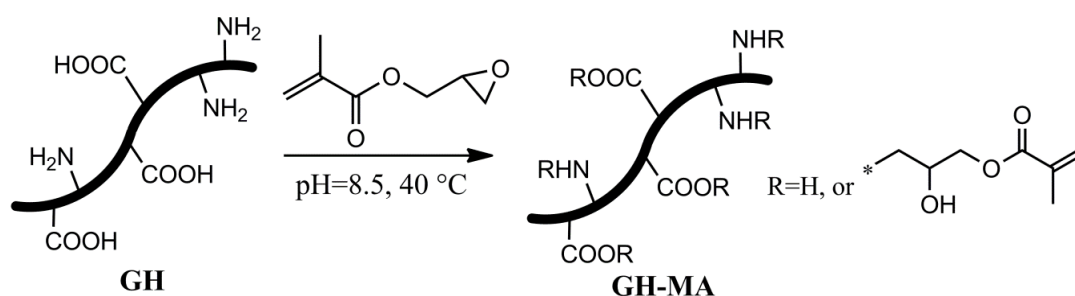


**Figure 25.** The reaction of GH with GMA

To confirm the synthesis, NMR spectrum of GH-MA was measured (Figure 26). The spectrum shows characteristic peaks at 6.2 ppm (**a**), 5.7 ppm (**b**) and 1.9 ppm (**c**) that are corresponding to the methacrylate groups. The degree of substitution of GH-MA was determined by calculating the integration ratio of unsaturated proton (**a**) relative to that of

–CH<sub>3</sub> protons of GH at 0.9 ppm.

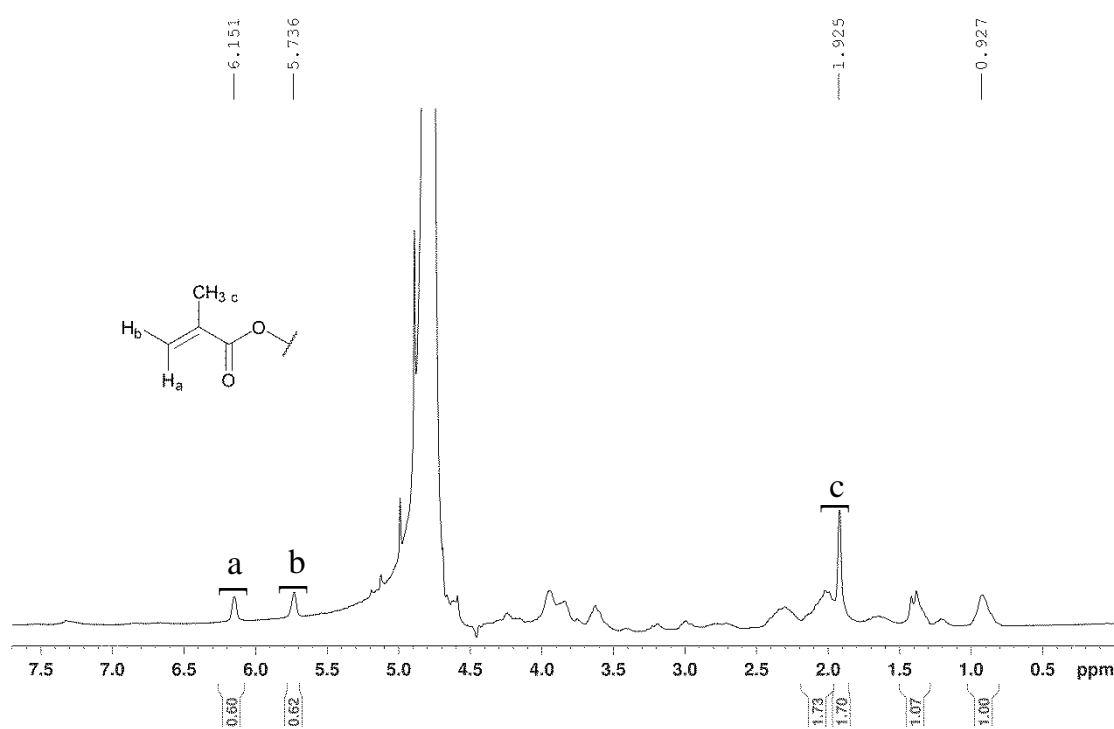


**Figure 26.** <sup>1</sup>H-NMR spectrum of GH-MA (D<sub>2</sub>O, 25 °C)

Based on the –CH<sub>3</sub> value (1.04 mmol/g), the concentration of methacrylate groups in GH-MA was calculated to be 1.90 mmol/g (0.38 mmol/g for lysine residues), indicating the involvement of acidic residues. This value is higher than the total value of accessible amino acids residues (Table 5). The difference is likely due to the involvement of the N-terminus and C-terminus of GH. By assuming 4750 Da as the average MW of GH, further calculation implies that ~9.0 methacrylate groups on average are present in one GH-MA peptide.

### 1.1.2 Synthesis of High MW Gelatin Methacrylates (gelMOD)

Besides low MW GH-MA (~5 kDa), gelatin methacrylamides (gelMOD) with higher MW (50-100 kDa) was also prepared as reference material. In an earlier study by Nicol et al.,<sup>87</sup> gelMOD was utilized as gel precursor for UV-photoencapsulation of fibroblasts with high viability (~92%). Ovsianikov et al. recently reported 2PP microfabrication of gelMOD-based hydrogel constructs.<sup>155</sup>

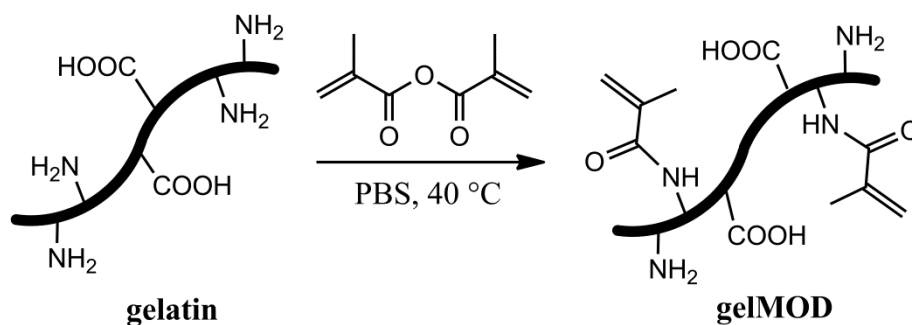


**Figure 27.** Reaction of high MW gelatin with methacrylic anhydride

GelMOD was prepared by reacting the lysine units of high MW gelatin (300 bloom) with excessive methacrylic anhydride (MA, 10 Eq. to lysines) as reported by Van den Bulcke (Figure 27).<sup>86</sup> Given that high MW gelatin solutions become physical gels at room temperature, the reaction was maintained at 40 °C in PBS solution. After overnight reaction, the solution was firstly washed with sodium bicarbonate solution to neutralize the unreacted MA and/or methacrylic acid. Next, the crude solution was purified by dialysis (cut-off: 12 kDa) against distilled water at 40 °C. After lyophilization, gelMOD was obtained as white foam (92 % of theory).

Owing to the thermo-reversible behavior of high MW gelatin, NMR analysis of gelMOD was measured at 40 °C, above the transition temperature (37 °C), to ensure a flat baseline. As shown in Figure 28, NMR spectrum of gelMOD in D<sub>2</sub>O includes more than 15 resonances of different amino acids in gelatin. Complete explanation of this spectrum is beyond the scope of this work. Similar to the spectrum of GH-MA, characteristic signals corresponding to methacrylate groups could be found at 5.8 ppm (**a**), 5.6 ppm (**b**), and 2.1 ppm (**c**), respectively.

In order to determine the DS of gelMOD, proton signals at 1.1 ppm corresponding to the –CH<sub>3</sub> groups of Val, Leu, and Ile residues are selected as the reference. It is reported that the concentration of these residues in high MW gelatin is 0.64 mmol/g.<sup>156</sup> Given that each of the residues has two methyl groups, the integration of the peak at 1.1 ppm (6 protons) corresponds to 3.84 mmol/g. In addition, initial amount of primary amine groups should be the concentration of (hydroxyl)lysine in gelatin (0.38 mmol/g).<sup>151</sup>

The DS calculation was carried out as below:

$$\text{DS (\%)} = 3.84 \times (I_{5.6\text{ppm}}/I_{1.1\text{ppm}}) \times (100/0.38)$$

The integration at 1.1 ppm is 1.00 and the integration at 5.6 ppm is 0.07. Thus, the DS value was calculated to be 70 % (65% in Lit.<sup>156</sup>), indicating ~70 methacrylamide groups per 100 lysines. By assuming the average MW of gelMOD to be 75 kDa, there are ~20 methacrylamide groups per gelMOD. Notably, this value is significantly higher than that of GH-MA (~9). A high concentration of methacrylamide groups per macromer might explain the usefulness of gelMOD in 2PP microfabrication.<sup>156</sup>

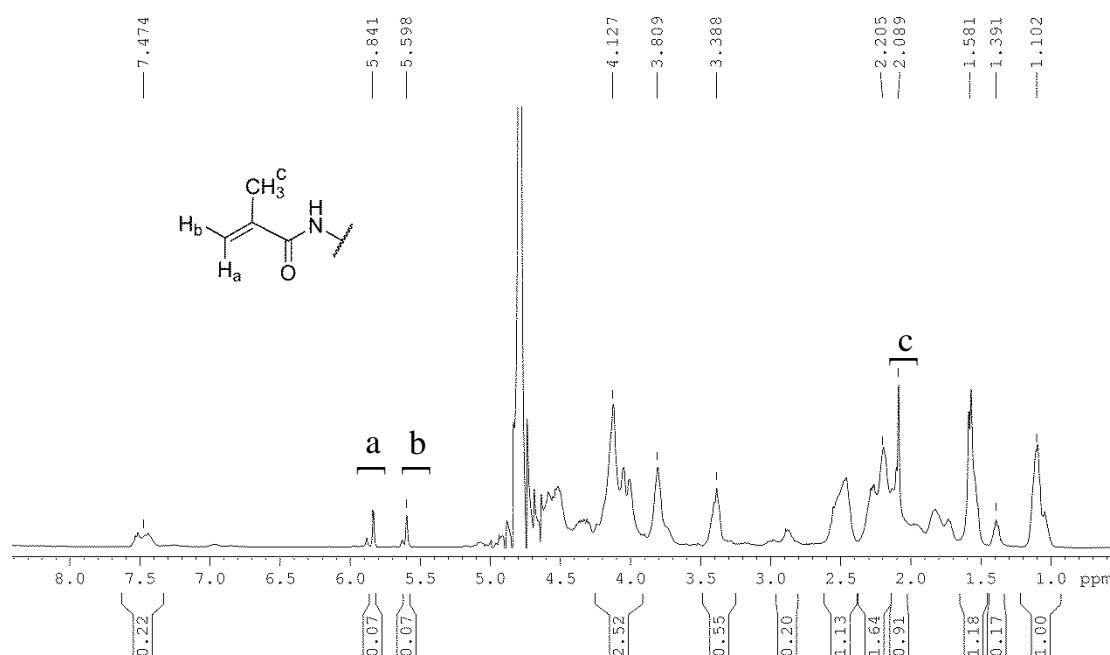


**Figure 28.** <sup>1</sup>H-NMR spectrum of gelMOD (D<sub>2</sub>O, 40 °C, 400 MHz)

### 1.1.3 Synthesis of Gelatin Acrylates (GH-AC)

The acrylate derivative of gelatin (GH-AC) remains unpublished in literature. To synthesize GH-AC, a direct modification approach was initially explored by reacting excessive acryloyl chloride with lysine residues in GH (Figure 29). Specifically, a pre-dissolved GH/DMSO solution containing triethylamine as acid scavenger was added dropwise into a DMSO solution of acryloyl chloride (5 eq. to lysine residues) at 20 °C with vigorous stirring. Notably, it was impractical to stir this reaction under ice bath since the melting point of DMSO is ~19 °C. Unfortunately, instant gelation was observed during the addition. It is presumably due to the fast substitution rate of acryloyl chloride and subsequent Michael-addition reaction between the substituted acrylate groups with neighboring amine groups, eventually causing intermolecular crosslinking.

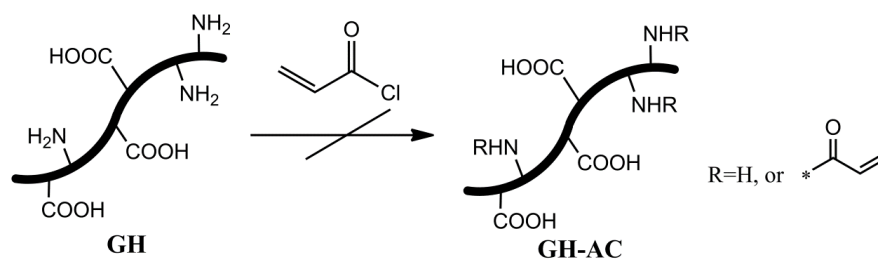


**Figure 29.** The reaction of GH with acryloyl chloride

To circumvent the gelation problem, alternative synthetic procedures were attempted. For instance, dilute NaOH or  $K_2CO_3$  solutions were utilized as both reaction media and acid scavenger, so that the reactions were performed at 5 °C. When 1-fold of acryloyl chloride to lysine units was used, no DS could be observed from the purified product. When a 5-fold excess of acryloyl chloride was used, gelation was still observed during the reaction. Besides, high MW gelatin (50-100 kDa) was also explored as an alternative substrate. The reaction of high MW gelatin in DMSO/TEA reached gelation earlier than the control reaction of GH. Without using DMSO, it was not feasible to carry out the reaction of high MW gelatin in alkaline solutions below 37 °C. In all, direct modification of gelatin with acryloyl chloride was not successful.

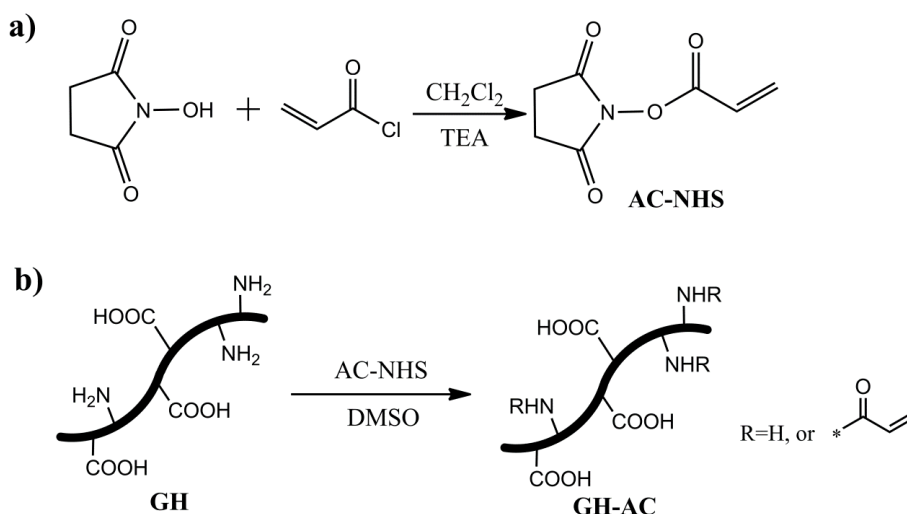


**Figure 30.** Two-step synthesis of GH-AC: **a)** synthesis of acrylated NHS ester; and **b)** the reaction of GH with AC-NHS (TEA: triethylamine)

Instead of direct using acryloyl chloride, a two-step modification approach (Figure 30) was devised. First, n-acryloxysuccinimide (AC-NHS, Figure 30a) was prepared by reacting NHS with acryloyl chloride in  $CH_2Cl_2$ /TEA at 4 °C as described by Whitesides and co-workers.<sup>157</sup> The product was recrystallized from a mixture of EE and Hexane

(1:1). AC-NHS was obtained as colorless crystals in 73 % yield. Second, the lysine residues of GH were allowed to react with AC-NHS (Figure 30b). Specifically, a GH/DMSO solution was added into a DMSO solution of AC-NHS (5 Eq. to lysine residues) and hydroquinone at room temperature. Notably, no gelation was observed during the reaction process (12 h). The crude product was purified by dialysis against deionized water for 24 h. After lyophilization, GH-AC was obtained as yellowish solid in 61% yield.

To evaluate the synthesis, NMR spectrum of GH-AC was measured (Figure 31). In comparison with the spectrum of GH (Figure 24), GH-AC shows new peaks in the range of 5.5-6.4 ppm, corresponding to three unsaturated protons of acrylate groups. Furthermore, proton signals at 3.2 and 1.3 ppm indicate the presence of methylene groups adjacent to the newly formed amide bonds.

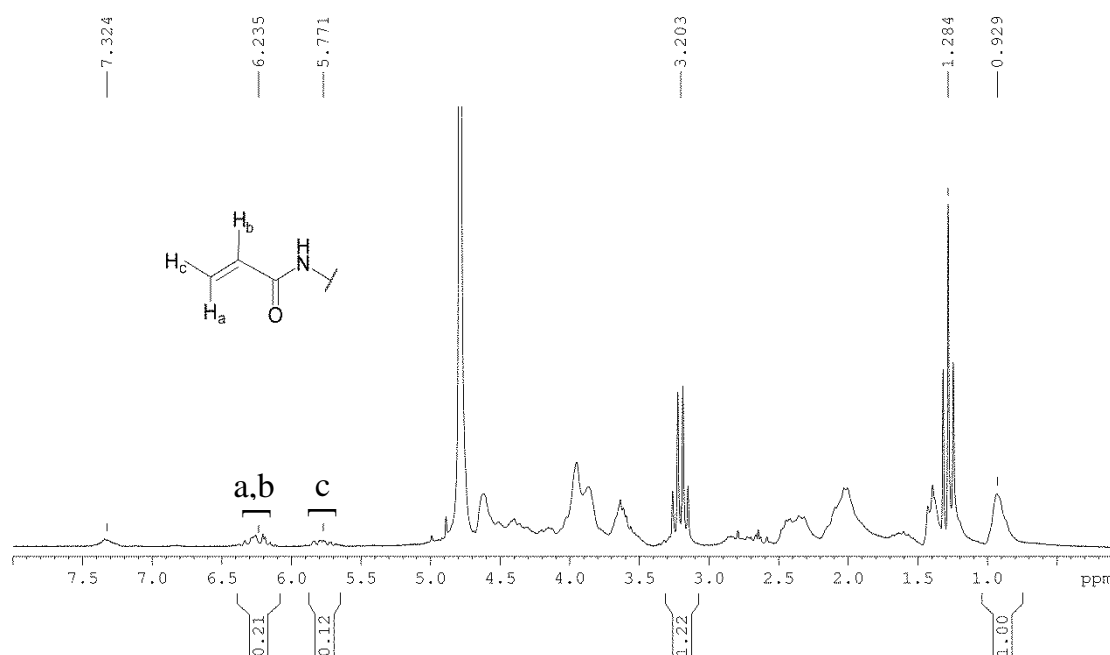


**Figure 31.** <sup>1</sup>H-NMR spectrum of GH-AC (D<sub>2</sub>O, 25 °C)

The DS of GH-AC was determined by calculating the relative ratio of the integration of acrylate protons to that of the -CH<sub>3</sub> reference at 0.9 ppm. Based on the -CH<sub>3</sub> value (1.04 mmol/g), the acrylate group concentration was calculated to be 0.34 mmol/g, corresponding to ~1.4 acrylate groups on average are present on one GH-AC peptide. This value (0.34 mmol/g) is much lower than the value of total amino groups in GH (0.59 mmol/g). Given that excessive AC-NHS was used, it is speculated that the difference is



attributed to the loss of acrylate groups after reacting with residual amino groups through Michael-addition reaction.

### 1.1.4 Synthesis of Gelatin Vinyl Esters (GH-VE)

To synthesize GH-VE, an aminolysis reaction was selected to functionalize GH using a commercial divinylester (divinyladipate, DVA). To carry out the synthesis, an appropriate solvent had to be determined first. As DVA is prone to hydrolysis in the presence of water, the aprotic polar solvent DMSO was selected as the solvent since it avoids hydrolysis of DVA while keeping good solubility for GH.

#### Model Reaction

At the first stage of this work, a model reaction (Figure 32) for the synthesis of GH-VE was performed on a low-molecular-weight model compound (1-hexyl-amine) in order to investigate the efficiency of aminolysis reactions between  $\epsilon$ -amino groups and a 10-fold excess of DVA. From the results of the model reaction (GC-MS analysis), 1-hexyl-amine was quantitatively converted (>98%) with DVA after 3 h reaction in anhydrous DMSO at 50 °C.  $^1\text{H-NMR}$  results provided further evidence on the successful modification. The proton signals at 2.7 ppm which correspond to the methylene protons next to the amine groups disappeared entirely. Furthermore, only negligible amounts of diamides were detected in GC-MS experiments.

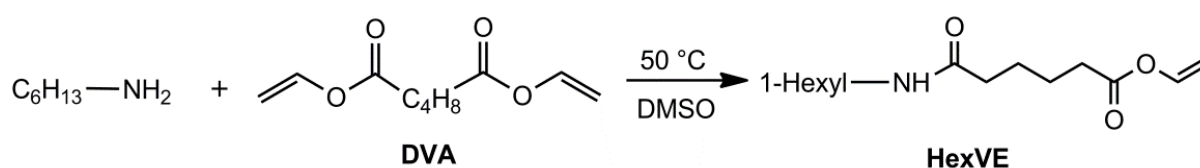


**Figure 32.** Reaction of 1-hexyl-amine with DVA

#### Synthesis of GH-VE

Based on the success of model reaction, GH was reacted with a ten-fold excess of DVA according to the conditions in the model reaction (Figure 33). It is hypothesized that the dropwise addition of GH solution into excessive DVA would minimize the possibility of intermolecular crosslinking by DVA. In order to remove the excessive DVA, DMSO was firstly removed by high vacuum distillation followed with a liquid-liquid extraction. After subsequent dialysis and lyophilization, the vinyl ester derivative of GH (GH-VE)

was obtained as yellow powder in 66 % yield. It is noteworthy that the only side product of this reaction is acetaldehyde (b.p., 20.2 °C) that can be easily removed.

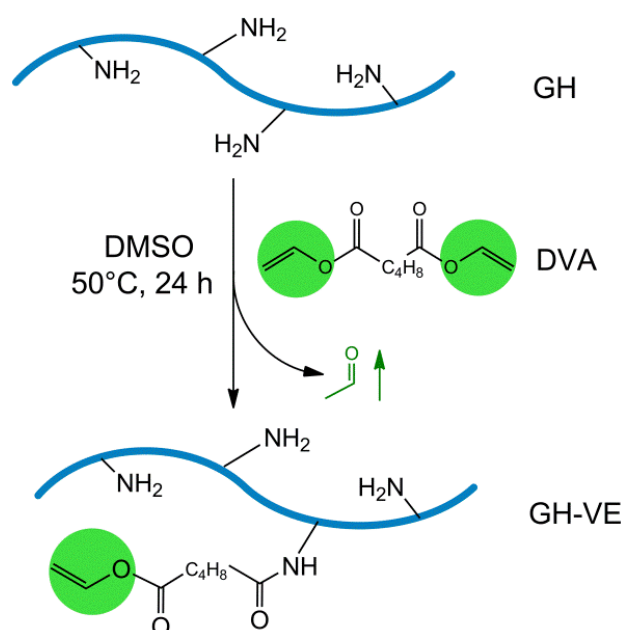


**Figure 33.** Synthesis of GH-VE by reacting GH with excessive DVA

### <sup>1</sup>H-NMR

As shown in Figure 34, the <sup>1</sup>H-NMR spectrum of GH-VE was measured to characterize the product. Proton signal **(a)** at 7.4 ppm corresponds to one of the unsaturated protons (C=CH–O–) of the pendant vinyl ester group, while signals **(b)** and **(c)** from the other two unsaturated protons (CH<sub>2</sub>=C–O–) were partly overlapped with the solvent peak (D<sub>2</sub>O) within the range 5.2–4.7 ppm. Compared to the spectrum of GH (Figure 24), an increase of the amide proton signal **(d)** could be observed at 3.5 ppm. Additionally, three kinds of methylene signals **(f, g, e)** centered at 2.7–2.5 ppm and 1.8 ppm showed obviously stronger signals due to the presence of DVA moieties. The combined evidence indicates that the aminolysis reaction of GH was successful.

To quantify the concentration of vinyl groups in GH-VE, the integration of vinyl proton **(a)** at 7.4 ppm (C=CH–O–) was used as reference in comparison with that of the –CH<sub>3</sub> proton signal at 1.12 ppm. Based on the –CH<sub>3</sub> value (1.04 mmol/g) in GH, the concentration of vinyl ester groups in GH-VE was calculated to be 0.57 mmol/g.

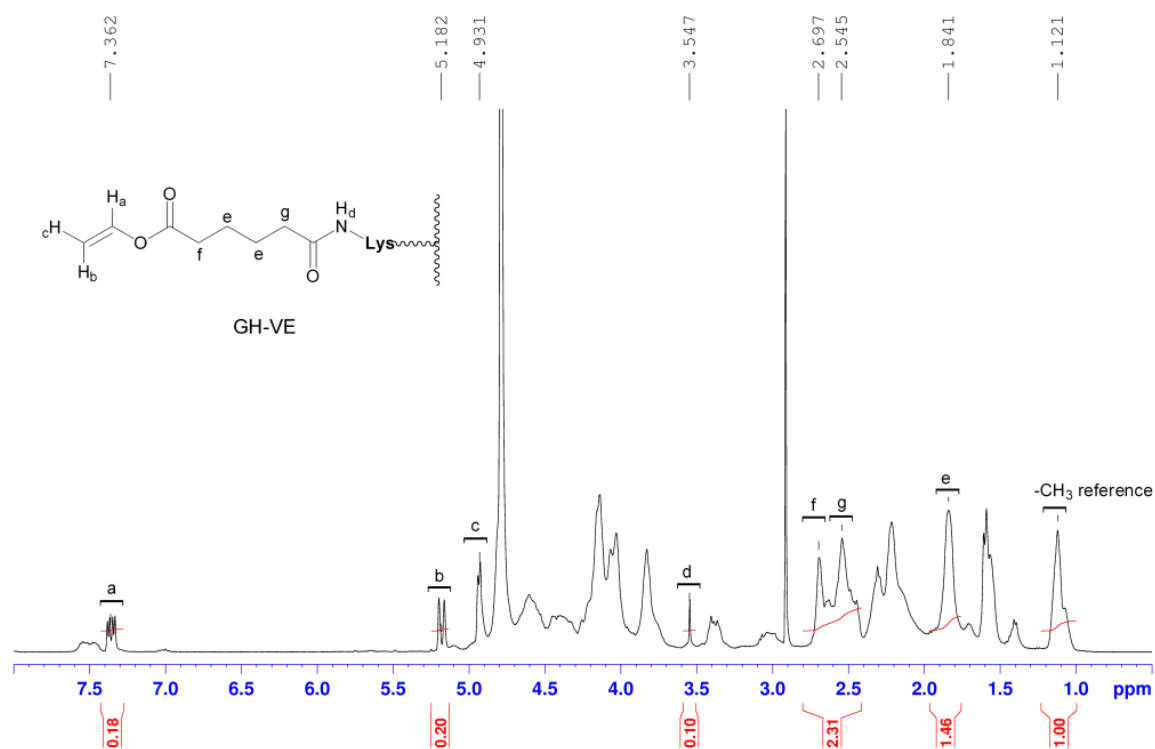


**Figure 34.**  $^1\text{H-NMR}$  spectrum of GH-VE ( $\text{D}_2\text{O}$ ,  $40\text{ }^\circ\text{C}$ ,  $400\text{ MHz}$ )

To design an efficient thiol-ene formulation for photocrosslinking, at least two thiol or ene functionalities should be incorporated to both thiol and ene macromers.<sup>55</sup> To roughly estimate the number of DVA moieties per GH-VE, calculation resulted in about 2.7 DVA moieties on average were attached on the GH backbone. Since this value was beyond the theoretical value of lysine units in GH (1.8 per GH), it is supposed that the amino group at the N-terminus contributed to this difference. Thus the substitution degree of amino groups was calculated as 96 %.

### MALDI-TOF

Apart from NMR analysis, MALDI-TOF mass spectroscopy was also applied to confirm the modification success. MALDI-TOF studies were carried out through coloration with Prof. Robert Saf at Graz University of Technology. Spectra typical for complex mixtures of peptides were obtained for GH as well as for GH-VE. The spectra are overlaid in Figure 35 to facilitate direct comparison.

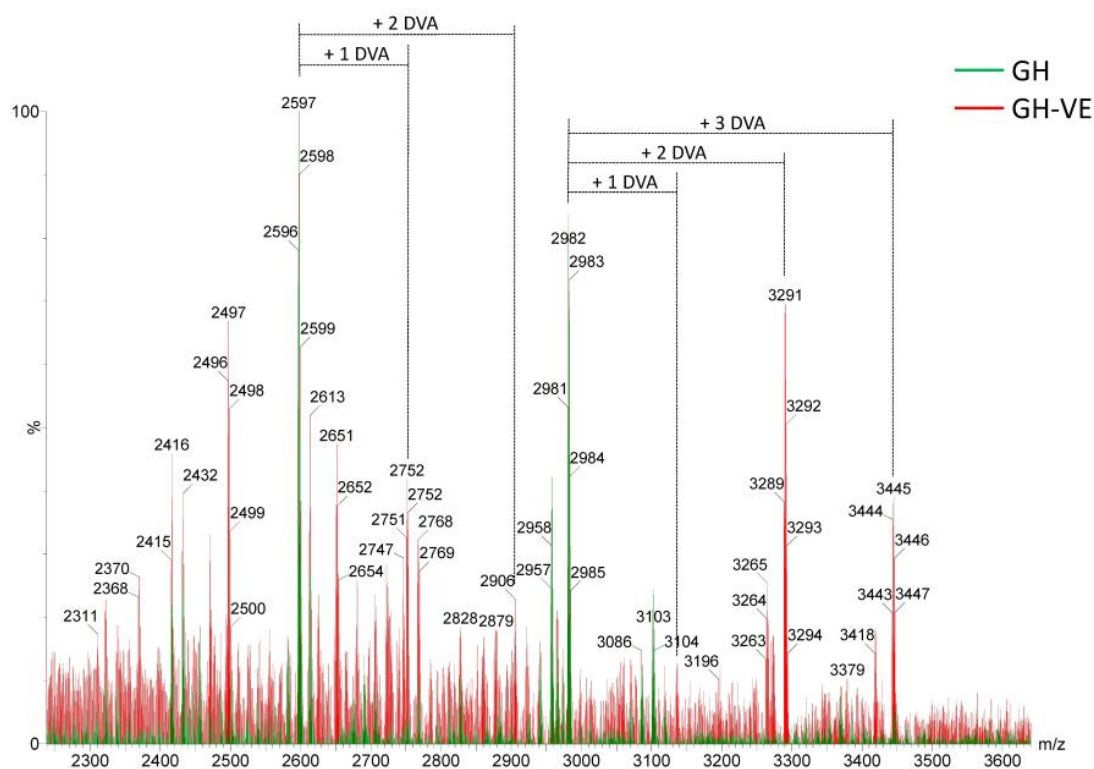


**Figure 35.** Overlaid MALDI-TOF mass spectra of GH (green) and GH-VE (red). Comparison of the fingerprints show that various signals observed for GH-VE can be correlated to peptides observed for GH assuming  $n$ -fold addition of divinyl adipate (DVA)

The fingerprints of the spectra clearly indicate that DVA was bound to peptides between one and three times. For example, a rather intense peak in the spectrum of GH was observed at  $m/z = 2981$  Da (monoisotopic peak). After single modification with DVA an increase of the mass of 154 Da should be observed due to introduction of the corresponding vinyl adipate moiety (compare Figure 33). The corresponding signal at 3135 Da was observed in the MALDI spectrum of GH-VE with low intensity. Signals with rather high intensities were also observed at 3289 and 3443 Da. These two signals are assigned to two- and three-fold modification of the peptide. As another example, the modification of a peptide with 2597 Da is marked in Figure 35. Several other signals observed in the spectrum of GH-VE can also be correlated to signals of GH, e.g. the signals at 3265/3419 Da can be interpreted as double/triple modification of the peptide originally observed at 2957 Da. Note, that these results correspond well to the average degree of modification of approximately 2.7, which was calculated from the NMR data. Another important aspect during the synthesis of GH-VE was the possibility for intramolecular reactions of already introduced vinyl ester groups with residual amino

groups, an undesired side reaction that would lead to loss of polymerizable ene groups or potential gelation. The MALDI spectrum of GH-VE indicates that the side reaction was negligible. As one example, the signal at  $m/z = 3289$  Da was already assigned to a double modified peptide. The species must contain at least one residual amino group, since three fold modification was observed too ( $m/z = 3443$  Da). Consequently, an intramolecular side reaction would be possible. After loss of  $C_2H_4O$  (44 Da) the corresponding product should be observed at 3245 Da. As shown in Figure 35, this signal was not detected with reasonable intensity.

## 1.2 Characterization of Gelatin Derivatives

Considering that gelatin-derivatives with varying functional groups (Figure 36) were prepared, it is intriguing to investigate how the functionality difference influences macromer properties. However, it is important to mention that the DS of these macromers was different from each other due to different modification approaches. Characterization of these macromers was carried out with a focus on photoreactivity and cytotoxicity.

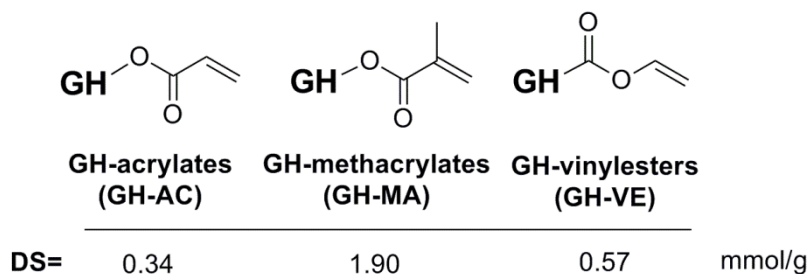


**Figure 36.** Chemical structures of (meth)acrylate and vinyl ester groups and the respective DS

### 1.2.1 Photo-rheometry

Photoreactivity of gelatin-derivatives listed in Figure 36 were analyzed using oscillatory, plate-to-plate *in-situ* photo-rheometry. Detailed explanation of this methodology including principle, set-up, and protocols is listed in **Methods**. For these measurements, the formulations consisted of 25 % respective macromer and 0.5 % PI (I2959). After a 60 s blank period, filtered UV light (320-500 nm) was allowed to irradiate the sample (gap thickness: 50  $\mu$ m) and initiate photopolymerization. The evolution of elastic modulus ( $G'$ ) and loss modulus ( $G''$ ) during the gelation process could be recorded and the  $G'$ -

plateau value correlates with the crosslinking density of a hydrogel network. The vicinity to the  $G'$ - $G''$  crossover could be determined as the gel point.

As shown in Figure 37, upon irradiation the GH-AC formulation underwent a rapid initiation process with a gel point of 18 s and finally reached a  $G'$ -plateau value of  $\sim 4$  kPa. In comparison, the GH-MA formulation underwent a relatively slower initiation with a gel point of 28 s, yet finally reaching a  $G'$ -plateau value of  $\sim 12$  kPa. These results can be explained from two aspects. On one hand, the robustness of acrylate chemistry provided GH-AC with a shorter induction period and a faster process to form intermolecular crosslinks. The lower efficiency of methacrylate groups on GH-MA led to a later gel point and relatively slower initiation process. On the other hand, the DS difference between GH-AC and GH-MA might explain the difference in  $G'$ -plateau values. It is very possible that as the polymerization proceeded, the acrylate groups in GH-AC were depleted much earlier than the methacrylate group in GH-MA.

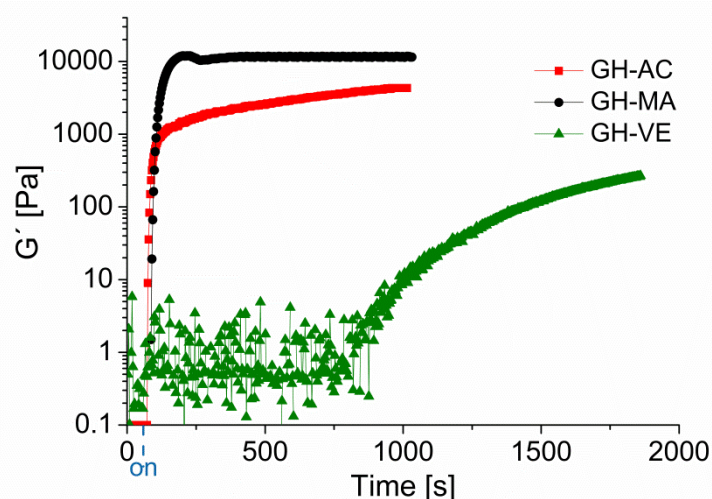


**Figure 37.** Photo-rheometry  $G'$ -curves of GH-AC, GH-MA and GH-VE (25% macromer content, 0.5 % I2959, 15 mW/cm<sup>2</sup>)

By contrast, the GH-VE formulation required more than 1700 s to reach a  $G'_{\text{plateau}}$  ( $\sim 300$  Pa) while the gel point was around 1050 s. These results (Table 6) indicate that the reactivity of GH-VE towards homopolymerization is quite limited. This limitation can be further explained as a consequence of: 1) the limited amount of vinyl ester groups per GH-VE peptide and 2) the moderate reactivity of vinyl ester groups which has been demonstrated in the PhD thesis of Christian Heller.<sup>43</sup>

**Table 6.** Detailed information on gel points, elastic and loss moduli of formulation I-III

Entry	GH-X	Gel point (s)	G'-plateau (kPa)	G''-plateau (kPa)
I	AC	18	4.3	0.4
II	MA	28	11.9	0.5
II	VE	1120	0.3	0.1

### 1.2.2 Cytotoxicity

To test the hypothesis that vinyl esters are less toxic than (meth)acrylates references, the macromer cytotoxicity of GH-VE was measured in comparison with GH-AC and GH-MA (Figure 36). Specifically, standard MTT assay was applied to quantify the influence of macromer solutions pre-dissolved in Dulbecco's modified eagle medium (DMEM) on the metabolic activity of osteosarcoma MG63 cells. Surprisingly, when the macromer concentration was 10 %, the GH macromer alone (Figure 38a) induced a drastic decrease of metabolic activity of MG 63 cells to ~50% of the control (cells in DMEM). This might be caused by the increased cellular uptake at high concentration of low molecular weight gelatin fragments and subsequent apoptosis.

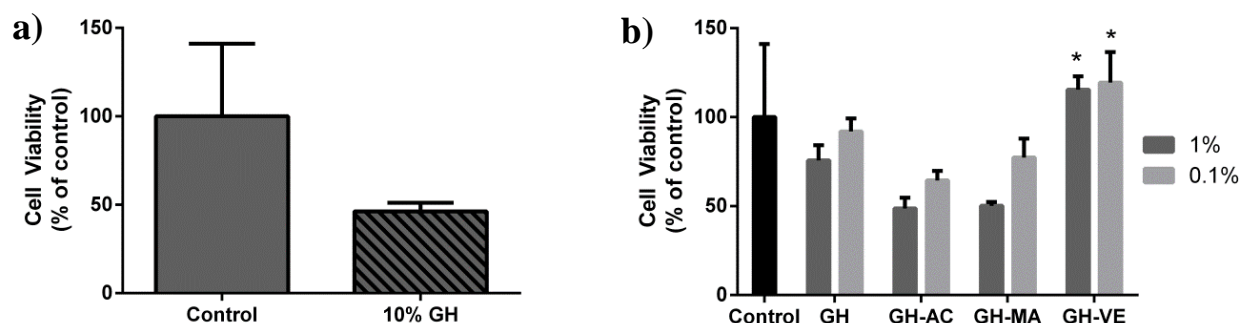


**Figure 38.** Cytotoxic effects of GH-VE in comparison with GH-AC and GH-MA investigated by MTT assay: **a)** macromer toxicity data of 10% GH; and **b)** toxicity data of 4 macromer solutions at 1% and 0.1% (mean values  $\pm$  SD,  $n=3$ , \* $P<0.05$  from GH-AC and GH-MA)

As such, further toxicity test was measured at lower macromer concentrations (1% and 0.1%). As shown in Figure 38b, GH-VE exhibited negligible toxicity on MG 63 cells at both concentrations whereas GH-AC and GH-MA induced significant cytotoxic effects. However, it is important to note the DS difference (Figure 36) in the tested macromers, especially GH-MA owes the highest DS. It is possible that toxicity of GH-MA may become less significant as the DS decreases to an extent that is comparable to that of GH-

VE. Nevertheless, these data suggest that the GH-VE was less cytotoxic than GH-AC analogue since the GH-VE has a higher DS than the GH-AC.

### 1.3 Preparation of Albumin Macrothiols (BSA-SH)

To overcome the reactivity limitation of GH-VE, the robust thiol-ene click chemistry was explored in this study. By using photo-differential scanning calorimetry (Photo-DSC), previous work by Mautner et al. proved that the addition of multifunctional thiols (macrothiols,  $n_{\text{SH}} \geq 3$ ) can substantially improve the reactivity of vinyl esters.<sup>158, 159</sup> The underlined mechanism lies on the highly efficient chain transfer reactions from carbon-centered radicals to thiyl radicals (Figure 39). While reaction kinetics of thiol-vinyl ester photopolymerization in the absence of solvents was demonstrated, further use of these reactions for preparing hydrogels remains unexplored.

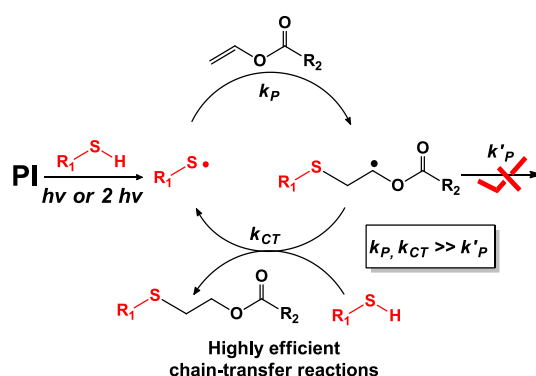


**Figure 39.** Proposed mechanism of photoinitiated thiol-vinylester photopolymerization

Notably, a number of commercial macrothiols have been explored in literature.<sup>55</sup> However, nearly all of these compounds are too hydrophobic to be used in hydrogel applications. Therefore, it is crucial to develop water-soluble macrothiols as gel precursors for a variety of biomedical applications. The material selected to prepare water-soluble macrothiols was bovine serum albumin (BSA), a 68 kDa protein widely used in biotechnology as tissue culture nutrient, blocking agent and enzymatic stabilizer.<sup>160</sup> In addition to its wide availability and good water solubility, BSA has a high number of cysteine residues making it a good candidate for thiol-ene chemistry. However, with the exception of a free thiol group at position 34, most cysteines are locked in disulfide bridges. These bridges could fortunately be cleaved through simple reduction, providing multiple free cysteines for radical-mediated thiol-ene copolymerization with the vinyl groups of ‘Ene’ macromers (Figure 40). Since the rate of



thiol-ene photopolymerization and the final mechanical properties of formed hydrogels depend on the thiol concentration, it was supposed that by adding varying amounts of the reducing agent such as tris(2-carboxyethyl)phosphine (TCEP), the final concentration of free cysteines could be controlled and allow further control over the physicochemical properties of hydrogels.

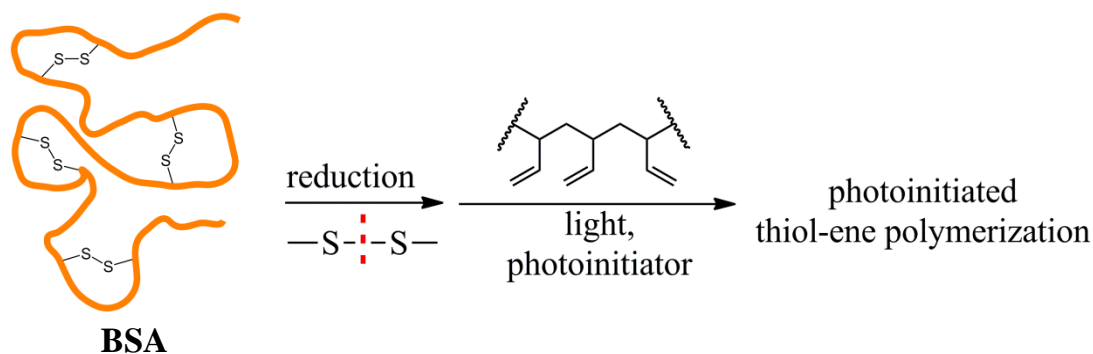


**Figure 40.** Schematic showing the reductive cleavage of disulfides in BSA and subsequent thiol-ene photopolymerization

### 1.3.1 Selection of Reducing Agent

In order to access the additional free cysteines in BSA, an appropriate reducing agent should be selected. In biochemistry, a variety of reducing agents are frequently used to break the disulfide bonds of proteins, generally for preventing the formation of intermolecular disulfide bonds.

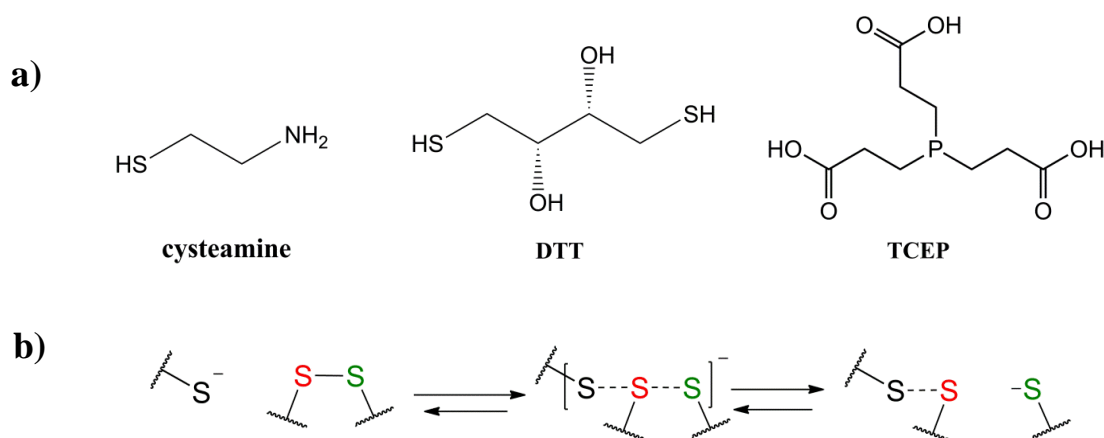


**Figure 41.** a) Chemical structures of reducing agents; and b) molecular mechanism of thiol-disulfide exchange

These reagents (Figure 41a) include cysteamine, dithiothreitol (DTT) and TCEP. It is important to mention that reduction mechanism and efficiency of these reagents varies

from one to another. For instance, cysteamine is a relatively mild reducing agent because it is only capable of reversible thiol-disulfide exchange reactions (Figure 41b).<sup>161</sup>

In comparison, DTT is a stronger reducing agent because it forms a stable six-membered ring with an internal disulfide bond (Figure 42a).<sup>162</sup> Since DTT suffers from its odor and poor stability, TCEP was developed as a non-volatile, odorless, stable and highly efficient reducing agent.<sup>163</sup> TCEP often reduces disulfides rapidly and completely in an irreversible manner at both alkaline and acidic conditions (unlike DTT), owing to the strength of P-O bonds (Figure 42b). Besides, since TCEP does not contain any thiol groups, the removal of reducing agent prior to further manipulation is often not necessary. Together, in this study, TCEP was selected as the optimal reducing agent to prepare reduced BSA macrothiols for subsequent thiol-ene copolymerization with GH-VE.

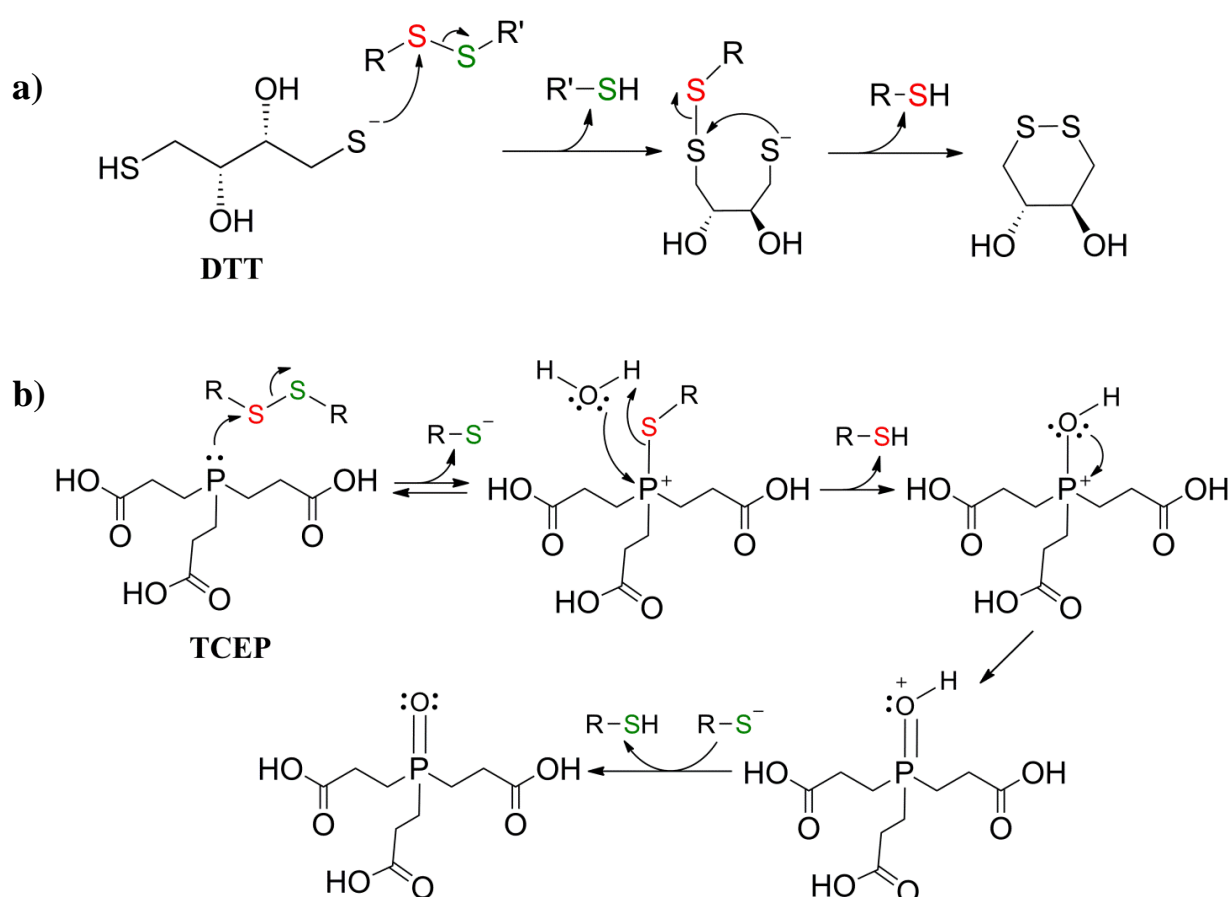


**Figure 42.** Reducing mechanism of DTT (a) and TCEP (b)

### 1.3.2 Ellman's Test

Once free cysteines are liberated from BSA through reduction, it is necessary to quantify the cysteine concentration prior to the design of a hydrogel formulation. Quantification of the concentration of free cysteines was determined by the method of Ellman.<sup>164</sup> The principle of Ellman's test (Figure 43) lies on a thiol-disulfide exchange reaction between Ellman's reagent (5,5'-dithio-bis-(2-nitrobenzoic acid), DTNB) and thiol groups. This reaction leads to a mixed disulfide and 2-nitro-5-thiobenzoic acid (TNB) which has a high molar extinction coefficient at 412 nm. Using a photometer and a standard solution of thiol compound, concentration of free sulfhydryl groups in the samples can be quantified.

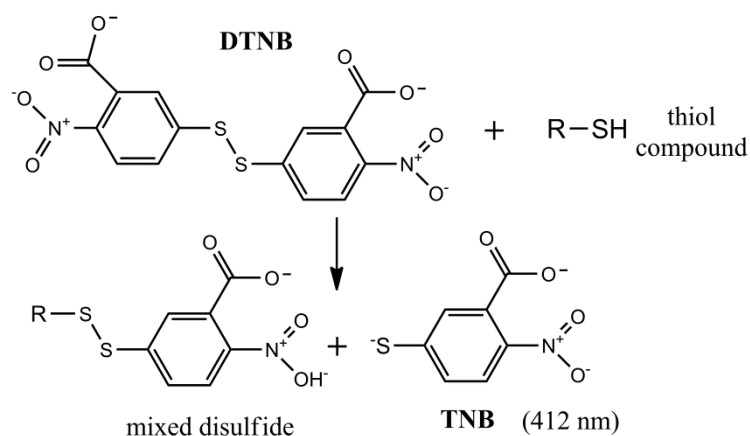


**Figure 43.** Working principle of DTNB in Ellman's test

N-acetyl-L-cysteine (Acetyl-Cys) was used as the standard thiol-containing compound and a calibration curve (see Experimental) was plotted from a series of Acetyl-Cys stock solutions (65  $\mu\text{M}$ -10 mM). An extinction value of TNB was calculated from Beer-Lambert law after linear regression and used to correlate the thiol concentration of BSA-SH. The molar extinction coefficient of TNB at 412 nm (25 °C, pH=7.4) was calculated to be 11963  $\text{M}^{-1}\text{cm}^{-1}$  (13600  $\text{M}^{-1}\text{cm}^{-1}$  in Lit.<sup>164</sup>). This value was used to further quantify the free sulfhydryl groups in reduced BSA solutions, in which varying amount of TCEP was added.

As aforementioned, native BSA has one free cysteine (Cys-34) and 17 disulfide bridges. It was supposed that the Cys-34 would contribute to the total cysteine concentration during the reduction procedure. The amount of free cysteines (or sulfhydryl groups) in

reduced BSA should depend on the amount of TCEP added. It was supposed that 1 unit of TCEP cleaves 1 disulfide bond while forming 2 free cysteines.

Although a series of early studies have shown that 17 disulfide bridges of BSA could be reduced completely and provide 35 free cysteines, the reported methods require very low working concentration of BSA (<1 wt%), presumably due to the decreased solubility of reduced BSA.<sup>165</sup> For this work, protein concentration has to reach a certain level to maintain adequate mechanical properties of the resultant gels. Practically, it was found that the reduced BSA would precipitate out of PBS buffer if excessive TCEP was added. For instance, for a 30 wt% BSA solution, the maximum dose of reducing agent is around 7 times the molar amount of BSA before precipitation was observed. By lowering BSA concentration, it was possible to achieve free cysteine/chain values from 2 up to 12. These reduced BSA macrothiols were however prone to air oxidization where formulation stability was dependent on: 1) working concentration of BSA, and 2) amount of TCEP added.

As shown in Table 7, three formulations of reduced BSA (BSA-SH-X, X=3, 6, 12) were prepared and later analyzed by Ellman's test. In order to minimize re-oxidation of -SH groups, both the preparative and analytical procedure was performed under Argon protection. The results suggest a good correlation between the calculated and measured values, showing the quantitative reduction efficiency of TCEP. It is consistent with the assumption that 1 unit of TCEP cleaves 1 disulfide bond and generates 2 thiols. These results enable further control on the thiol concentration prior to hydrogel design.

**Table 7.** Results showing the calculated and measured concentration of free thiol groups in 25 % (3.76 mM) reduced BSA (BSA-SH-X, X=3, 6, 12) after treatment with varying amounts of TCEP

Entry	Reduced disulfides per BSA	Calculated Cys per BSA	TCEP [mM]	C <sub>SH</sub> [mM]
BSA-SH-3	1.0	3.0	3.79	11.35
BSA-SH-6	2.5	6.0	9.47	22.73
BSA-SH-12	5.5	12.0	20.83	45.48

## 1.4 Characterization of GH-VE/BSA-SH Hydrogels

Since the reactivity of GH-VE towards homopolymerization was too low to be used in photolithographic applications, the highly efficient thiol-ene reaction was chosen as a polymerization strategy. Reduced BSA was used as a model macrothiol where its multiple cysteines can donate free thiol units to efficiently react with vinyl ester groups in GH-VE (Figure 44).

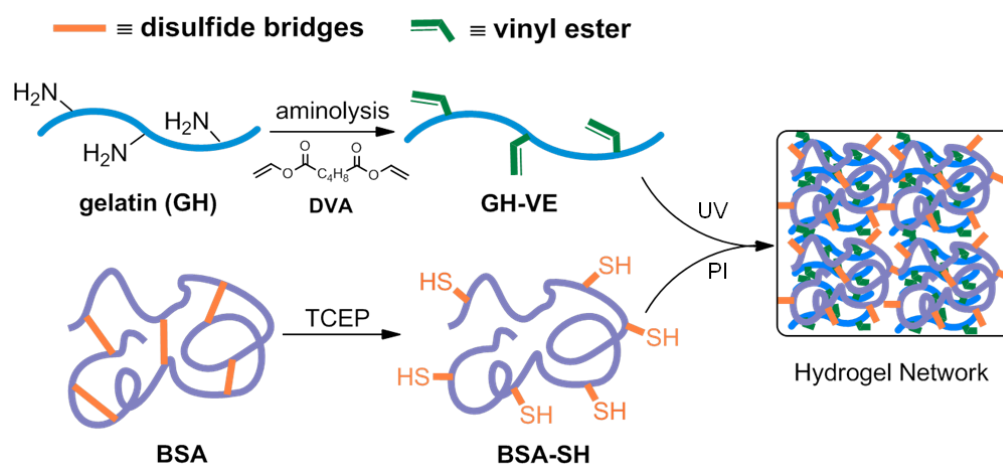


**Figure 44.** Schematics of GH-VE/BSA-SH hydrogel formation by photoinitiated thiol-ene polymerization

To test whether the reduced BSA can influence the gel formation of GH-VE and to which extent, four formulations (Table 8, 0-iii) with different thiol/ene ratios were prepared and used while holding the weight ratio between GH-VE and reduced BSA constant (except control 0). Due to a fairly low number of thiols per weight, a high concentration of BSA (16 %, w/w) was used. GH-VE was used at 9 % to give a total macromer concentration of 25 %.

**Table 8.** Details related to the macromer concentration and thiol/ene ratio in formulation 0-iii

Entry	GH-VE %	BSA-SH-X % (X)	C <sub>-SH</sub> [mM]	C <sub>-ene</sub> [mM]	n <sub>-SH</sub> :n <sub>-Ene</sub>
0	25	-	-	202.0	0
i	9	16 (3)	7.27	72.73	0.1
ii	9	16 (6)	14.55	72.73	0.2
iii	9	16 (12)	29.09	72.73	0.4

Reduced BSA with different degrees of free thiols was prepared by controlling the amount of TCEP as described in (section 1.3.2) and then used in combination with GH-VE, providing formulation 0-iii with four thiol/ene ratios (0, 0.1, 0.2, and 0.4).

### 1.4.1 Photo-rheometry

Since it is accepted that cysteine-containing proteins are prone to oxidation due to disulfide recombination, the stability of thiol-ene formulations (i, ii, iii) were firstly tested under varying conditions: 1) with initiator but without light (Figure 45a); and 2) without initiator but with light (Figure 45b). These control experiments indicated that the selected three formulations are stable under the selected conditions. To further investigate the influence of thiol/ene ratio on photoreactivity and final physical properties, formulations (0-iii) were evaluated.

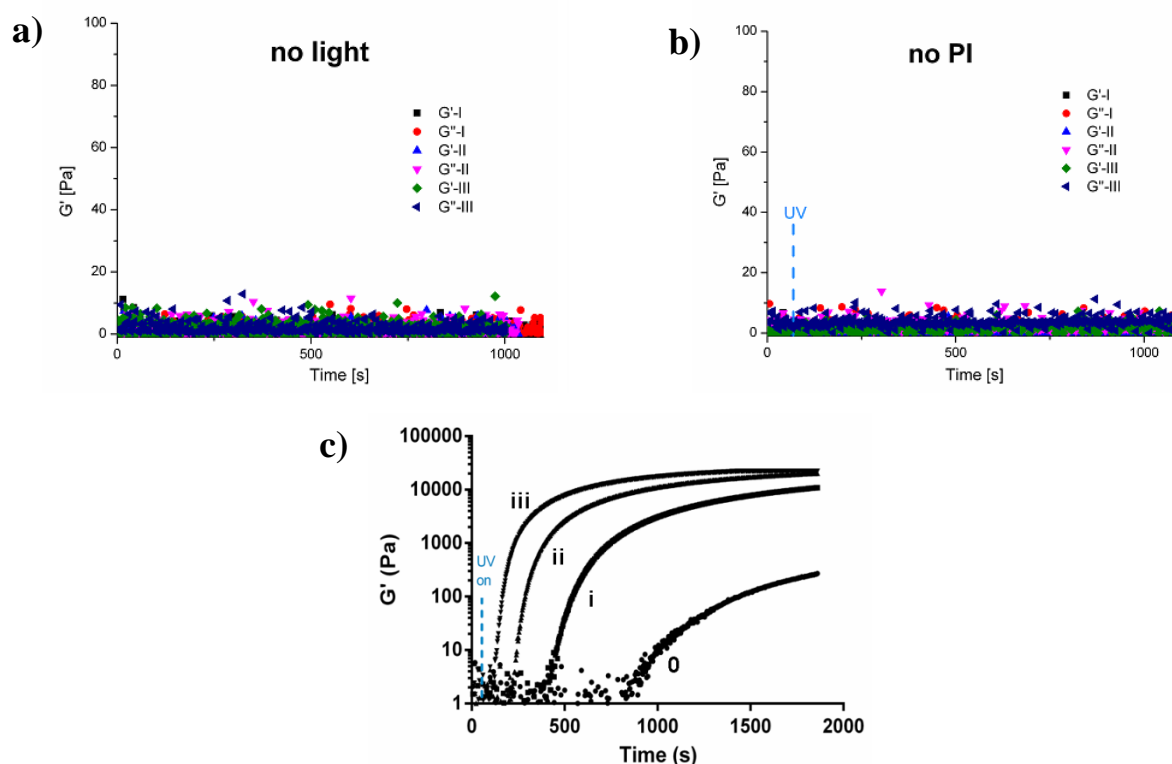


**Figure 45.** Photo-rheology plots of formulation i-iii: **a)** in the absence of light but with photoinitiator; **b)** with light but without photoinitiator; and **c)** with both light and photoinitiator. (Entry 0: GH-VE control)

As aforementioned, photoreactivity of GH-VE was initially quite limited, as evidenced by the photo-rheometry plot of 25% GH-VE in Figure 45c (Entry 0). The homopolymerization of GH-VE took more than 1000 s to reach the gel point. However,

when reduced BSA was added as macrothiols to donate free cysteines, the plots significantly changed. As the thiol/ene ratio was increased from 0 to 0.1, 0.2 and 0.4 (Table 9), the gel points were shifted from 1120 to 442, 205, and 95 seconds, suggesting increased reactivity. Meanwhile, elastic modulus increased from 0.27 to 10.9, 20.2, and 22.1 kPa, indicating an increased crosslinking density. Collectively, it was shown that the thiol/ene ratio could influence the onset of gelation and the crosslinking density of the network.

**Table 9.** Influence of the thiol/ene ratio on gel points, elastic and loss moduli of hydrogels 0-iii

Entry	$n_{\text{SH}} : n_{\text{ene}}$	Gel point (s)	$G'$ (kPa)	$G''$ (kPa)
0	0	1120	0.27	0.07
i	0.1	442	10.87	1.15
ii	0.2	205	20.24	1.84
iii	0.4	95	22.11	2.01

#### 1.4.2 Swelling Test

The swelling ability of a hydrogel is important for numerous applications since it influences both mechanical properties and solute transport activities.<sup>166</sup> The extent to which a gel can swell is primarily dependent on the crosslinking density of the network. In this study, the influence of thiol/ene ratio on swelling characteristics of GH-VE/BSA-SH hydrogels was tested. In the case of the neat GH-VE hydrogel without BSA-SH (Entry 0), the gel was too weak to accurately determine its swelling ratio. For gels containing BSA-SH (entries i-iii), the extent of water uptake was found to depend on the concentration of thiol groups (Figure 46). The mass swelling ratio decreased from 5.09 to 4.66 and 4.30 as the thiol/ene ratio increased from 0.1 to 0.2 and 0.4, suggesting an increased crosslinking density of the network. These results are consistent with the photo-rheology measurements as described in section 1.5.1.

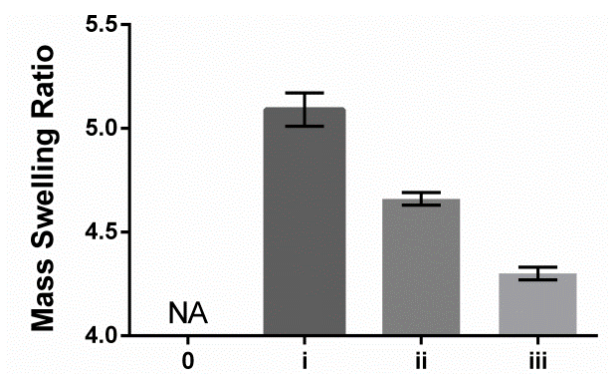


**Figure 46.** Mass swelling ratio of GH-VE/BSA-SH photopolymerized hydrogels with different thiol/ene ratio ( $n_{\text{thiol:ene}}=0$  (0), 0.1(i), 0.2(ii) and 0.4(iii); NA: not applicable, error bars:  $\pm$  SD)

### 1.4.3 Hydrogel Toxicity

Besides macromer toxicity, quantitative MTT assays were also performed to evaluate the cytotoxicities of extractions of gel pellets (i-iii) on MG63 cells (Figure 47). As described in section 1.2.2, MTT results showed that GH-VE displayed negligible cytotoxicities after 24h culture as compared to cell culture media (control). For GH-VE/BSA-SH gel pellets, a similar phenomenon was also observed with extractions out of pellets (i, ii). In contrast, extractions out of pellets (iii) decreased the cell viability to 70% of control. This might be due to the remaining traces of reducing agent although dialysis was performed prior to hydrogel preparation. These results were unexpected and further tests using different cell lines are warranted.

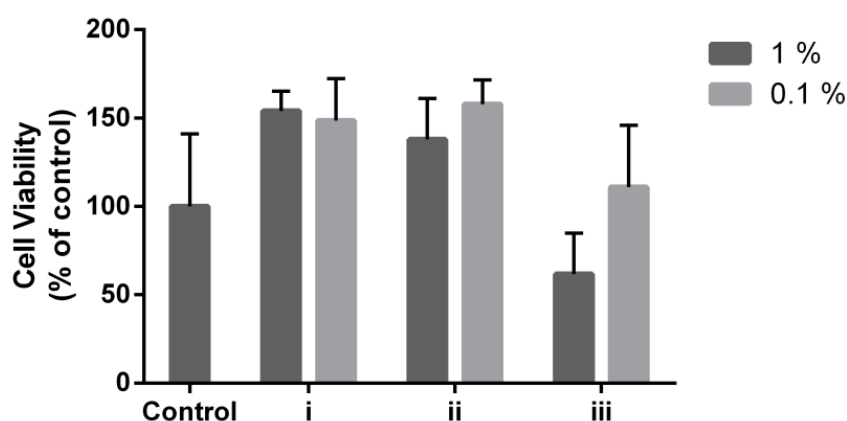


**Figure 47.** Viability of MG63 cells in contact with the pellet extracts (i-iii) investigated by MTT assay (mean values  $\pm$  SD, n=4)



### 1.4.4 Cell Adhesion

The ability for cells to adhere to a surface has important consequences on several cellular functions including migration, proliferation and apoptosis. Gelatin has a plurality of RGD motifs to promote cell adhesion. By contrast, BSA tends to resist cell adhesion due to its negative surface charge.<sup>167</sup> It is hypothesized that cell attachment could be adjusted by tuning the relative ratio between GH-VE and BSA-SH. To verify how the macromer relative ratio influences cell attachment, MG 63 cell suspension was loaded on the top of gel pellets in which GH-VE and BSA-SH-6 were mixed and polymerized at varying ratios. As shown in Figure 48A, when the GH-VE/BSA-SH relative ratio was 9:16, cells maintained round shapes, suggesting the pellets were not adhesive. Interestingly, as the ratio was increased to 12.5:12.5 (Figure 48B) and 20:5 (Figure 48C), there was increasing number of cells exhibiting a typical MG63 morphology. All together, these results indicate that the GH-VE supported cell adhesion. Since reduced BSA tends to discourage adhesion, it is intriguing to explore alternative disulfide-rich proteins that are also cell-adhesive.

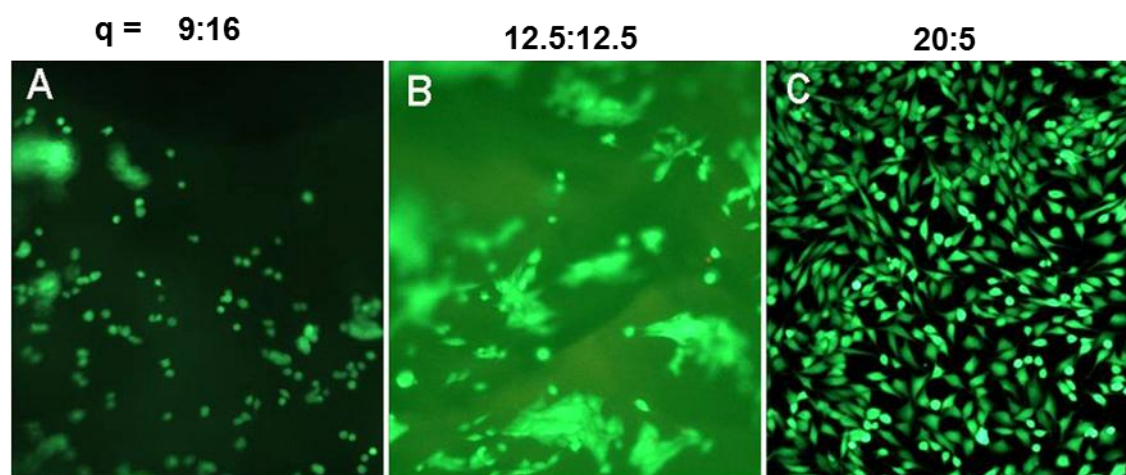


**Figure 48.** Influence of GH-VE/BSA-SH ratio ( $q$ ) on MG 63 cell adhesion (100 X):  $q = 9:16$  (A), 12.5:12.5 (B) and 20:5 (C)

## 1.5 2PP Microfabrication

### 1.5.1 Selection of Two-photon Initiator

To carry out 2PP microfabrication of hydrogels, one has to select a two-photon initiator (2PI) with high efficiency and good water-solubility. Although researchers have used certain water-soluble dyes (e.g., eosin-Y) as 2PI to fabricate hydrogels,<sup>168</sup> these dyes

generally lack efficiency due to their low two-photon-absorption (2PA) cross-section. For instance, it was reported that the 2PA cross-section value of eosin-Y was below 10 GM (Goepfert-Mayer units), which necessitates high laser powers for patterning.<sup>168</sup> It has been reported that the 4, 4'-dialkylamino bis(styryl)benzene (R1) chromophore shows a comparatively large 2PA cross section (318 GM).<sup>169</sup> The oil-soluble R1 has been utilized as a highly efficient initiator for 2PP microfabrication of acrylates. The underlined mechanism was thought to be a bimolecular electron transfer process from the photo-excited chromophore to acrylate monomers.<sup>30</sup>

Given the efficiency of the R1 chromophore, the water-soluble analogue (WSPI, Figure 49) which has a much larger 2PA cross-section value (144 GM) than eosin-Y was developed by Dr. Niklas Pucher (IAS) according to a protocol of Woo et al.<sup>170</sup>

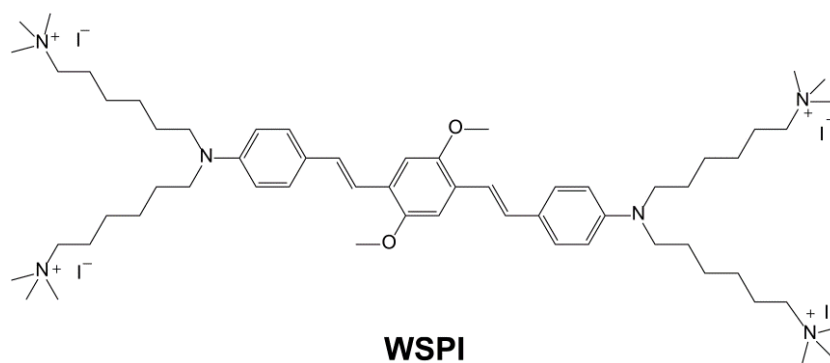


**Figure 49.** Chemical structure of the water-soluble two-photon initiator (WSPI)

WSPI and its derivatives were previously studied to investigate the solvent effects in a variety of media for biological imaging applications.<sup>36</sup> The addition of four quaternary ammonium pendant groups to the R1 chromophore provided enhanced solubility of WSPI in aqueous medium which is essential for biological applications. The charged end groups bonded to the aniline functionality through long aliphatic chains do not appear to interact with the electronic structure of the 2PA chromophore and thus do not affect its photoinitiating behavior. Very few groups have used WSPI as photoinitiator for 2PP microfabrication of hydrogels. Torgersen et al. previously explored the use of WSPI for the microfabrication of PEGDA based hydrogels in the presence of *C. Elegans*.<sup>39</sup> It was demonstrated that WSPI was a highly efficient water-soluble 2PI which enabled a broad processing window and high writing speed (10 mm/s).

### 1.5.2 Scaffold Design

For tissue engineering applications, 3D hydrogel scaffolds with free-transport properties are critical to maintain cell functions since diffusive nutrient/waste transport is only limited to short distances.<sup>21, 102</sup> In liver tissue engineering, for instance, it is still challenging to succeed the long-term culture of hepatocytes owing to their highly metabolic nature. Primarily it is due to the lack of a technique to precisely recapitulate the complex structure of liver tissue which is composed of thousands of hundreds of liver lobules (Figure 50a). These lobular microstructures allow the free transport of nutrients and wastes of hepatocytes.

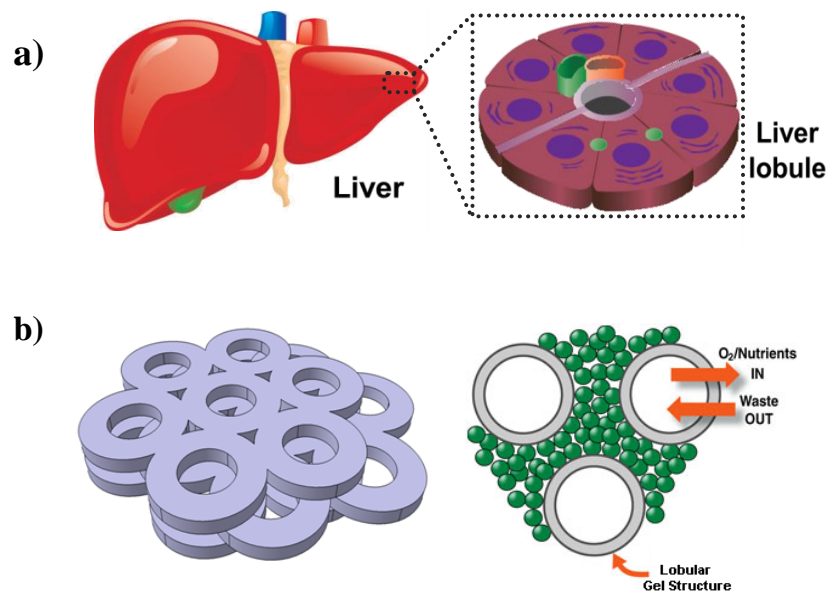


**Figure 50.** Schematic showing the structure units of liver tissue (a); and design of a biomimetic CAD scaffold with free-transport properties (b)

Therefore, a 3D CAD model (Figure 50b) was designed to mimic the geometry of liver lobules. This model ( $480 \times 580 \times 75 \mu\text{m}^3$ ) consists of three layers of packed cylinders with a hexagonal arrangement. It is supposed that these rationally-designed structures would likely enable long-term culture of hepatocytes on the 2PP fabricated scaffolds. In particular, these scaffolds are promising for liver tissue engineering when integrated with a perfusion bioreactor.<sup>1</sup>

### 1.5.3 Microfabrication

The 2PP microfabrication of GH-VE/BSA-SH hydrogels was carried out by Dr. Jan Torgersen. By using the 2PP technique, well-defined gel structures were written in accordance with the CAD model in the GH-VE/BSA-SH matrices. Laser scanning microscope (LSM) images of the hydrogel constructs are shown in Figure 51. The structures' feature sizes were around tens of microns, which are relevant to the size range of most mammalian cells.

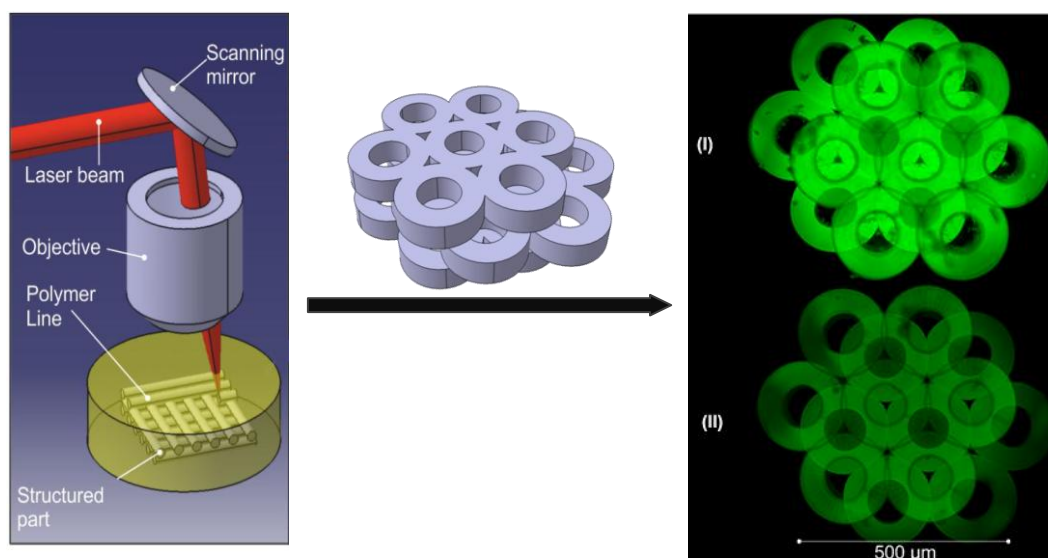


**Figure 51.** Schematics of 3D microfabrication of hydrogel constructs via 2PP and z-stacked LSM images of the constructs (0.5 % WSPI in PBS, 16 % BSA-SH-X (X=3, 6) and 9 % GH-VE,  $n_{\text{thiol:ene}}=0.1$  (i) and 0.2 (ii), respectively)

Generally, although high spatial resolution could be achieved by 2PP, a major challenge still exists in terms of the long processing time which greatly limits potential applications. Very recently, Li et al. reported the optimization of 2PP writing speed to a maximum level of 80 mm/s in non-aqueous media by using an optimized setup and an efficient 2PI.<sup>171</sup> However, ultrafast 2PP of hydrogels in the context of aqueous medium is more challenging when compared to 2PP in non-aqueous media, since hydrogel precursor solutions generally contain much lower concentrations of initiators and monomers. Nevertheless, it is noteworthy that a comparatively high writing speed (50 mm/s) was achieved in this study compared to previously reported results (10 mm/s for PEGDA),<sup>39</sup> presumably due to the optimized fabrication setup and the robustness of two-photon-induced thiol-ene chemistry.

To investigate the influence of the thiol/ene ratio on the reactivity and the resultant 2PP processing window, comparative 2PP fabrication of simplified structures were performed with constant writing speed (15 mm/s). It was found that all of the formulations were processable at 15 mm/s. As shown in Table 10, formulation-i ( $n_{\text{thiol}}:n_{\text{ene}}=0.1$ ) showed a broad processing window(75-375 mW) while formulation-ii ( $n_{\text{thiol}}:n_{\text{ene}}=0.2$ ) showed a comparable processing window(100-300 mW). Notably, formulation-iii ( $n_{\text{thiol}}:n_{\text{ene}}=0.4$ ) could be processed in a power as low as 50 mW, indicating that higher photoreactivity was obtained as a result of the increase of thiol concentration. However, the maximum processing power of formulation-iii was much lower than formulation-I and formulation-II, which could be explained as the decrease of protein tolerance against light-induced denaturation when BSA was reduced to a certain extent.

**Table 10.** Influence of the thiol-ene ratio on 2PP fabrication threshold (16 wt% BSA-SH-X (X= 3, 6, 12) and 9 wt% GH-VE, 0.5 wt% WSPI in PBS, writing speed: 15 mm/s)

Entry	$n_{\text{SH}} : n_{\text{ene}}$	Average Power Window
		[mW]
i	0.1	75-375
ii	0.2	100-300
iii	0.4	50-125

## 1.6 Attempts to Increase Crosslinking Density

Considering that GH-VE macromers suffers from low crosslinking efficiency and very few reactive sites (i.e.,  $-\text{NH}_2$  groups) are available in GH for aminolysis, it is invaluable to increase the  $-\text{NH}_2$  group concentration. Previous work on GH-MA (section 1.1) has demonstrated that a rather high DS value was achieved because the acidic amino acids in GH were also involved in a ring-opening reaction.

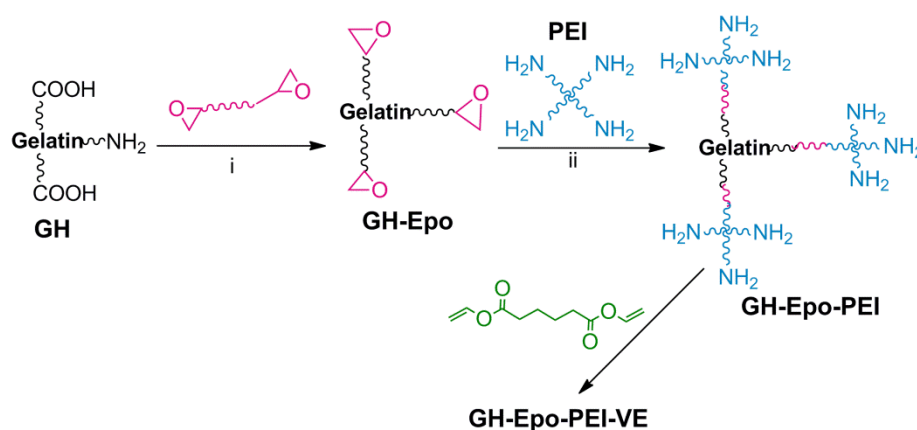


**Figure 52.** Schematic showing the synthesis for increasing  $-\text{NH}_2$  concentration and subsequent vinylation (i. 1,4-butanedioldiglycidyl ether, potassium phosphate buffer, pH=8.0; ii. polyethylenimine, ethylenediamine branched, Mw~800 Da, potassium phosphate buffer, pH=8.0)

Therefore, a multi-step synthetic approach was devised (Figure 52). Firstly, the substrate GH was allowed to react with an excess of di-epoxide (1,4-butanedioldiglycidyl ether). Then the intermediate (GH-Epo) was reacted with a branched molecule (polyethylenimine, PEI) which is rich in primary  $-\text{NH}_2$  groups, giving GH-Epo-PEI as product. At last, the GH-Epo-PEI was functionalized with excessive DVA, providing GH-Epo-PEI-VE as the final product.

### 1.6.1 Synthesis of GH-Epo

The synthesis of epoxide derivative of GH (GH-Epo) was carried out according to a procedure described by Dr. Monika Schuster (IAS).<sup>154</sup> As shown in Figure 53, GH-Epo was synthesized by reacting GH with a 10-fold excess of 1,4-butanediol diglycidyl ether in 0.1 M potassium phosphate buffer (pH=8.0) at 40 °C. The product was purified by dialysis against distilled water for 24 h. After lyophilization, GH-Epo was obtained as yellowish solid in 55 % yield.

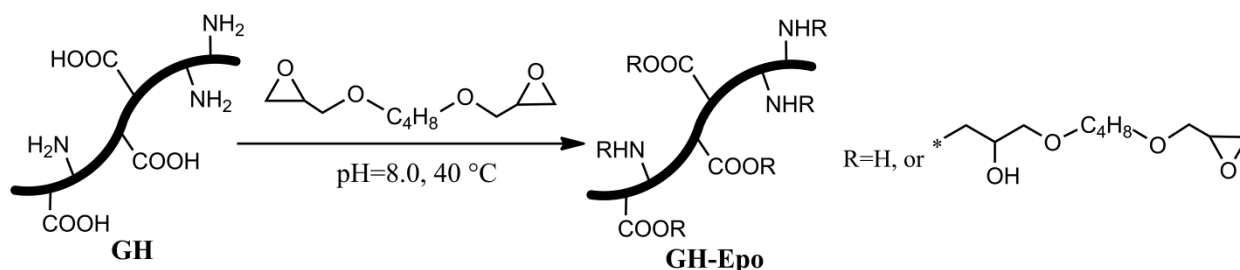


**Figure 53.** Reaction with 1,4-butanediol diglycidyl ether

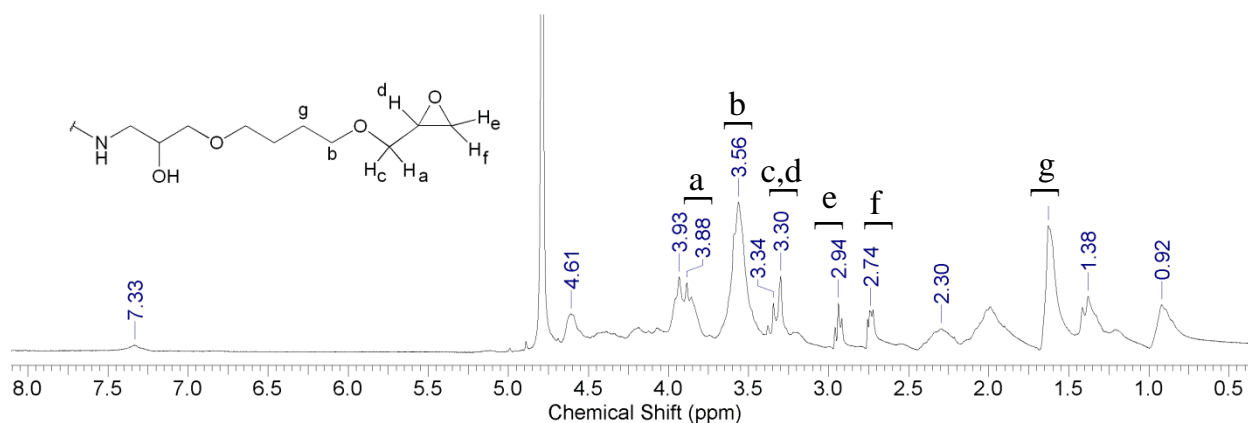


**Figure 54.**  $^1\text{H}$ -NMR spectrum of GH-Epo ( $\text{D}_2\text{O}$ , 25 °C)

To confirm the synthesis, NMR spectrum (Figure 54) of GH-Epo was measured in  $\text{D}_2\text{O}$ . The spectrum shows new peaks at 3.9, 3.6, 2.9, 2.7 and 1.6 ppm compared to that of neat GH. These signals are corresponding to protons on the oxyrane ring and the adjacent methylene group. Due to signal overlapping, however, it was hard to determine the DS of GH-Epo merely by NMR spectrum.

To quantify the concentration of epoxy groups in GH-Epo, a general protocol for titration of epoxy groups was applied.<sup>172</sup> The principle (Figure 55) of this method is that terminal epoxy groups can be quantified by titrating the alkali liberated on reaction with sodium thiosulphate.

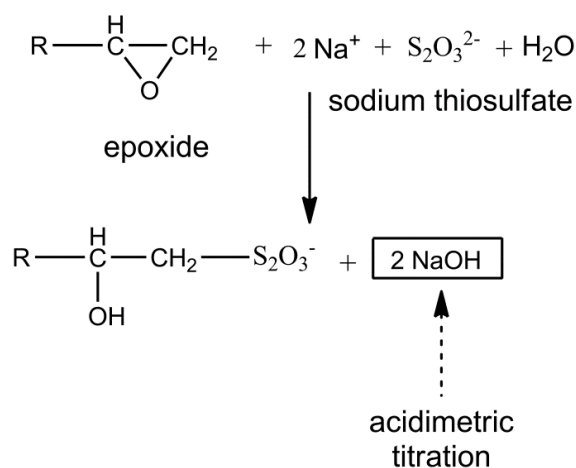


**Figure 55.** Principle of epoxide titration

From the titration results, the epoxy group concentration in GH-Epo was calculated as  $0.529 \pm 0.017$  mmol/g. Further calculation led to an epoxy-concentration of  $\sim 2.5$  groups

per peptide. By assuming that amino groups (0.59 mmol/g) were the primary targets for ring-opening reaction, the DS of amino groups was calculated as ~90 %.

### 1.6.2 Synthesis of GH-Epo-PEI

In order to increase the  $-\text{NH}_2$  concentration, a branched polyamine (PEI, Figure 56) was selected as the reagent to further react with GH-Epo. PEI is widely used as carrier materials in non-viral gene delivery applications due to its strong proton sponge effects.<sup>173</sup>

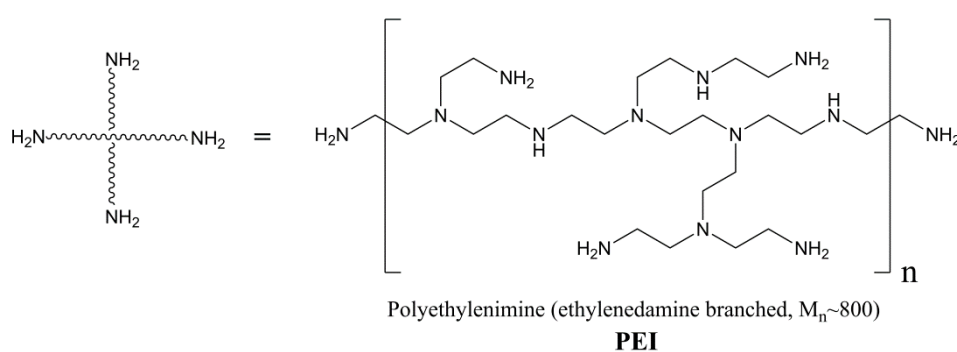


**Figure 56.** Chemical Structure of PEI

To minimize the probability of intermolecular crosslinking and loss of  $-\text{NH}_2$  groups, a pre-dissolved GH-Epo solution (5 % in water) was allowed to react with a 10-fold excess of PEI (based on epoxy groups) in 0.1 M potassium phosphate buffer (pH=8.0) at 40 °C for overnight. As shown in Figure 57, it is supposed that the lone pair of amine groups on PEI could attack the polarized carbon atom on epoxy groups of GH-Epo. Such a ring-opening reaction would covalently link PEI molecule onto the GH-Epo substrate. The product was purified by dialysis against distilled water for 1 week in order to remove residual PEI that was physically bound. After lyophilization, GH-Epo-PEI was obtained as yellow oil in 48 % yield.



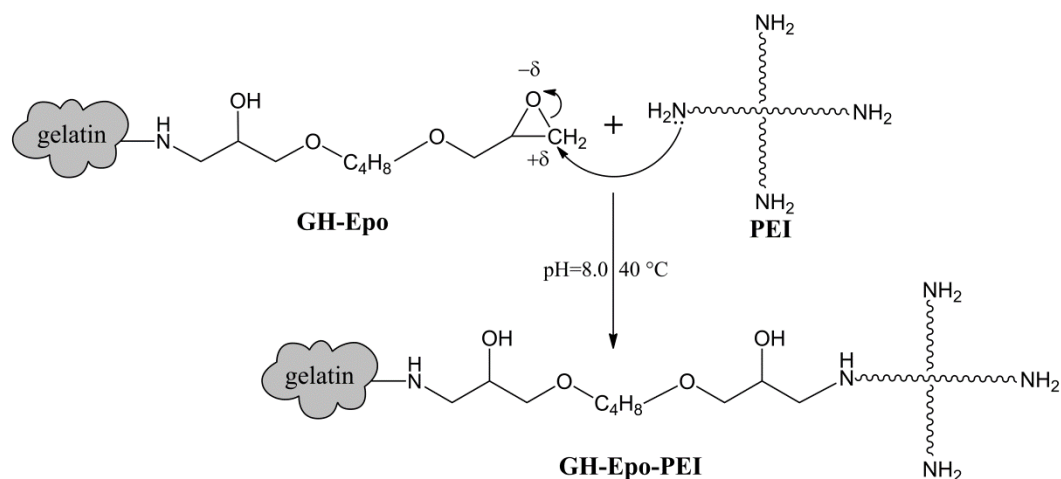


**Figure 57.** Reaction of GH-Epo with PEI

To confirm the synthesis, NMR spectrum (Figure 58) of GH-Epo-PEI was measured in  $D_2O$ . The spectrum shows significantly strong signals in the range of 2.5-3.0 ppm, corresponding to the characteristic proton signals of methylene groups in PEI.

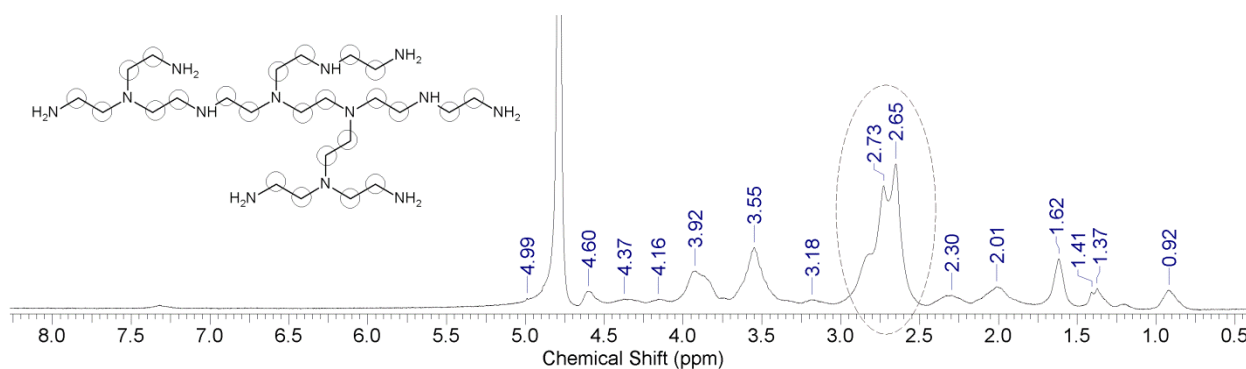


**Figure 58.**  $^1H$ -NMR spectrum of GH-Epo-PEI ( $D_2O$ , 25 °C)

### 1.6.3 Synthesis of GH-Epo-PEI-VE

The vinyl ester derivative of GH-Epo-PEI (GH-Epo-PEI-VE) was prepared according to the synthesis procedure of GH-VE (section 1.1). Specifically, GH-Epo-PEI was firstly dissolved in DMSO and afterward this solution was added dropwise into an excess of DVA (10 eq.) at 50 °C. It is supposed that the GH-Epo-PEI would undergo an aminolysis reaction (Figure 59) with one side of DVA through nucleophilic substitution and form amide linkages while leaving the other side unreacted to provide vinyl ester functionalities.

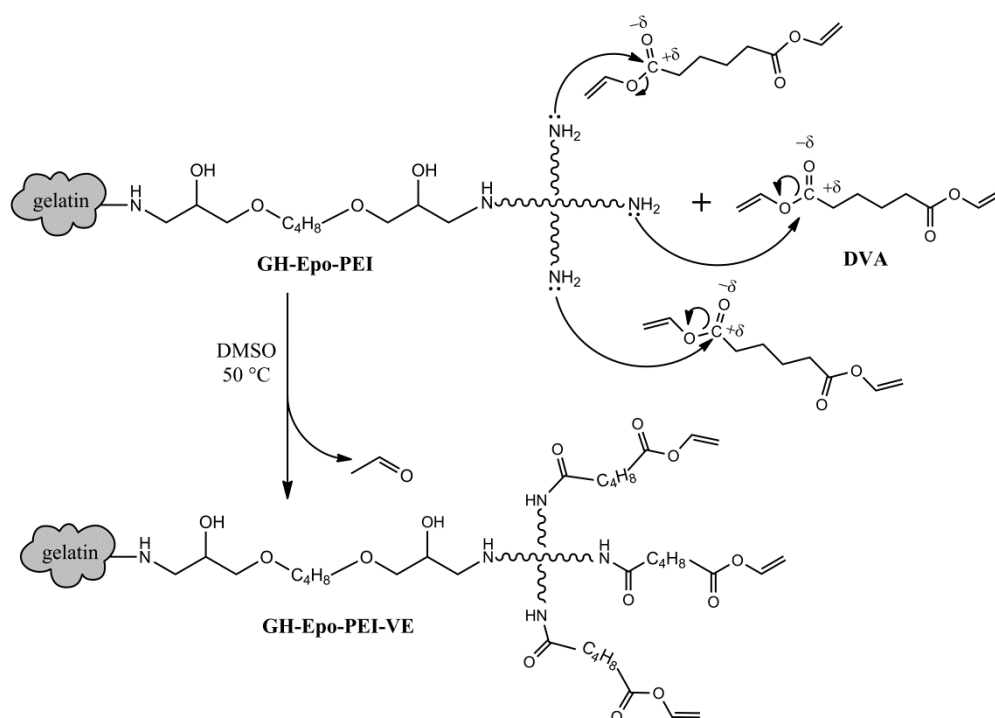


**Figure 59.** Proposed reaction of GH-Epo-PEI with divinyladipate

However, precipitation was observed during the reaction, presumably due to di-substitution-induced crosslinking. The left part was purified by dialysis against distilled water. After lyophilization, GH-Epo-PEI-VE was obtained as yellowish solid in 59% yield.

As shown in Figure 60, NMR spectrum of GH-Epo-PEI-VE was measured in  $\text{D}_2\text{O}$ . The spectrum showed characteristic signals of unsaturated protons of DVA moieties at 7.1, 5.0, and 4.8 ppm. However, the integration value of the unsaturated proton at 7.1 ppm was only 0.17. Considering that the corresponding value of GH-VE was 0.18 (section 1.1.4) and the reference ( $-\text{CH}_3$ ) signal at 0.9 ppm is supposed to be constant, this led to a conclusion that the vinyl ester concentration did not increase after the final step of modification.

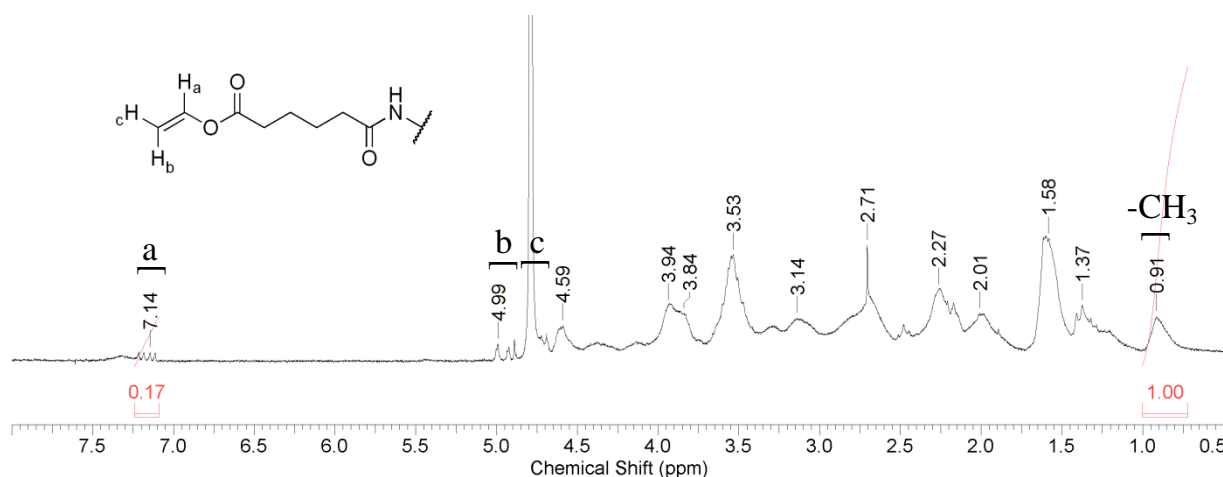


**Figure 60.**  $^1\text{H-NMR}$  spectrum of GH-Epo-PEI-VE ( $\text{D}_2\text{O}$ ,  $25\text{ }^\circ\text{C}$ )

In all, these results suggest that the attempts for increasing  $-\text{NH}_2$  concentration were not successful. Although one epoxide group was supposed to react with only one PEI molecule, it is very likely that multi-sites reaction between GH-Epo and PEI cause the significant loss of  $-\text{NH}_2$  concentration prior to the final vinylation reaction. The data lead to the assumption that one GH-Epo consumed more than one amine groups per PEI. Another two probable explanations could be that: 1) the highly cationic nature of PEI induces very strong electrostatic interactions with GH-Epo and the GH-Epo-PEI product may contain PEI traces albeit it was dialyzed more than 10 days; 2) even PEI was successfully attached on GH-Epo, the significantly increased charge may decrease the efficiency of subsequent aminolysis reaction; which is based on nucleophilic attack on the carbonyl group.



## 2 Hyaluronan-based Hydrogels

Another objective of this thesis research is to develop naturally-derived gel precursors with high photoreactivity and low cytotoxicity for creating artificial ECM gels via two-photon lithography. Given a limited number of lysine residues in gelatin, one type of polysaccharides, hyaluronic acid (HA), was selected as the substrate for providing hundreds of sites for chemical modification. While HA derivatives (Figure 61) such as thiolated HA and (meth)acrylated HA have been reported in literature,<sup>92</sup> HA vinyl esters (HA-VE) remain unexplored. Therefore, it was intriguing to synthesize HA-VE and explore its physicochemical properties in comparison with its photopolymerizable references: acrylated HA (HA-AC) and methacrylated HA (HA-MA). In addition, the air oxidizable reference, thiolated HA (HA-SH), was synthesized as macrothiols.

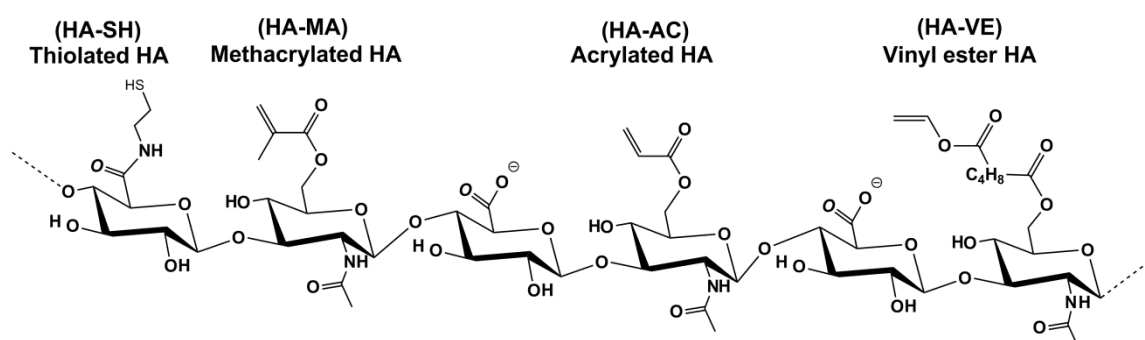


**Figure 61.** Chemical structures of HA derivatives: HA-SH, HA-MA, HA-AC and HA-VE

### 2.1 Background

Hyaluronic acid (HA or hyaluronan), is a linear polysaccharide consisting of D-glucuronic acid and D-N-acetylglucosamine as repeating units (Figure 62). HA is an anionic, nonsulfated glycosaminoglycan (GAG) distributed widely throughout connective, epithelial, and neural tissues. Unlike most GAGs, HA is formed in the plasma membrane instead of the Golgi and its molecular weight often reaches several millions.<sup>92</sup>

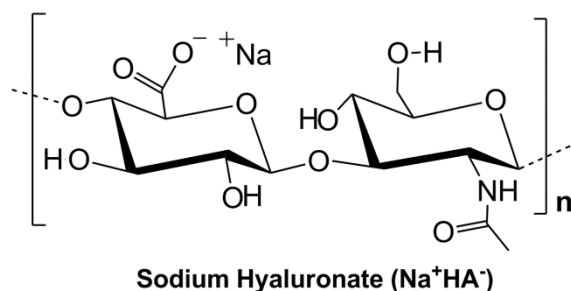


**Figure 62.** Chemical structure of one HA repeating unit

As an essential ECM component, HA plays important roles in tissue development, cell signaling, tumor progression and wound healing.<sup>88</sup> Due to its unique biological functions, HA has been widely used in biomedical applications such as the treatment of osteoarthritis. Nevertheless, the native HA suffers from poor mechanical properties and short half-lives *in vivo* which makes it inappropriate for certain clinical applications such as articular cartilage regeneration. As such, many researchers have explored a variety of methods to chemically modify HA with polymerizable groups and finally provide covalently crosslinked hydrogel networks.<sup>91-93</sup> These methods could effectively improve the mechanical strength and prolong the half-lives *in vivo*.

The principle targets for chemical modification in HA are the carboxyl and hydroxyl groups. Notably, Shu and Prestwich reported a synthetic method (Figure 63) for the preparation of thiolated HA.<sup>91</sup> First, carboxyl groups on HA were allowed to react with a disulfide-containing dihydrazide through carbodiimide-mediated reactions in water (pH 4.8). Second, the mono- and/or di-substituted intermediates were reduced using DTT to liberate free sulfhydryl groups. Although the first reaction lacks chemo-selectivity while generating urea byproducts, thiolated HA with tunable DS (20 %-70 %) and high purity could be obtained after exhaustive dialysis against dilute HCl (pH 3.5).

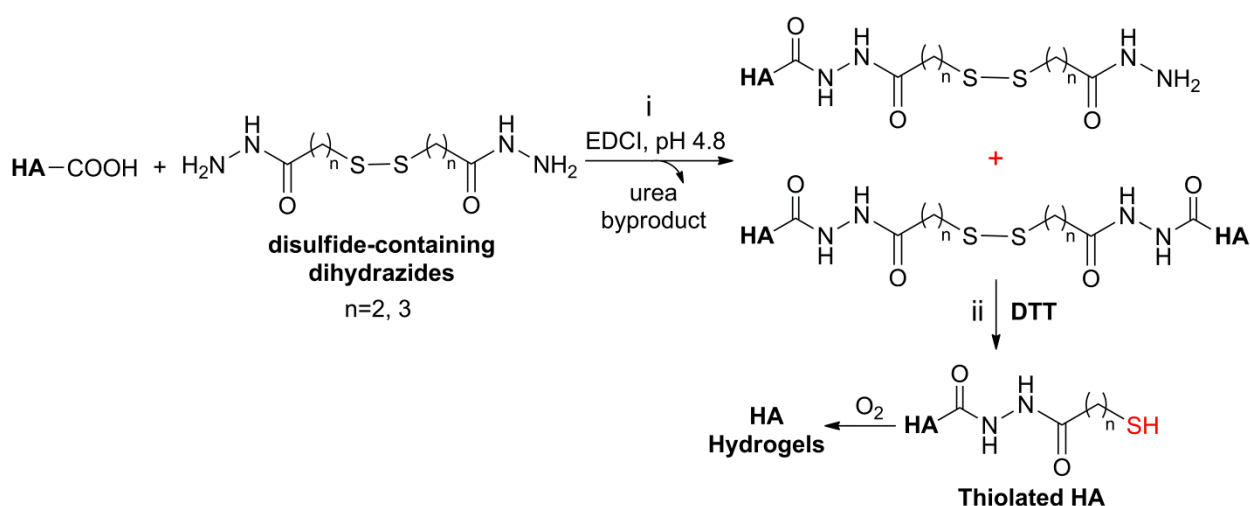


**Figure 63.** Synthesis of thiolated HA through EDCI-coupling (i) and subsequent disulfide-cleavage (ii)<sup>91</sup>: EDCI, 1-Ethyl-3-(3-dimethylaminopropyl)carbodiimide; DTT, dithiolthretol

The sulfhydryl groups on thiolated HA could be oxidized in air to reform disulfide linkages, providing HA hydrogels that could be again reduced into sols with DTT.<sup>91</sup> Since rapid gelation under physiological conditions could be achieved, the authors

demonstrated the feasibility of this hydrogel system for *in situ* cell encapsulation. It was proved that the L929 fibroblasts encapsulated in the HA hydrogel remained viable and proliferative after 3 days of culture *in vitro*.<sup>91</sup>

On the other hand, photopolymerizable HA-derivatives such as HA-MA (Figure 67) were synthesized by reacting either methacrylic anhydride or glycidyl methacrylate with the primary hydroxyl groups in HA.<sup>94, 95</sup> Recently, Burdick and colleagues reported acrylated HA (AHA, DS~38%) with degradable ester linkages (Figure 64) as well as a sequential crosslinking approach.<sup>97</sup> First, 2-hydroxy ethyl acrylate (HEA) was allowed to react with succinic anhydride under the catalysis of 1-Methylimidazole in DCM at 65 °C for 18 h, giving the intermediate (HEA-suc). Second, the carboxyl group of HEA-suc was allowed to react with the hydroxyl group of HA under the catalysis of dimethylaminopyridine (DMAP) and di-tert-butyl dicarbonate (Boc<sub>2</sub>O) in DMSO at 45 °C for 18 h. Importantly, the authors utilized the tetrabutylammonium salt of HA (HA-TBA) to meet the required anhydrous conditions for esterification reactions, given that HA-TBA is well soluble in DMSO.

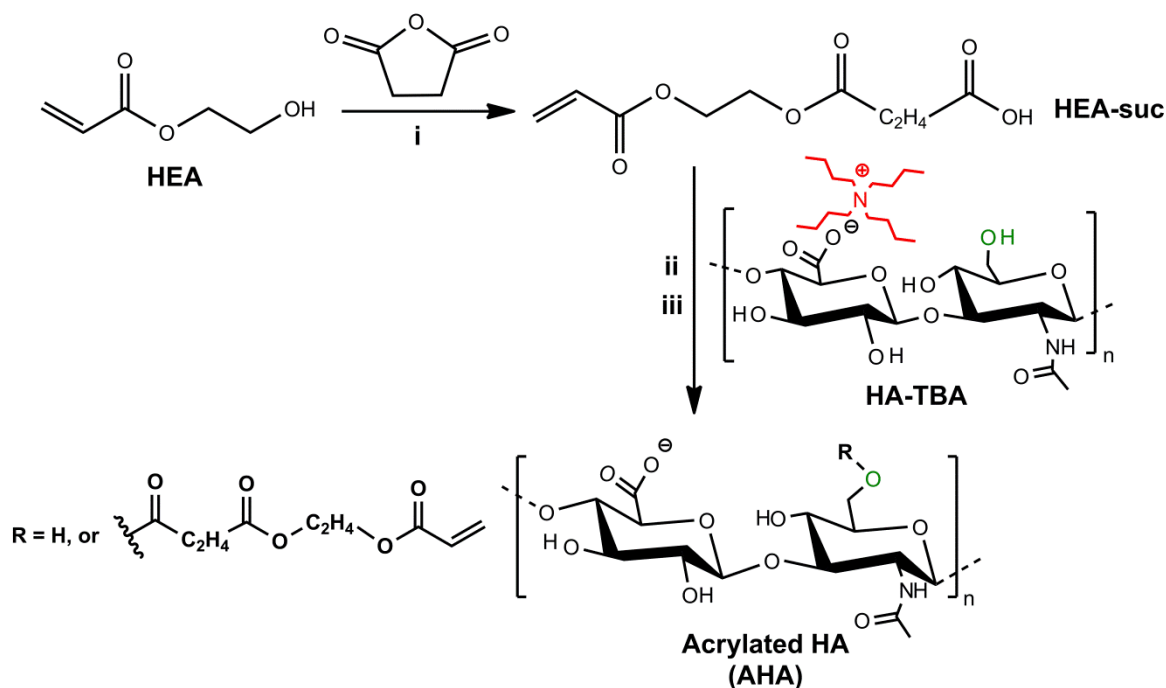


**Figure 64.** Synthesis of acrylated HA (AHA) with hydrolytically degradable linkages<sup>97</sup>: **(i)** anhydrous DCM, 2-hydroxy ethyl acrylate (HEA, 1 eq.), succinic anhydride (1.5 eq.), 1-Methylimidazole (0.06 eq.), N<sub>2</sub> protection, 65 °C, 18 h; **(ii)** anhydrous DMSO, dimethylaminopyridine (DMAP, 0.075 eq.), di-tert-butyl dicarbonate (Boc<sub>2</sub>O, 1.5 eq.), HA-TBA (1 eq. units), N<sub>2</sub> protection, 45 °C, 18 h; **(iii)** dialysis against DI H<sub>2</sub>O for 24 h and lyophilization

In order to render AHA hydrogel bioactive, the authors devised a sequential crosslinking approach (Figure 65). Firstly, both cysteine-containing RGD peptide (GCGYGRGDSPG) and matrix metalloproteinase (MMP)-degradable peptide (GCRDGPQG↓IWGQDRCG) were allowed to react with AHA macromers via Michael-addition, forming soft hydrogels that were cell adhesive and MMP-degradable. Second, remaining acrylate groups on the partially crosslinked gel were further photopolymerized with I2959, providing stiffer gels that blocked cell spreading.

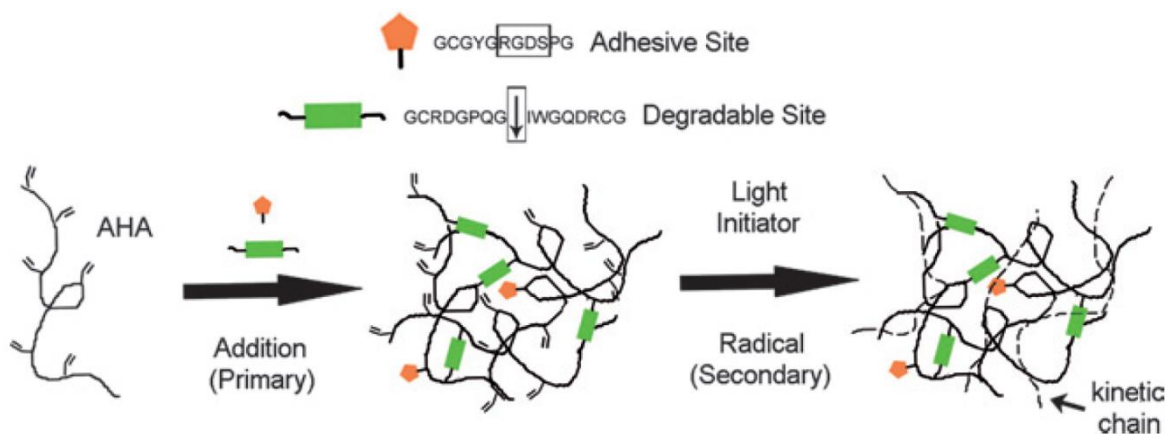


**Figure 65.** Schematic showing sequential crosslinking of AHA using a primary addition reaction and a secondary photocrosslinking reaction (adapted with permission from lit.<sup>97</sup>)

## 2.2 Synthesis of HA-derivatives

### 2.2.1 Preparation of Low MW HA

Native HA are high molecular weight (>1 MDa) macromolecules and often require long dissolution time. Practically, it is hard to prepare a HA solution with a concentration over 3%. For 2PP lithography, the gel crosslinking density needs to be sufficiently high to withstand the developing process and sample transfer. In order to increase the crosslinking density, HA with low molecular weights seems to be better candidates for the purpose of this research. Therefore, in this study low molecular weight HA was selected as the substrates for further modification.

Low molecular weight HA was prepared through acidic degradation (pH=1, 50°C) of high molecular weight HA (1.3 MDa) according to literature.<sup>174</sup> After 24 h degradation, the reaction media was firstly neutralized by adding diluted NaOH and then transferred into a dialysis tube (MWCO: 3.5 kDa). The solution was dialyzed against deionized



water for 24h with several changes of water. So that only selected HA fragments (> 3.5 kDa) were used in further modification. After lyophilization, the molecular weight of these selected HA was evidenced by GPC ( $M_n = 11.4$  kDa, PDI:  $\sim 1.6$ ).

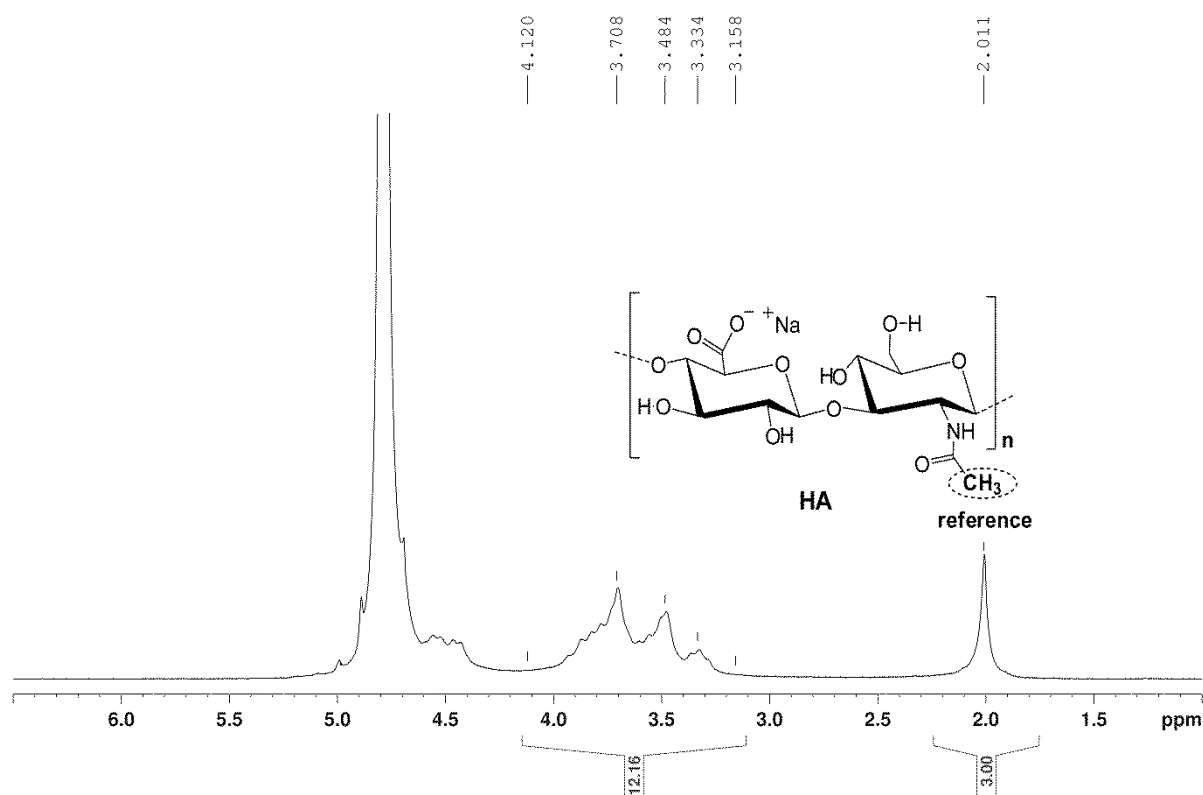


**Figure 66.**  $^1\text{H-NMR}$  spectrum of low molecular weight HA ( $\text{D}_2\text{O}$ ,  $25^\circ\text{C}$ )

As shown in Figure 66, NMR spectrum of low molecular weight HA was measured in  $\text{D}_2\text{O}$ . Well-separated singlet of the acetamide (s, 3H, acetyl) was observed at 2.0 ppm while other non-active protons were located from 3.2 ppm to 4.6 ppm. Importantly, the acetyl protons can be utilized as reference for further quantification of DS of HA derivatives.

### 2.2.2 Synthesis of Hyaluronate Methacrylates (HA-MA)

The HA methacrylates (HA-MA) was prepared as described by Leach and co-workers.<sup>95</sup> Specifically, HA was allowed to react with excessive methacrylic anhydride (10 eq. to HA units) at  $5^\circ\text{C}$  and pH 8.5 for 3 h (Figure 67). During addition of methacrylic anhydride, the reaction media was maintained at pH (8.5-9.0) by simultaneously adding diluted NaOH. It was supposed that primary hydroxyl groups in HA were the major targets towards esterification. In order to remove the unreacted methacrylic anhydride

and/or methacrylic acid, the reaction mixture was neutralized with sodium bicarbonate. The resultant solution was dialyzed against distilled water for 24 h. After lyophilization, HA-MA was obtained as colorless solid in 80 % yield.

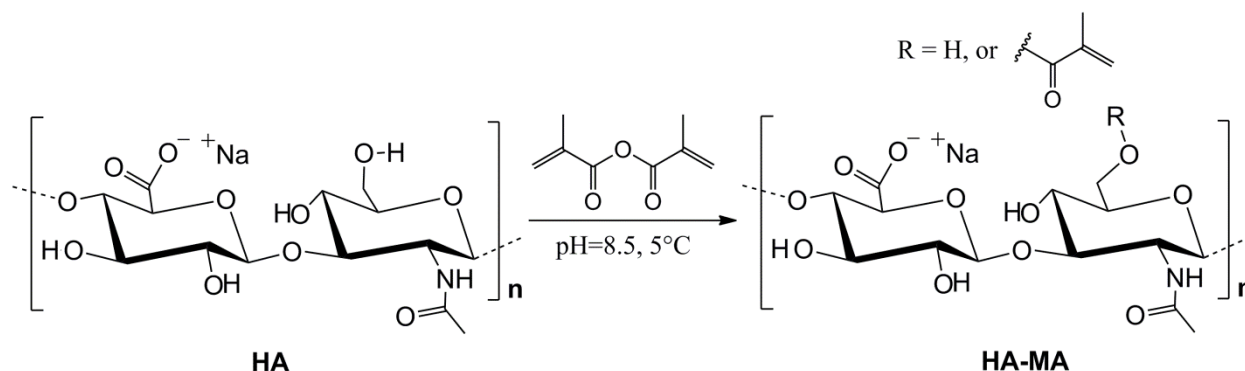


**Figure 67.** Reaction of HA with methacrylic anhydride

To confirm the synthesis, NMR spectrum of the lyophilized product was measured in  $D_2O$  (Figure 68). Characteristic signals of methacrylic groups were found at 5.6 ppm (s, 1H,  $CH_2=C-$ ), 5.3 ppm (s, 1H,  $CH_2=C-$ ) and 1.9 ppm (s, 3H,  $C=C-CH_3$ ). By comparing the peak area of these signals with that of reference signal at 2.0 ppm (s, 3H, acetyl), the DS of HA-MA was determined as 0.57, indicating the presence of approx. 57 acrylic groups per 100 HA repeating units.

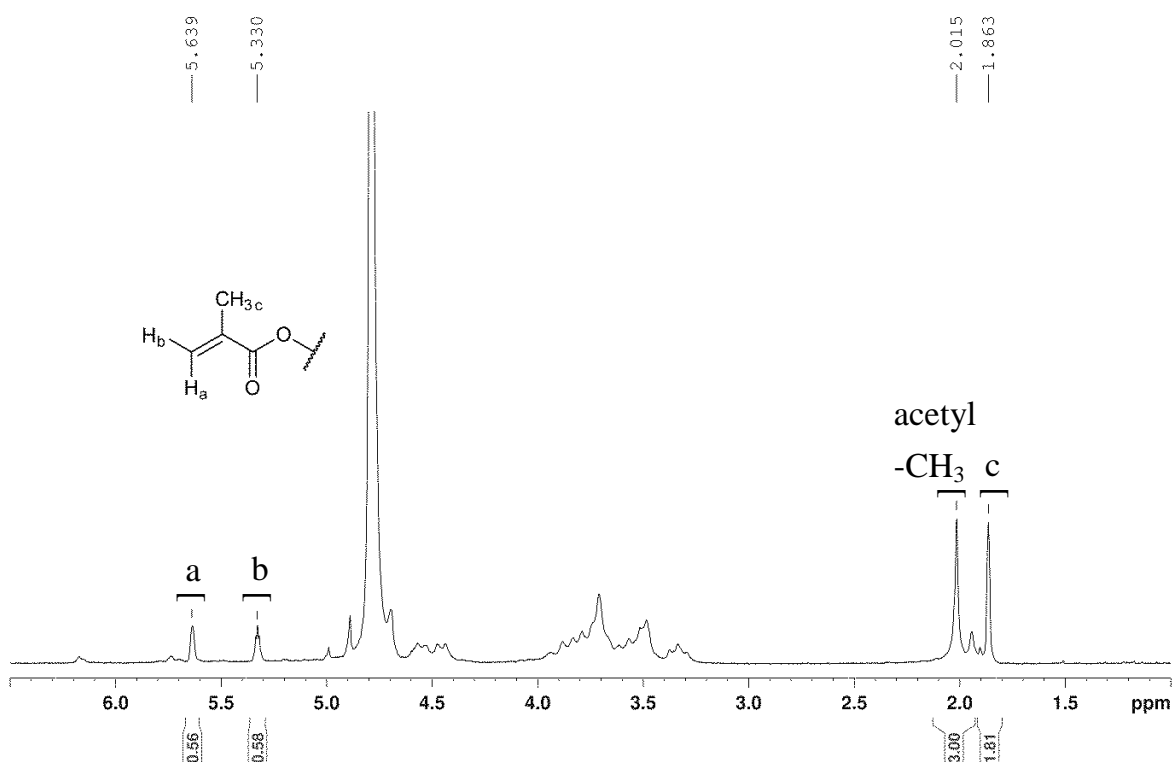


**Figure 68.**  $^1H$ -NMR spectrum of HA-MA ( $D_2O$ )

### 2.2.3 Synthesis of Hyaluronate Acrylates (HA-AC)

The HA acrylates (HA-AC) was synthesized according to a procedure described by Novozyme.<sup>175</sup> HA was allowed to react with a 30-fold excess of acryloyl chloride at 5 °C for 1 h (Figure 69). During addition of acryloyl chloride, the reaction media was maintained at pH (8.5-9.0) by simultaneously adding diluted NaOH. After reaction, the unreacted acryloyl chloride and/or acrylic acid was removed by neutralization with sodium bicarbonate. The resultant solution was purified by dialysis against deionized water for 24 h. After lyophilization, HA-AC was obtained as colorless solid in 85 % yield.

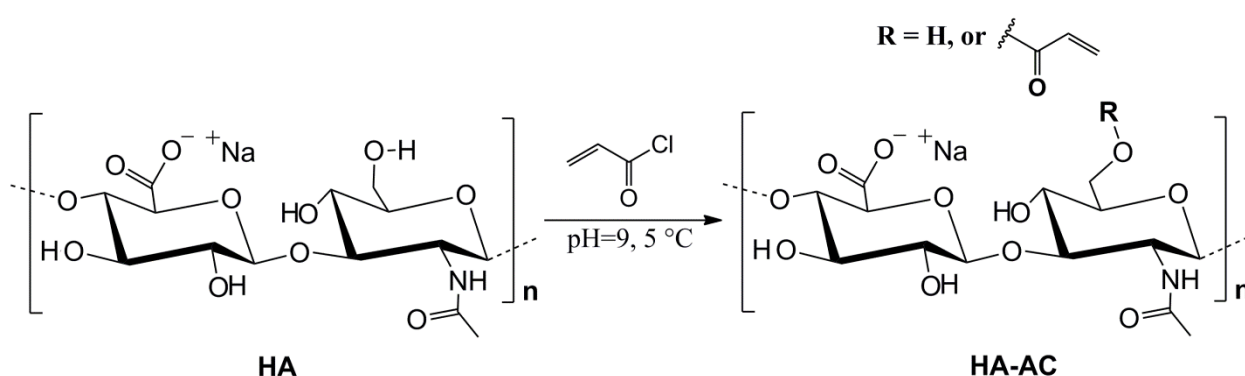


Figure 69. Reaction of HA with acryloyl chloride

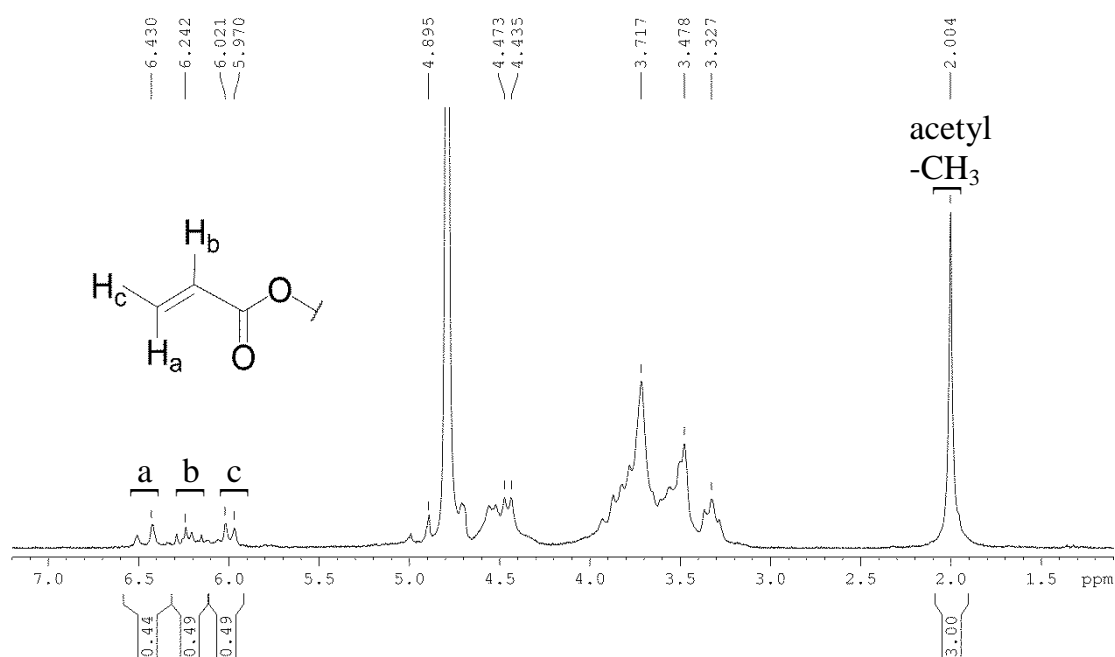
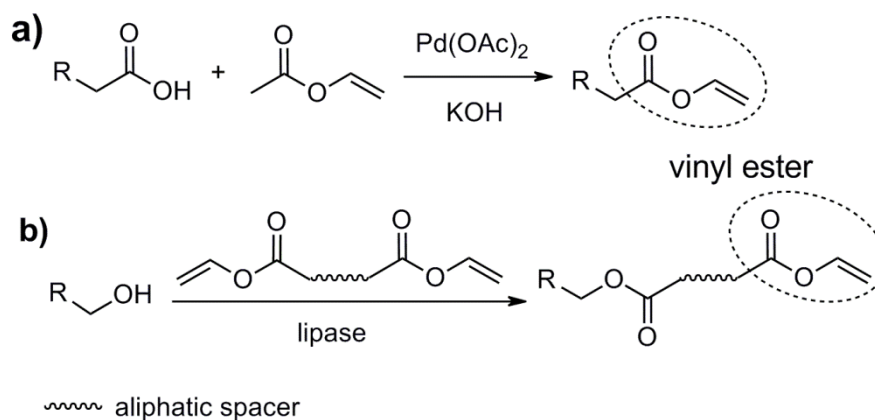


Figure 70. <sup>1</sup>H-NMR spectrum of HA-AC (D<sub>2</sub>O)

As shown in Figure 70, NMR spectrum of the lyophilized product was measured in D<sub>2</sub>O. Characteristic signals corresponding to acrylate groups were observed within 5.9-6.6 ppm. By comparing the peak area of these signals with that of reference signal at 2.0 ppm (s, 3H, acetyl), the DS of HA-MA was determined as 0.49, indicating that approx. 49 acrylic groups were present in 100 HA repeating units.

#### 2.2.4 Synthesis of Hyaluronate Vinyl esters (HA-VE)

Unlike HA-MA and HA-AC, the synthetic route to vinyl ester derivative of HA (HA-VE) remains unknown. To introduce vinyl ester groups onto HA, it is essential to look into available synthetic approaches for vinyl esters (Figure 71).



**Figure 71.** Synthetic routes to vinyl esters

In the thesis research of Dr. Christian Heller (IAS),<sup>176</sup> a variety of vinyl esters have been successfully prepared by reacting diacids with a huge excess of vinyl acetate under the catalysis of Pd(OAc)<sub>2</sub> and powdered KOH. Although HA also has carboxylate groups, this synthetic route seems inappropriate due to the facts that: 1) it is impossible to dissolve HA in vinyl acetate and 2) this method necessitates the use of expensive metal catalysts (i.e., Pd(OAc)<sub>2</sub>) which is highly sensitive to moisture.

Alternatively, vinyl ester group can be indirectly introduced by reacting primary alcohol with divinyl dicarboxylates under the catalysis of lipases. Notably, Lin's group reported the preparation of polymerizable prodrug of cytarabine using this method (Figure 72).<sup>177</sup> In particular, enzymatic regioselectivity in transesterification reactions were demonstrated in this study. For instance, a *Candida antarctica* lipase B (CAL-B) lipase enabled the single step synthesis of 5'-O-acyl cytarabine derivatives in acetone with high

yields while using a subtilisin protease in pyridine afforded the mixtures of 5'-O-acyl and 4-N-acyl cytarabine derivatives.<sup>177</sup> Interestingly, there are both primary and secondary hydroxyl groups available in HA.

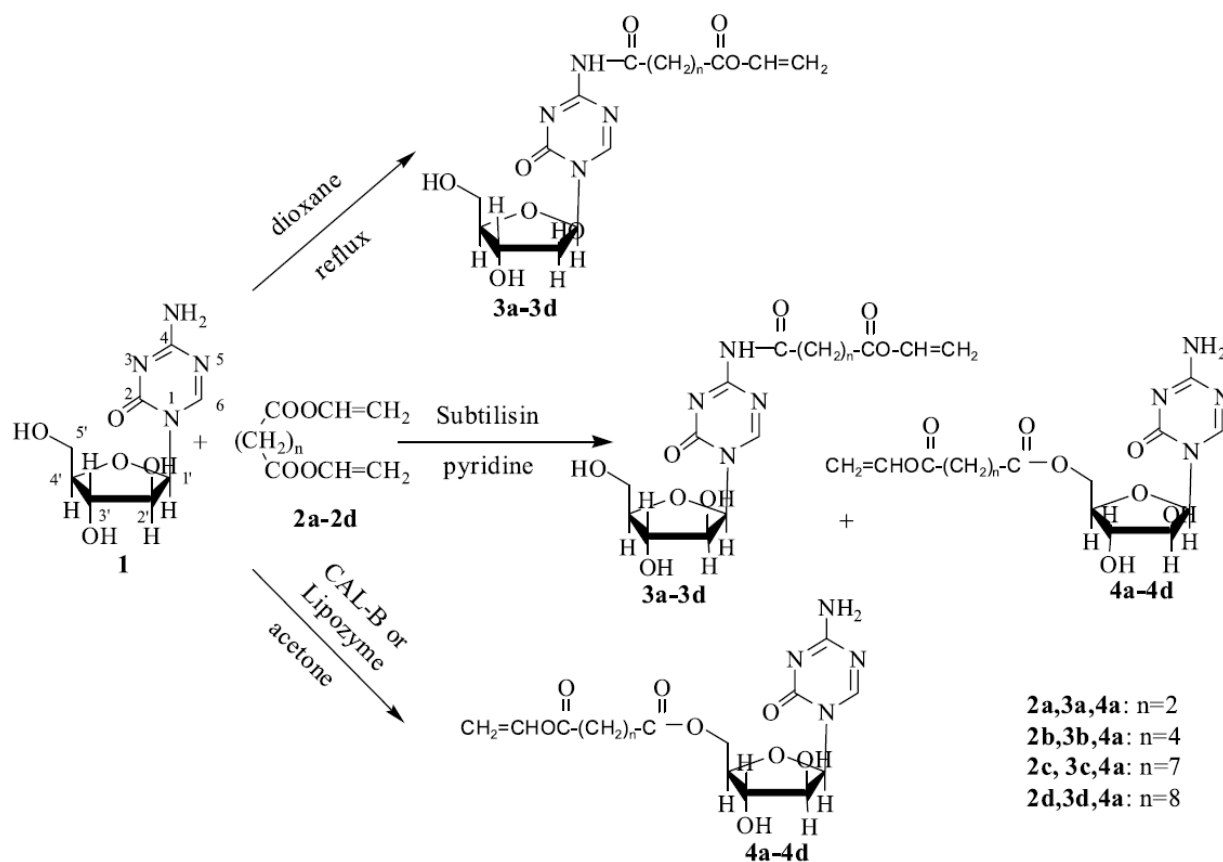


**Figure 72.** Synthesis of 4-N-acyl and 5'-O-acyl cytarabine vinyl esters<sup>177</sup>

With this information in mind, lipase-catalyzed transesterification reaction seems to be a better approach for the synthesis of HA-VE than the former one. Given that divinyladipate (DVA) is one type of divinyl dicarboxylates and commercially available, DVA was selected as the reagent for transesterification reaction with HA. It was supposed that primary hydroxyl groups of HA should primarily react with excessive DVA under the catalysis of CAL-B and give HA-VE as the products.

DVA has been used for the preparation of biodegradable and biocompatible polymers through lipase-catalyzed condensation.<sup>178</sup> As such, it is assumed that the use of DVA would provide an additional degradation mechanism into HA-VE since DVA is prone to hydrolysis.

Although similar lipase-catalyzed reactions have been explored in literature,<sup>177, 179</sup> most work focused on the functionalization of di-saccharides or tri-saccharides with polymerizable moieties. It is accepted that the choice of solvent plays an important role on the reaction efficiency. On one hand, the solvent should render the substrates soluble and provide a homogeneous reaction media; on the other hand, the solvent should be benign to keep the activity of lipases. Wang et al. proved that a mixture of acetone and ionic liquids was an ideal solvent pair for lipase-catalyzed reactions.<sup>177</sup> As such, such a solvent system was attempted to functionalize HA with DVA moieties (Figure 73). However, no substitution was observed, probably due to the limited solubility of HA.

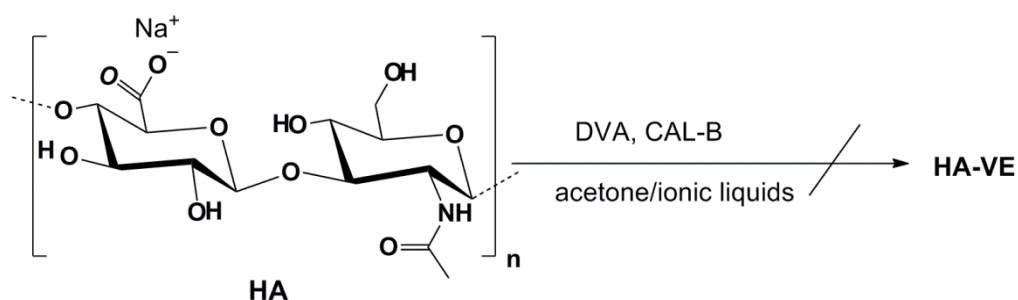


**Figure 73.** The reaction with DVA in acetone and ionic liquids [(BMIM) BF<sub>4</sub>]

In the search for an ideal solvent that permits HA dissolution while being lipase-friendly, previous work related to HA modification was reviewed. Importantly, Khetan and Burdick reported a multistep synthetic procedure where acrylated HA (AHA, Figure 64) was synthesized through esterification of a tetrabutylammonium salt of HA (HA-TBA) in anhydrous DMSO.<sup>97</sup> This work suggests that once the sodium salt of HA is exchanged with the bulky quaternary TBA cation, the HA substrate gets more hydrophobic and consequently soluble in DMSO. Although it was unclear that whether the use of DMSO would destroy the catalytic activity of lipase, it was worthwhile to prepare the HA-TBA salt and then attempt the transesterification reaction in DMSO by reacting HA-TBA with excessive DVA under the catalysis of CAL-B.

#### 2.2.4.1 Preparation of Tetrabutylammonium Salt of HA (HA-TBA)

The HA-TBA salt (Figure 74) was prepared according to Khetan et al.<sup>97</sup> Specifically, sodium salt of HA was firstly dissolved in deionized water and then incubated with strongly acidic ion-exchanger resin. After filtering off the resin, the protonated HA was neutralized to a specific extent (pH=7.02-7.05) by carefully adding tetrabutylammonium

hydroxide (TBA-OH, 20%). Since the side product of this step was only water, the solution was directly lyophilized and analyzed without further purification.

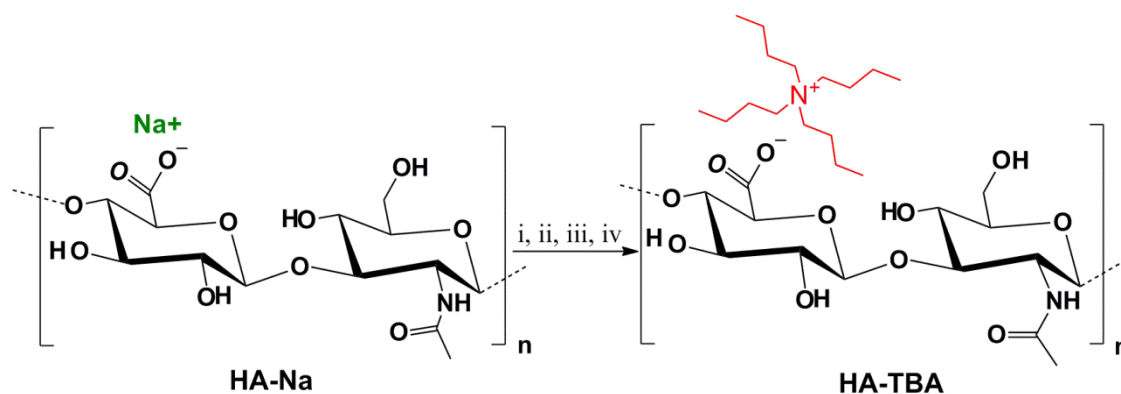


**Figure 74.** Preparation of tetrabutylammonium salt of HA (i: protonation, strongly acidic ion-exchanger resin, 6 h; ii: filtration; iii: neutralization, 20% TBA-OH; iv: lyophilization)

To confirm the preparation, NMR spectrum (Figure 75) of the lyophilized product was measured in  $\text{D}_2\text{O}$ . Characteristic signals corresponding to the TBA cation was evidenced at 3.3 ppm (m, 8H,  $4 \times -\text{CH}_2-\text{N}^+$ ), 1.6 ppm (m, 8H,  $4 \times -\text{CH}_2\text{CH}_2-\text{N}^+$ ), 1.3 ppm (m, 8H,  $4 \times -\text{CH}_2-\text{CH}_3$ ) and 0.9 ppm (m, 12H,  $4 \times -\text{CH}_3$ ).

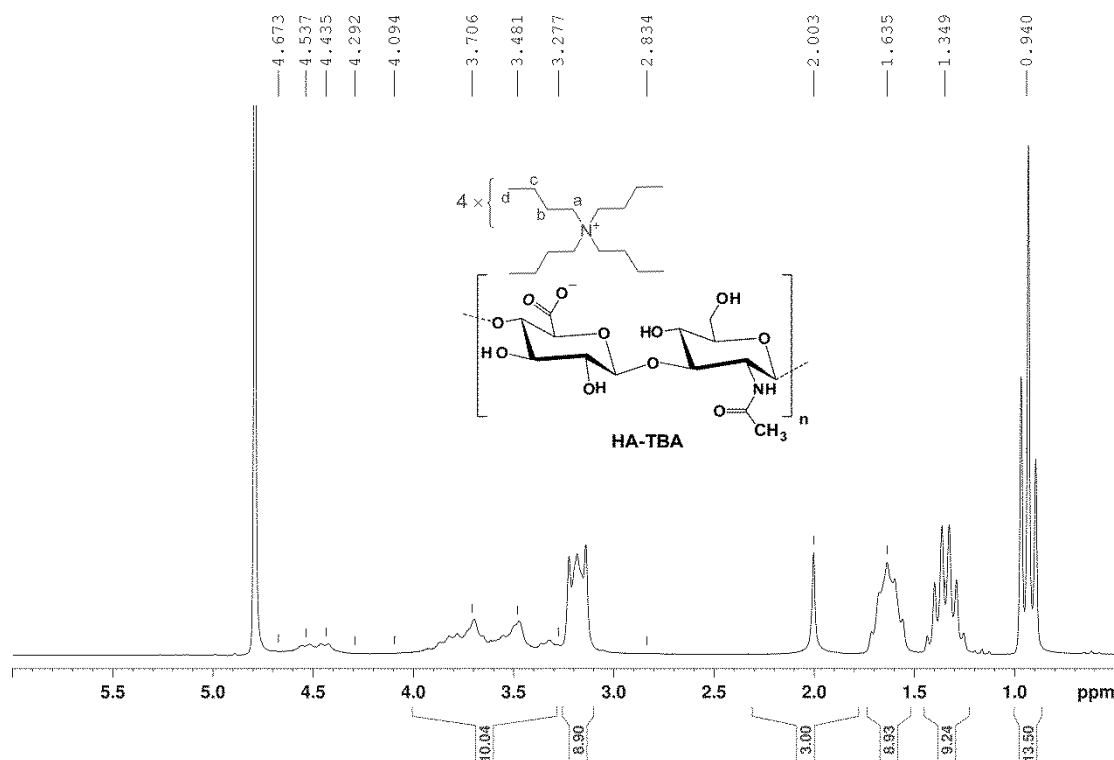


**Figure 75.**  $^1\text{H}$ -NMR spectrum of HA-TBA ( $\text{D}_2\text{O}$ )

### 2.2.4.2 Synthesis of HA-VE

The HA-TBA was allowed to react with excessive DVA (i.e., 5 eq. to HA repeating units) under the catalysis of CAL-B at 50 °C in DMSO. The reaction (Figure 76) was maintained for 24 h under anhydrous conditions in order to avoid the hydrolysis of DVA. Notably, the side product out of this reaction is acetaldehyde (b.p., 20.7 °C) that can be easily removed. After filtering off the lipase resin, the crude products were purified in three steps. First, DMSO was removed by high vacuum distillation in the presence of hydroquinone (1000 ppm). Second, the reaction slurry was purified by liquid-liquid extraction to remove excessive DVA. Third, the TBA cation was exchanged with Na<sup>+</sup> cation through dialysis of the crude product against 100 mM NaCl and subsequent deionized water. As the NaCl dialysis went on, the TBA salt of HA-VE (white) became colorless, indicating the formation of sodium salt of HA-VE which is more hydrophilic than the TBA salt. Although the incorporation of DVA moieties may increase the substrate hydrophobicity, it was found that the HA-VE products possessed good water solubility (max.: ~30%, w/w).

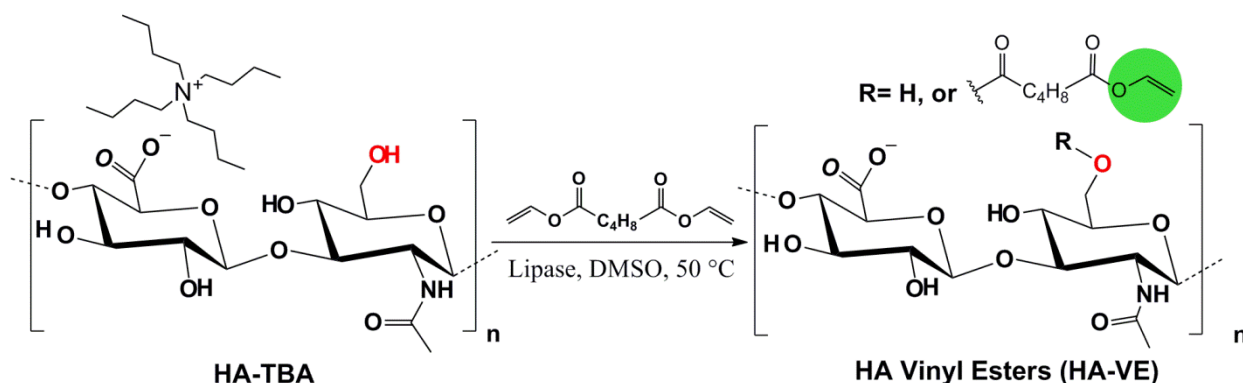


**Figure 76.** Reaction of HA-TBA with DVA

To evaluate the synthesis, comparative NMR spectra of HA and HA-VE were measured in D<sub>2</sub>O. In comparison with HA, the spectrum of HA-VE (Figure 77) showed new peaks at 1.7 (f), 2.52 (e), 4.80-5.03 (b, c) and 7.20 (a) ppm that correlate with the proton signals of DVA. The peak area under acetyl protons of HA at 2.0 ppm was utilized as reference for the determination of DS by calculating its relative ratio to that of the unsaturated proton (a) at 7.20 ppm. The DS of HA-VE was determined as 0.54, showing the presence of approx. 54 vinyl esters per 100 HA units.



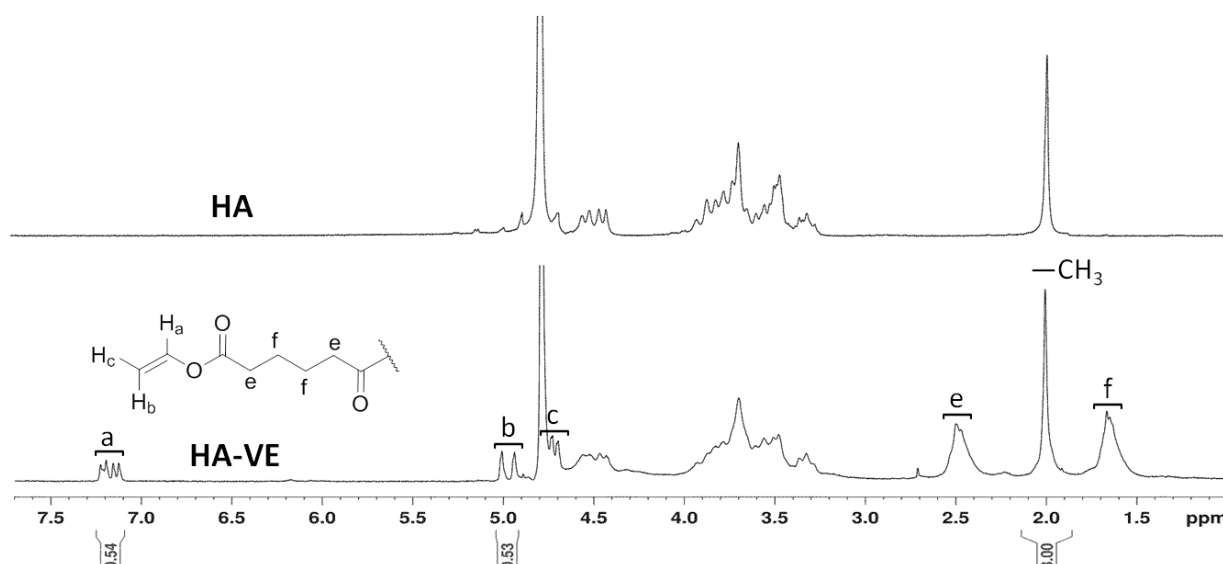


**Figure 77.**  $^1\text{H-NMR}$  spectra of HA and HA-VE ( $\text{D}_2\text{O}$ )

To further confirm the success of synthesis, comparative ATR-FTIR spectra (i.e., HA, DVA and HA-VE) were measured (Figure 78). Spectrum of HA-VE showed characteristic signals of DVA at  $1735\text{ cm}^{-1}$  ( $\text{C}=\text{O}$ ), and  $1640\text{ cm}^{-1}$  ( $\text{C}=\text{C}$ ) in comparison with that of HA. Together, these results proved that the synthesis of HA-VE was successful.

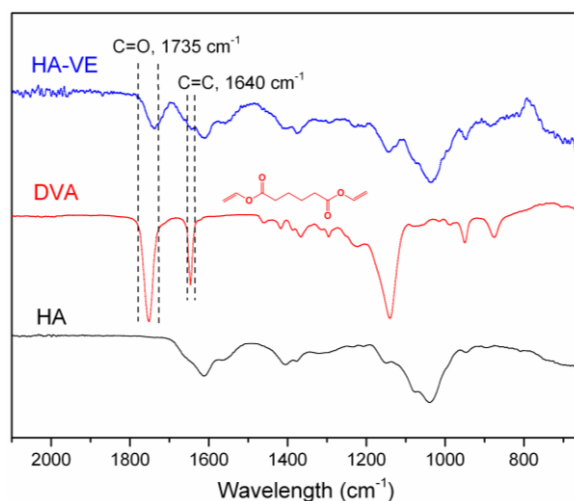


**Figure 78.** Comparative ATR-FTIR spectra of HA, DVA and HA-VE

To test the feasibility of HA-VE with tunable DS, the influence of reaction time and reactants stoichiometry on DS was investigated (Table 11). As the reaction time increased from 24 h to 72 h (Entry 1-3), the DS increased from 0.13 to 0.34. On the other hand, as the stoichiometry increased from 1:1 to 3:1 (Entry 1-6), the DS was raised in varying degree from 0.33 to 1.04. When we prolonged the reaction time to 96 h (Entry 7),

the DS value as high as 1.25 was obtained. This could be explained as the contribution of the secondary hydroxyl groups although in comparison primary hydroxyl groups are thought to be more reactive towards transesterification reactions.

**Table 11.** The influence of reaction time and stoichiometry on DS (\*stoichiometry: the molar ratio between DVA and HA repeating units)

Entry	Stoichiometry *	Reaction Time (h)	DS
1	1:1	24	0.13
2	1:1	48	0.21
3	1:1	72	0.34
4	3:1	24	0.33
5	3:1	48	0.71
6	3:1	72	1.04
7	3:1	96	1.25

### 2.2.5 Synthesis of Thiolated Hyaluronan (HA-SH)

Although disulfide-crosslinked HA hydrogels has been reported in literature,<sup>91</sup> the reported method is relying on the use of disulfide-containing dihydrazides that are not commercial available and difficult to synthesize. Thus, facile approaches for the synthesis of thiolated HA are in demand.

Given that water is the most appropriate solvent for HA, the water-soluble carbodiimide (1-ethyl-3-(3-dimethylaminopropyl)carbodiimide, EDCI) seems to be an 'idea' catalyst to activate carboxyl groups of HA. In 1991, however, Prestwich and co-workers reported that EDCI-mediated coupling of HA to primary amines was not successful.<sup>180</sup> It was found that the reaction of HA and EDCI in the presence of excessive 1,6-diaminohexane did not lead to formation of amide bonds, but N-acylurea. The authors attributed this to the fact that the reactive intermediate (O-acylurea) could rapidly rearrange to a stable N-acylurea adduct (Figure 79).

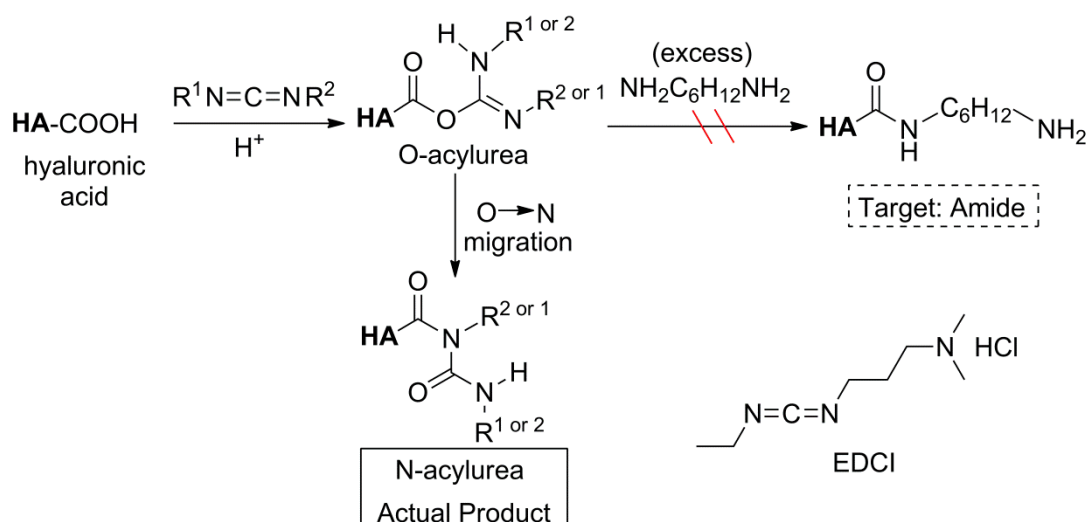


**Figure 79.** Reaction products of HA and EDCI in the presence of excessive 1,6-diaminohexane were N-acylurea (instead of amide)<sup>180</sup>

In a later study by Kafedjiiski et al.,<sup>181</sup> it was proved that the use of N-hydroxysuccinimide (NHS, Figure 80) could provide a non-rearrangeable active ester of HA for effective conjugation with cysteine ethyl ester. The product, HA-cysteine ethylester (HA-Cys), presented lower hydrolysis degree than the unmodified HA. Moreover, *in vivo* studies of HA-Cys gels exhibited improved mucoadhesive properties and prolonged degradation profile owing to the presence of disulfide crosslinks. Importantly, the synthetic approach for HA-Cys is one-step and thus more straightforward than the aforementioned approach (Figure 63) using dihydrazide.

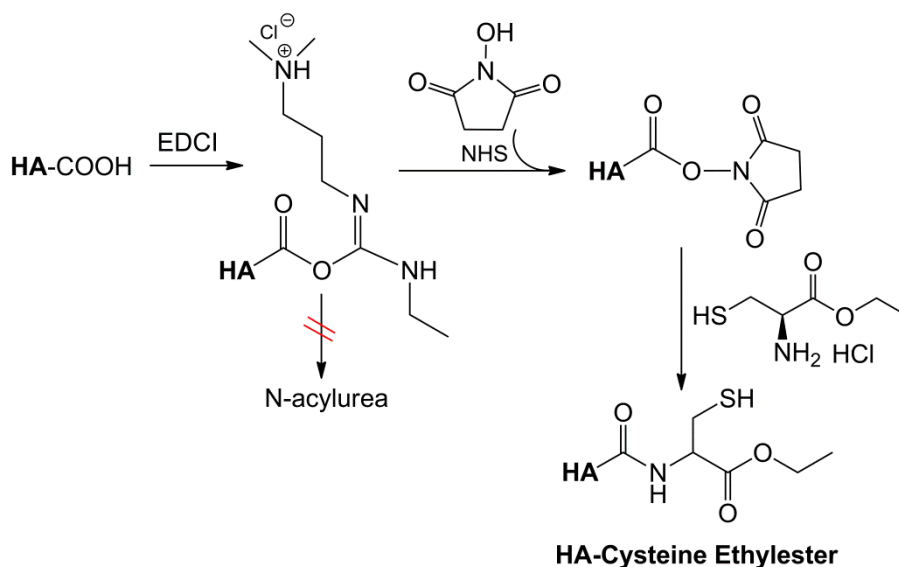


**Figure 80.** Synthesis of HA-cysteine ethyl ester via EDCI/NHS coupling<sup>181</sup>

With these information in mind, the thiolated HA (HA-SH) was prepared in one-step using a dual catalysis system-EDCI/NHS (Figure 81). Activated carboxyl groups of HA were supposed to be reactive with primary amine groups in cysteamine and form amide bonds. Specifically, HA (1 eq.  $-\text{COOH}$ ) was allowed to react with excessive cysteamine (3 eq.) in dilute HCl (pH 6.0) at room temperature for 24 h. Since the thiolated compounds are prone to oxidation and disulfide reformation, the dialysis was performed under acidic conditions (pH=3.0). After lyophilization, HA-SH was obtained as colorless solid in 92 % yield.

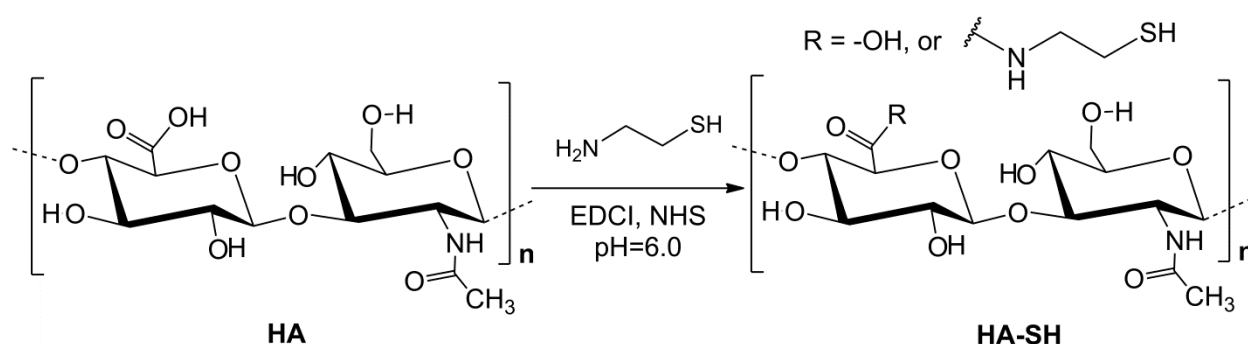


**Figure 81.** Reaction of HA with cysteamine under the catalysis of EDCI and NHS

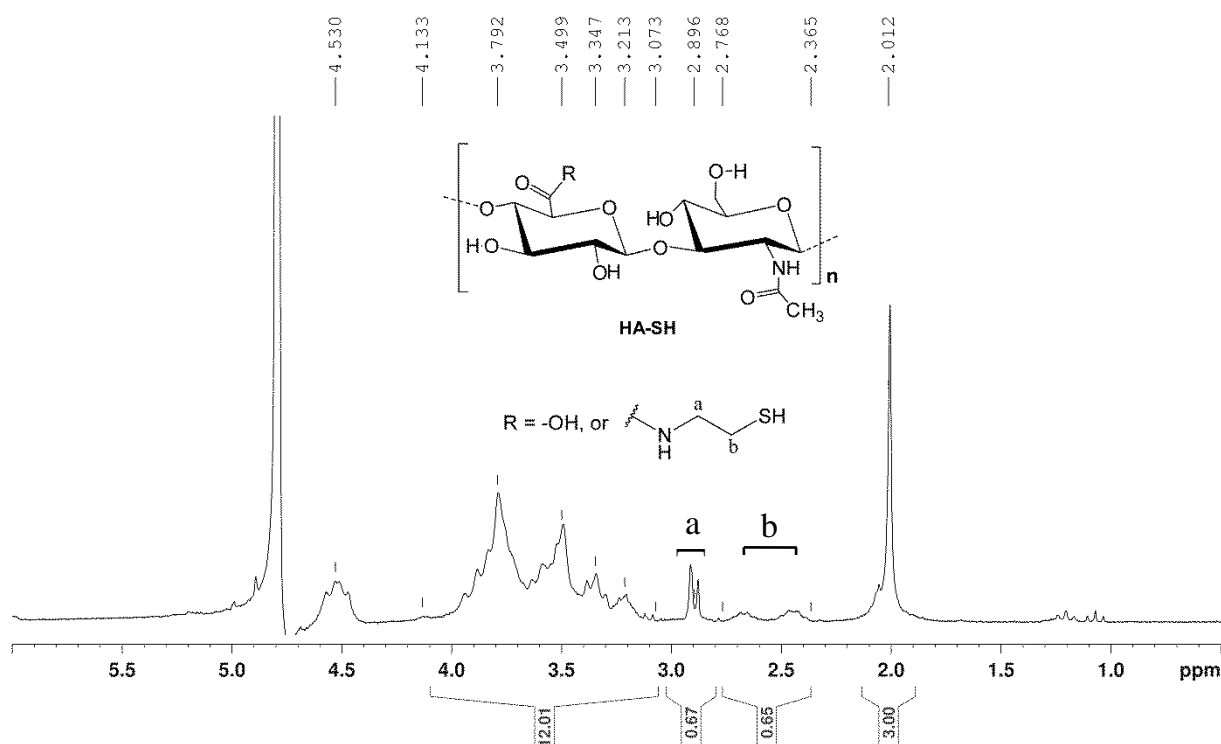


**Figure 82.**  $^1\text{H-NMR}$  spectrum of HA-SH ( $\text{D}_2\text{O}$ )

To confirm the modification, NMR spectrum (Figure 82) of HA-SH was measured in D<sub>2</sub>O. Compared to neat HA, characteristic signals corresponding to cysteamine moieties were observed at 2.9 ppm (m, 2H, NH-CH<sub>2</sub>-) and 2.4-2.8 ppm (m, 2H, -CH<sub>2</sub>-SH). By taking the N-acetyl protons (s, 3H, -CH<sub>3</sub>) at 2.0 ppm as reference, the DS of HA-SH was determined as 0.33, indicating the presence of ~33 sulfhydryl groups per 100 HA units.

## 2.3 Characterization of HA Derivatives

Given that the HA derivatives were successfully synthesized, properties of these macromers and the corresponding hydrogels were characterized from different aspects, including photoreactivity, cytotoxicity, crosslinking efficiency, water uptake and gel stiffness. This work could be divided into two categories:

- 1) Characterization of HA-VE with different DS (section 2.3.1);
- 2) Comparative analysis of HA-VE, HA-AC, and HA-MA with similar DS (section 2.3.2).

### 2.3.1 HA-VE Hydrogels

In order to investigate the influence DS on HA-VE properties, HA-VE macromers with three DS (Table 12) were used as the gel precursors while I2959 (0.5 %) was selected as the photoinitiator for UV photopolymerization. Under light irradiation (320-500 nm), photopolymerization of HA-VE solutions (10% in PBS) were performed either in a PDMS mold for preparing hydrogel pellets, or in a photo-rheometry setting for real-time monitoring the gel formation.

**Table 12.** DS of HA-VE macromers used in this study

HA-VEs	DS
Low	0.13
Middle	0.21
High	0.54

### 2.3.1.1 Photopolymerization

As shown in Figure 83, photoinitiated formation of HA-VE gel networks is depicted. In reality, the appearance of HA-VE gel pellets (Figure 83, right bottom) was slightly yellowish but transparent. It is supposed that the gel formation was based on radical-mediated homopolymerization of vinyl ester groups and subsequent formation of intermolecular crosslinks.

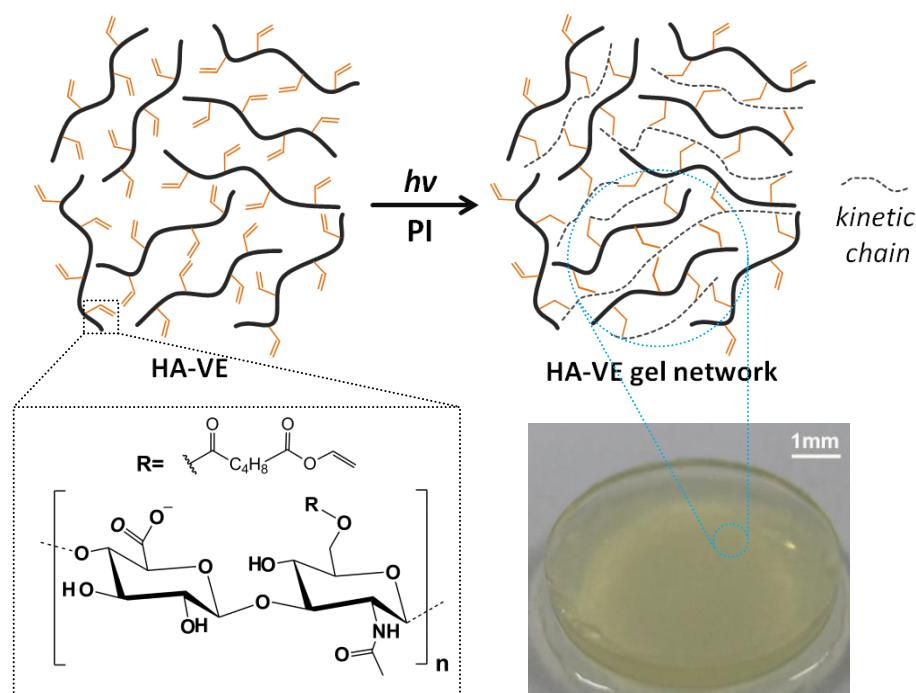


**Figure 83.** Schematics of the hydrogel formation by photopolymerization and a captured image of HA-VE gel pellet (scale bar: 1 mm)

### 2.3.1.2 Influence of DS on Photoreactivity

To test the hypothesis that DS of macromer can influence gel physicochemical properties, HA-VEs with three different DS (0.13, 0.21, and 0.54) were screened using photorheometry at 10% macromer content and 0.5% I2959 concentration in PBS. As shown in Figure 84, the elastic modulus ( $G'$ ) of HA-VE formulations were monitored as a function of UV irradiation time (from 60 s) till a  $G'$ -plateau was observed. As the increase of DS from 0.13, 0.21 to 0.54 (Table 13),  $G'$  was gradually shifted from 11.5 kPa, 23.2 kPa to 36.4 kPa respectively, indicating the increase of network crosslinking density.

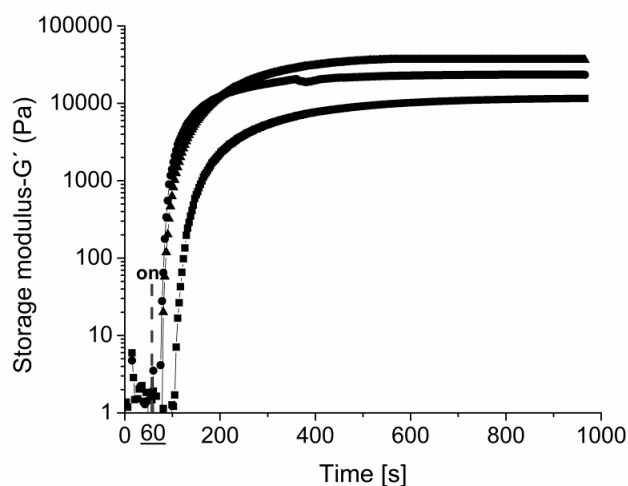


**Figure 84.** Photo-rheometry plots of 10% HA-VE with varying DS: 0.13(■), 0.21 (●), or 0.54 (▲); 0.5 % I2959, 15 mW cm<sup>2</sup>

Furthermore, gel points are defined in the vicinity of the elastic and viscous moduli crossover ( $G'$ ) as described elsewhere.<sup>182</sup> It was found that the gel point was shortened from 95 s to 20 s and 16 s respectively, showing that photoreactivity was improved owing to the increase of VE group concentration. Together, these results suggest that by tuning the DS it is feasible to finely control both photoreactivity and physical properties of HA-VE gel formulations.

**Table 13.** Influence of DS on gel points,  $G'_{\text{plateau}}$  and  $G''_{\text{plateau}}$  values

DS	Gel point (s)	$G'_{\text{plateau}}$ (kPa)	$G''_{\text{plateau}}$ (kPa)
0.15	45	11.5	0.03
0.20	20	23.2	0.1
0.53	16	36.4	3.0

### 2.3.1.3 Influence of Macromer Content on Gel Stiffness

To further prove that mechanical properties of HA-VE hydrogels are physiologically-relevant and comparable to varying soft tissues,<sup>16</sup> the influence of the macromer (HA-VE, DS=0.13) concentration on  $G'$ -plateau values (Figure 85) was investigated. It was found that for 4-10 % HA-VE gels, the  $G'$ -plateau values were located in a broad range from 200 Pa to 12 kPa (Table 14). In addition, as the macromer content decreased from 10 % to 4 %, the gel point was prolonged from 45 s to 123 s gradually, indicating the decreased photoreactivity.

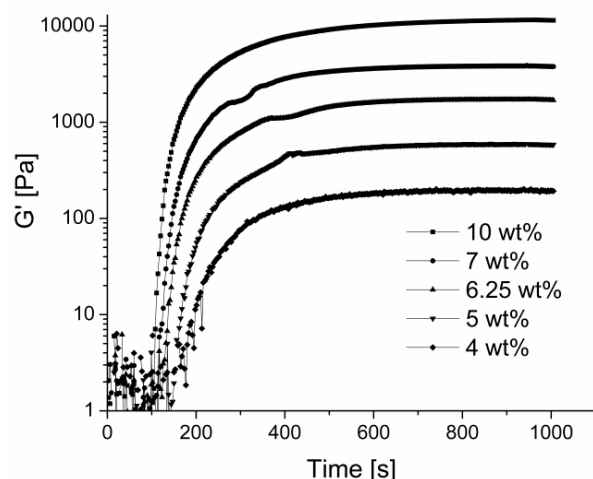


**Figure 85.** Rheometry plots of HA-VE gels formed at varying macromer contents: DS-0.13, 0.5 % I2959, 15 mW cm<sup>2</sup>

**Table 14.** Influence of macromer contents on gel points,  $G'_{\text{plateau}}$ , and  $G''_{\text{plateau}}$  values

wt %	Gel point (s)	$G'_{\text{plateau}}$ (kPa)	$G''_{\text{plateau}}$ (kPa)
10	45	11.5	0.03
7	66	3.8	0.04
6	80	1.7	0.01
5	103	0.6	0.01
4	123	0.2	0.01

### 2.3.1.4 Temporal Control

An unique advantage of photocurable hydrogels is that macromer solutions can be injected into an prescribed area in a minimally invasive surgery and the subsequent curing process can be precisely controlled with light.<sup>183</sup> To prove that HA-VE hydrogels is formed exclusively due to light exposure (i.e., under temporal control), another rheometry measurement of HA-VE was performed (Figure 86) where the UV-light was switched off for 80s at 100s and again at 260s. Without light exposure, negligible modulus change was evidenced by the horizontal plots in the ‘off’ regions.



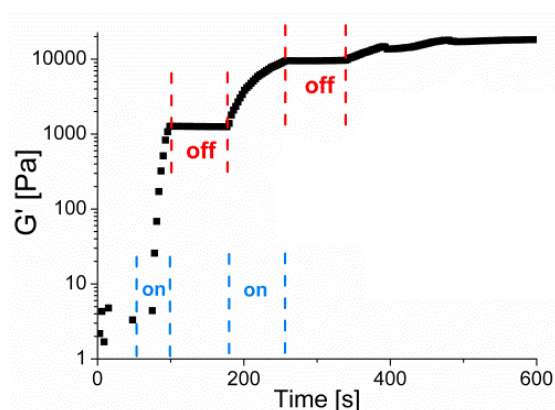


**Figure 86.** A case study showing temporal control on gel formation: 10 % HA-VE, DS=0.13; 0.5 % I2959, 15 mW cm<sup>2</sup>

### 2.3.1.5 Degradation

Another design criterion for a hydrogel system is the ability to be biodegradable (either by enzyme or hydrolysis), which is an important feature for tissue remodeling. Based on an adapted protocol as described by Fairbanks et al.,<sup>54</sup> in-situ rheometry was applied to monitor the enzymatic degradation process (Figure 87) of HA-VE gels upon exposure to varying amount of hyaluronidase (Hase). Both the elastic moduli ( $G'$ ) and loss modulus ( $G''$ ) could be monitored in real time within the degradation process (Figure 87a). It was found that all the elastic moduli ( $G'$ ) decreased exponentially owing to the biochemical response of HA-VE to Hase, which can be explained as the cleavage of linkages between HA repeating units by Hase. Moreover, it is demonstrated that the rate of degradation processes was dose-dependent (Figure 87b).

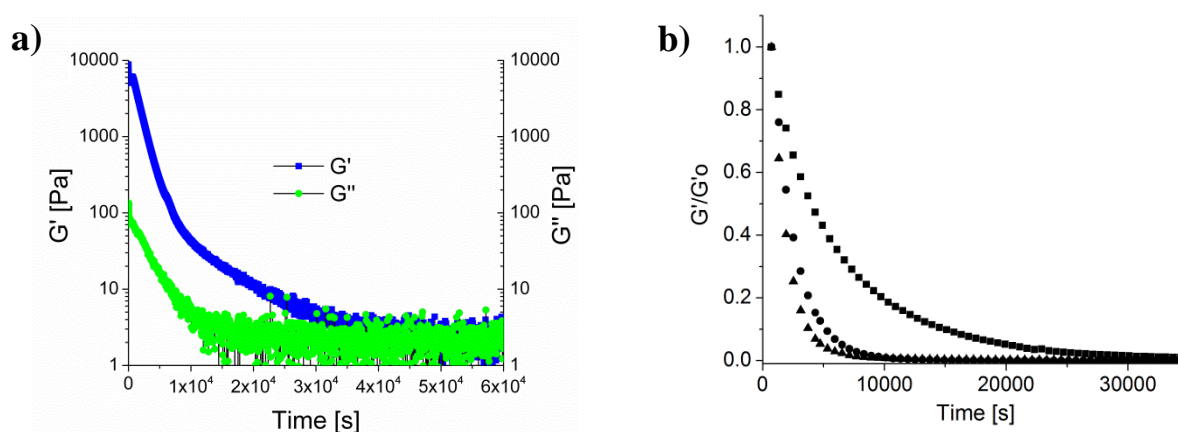


**Figure 87.** in-situ monitoring the degradation process of HA-VE gels (a) and influence of Hase dose (b): 10 (■), 30 (●), or 60 (▲) mg/mL

Alternatively, it is supposed that HA-VE gels are also degradable through hydrolysis. Heller et al. previously studied the in-vitro degradation process of polyVEs in comparison with polylactide (PLA) and poly(meth)acrylates.<sup>184</sup> It was observed that polyVEs degraded ~2 times slower than PLA and much faster (>10 times) than poly(meth)acrylates.

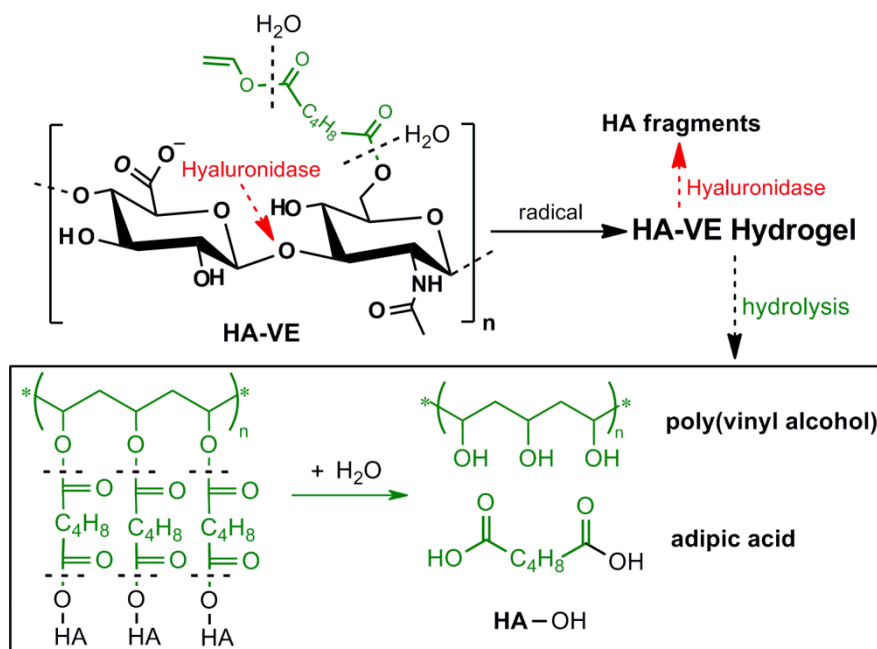


**Figure 88.** Proposed degradation mechanisms of HA-VE hydrogel

Together, the degradation pathways of HA-VE hydrogels are proposed (Figure 88). The degradation products of HA-VE hydrogels should be PVA, adipic acid and HA fragments. It is noteworthy that the toxicity of adipic acid is as low as that of citric acid.<sup>185</sup> These analyses lead to a conclusion that HA-VE hydrogels are biodegradable and generate non-toxic degradation products, making it promising for potential biomedical applications. However, it is challenging to compare *in vitro* and *in vivo* situations. Thus, further investigation into the degradation kinetics under physiological conditions is warranted for clinical applications.

### 2.3.2 Comparative Characterization

Hydrogel properties are largely dependent on the crosslinking density which is further dictated by the macromer chemistry. As shown in Figure 89, the target of this section is to investigate the influence of chemical groups (AC, MA, or VE) on hydrogel properties. Specifically, HA-VE (DS=0.54) was characterized in comparison with two references:

HA-AC (DS=0.49) and HA-MA (DS=0.57). It is supposed that physicochemical properties of these hydrogels could be compared from different aspects: photoreactivity, cytotoxicity, gel stiffness and water-uptake.

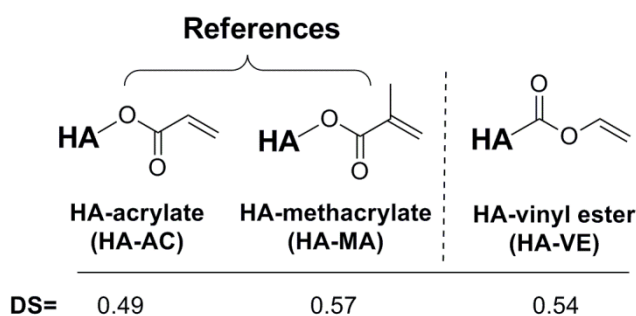


**Figure 89.** Chemical structures of (meth)acrylate and vinyl ester groups and the respective DS

### 2.3.2.1 Cytotoxicity

In order to confirm that HA-VE is less cytotoxic than its (meth)acrylate analogs (Figure 89), cytotoxicity of three macromers on L929 fibroblasts were evaluated using Presto-Blue assay. Initially, the toxic effects of HA substrate was tested at three concentrations (10%, 1% and 0.1%, Figure 90). Surprisingly, it was found a 10% HA solution induced a significant decrease of cell metabolic activity. This can be attributed to the interaction between HA and CD44 receptor on L929. A similar phenomenon has been reported in a recent study where metabolic activity of NIH-3T3 fibroblast was influenced due to the presence of HA.<sup>186</sup> Hence, 1% and 0.1% were used as working concentrations in further toxicity measurements.

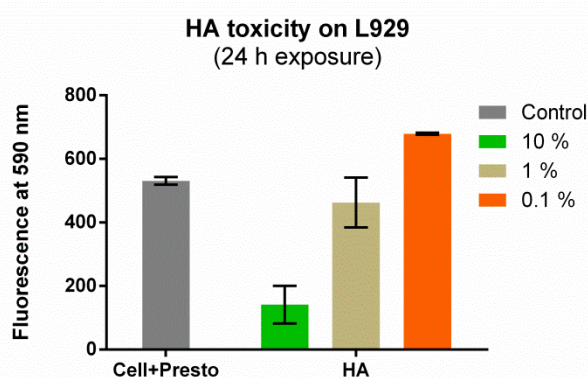


**Figure 90.** Cell metabolic activity influenced by HA macromer concentrations investigated by Presto-blue Assay (mean  $\pm$  SD, n=4)

As shown in Figure 91, the toxicity of HA-VE solution (1%) was significantly lower than that of HA-AC ( $P < 0.01$ , Student T-test) and that of HA-MA ( $P < 0.05$ ). When the

macromer solutions were diluted to 0.1%, no significant differences between the four samples could be observed (data not shown). Together, these data suggest a toxicity order: **HA-AC > HA-MA > HA-VE**.

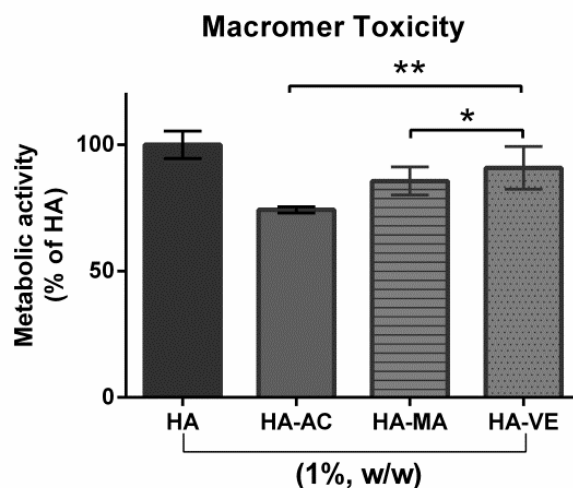


**Figure 91.** Cell viability of four macromer solutions at 1% investigated by Presto-blue Assay (mean  $\pm$  SD, n=4)

### 2.3.2.2 Photoreactivity

The photoreactivity difference among the three macromers (Figure 89) was analyzed using photo-rheometry. To quantify the reactivity, two important parameters of photopolymers were focused: 1) slope value of the plotted  $G'$  curves and 2) induction time. As shown in Figure 92, slope values indicate the respective reactivity follows this order: **HA-AC >> HA-VE > HA-MA**. Notably, homopolymerization rate of HA-VE was at least three times lower when compared to HA-AC.

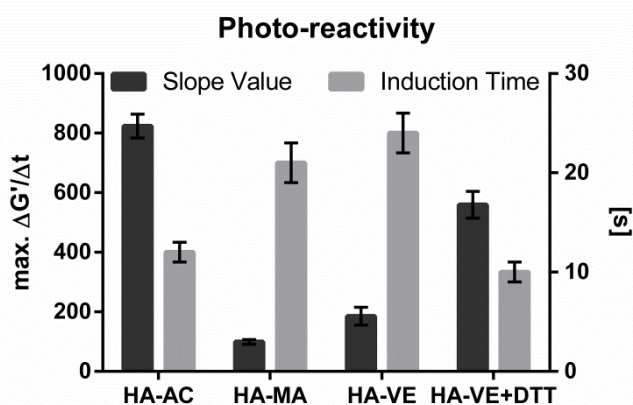


**Figure 92.** Slope values (black) and induction time (grey) of four HA gel formulations: 10% macromer, 0.5 % I2959, 15 mW cm<sup>2</sup>

The reactivity difference can also be evidenced by the differences in induction time where the onset time of HA-VE or HA-MA was nearly the twice relative to that of HA-AC. Furthermore, the lower macromer content limit (Table 15) of HA-AC, HA-MA, and HA-VE to form a gel were tested upon a 15 min UV exposure. Both HA-AC and HA-VE form gels as low as 2.5% whereas the lower limit of HA-MA was 5%, indicating the lower crosslinking efficiency.

**Table 15.** The lower macromer content limit for gel formation

	min. wt%
HA-AC	2.5
HA-MA	5
HA-VE	2.5

### 2.3.2.3 Influence of Thiol-ene Chemistry

Given the limited reactivity of HA-VE towards homopolymerization, thiol-ene chemistry was explored in this study (Figure 94a). It is supposed that the highly efficient chain transfer reactions can be utilized to boost the reactivity of HA-VE.<sup>55</sup> By using photorheometry, the influence of a model compound (dithiothreitol, DTT) on the gelation kinetics of HA-VE was analyzed. It was found that addition of appropriate amount of DTT ( $n_{\text{SH}}:n_{\text{ene}}=0.2-1$ ) can drastically improve the photoreactivity of HA-VE and shorten the time required to reach a  $G'$ -plateau (Figure 93). When DTT was absent, homopolymerization of HA-VE required 52 s to reach the gel point and ~500 s for reaching a  $G'$ -plateau value of 9.2 kPa (Entry 0). When the thiol/ene ratio was increased from 20 % to 100 % by adding varying amount of DTT, the gel point decreased gradually from 39 s to 15 s, indicating a trend of reactivity increase.

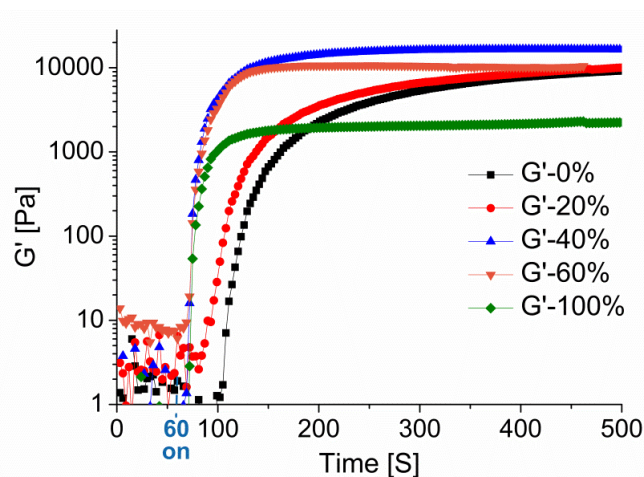


**Figure 93.** Influence of varying amount of DTT on gelation kinetics of HA-VE: 10 % HA-VE, DS-0.15; 0.5 % I2959, 15 mW cm<sup>2</sup>

Although the reactivity was initially increased by DTT, a decline of  $G'$ -plateau value was also observed when the thiol/ene ratio exceeded a certain extent ( $\sim 0.6$ , Table 16). The  $G'$ -plateau value was 16.5 kPa (Entry 2,  $n_{\text{-SH:-ene}}=0.4$ ) whereas it declined to 10.6 kPa (Entry 3,  $n_{\text{-SH:-ene}}=0.6$ ) and 2.3 kPa (Entry 4,  $n_{\text{-SH:-ene}}=1$ ), respectively. Although the gel point showed no significant differences when thiol/ene ratio exceeded 40 % (Entry 2-4), the decrease of  $G'$ -plateau value indicates the decrease of crosslinking density. This could be explained as the interplay between the thiol/ene ratio and polymerization kinetics of HA-VE. When DTT is present, photopolymerization of HA-VE is supposed to proceed in a mix-mode (chain- and step-growth) fashion. These observations are consistent with previous studies related to thiol-ene mix-mode polymerization.<sup>56</sup>

**Table 16.** Influence of thiol/ene ratio on gel points and  $G'$ -/ $G''$ -plateau values

Entry	Ratio -SH:-VE	Stoichiometric ratio	Gel Point (s)	$G'$ -plateau (kPa)	$G''$ -plateau (kPa)
0	0:1	0	52	9.2	0.03
1	1:5	0.2	39	9.9	0.05
2	2:5	0.4	13	16.5	0.03
3	3:5	0.6	16	10.6	0.05
4	1:1	1	15	2.3	0.07

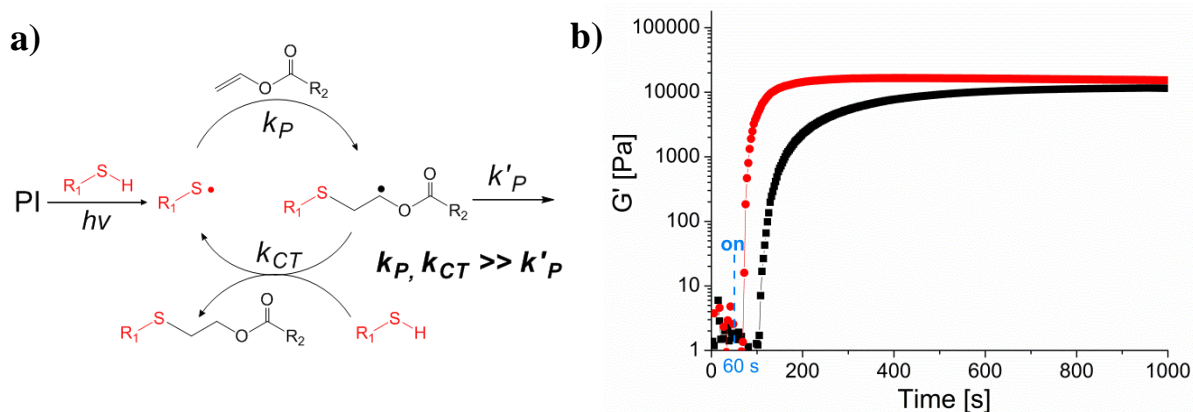


**Figure 94.** Proposed mechanism of photoinitiated thiol-vinyl ester chemistry (a) and plotted  $G'$  curves of HA-VE formulations (b): HA-VE only (■) versus the optimal HA-VE/DTT formulation (●),  $n_{SH}:n_{ene}=0.4$ ; 10 % HA-VE, DS-0.15; 0.5 % I2959, 15 mW cm<sup>2</sup>

To ensure fast gelation (short gel point) while maintaining the gel modulus, an optimal HA-VE/DTT formulation (Figure 94b,  $n_{SH}:n_{ene}=0.4$ ) was selected for 2PP microfabrication. It is To prove whether the reactivity of this formulation was comparable to that of HA-AC, further analysis (Figure 92) showed that the slope value increased from 180 to 570 (800 for HA-AC) while the induction time was shortened from 24 s to 9 s (11 s for HA-AC).

### 2.3.2.4 Swelling Test

Swelling behavior is a characteristic feature of hydrogels and important for one to target specific applications. The swelling ratio can give a good indication of the network structure: i.e., the higher swelling ratio, the looser gel network. The equilibrium mass swelling ratio of HA-AC, HA-MA, and HA-VE gels with varying macromer contents (Figure 95) were screened. Equilibrium mass swelling ratio ( $Q_m$ ) of HA-VE gels was around 45 (2.5%), 20 (5%) and 10 (10%), respectively. These values are comparable to those of HA-AC gels, showing similar network structures and final macromer conversion. In comparison, HA-MA gels present much higher  $Q_m$  values of 50 (5%) and 25 (10%). Together, the observed differences in  $Q_m$  values not only reflects the varying network structures, but in turn implies the influences of macromer reactivity and crosslinking efficiency.

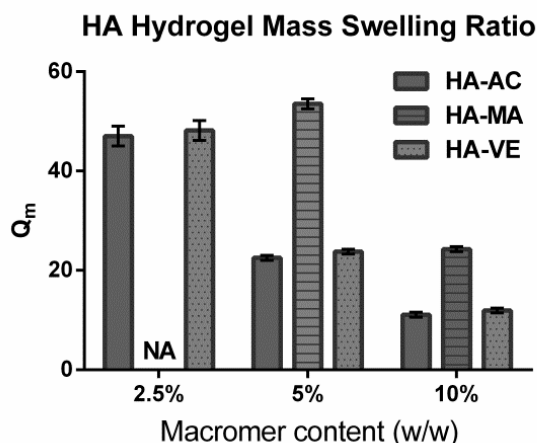


**Figure 95.** HA hydrogel mass swelling ratio at varying macromer contents (2.5%, 5%, 10%), NA: not applicable

### 2.3.2.5 AFM Modulus Test

Given that rheometry is limited to measure gel modulus at the bulk scale whereas cells respond to local forces at the micro- and nanoscale level,<sup>187-189</sup> the Young's modulus of HA gels were measured by nanoindentation using atomic force microscopy (AFM). The AFM test was made possible under the assistance of Drs. Enrico Klotzsch and Birgit Plochberger from the lab of Prof. Gerhard Schütz located in the Institute of Applied Physics (TU Wien). Prior to AFM test, hydrogel samples were UV-polymerized on top of methacrylated glass slides and then soaked in H<sub>2</sub>O for 24 h. Since HA-MA gels formed at 5% were too sticky to be measured, hydrogel samples were measured at 10% macromer content. Comparison in Young's modulus values (Figure 96) suggests a gel elasticity order: **HA-AC** > **HA-VE** > **HA-MA**, consistent with the swelling ratio values (Figure 95).

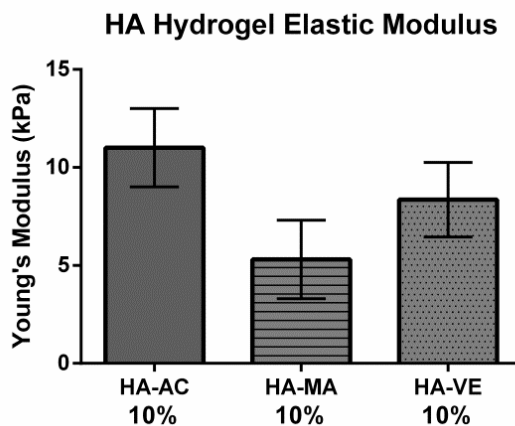


**Figure 96.** Young's modulus values of HA gels formed at 10%



Interestingly, the network density difference of HA-AC and HA-VE gels is less significant than the reactivity difference of corresponding macromers. This is attributed to the unique polymerization kinetics of VEs which was previously demonstrated by Heller and Liska: i.e., VEs undergo homopolymerization at a much lower rate relative to that of acrylates analogs but finally achieve a comparable conversion.<sup>184</sup>

## 2.4 2PP Microfabrication

Based on one-photon characteristics of HA-VE gels, 2PP microfabrication of HA-VE gels (10%) was attempted using an efficient two-photon initiator (2.2 mM P2CK, Figure 97) which was developed by Dr. Zhiqian Li at the IAS institute. Preliminary fabrication was performed by Jan Torgersen while the later trials were made by Peter Gruber. However, the initial structuring did not succeed even at the maximum laser dosage (>200 mW). This should be addressed to the limited reactivity of HA-VE towards homopolymerization.

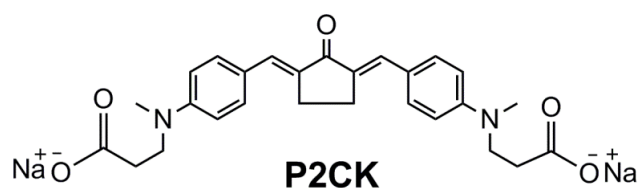


**Figure 97.** Chemical structure of P2CK (two-photon cross section: 176 GM at 800 nm)<sup>37</sup>

Based on the success of thiol-ene photo-rheometry, an optimal formulation (20% HA-VE+DTT,  $n_{\text{SH}}:n_{\text{ene}}=0.4$ , 2.23 mM P2CK) was prepared. By scanning the laser beam (Figure 98a) inside this formulation with high water content (80%), a complex hydrogel construct (Figure 98b) was directly built up in 3D according to a computer-aided-design. After developing the sample in PBS, the gel construct was visualized by a confocal laser scanning microscope. The spatial feature size of this construct is around 4  $\mu\text{m}$ , which is an intriguing size scale for a wide range of biological relevant studies.

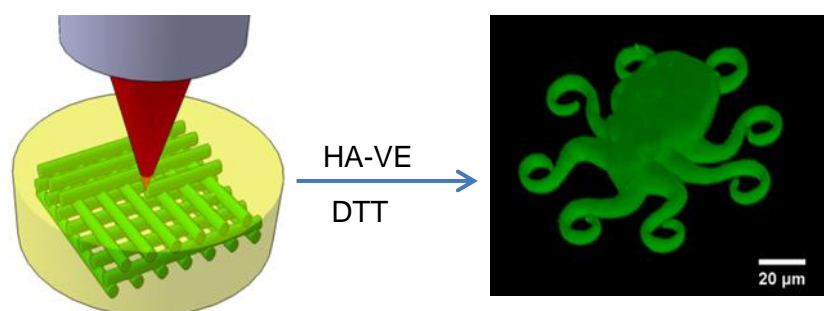


**Figure 98.** 2PP microfabrication of a 3D hydrogel construct: schematic showing the 2PP setup (**left**) and stacked laser scanning microscope image of the gel construct after developing (**right**); 10% HA-VE, DS=0.54,  $n_{\text{SH}}:n_{\text{ene}}=0.4$ , scale bar: 20  $\mu\text{m}$

The robustness of thiol-VE reactions enabled the access to a broad processing window. Arrays of cubic structures were screened at varying scanning speeds and laser powers. As shown in Figure 99, writing speed as high as 56 mm/s was accessible, providing the feasibility of 2PP processing within a clinical relevant time. Meanwhile, the formulation is processable at laser power as low as 20 mW. At this level, photo-induced cellular damage is supposed to be minimal. Also, the size variance in the gel structures provides a good indication of how spatiotemporal control of photon density influences the gel crosslinking density and the resultant volumetric swelling ratio. Together, these results suggest that HA-VE holds great potentials for high-throughput 2PP lithography of 3D hydrogels.

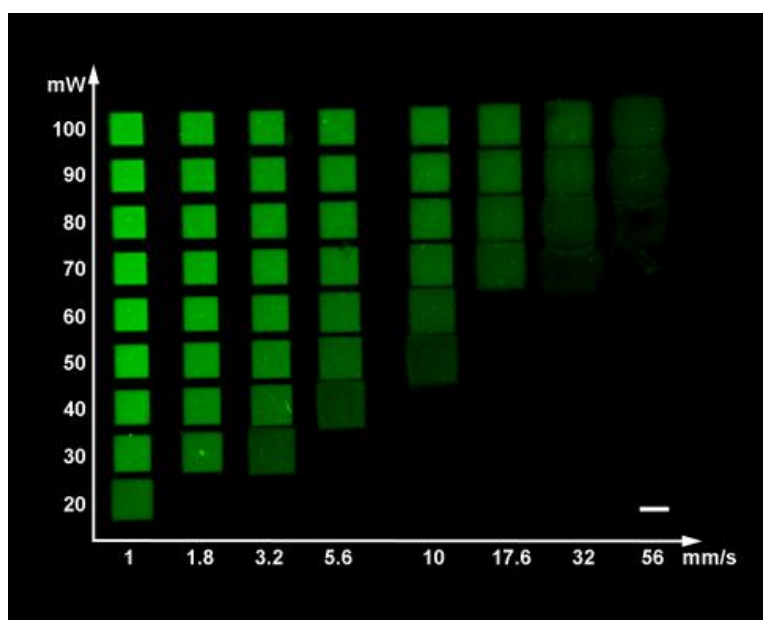


**Figure 99.** 2PP processing window of a HA-VE/DTT formulation (10% HA-VE, DS=0.54, 2.23 mM P2CK,  $n_{\text{SH}}:n_{\text{ene}}=0.4$ , scale bar: 50  $\mu\text{m}$ )

## 2.5 Engineering Cell Adhesion

Although HA-VE presented low cytotoxicity and capability for one- and two-photon polymerization, bioactivity of HA-VE gels was unknown. Generally, it is accepted that HA is not cell adhesive and even resistant with cell attachment due to its anionic nature. Given that cell adhesion plays a critical role in regulating other cell functions, this section is focused on the design of engineering approaches for optimizing the bioactivity of HA-VE gels.

### 2.5.1 Preliminary Cell Top-seeding

In order to test whether cells could adapt themselves on HA-VE gels, preliminary top-seeding of MG 63 cells on gel pellets were carried out. This part of work was performed by Severin Mühleder (LBI-Trauma). Specifically, MG 63 cells were loaded on the top of HA-VE gels with varying DS (Figure 100, a-c) or with DTT (d). After 6 h incubation, the cells were stained using a live (green)-dead (red) kit and visualized using a fluorescent microscope.

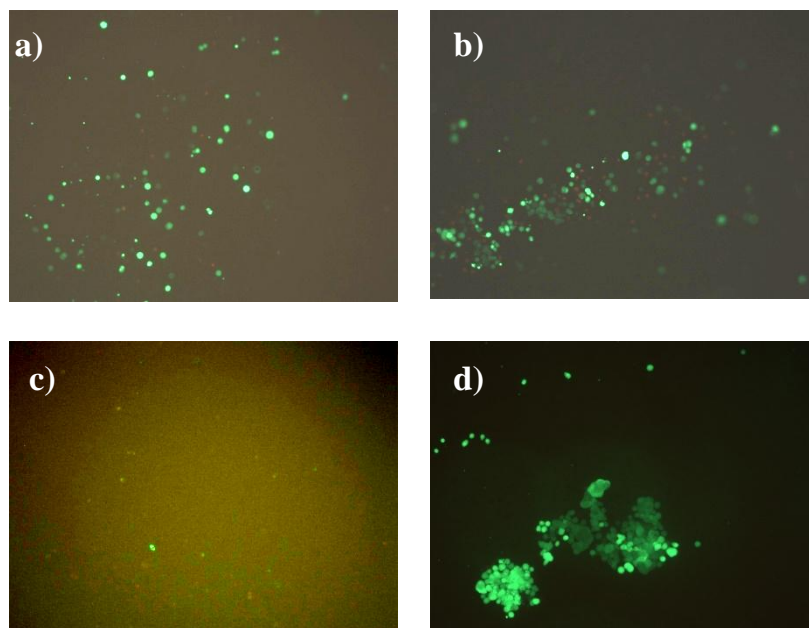


**Figure 100.** MG 63 cell top-seeding on UV-polymerized HA-VE pellets: DS=0.13 (a), 0.21 (b), 0.54 (c) and HA-VE+DTT (d, DS=0.13,  $n_{SH}:n_{enc}=0.4$ )

As shown in Figure 100a-b, as the DS increased from 0.13 to 0.21, the cell distribution became denser. This is due to the increased crosslinking density. When the DS was 0.54

(Figure 100c), the gel background was too poor to be visualized, presumably owing to the increased hydrophobicity of macromer. Notably, the thiol-ene photopolymerized gel (Figure 100d) provided the highest cell viability (>98%) in comparison with the homopolymerized gels. In all cases, however, the cells remain round-shaped, indicating the absence of cell attachment.

## 2.5.2 A Photopatterning Approach

In natural situations, cell attachment is regulated by the crosstalk (Figure 101a) between the integrin receptor on cell surfaces and adhesive ligands (e.g., fibronectin) distributed in the ECM. Interestingly, several cell-adhesive ECM components share the same functional domain which is a tripeptide sequence (Figure 101b, Arg-Gly-Asp, RGD). In the biomaterials community, RGD-relevant peptides have been widely used for building up cell-biomaterial interactions.<sup>190</sup>

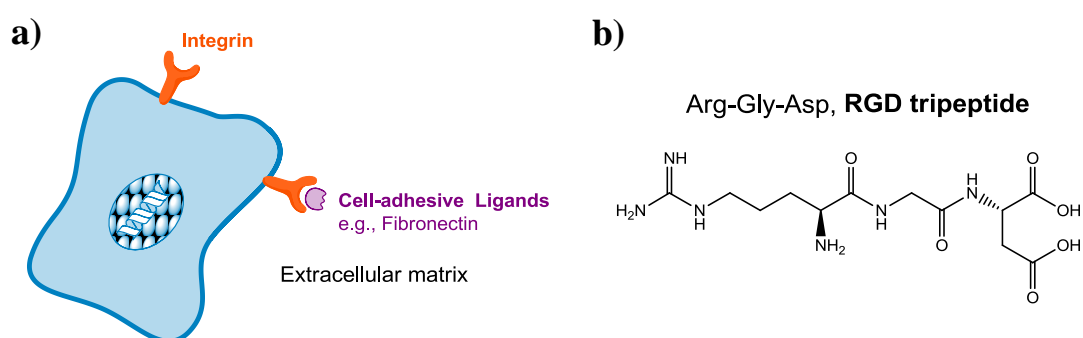


**Figure 101.** Schematics of cell attachment through integrin-binding (a) and chemical structure of the fibronectin domain (RGD motif) for integrin binding (b)

A series of recent work has proved the feasibility to engineer a cysteine residue into the RGD sequence.<sup>28, 145</sup> The cysteine residue allows for further conjugation with several alkene groups including maleimide and acrylate under Michael-addition conditions. Nevertheless, biofunctionalization of hydrogels using thiol-vinyl ester conjugation remains unpublished. Previous work on HA-VE gels proved the robustness of photoinitiated thiol-vinyl ester reactions.

Given that there should be unreacted vinyl ester groups on HA-VE gels, a sequential approach was devised for photopatterning of cell-adhesive RGD peptides. As shown in Figure 102, the first step of this approach is to prepare a HA-VE gel pellet by UV-

photopolymerization. Second, the gel pellet is soaked in a solution consisting of cysteine-containing RGD peptide and photoinitiator. Third, the pellet is allowed to be photopatterned using a photomask. Since it is well known that hydrogels are transparent to near-IR beam, it is reasonable to apply the same chemistry (Figure 102a) but with different light wavelength to realize the spatiotemporal control in 3D. It is hypothesized that two-photon patterning of cell-adhesive ligands could be realized in 3D within HA-VE gels, allowing precise engineering of cell adhesion.

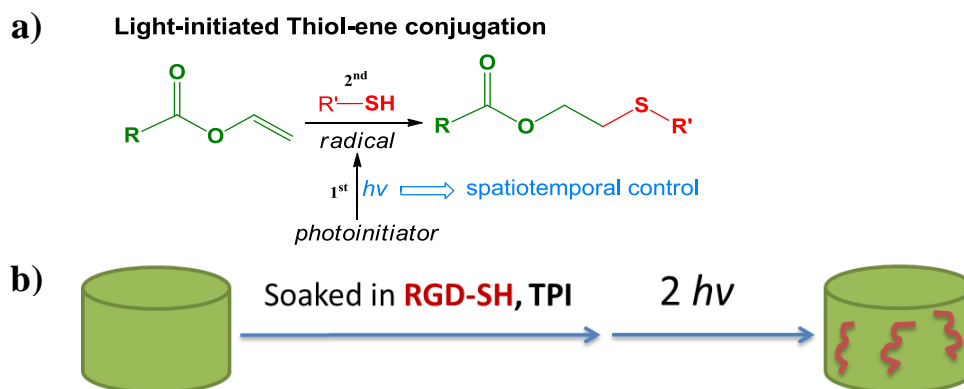


**Figure 102.** Mechanism of photoinitiated thiol-ene conjugation (**a**) and schematic showing the photopatterning approach (**b**)

### 2.5.3 Model One-photon Patterning

In order to test the hypothesis, one-photon model patterning was firstly performed. Specifically, I2959 was used as the photoinitiator. Thiolated fluorescein (Flu-SH, Figure 103) was used as the model reagent of cysteine-containing RGD peptides. The use of this compound would visualize the photopatterning process. The precursor of this compound (Acetyl Flu-SH) was developed by Patrick Knack at the IAS institute.

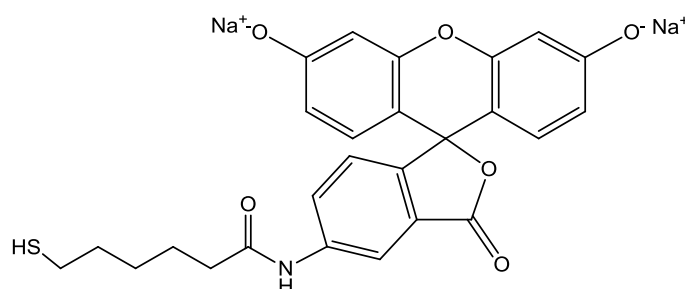


**Figure 103.** Chemical structure of thiolated fluorescein

As shown in Figure 104a, the photopatterning protocol was depicted. A lab-made 'TU-Wien' logo was used as the photomask. After developing the sample in PBS, it was found that the logo pattern was successfully patterned on the HA-VE gel.

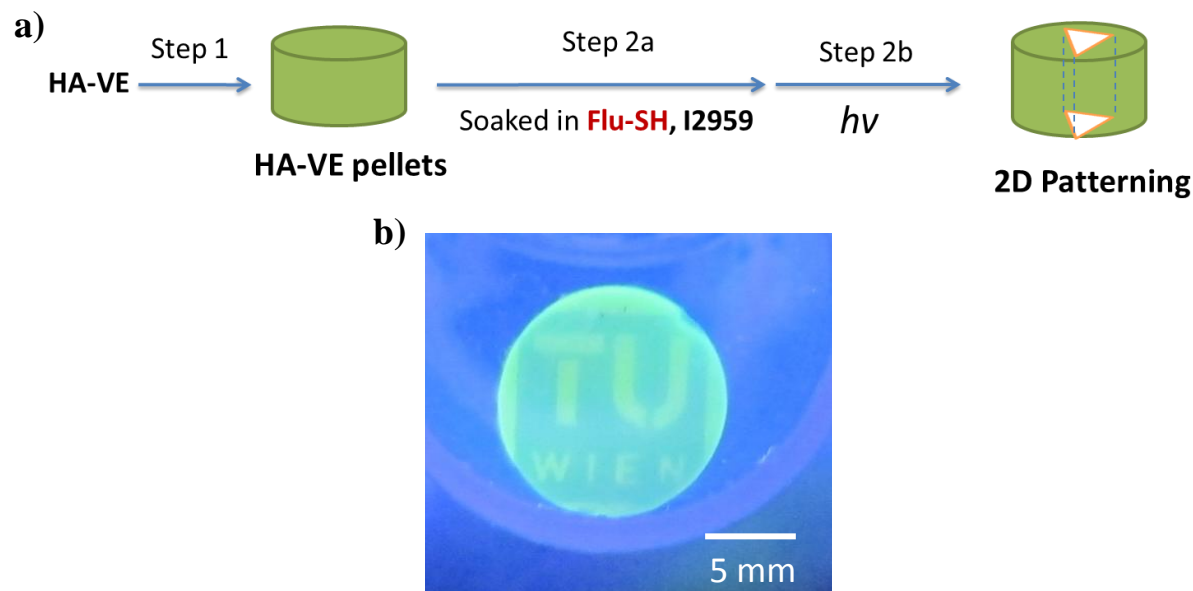


**Figure 104.** Schematic showing the UV photopatterning approach (a) and the patterned HA-VE pellet (b)

#### 2.5.4 Model Two-photon Patterning

Based on the success of one-photon model patterning, two-photon model patterning was performed using a two-photon active initiator (WSPI) under the assistance of Dr. Aleksandr Ovsianikov. However, the initial patterning did not succeed, presumably due to photoluminescence overlapping between WSPI and Fluo-SH. In other words, the excited WSPI may act as the donor-chromophore and transfer energy to the acceptor-chromophore through non-radiative dipole–dipole coupling. This process is termed as Förster resonance energy transfer (FRET).

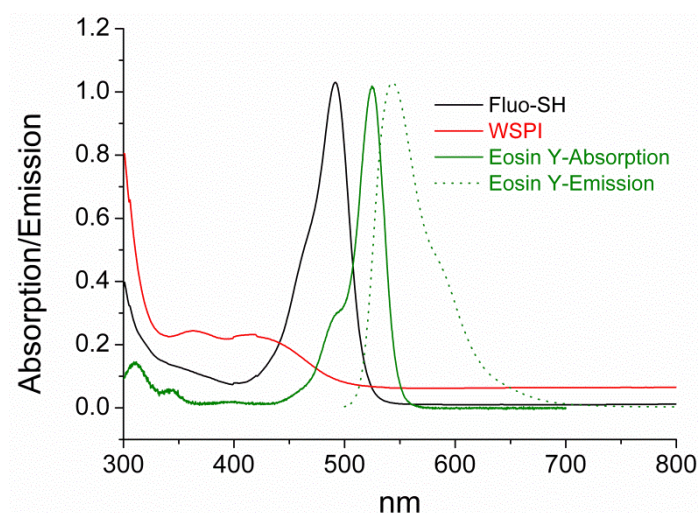


**Figure 105.** Absorption/emission spectra of the fluorophores (10  $\mu\text{mol}$  in deionized water)

In order to elucidate the mechanism, photophysical properties (Figure 105) of WSPI, Fluo-SH and eosin Yellow were measured using a photometer. Table 17 presents the specific photophysical values ( $\lambda_{\text{absorption}}$  and  $\lambda_{\text{emission}}$ ) of the fluorophores. It is hypothesized that the use of alternative PI with longer wavelength (e.g., eosin Yellow) may avoid the aforementioned problem.

**Table 17.** Photophysical properties of WSPI, Fluo-SH, and eosin Yellow

fluorophores	Structures	$\lambda_{\text{absorption}}$	$\lambda_{\text{emission}}$
WSPI		423	567
Fluo-SH		490	542
eosin Yellow		524	545

The optimization work was performed under the assistance of Evaldas Stankevičius (IMST). As shown in Figure 106, the two-photon patterning using eosin Yellow was successful, as evidenced by the LSM image.

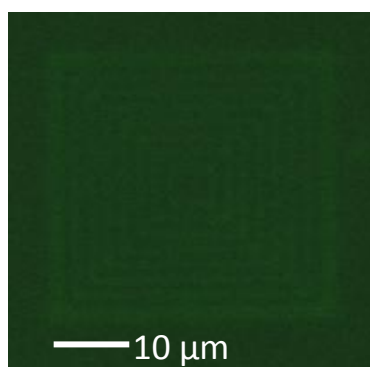


**Figure 106.** LSM image of two-photon patterned HA-VE gel

The patterning model was designed as a series of squares each of which is separated with a 1  $\mu\text{m}$  gap. The resolution of this process was about 1  $\mu\text{m}$  which is at the subcellular scale. This resolution is even higher than the reported resolution (3  $\mu\text{m}$ ) of two-photon grafting where aromatic azide was photografted on PEG matrices through nitrile insertion reactions.<sup>148</sup> Another advantage of this method is the processability in water whereas very few aromatic azides are water-soluble, making this method promising for two-photon patterning of other biological molecules.



### 3 Synthetic Hydrogels

Apart from developing naturally-derived materials, designing novel synthetic mono- or macromers as gel precursors for 2PP has also been one of the major targets in this research. Compared to natural polymers, synthetic polymers present several advantages including easy access, cost efficacy, low batch-to-batch variance, well-defined structure and low immunogenicity. As mentioned in the Introduction part, HEMA, PEG and PVA are the most typical materials for preparing hydrogels. Given that HEMA is not reactive enough for 2PP and the reported PEG/PVA hydrogels are typically based on acrylate chemistry, this chapter is aiming at developing low cytotoxic, synthetic monomers or macromers that are water-soluble and photopolymerizable in a 2PP setting.

The efforts in this chapter could be divided into three parts:

- 1) Synthesis and characterization of hydrophilic monomers with vinyl carbonate/carbamate functional group(s);
- 2) Synthesis and characterization of PEG-based macromers with vinyl ester functional groups;
- 3) Synthesis and characterization of PVA-based macromers with norbornene functional groups.

#### 3.1 Vinyl Carbonates/Carbamates-based Hydrogels

While (meth)acrylates-based hydrogels have been extensively used for biomedical applications, the irritancy and potential toxicity of unreacted acrylate groups and/or monomers is still an controversial issue.<sup>191</sup> To address this problem, previous research by Liska and co-workers has established the concept of PVA-based photopolymers, including vinyl esters and vinyl carbonates/carbamates.<sup>192</sup> In a long-term *in-vivo* study, Heller et al. have proved the superior biocompatibility and biodegradability of vinyl carbonates.<sup>184</sup> Unlike polyvinyl esters, the degradation products (Figure 107) of polyvinyl carbonates include low MW alcohol instead of free acids. Thus, it is assumed that vinyl carbonates-based scaffolds only pose negligible or minimal inflammatory effects. On the

other hand, polyvinyl carbamates are supposed to be non-inflammatory but rather hydrolytically stable due to the presence of amide linkages.

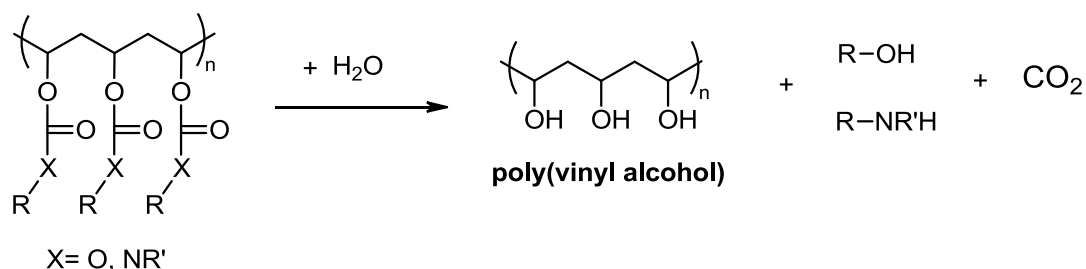


**Figure 107.** Degradation of polyvinyl carbonates/carbamates

Till now, there are no hydrophilic vinyl carbonates/carbamates commercially available. Therefore, these monomers should be synthesized in order to target hydrogel related applications. The structures of these monomers are devised according to the following benchmark monomers (Figure 108): 2-hydroxyethyl acrylate (HEA), 2-hydroxyethyl methacrylate (HEMA) and trimethylolpropane triacrylate (TTA). Given that HEMA is the frequently used monomer for contact-lenses applications,<sup>193</sup> the vinyl carbonate/carbamate counterparts, 2-hydroxyethyl carbonate/carbamate (HEVC/HEVCa) should be prepared. Since hydrogels are crosslinked networks of hydrophilic monomers, it is essential to develop an appropriate crosslinking agent. A trifunctional crosslinker based on glycerol (glycerol trivinyl carbonate, GTVC) should be considered as the non-cytotoxic analogue of the benchmark crosslinker (TTA), since glycerol naturally exists as a precursor for the synthesis of phospholipids in the liver.

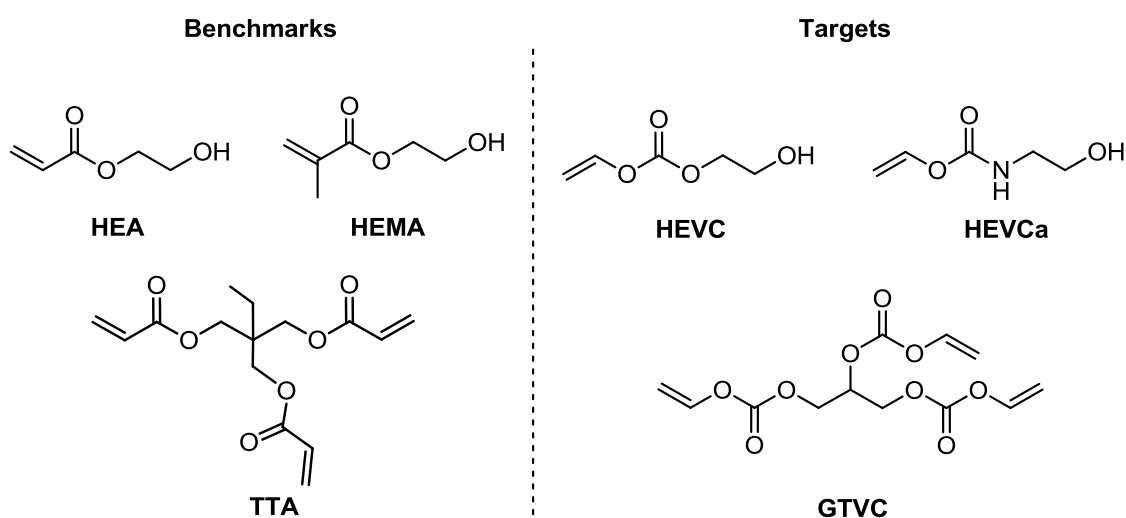


**Figure 108.** Chemical structures of the benchmark and targeted monomers/crosslinkers

### 3.1.1 Synthesis

#### 3.1.1.1 Synthesis of Hydroxyethyl Vinyl Carbonate

Since HEMA is widely used for a variety of biomedical applications such as contact lenses,<sup>193</sup> it is intriguing to prepare the vinyl carbonate analogue of HEMA. Hydroxyethyl vinyl carbonate (HEVC) was synthesized (Figure 109) in a mixture of DCM (solvent) and pyridine ( $H^+$  scavenger) under ice bath. In order to minimize the possibility of forming di-substituted product, vinyl chloroformate was added dropwise into a 10-fold excess of ethylene glycol.

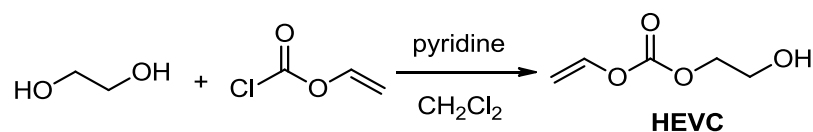


**Figure 109.** Synthesis of 2-hydroxyethyl vinyl carbonate

Since HEVC is expected to be more hydrophilic than the di-substituted side product, HEVC was firstly extracted into the aqueous layer. From this layer, HEVC was re-extracted into DCM by adding NaCl. The crude product was further purified by kugelrohr distillation. The distilled product was analyzed by NMR. It was found that ~5% ethylene glycol was still present. The boiling point (B.P.) of ethylene glycol is 197.3 °C while the B.P. of HEMA is 198 °C. Due to B.P. proximity, it was challenging to get rid of the ethylene glycol traces from HEVC.

Alternative purification by column chromatography (silica gel) was also attempted. However, no products could be isolated although the product was visible in TLC.

#### 3.1.1.2 Synthesis of Glycerol Trivinyl carbonate

Given the importance of crosslinking agent in hydrogel formation, a trifunctional vinyl carbonate based on glycerol, which is a biocompatible precursor, was prepared.

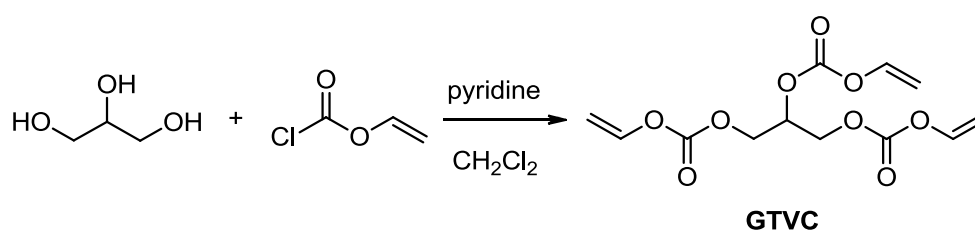


**Figure 110.** Synthesis of glycerol trivinyl carbonate

The glycerol trivinyl carbonate (GTVC, Figure 110) was synthesized according to a generic protocol as described by Heller.<sup>176</sup> Specifically, glycerol was allowed to react with a 3-fold excess of vinyl chloroformate in a mixture of DCM and pyridine. After conventional work-up and purification by column chromatography, GTVC was obtained in 63% yield as a colorless liquid.

To evaluate the access to 2PP, water solubility of GTVC was tested in PBS buffer. Unfortunately, it was found that the solubility of GTVC was quite limited (< 2%).

### 3.1.1.3 Synthesis of Hydroxyethyl Vinyl Carbamate

When one needs to design a hydrogel system, it is desirable to tune the degradation rate to match the speed of tissue regeneration. Since polyvinyl carbamates are expected to be hydrolytically stable, vinyl carbamate may serve as a non-degradable component for better control of the degradation rate of a fast-degradable hydrogel. Thus, the vinyl carbamate derivative of HEMA was prepared.

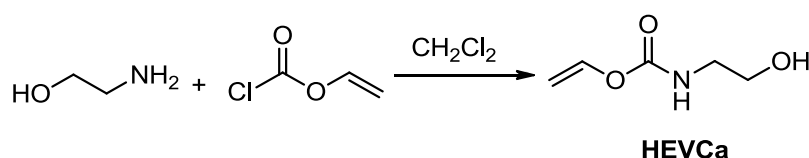


**Figure 111.** Synthesis of 2-hydroxyethyl vinyl carbamate

The 2-hydroxyethyl vinyl carbamate (HEVCa, Figure 111) was synthesized according to a procedure described by Bambury and Seelye.<sup>194</sup> Vinyl chloroformate was allowed to react with a 2-fold excess of ethanol amine which was acting as both reactant and acid scavenger. After extractive work-up and purification by kugelrohr distillation, HEVCa was obtained in 71% yield as a colorless liquid.

## 3.1.2 Characterization

### 3.1.2.1 Cytotoxicity

The cytotoxicity test was performed by Mag. Barbara Kapeller at the Medical University of Vienna and under assistance from Dr. Andreas Mautner. The test was based on a MTT assay using an osteoblast cell line. All of the samples were firstly dissolved in DMSO to

give concentrations from 0.6 mM to 10 mM. The lethal concentration ( $LC_{50}$ ) was defined as the sample concentration that caused 50% of the cell death.

Due to the inability to get HEVC with high purity (>99%), HEVC was not included in this study. Besides TTA, the trimethylolpropane ethoxylate triacrylate (ETA) was also included. Thus, the materials selected for toxicity test could be divided into two groups:

- 1) Monomer group: HEMA and HEVCa,
- 2) Crosslinker group: TTA, ETA and GTVC.

As shown in Figure 112, the control sample (cell + cell medium) was defined as the reference to stand for 100% viability. To test the toxicity of DMSO, cells were incubated with 1% DMSO. It was found that the use of DMSO caused ~20% decrease of cell viability.

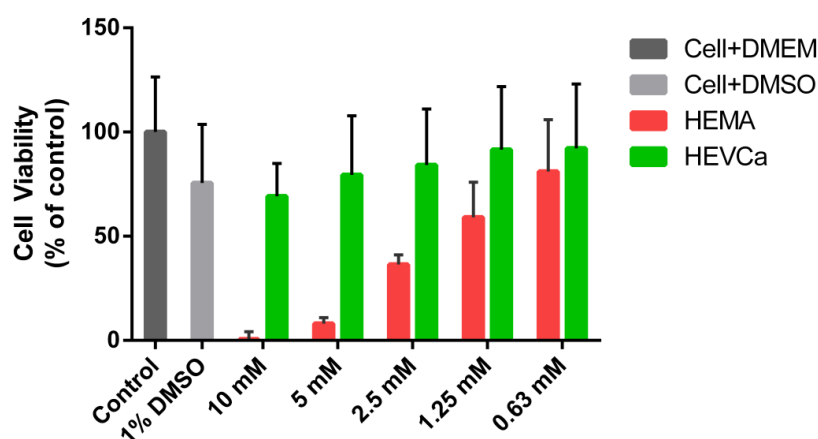


**Figure 112.** Influences of HEMA and HEVCa at varying concentrations on osteoblast investigated by MTT assay (mean  $\pm$  SD, n=3)

In comparison, the toxic effects of HEMA could be evidenced by the drastic decline of cell viability at concentrations from 1-10 mM. Notably, at all concentrations the toxic effects of HEVCa were not significant when compared to the DMSO control. These results show that the toxicity of HEMA is significantly higher than that of HEVCa.

The toxicity variance could also be evidenced by the  $LC_{50}$  values of these monomers (Table 18). Freidig et al. reported that the  $LC_{50}$  value of HEA was 0.28 mM for rat hepatocytes. The acute toxic effects were attributed to the depletion of glutathione.<sup>195</sup> As expected, the  $LC_{50}$  value of HEMA in this study was nearly one order of magnitude

higher than that of HEA, showing the lower toxicity of methacrylate groups. Notably, the LC<sub>50</sub> value of HEVCa was at least five times higher than that of HEMA, indicating the even lower cytotoxicity of vinyl carbamate groups.

**Table 18.** LC<sub>50</sub> values of the selected monomers and crosslinkers

monomer/crosslinker	LC <sub>50</sub> [mM]
HEMA	2
HEVCa	>10
HEA	0.28 <sup>195</sup>
GTVC	5
ETA	0.2
TTA	0.1

Cytotoxicity of the vinyl carbonate crosslinker (GTVC) was measured in comparison with the acrylated crosslinkers (TTA and ETA). As shown in Figure 113, the toxic effects of the three crosslinkers follow an order: **TTA > ETA >> GTVC**. Since these crosslinkers were tested at equal molar concentration as for the monomers (Figure 112), the significantly lower cell viability in cases of TTA and ETA suggests that the increase of acrylate group concentration could substantially enlarge the cellular damage and resultant cell death. In comparison, at all concentrations the vinyl carbonate analogue (GTVC) did not cause significant decrease of cell viability. These results confirmed the hypothesis that vinyl carbonates are much less cytotoxic monomers in comparison with acrylates references.

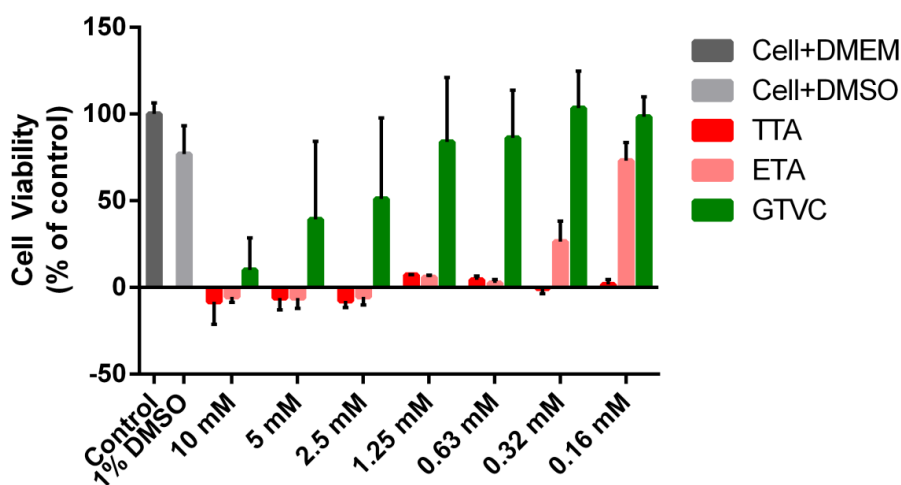


**Figure 113.** Cytotoxicity of TTA, ETA and GTVC at varying concentrations investigated by MTT assay (mean  $\pm$  SD, n=4)

### 3.1.2.2 Photo-Differential Scanning Calorimetry

When one designs a photopolymerization system for biomedical applications, it is critical to determine the polymerization extent of monomers. Specifically, the double bond conversion (DBC) is an essential factor to be quantified. On one hand, low DBC values would significantly compromise the mechanical properties of implants. On the other hand, low DBC always stands for high possibility of monomer leaching, which can cause serious toxicity effects and clinical complications.<sup>196</sup>

Besides photo-rheometry, photo-differential scanning calorimetry (Photo-DSC) is another useful method for characterizing the reactivity of photopolymers. In this study, the usage principle is that photo-rheometry is used for water-based formulations while Photo-DSC used for non-water formulations. A detailed illustration of the principle and protocol of Photo-DSC could be found in **Methods**.

To test the reactivity of monofunctional vinyl carbonates/carbamates, the hydrophilic vinyl carbonate HEVC and vinyl carbamate HEVCa were tested using Photo-DSC in comparison with the respective (meth)acrylate analogues (Figure 114). In addition, for the crosslinker category, GTVC was tested in comparison with TTA. Samples were measured with 5 wt% of I2959.

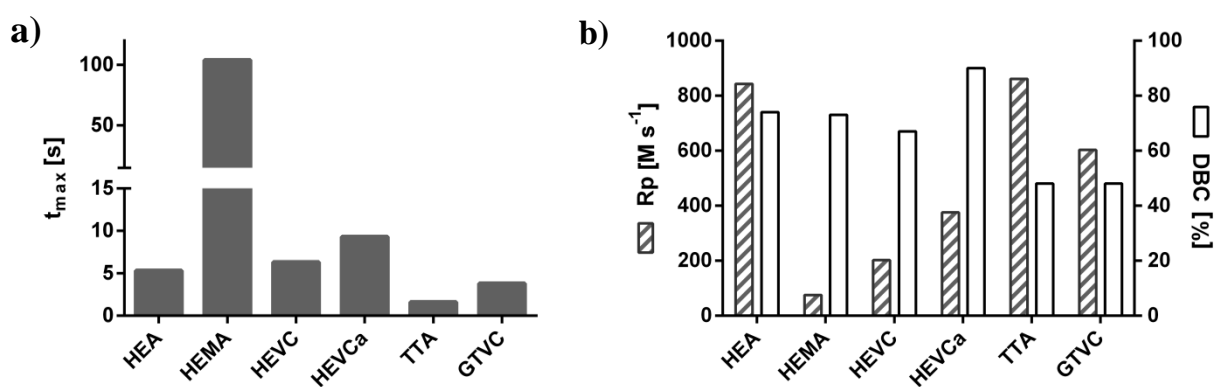


**Figure 114.** Photo-DSC results of the monomers: **a)**  $t_{max}$ ; and **b)**  $R_p$  and DBC

As shown in Figure 114b, polymerization rate ( $R_p$ ) of the acrylate analogue (HEA) was significantly higher than those of the vinyl carbonates/carbamates (HEVC/HEVCa) and/or the methacrylate (HEMA). In other words, the reactivity of vinyl carbonates/carbamates is between acrylates and methacrylates, which is consistent with

previous findings by Heller.<sup>176</sup> Interestingly, the amide-containing monomer (HEVCa) proves to be more reactive by about 50 % (higher  $R_p$  and higher DBC) than that of HEVC. This is due to the accelerated polymerization as a result of hydrogen-bonding effects by amide linkages. Although the  $R_p$  of trivinylcarbonates crosslinker (GTVC) is ~70% of triacrylates (TTA), the DBC of GTVC was comparable to that of TTA.

**Table 19.** Values for  $t_{\max}$ ,  $R_p$  and DBC of the monomers/crosslinkers

	$t_{\max}$ [s]	$R_p$ [ $\times 10^3$ M/s]	DBC [%]
HEA	5.3	843	74
HEMA	104	75	73
HEVC	6.3	202	67
HEVCa	9.3	375	90
TTA <sup>176</sup>	1.6	861	48
GTVC <sup>176</sup>	3.8	603	48

### 3.1.2.3 Proof-of-Concept 2PP

As demonstrated in section 3.1.2.2.2, the photoreactivity of GTVC was comparable to that of TTA, which is one of the most reactive crosslinkers. To prove the processability of vinyl carbonates in 2PP, a formulation consisting of GTVC and 1 wt% R1 (Figure 115) as two-photon initiator was prepared for 2PP fabrication. R1, the oil-soluble analogue of WSPI, was prepared by Dr. Zhiquan Li (IAS). The fabrication work was performed by Dr. Jan Torgersen.

During the initial attempt, it was found that the solubility of R1 in GTVC was quite limited. Since the boiling point of R1 is ~149 °C, it was not feasible to dissolve R1 by direct heating. In order to prepare a homogeneous formulation, alternative approach was applied. First, the initiator was dissolved in acetone and then mixed with GTVC. Second, the sample was dried under high vacuum to remove acetone.



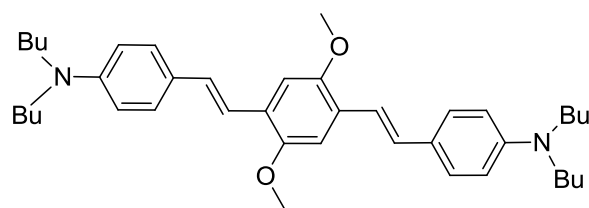


**Figure 115.** Chemical structure of the two-photon initiator (R1)

As shown in Figure 116, a GTVC scaffold ( $300 \times 300 \times 20 \mu\text{m}^3$ ) was directly fabricated according to a lattice CAD model (line distance:  $5 \mu\text{m}$ ). The sample was processable at low laser power (75 mW) and a reasonable writing speed ( $100 \mu\text{m/s}$ ). The structure quality was comparable to that of the gold-standard formulation (ETA/TTA), showing the high crosslinking efficiency of GTVC. The defects inside the structure were aggregates of poorly dissolved photoinitiator. Reducing the initiator amount to a better degree is warranted.

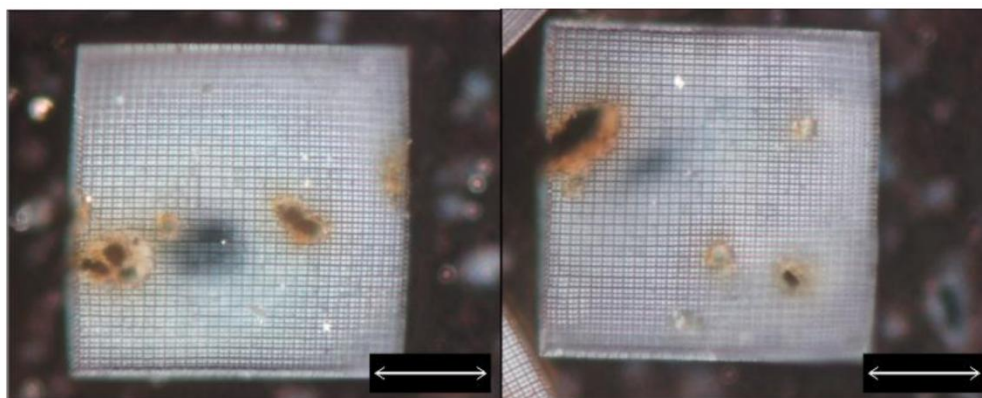


**Figure 116.** Phase contrast LM images of the polymer lattices consisting of GTVC and 1 wt% R1 ( $20 \times$  NA 0.8 objective, scale bars:  $100 \mu\text{m}$ )

While the initial 2PP structuring of vinyl carbonates was successful, it is notable that the water solubility of the crosslinker (GTVC) is too low to be used in hydrogel applications. Furthermore, the synthesis of vinyl carbonates/carbamates necessitates the use of expensive reagent (vinyl chloroformate). Nevertheless, GTVC scaffolds may be promising for bone tissue engineering applications.



## 3.2 PEG-based Hydrogels

In recent years, researchers have witnessed the popularity of PEG hydrogels due to their superior hydrophilicity, biocompatibility, and negligible immunogenicity.<sup>58</sup> PEG-based hydrogel precursors could be synthesized by introducing multifunctional vinyl groups to the pendant hydroxyl groups (Figure 117). For example, high MW (3-20 K Da) (meth)acrylated PEG (PEGDA/PEGDMA) can be synthesized in one step by reacting (meth)acryloyl chloride with pendant hydroxyl groups,<sup>59</sup> while lower MW ones (0.3-1 kDa) are commercially available.

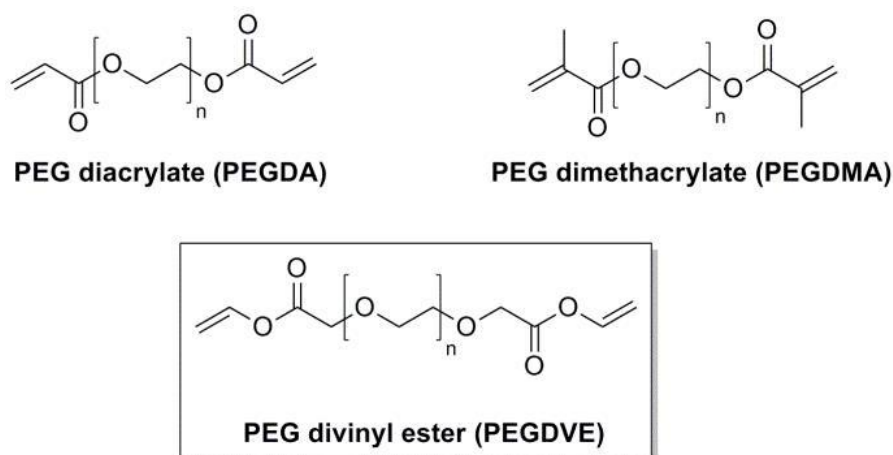


**Figure 117.** Chemical structures of PEG -diacrylates, -dimethacrylates, -divinyl esters

While PEGDA hydrogels have been widely studied in literature, one has to note the toxicity issue of acrylate chemistry. Up to date, synthetic hydrogels based on vinyl ester chemistry remain unexplored. Thus, the major objective in this section is to develop an alternative PEG hydrogel system based on vinyl ester chemistry. These hydrogels are supposed to be injectable, photopolymerizable, and biodegradable. Considering the acute toxicity of low MW PEGDA, high MW PEGDA should be developed as reference material for 2PP.

### 3.2.1 Synthesis

#### 3.2.1.1 Synthesis of PEG-600-Divinyl Esters

PEG divinyl esters (PEG600DVE) was synthesized according to a general method as described by Heller.<sup>176</sup> Specifically, PEG diacids (600 Da) were reacted with a huge excess of vinyl acetate under the catalysis of  $\text{Pd}(\text{OAc})_2$  (12 mol%) and powdered KOH

(10 mol%) at 60 °C for 48 h. As the reaction proceeded, the palladium catalyst turned from orange to black. It was found that conventional paper filtration was not effective to get rid of the black species. Instead, the use of Kieselgel could efficiently get rid of these species. After general workup, NMR analysis showed that the crude product had a purity of ~45% and the major impurity was the mono-substituted product.

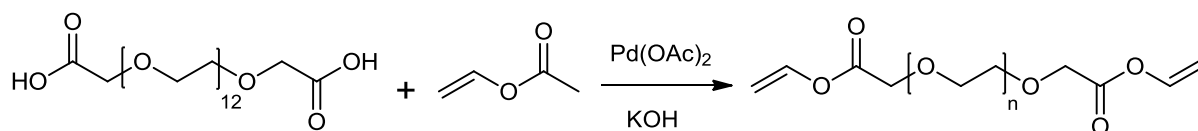


**Figure 118.** Synthesis of PEG-600-divinyl esters

An optimized workup procedure was adopted. Specifically, the crude product was washed with sodium bicarbonate solution to neutralize the carboxylate group of mono-substituted product. As a result, the sodium salt is supposed to be in the aqueous layer. However, NMR analysis showed that the purity of the optimized product was ~81%. Further purification by column chromatography was not successful, presumably due to its large molecular size. The crude PEG-600-DVE was obtained in 47% yield as a yellowish oil.

### 3.2.1.2 Synthesis of PEG-10k-Diacrylates

Given that PEGDA with a higher MW (> 3.4 kDa) have been used in cell-encapsulation studies and have exhibited much lower toxicity than PEGDA (700 Da), high MW PEGDA should be synthesized as reference. High MW PEGDA was prepared according to a procedure published by the Anseth group.<sup>197</sup>

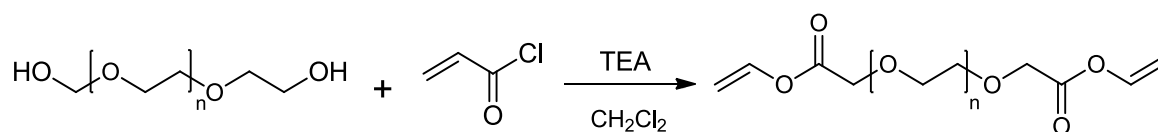


**Figure 119.** Synthesis of PEG diacrylates

Prior to synthesis, PEG (10 kDa) was firstly dried by azeotropic distillation with toluene. The dried PEG was allowed to react with 5-fold excess of acryloyl chloride (Figure 119) at 0 °C in a mixture of dichloromethane (solvent) and triethylamine (acid scavenger). After precipitation in cold diethyl ether, the crude product was further purified by dialysis against distilled water for 24 h. After lyophilization, high MW PEGDA was obtained as a white solid in 75 % yield.

### 3.2.1.3 Synthesis of Water-soluble Thiols

While vinylated PEG were successfully prepared, for thiol-ene photopolymerization, a water-soluble "thiol" crosslinker is necessary. However, the number of commercial water-soluble macrothiols is only limited to PEG dithiol (MW: 1-5 kDa, Sigma) and ethoxylated trifunctional thiols (MW: 700, 1300, 2000 Da, THIOCURE<sup>®</sup> ETTMP). This is likely due to the hydrophobicity nature of sulfhydryl group. Thus, it is intriguing to design novel approaches for the synthesis of water-soluble thiols.

Inspired by the "buffering" property of hydrophilic amino acids such as aspartic acid, a synthetic approach was proposed (Figure 120). The idea was to conjugate the amino group of L-cysteine with the oxyrane group of a substrate through ring-opening reaction. It is supposed that amino groups should react with oxyrane groups in a much higher rate than that of carboxylate groups. After reaction, the carboxylate could be neutralized into a sodium salt form to provide the solubility.

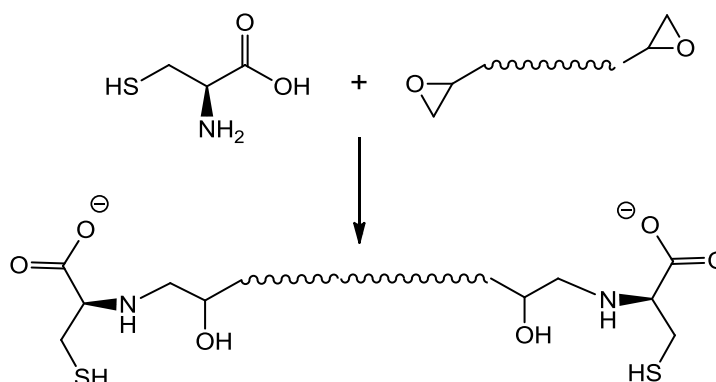


**Figure 120.** Proposed synthetic approach for water-soluble dithiol

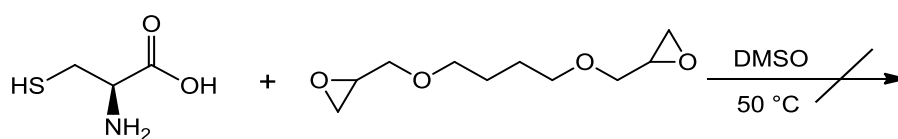


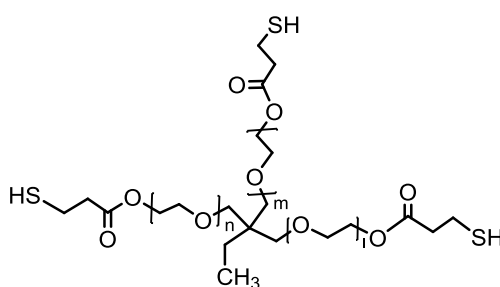
**Figure 121.** Model reaction of L-cysteine with 1,4-butanedioldiglycidyl ether

To test the hypothesis, a model reaction (Figure 121) was performed using 1,4-butanedioldiglycidyl ether as the substrate. This compound was allowed to react with L-cysteine (2 eq.) in DMSO at 50 °C. However, white precipitation was observed as soon as the reactants were mixed, showing the formation of intermolecular crosslinks. This observation could be explained in two aspects. On one hand, once primary amine groups

undergo ring-opening reaction, the formed secondary amine groups are still reactive towards ring-opening reactions. On the other hand, sulfhydryl groups may also contribute to the ring-opening reaction. The reactivity of sulfhydryl groups towards oxirane groups has been demonstrated in a recent study by Jian et al.<sup>198</sup>

### 3.2.1.4 Preparation of Macrothiols by Inclusion Complexation

Given that the synthesis of water-soluble thiols was unsuccessful and most commercial thiols only have limited water solubility, alternative approaches should be devised to improve the applicability of macrothiols for hydrogel preparation.



**ETTMP700 (I+m+n =7)**

**ETTMP1300 (I+m+n =21)**

Commercial trifunctional thiols (ethoxylated trimethylolpropane tri(3-mercaptopropionate), ETTMP-700/-1300) were initially selected as the macrothiol substrates since ethylene glycol units are supposed to enhance hydrophilicity. However, it was found that the water solubility of ETTMP-700 and ETTMP-1300 was ~0.5 wt% and ~1 wt%, respectively. While longer ethylene glycol spacer indeed provides better water solubility, the poor solubility of ETTMP-1300 may still pose problems for further used in hydrogel preparation.

In the field of supramolecular chemistry, it is well known that cyclodextrins have the ability to form complexes with hydrophobic compounds and improve the water solubility of host molecules.<sup>199</sup> The cyclodextrin family (Figure 122) includes several subtypes with varying sizes of sugar ring:  $\alpha$ -cyclodextrin (6-membered),  $\beta$ -cyclodextrin (7-membered),  $\gamma$ -cyclodextrin (8-membered). In addition, the methylated form (M $\beta$ CD) was found to be more efficient than  $\beta$ -cyclodextrin for complexation.<sup>200</sup> Owing to its superior water-solubility, M $\beta$ CD could form soluble inclusion complexes with cholesterol, consequently enhancing the solubility of cholesterol in aqueous solution.<sup>200</sup>

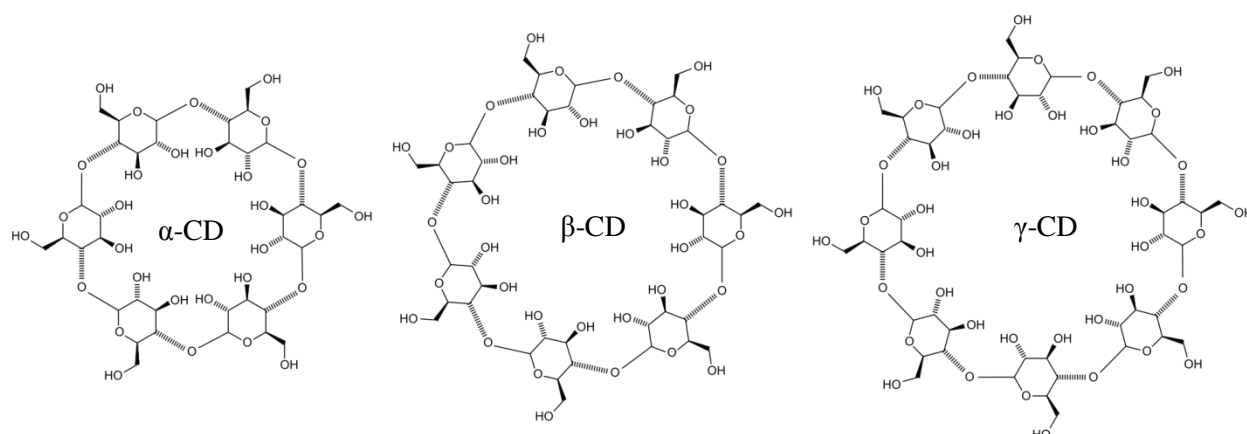


**Figure 122.** Chemical structures of cyclodextrin subtypes

Inspired by the aforementioned CD chemistry, it is supposed that the M $\beta$ CD could similarly form soluble inclusion complexes with ETTMP-1300 and this solution could be utilized as macrothiols for preparing hydrogels. To prepare the inclusion complex, M $\beta$ CD was firstly dissolved in distilled water to form a 22 wt%, homogeneous solution. Subsequently, varying amounts of macrothiol ETTMP-1300 were added to aliquoted M $\beta$ CD/water solution. The solutions were incubated for 10 h under stirring at room temperature. The maximum solubility of ETTMP-1300 in these solutions was determined by turbidity observation. It was found that after complexation the max. solubility of ETTMP-1300 was increased to a level of  $\sim$ 12 wt%.

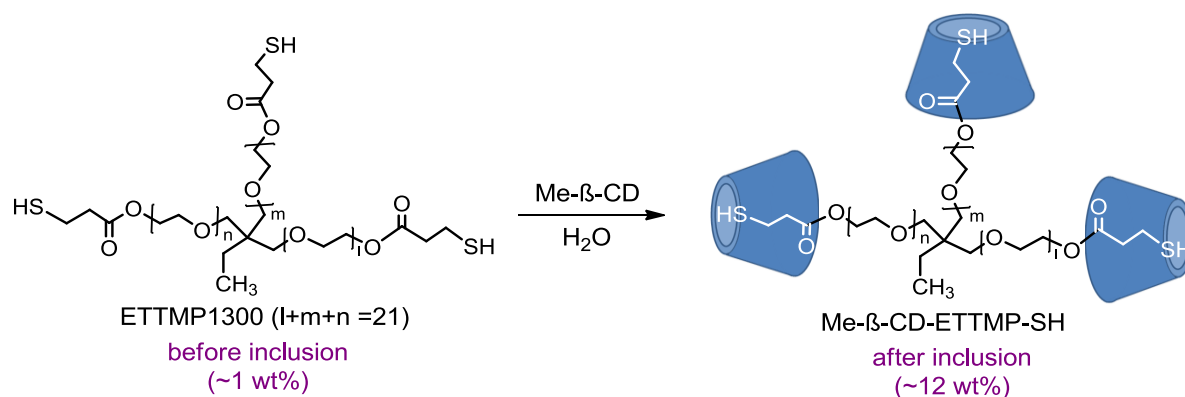


**Figure 123.** Schematics of preparation of M $\beta$ CD/ETTMP-1300 inclusion complexes as macrothiols

M $\beta$ CDs are hydrophobic inside the ring and hydrophilic outside the ring, they should form complexes with hydrophobic compounds. It is hypothesized that after complexation the hydrophobic sulfhydryl groups are covered inside the M $\beta$ CD ring and thus the solubility was significantly increased.

### 3.2.2 Characterization

PEG-600-DVE was characterized with a focus on photoreactivity in comparison with its (meth)acrylates analogues: PEG-600-DA and PEG-600-DMA. These analogues are commercially available and thus used as received. To investigate the influence of thiol-ene chemistry on photoreactivity, these materials (Figure 124) were tested with varying amount of sulfhydryl groups that are donated either by a trifunctional thiol (ethoxylated trimethylolpropane tri(3-mercaptopropionate), ETTMP700) or by a tetrafunctional thiol (pentaerythritol tetrakis(3-mercaptopropionate), TT). On one hand, photo-DSC was initially employed to test the photoreactivity of formulations in the absence of water; on the other hand, for hydrogel formulations photo-rheometry was applied instead.

Besides photoreactivity, cytotoxicity of the aforementioned materials should also be tested.

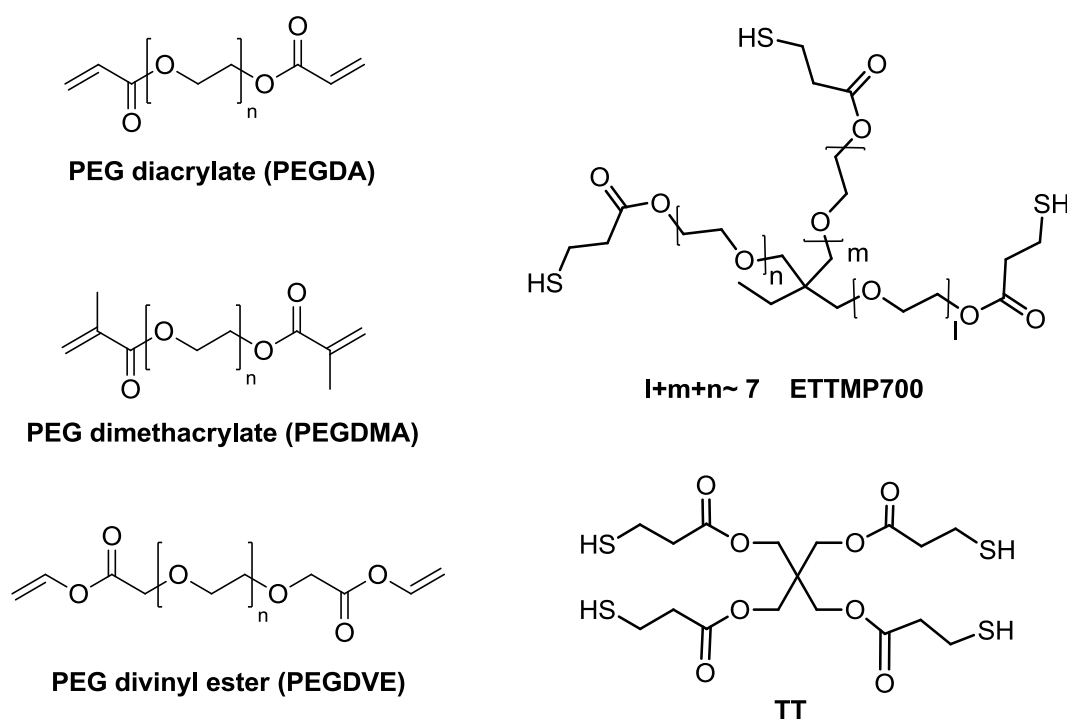


**Figure 124.** Chemical structures of the selected materials

#### 3.2.2.1 Cytotoxicity

Cytotoxicity study was carried out using a MTT assay as same as described in section 3.1.2.1. In the vinyl ester category, PEG-600-VE was tested at same molar concentrations



in comparison with DVA, which is commercially available. In the thiol category, only TT was tested in this study.

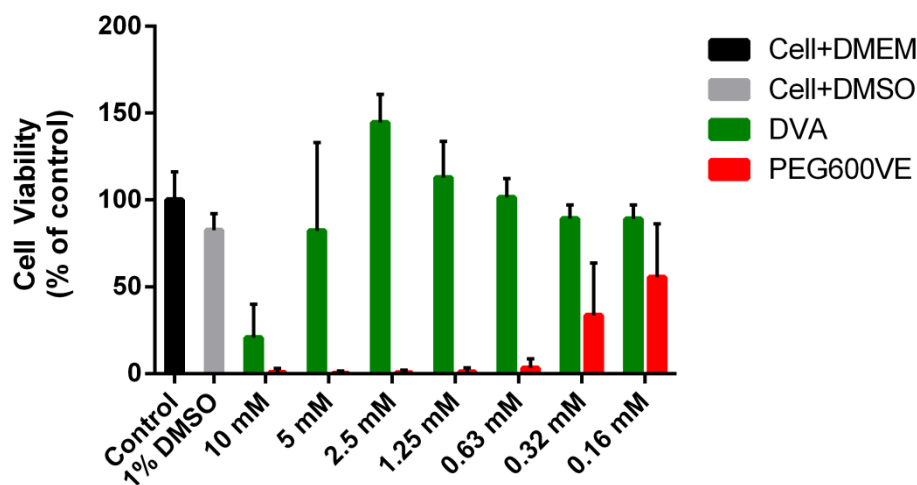


**Figure 125.** Cytotoxicity of DVA and PEG-600-DVE at varying concentrations on osteoblasts as investigated by MTT assay (mean  $\pm$  SD, n=3)

As shown in Figure 125, DVA exhibited low toxicity at most concentrations (<5 mM), as compared to the DMSO control. Surprisingly, PEG-600-VE induced a significant decrease of cell viability at most concentrations. It is likely due to the presence of mono-substituted product where carboxylate groups may induce a charge-dependent cell apoptosis. However, in the thesis research of Dr. Andreas Mautner, PEG-250-DVE with high purity also exhibited comparable toxic effects as PEG-600-DVE.<sup>201</sup> Together, these results are not expected and further toxicity study using different cell lines is warranted.

While thiol-ene polymerization has aroused wide interests for biomedical applications,<sup>55</sup> biocompatibility of "thiol" compounds is still a controversial issue. Generally, "thiol" compounds are supposed to be inappropriate for medical uses, due to their distinct odor and poor storage stability. However, the extent to which "thiol" compounds such as TT can influence cell viability is not reported.

To clarify the biocompatibility of "thiols", influence of varying amount of tetrathiol (TT) on osteoblasts was tested in this study. As shown in Figure 126, it was found that at most concentrations TT did not induce significant influence on the cell viability as compared to the DMSO control. Although these preliminary results are promising, one has to bear in mind that the working principle of MTT assay is based on the reduction of

tetrazolium dyes by oxidoreductase enzymes. It is unclear that whether sulfhydryl groups of TT could influence the reduction process of these enzymes.

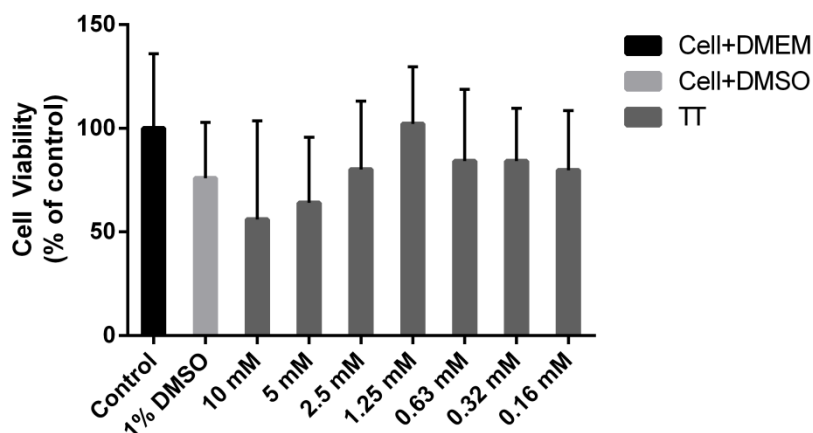


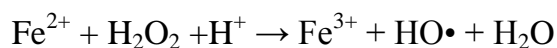
**Figure 126.** Cytotoxicity of TT at varying concentrations investigated by MTT assay (mean  $\pm$  SD, n=3)

In another study by Mautner et al.,<sup>158</sup> the toxicity of ETTMP-700 and TT was measured using Alamar-Blue assay. It was found that the LC<sub>50</sub> value of ETTMP-700 and TT was 1.25 mM and >10 mM, respectively. Although these compounds were tested in equal molar concentration, the underlined mechanisms causing the toxicity difference these different “thiol” compounds are not clear.

**Table 20.** LC<sub>50</sub> values of ETTMP-700 and TT from toxicity assay

Reagents	LC <sub>50</sub> [mM]
ETTMP-700 <sup>158</sup>	1.25
TT	>10

In an early study by Held and Melder,<sup>202</sup> cytotoxicity of a water-soluble dithiol (dithiothreitol, DTT) was measured using a Chinese hamster V79 cell line. Interestingly, it was found that at low concentrations (0.4-1.0 mM) DTT caused cell death whereas at higher concentrations (> 2 mM) or lower concentrations (0.1 mM) did not. The authors attributed this phenomenon to an oxidative-toxicity mechanism. It was proposed that the toxicity resulted from autoxidation of DTT and the release of H<sub>2</sub>O<sub>2</sub>, which could further change into the cytotoxic hydroxyl/superoxide radicals ( $\bullet$ OH or HOO $\bullet$ ) through metal-catalyzed Fenton reaction (below).



In all, these results suggest that MTT assay is likely inappropriate for the determination of the toxicity of “thiol” compounds. This preliminary study asks for alternative methodologies (e.g., flow cytometry) that circumvent the reduction-dependent mechanism.

### 3.2.2.2 Photo-DSC

#### Homopolymerization

Photoreactivity of the three “PEG-600-X” oligomers towards homopolymerization were screened using Photo-DSC according to a generic protocol as described in **Methods**. The PEG oligomers were mixed with 1 wt% photoinitiator (I2959).

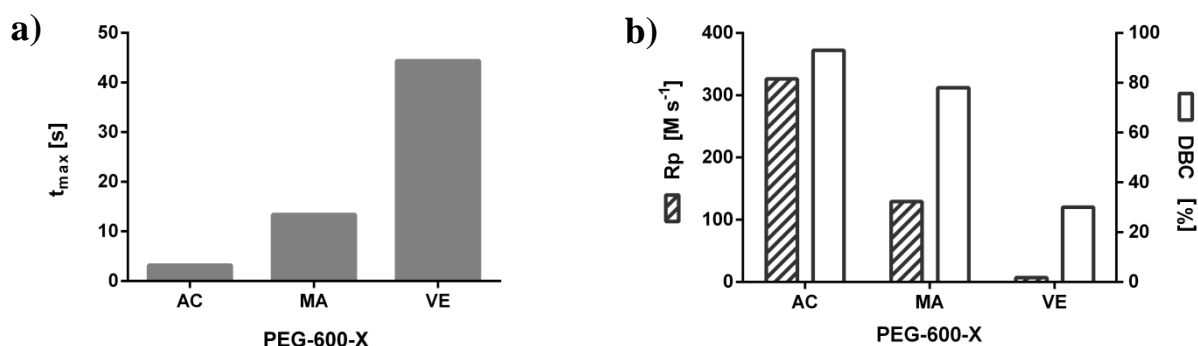
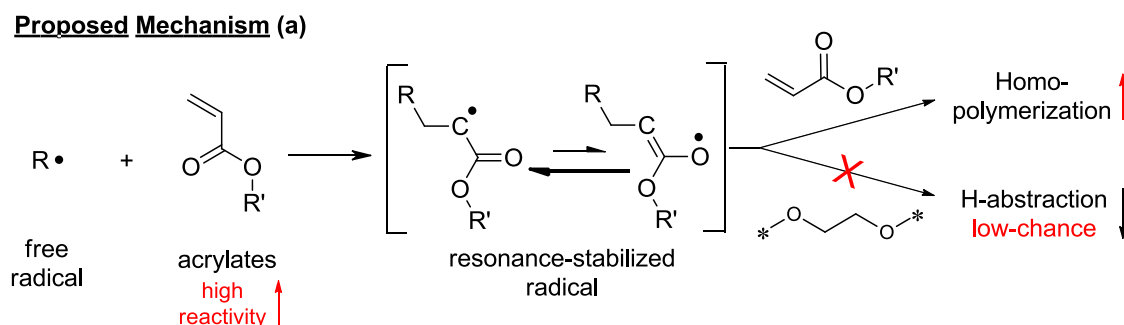


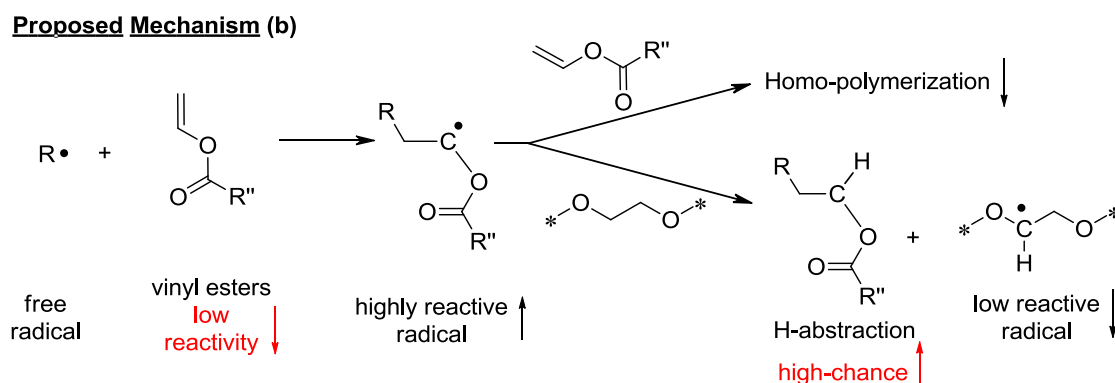
**Figure 127.** Photo-DSC results of the PEG-600-X oligomers: (a)  $t_{max}$ ; and (b)  $R_p$  and DBC

As shown in Figure 127, the  $t_{max}$  of PEG-600-DA is the shortest and the  $R_p$  and DBC values are the highest ones in comparison with those of other two samples (-MA, -VE), indicating the highest reactivity. However, the reactivity of PEG-600-VE was even significantly lower than that of the methacrylate analogue. To clarify the reactivity variance, it is important to analyze the underlined molecular mechanisms how different vinyl groups react with free radicals.

The extremely high polymerization rate of acrylates is attributed to the high reactivity of acrylate monomers. Due to resonance-stabilization of the carbon-centered radicals, side reactions such as H-abstractions from the ethylene glycol backbone are in low chance. Owing to the high reactivity of the acrylate monomer, homopolymerization proceeds to a large extent.



Compared to acrylates, vinyl esters are often supposed to be less reactive monomers, presumably because the associated carbon-centered radicals (b) lack of resonance stabilization. Interestingly, in a control measurement the  $t_{\max}$  of DVA (without ethylene glycol units) was found to be  $\sim 5$  s while the  $t_{\max}$  for acrylate and methacrylate analogues was 2.7 s and 39.5 s, respectively.<sup>159</sup> By contrast, the  $t_{\max}$  of PEG-600-VE ( $\sim 45$  s) was nearly one magnitude longer than that of DVA. Therefore, one can assume that there exist different polymerization mechanisms for vinyl esters with or without ethylene glycol units.



It is supposed that in the presence of ethylene glycol units, vinyl ester radicals are highly reactive towards H-abstractions while forming radicals of low reactivity and causing the termination. In other words, H-abstractions from ethylene glycol units can greatly compromise the homopolymerization rate of PEG-600-VE.

### Thiol-ene Copolymerization

In order to test the influence of thiol-ene chemistry on photoreactivity, the three oligomers were mixed with varying amounts of "thiol" compounds (TT or ETTMP-700) and 1 wt% 2959, so that the thiol to ene ratio was adjusted to be 10%, 20%, and 40%, respectively. To minimize the possibility of premature polymerization, 0.1 wt% pyrogallol was always added as stabilizer.

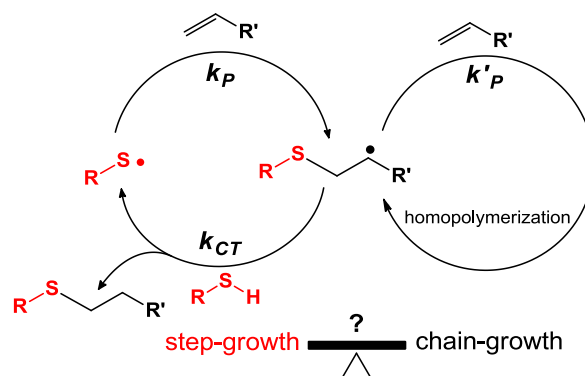


**Figure 128.** Schematic showing that the carbon-centered radical can undergo either a chain transfer reaction (left cycle) or an additional propagation (right cycle)

Based on the pioneering work by Hoyle and Bowman,<sup>55</sup> basic principles in radical-mediated thiol-ene reactions have been established (Figure 128). It is accepted that depending on the structure of "ene" groups, addition of thiols can influence the probability of chain-transfer reactions to varying extent. Specifically, whether the reactions proceed in a step-growth or a chain-growth manner, primarily depends on relative values of chain transfer constant ( $k_{CT}$ ) and propagation constants ( $k_p$  and  $k'_p$ ).

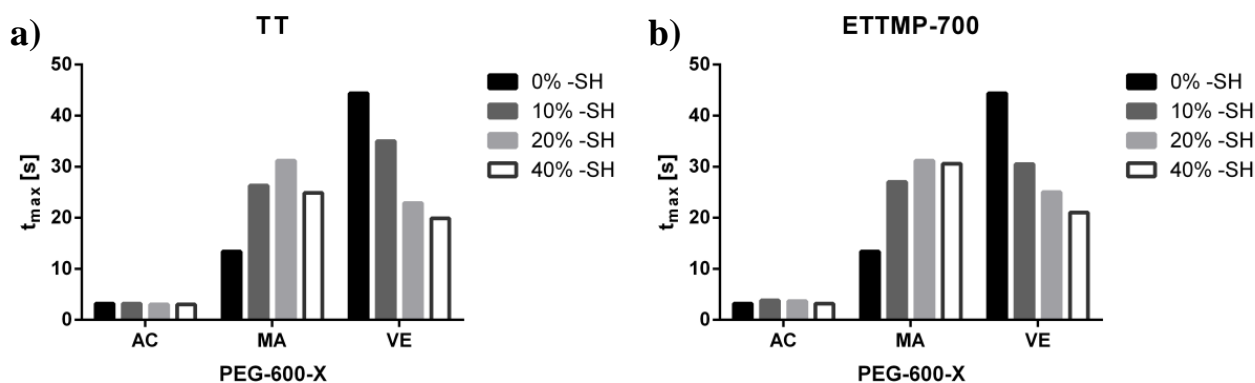


**Figure 129.** Photo-DSC results ( $t_{max}$ ) of the thiol-ene formulations: (a) TT and (b) ETTMP-700

Influence of TT or ETTMP-700 on the  $t_{max}$  values of the PEG oligomers was shown in Figure 129. For PEG-600-DA, the  $t_{max}$  values almost remained the same at all concentrations of TT, showing that the polymerization rate is not significantly influenced by the presence of thiols. This is consistent with previous findings related to thiol-acrylate photopolymerization by Cramer and Bowman.<sup>203</sup> In the case of ETTMP-700, the  $t_{max}$  values even increased as a result of addition of thiol groups. The reactivity decrease could be addressed to the prevalence of abstractable hydrogens in ETTMP-700 and the increased probability of H-abstraction and chain termination.

For PEG-600-DMA, in all cases the use of thiol-ene chemistry significantly increased the  $t_{\max}$  values, indicating the decreased reactivity. The ineffectiveness of thiol-ene chemistry for methacrylate is consistent with previous studies. For instance, in 2001 Lecamp et al. reported the kinetic study of thiol-methacrylate polymerization.<sup>204</sup> The authors found that thiol-ene addition is slower than homopolymerization and as a result the propagation is often stopped due to the complete consumption of the methacrylate "enes". By using theoretical calculation, a transfer constant value was defined as 0.26: i.e., the ratio of the rate constant for the H-abstraction to the rate constant of methacrylate homopolymerization was 0.26:1.

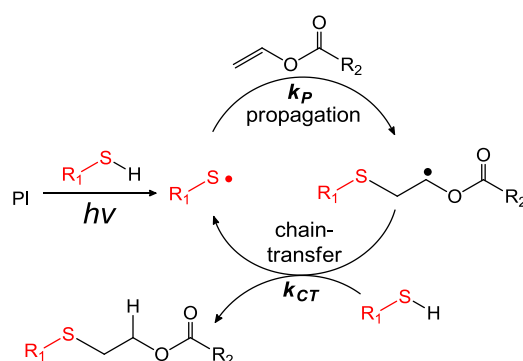


**Figure 130.** Proposed mechanism of thiol-vinyl ester photopolymerizations

For PEG-600-DVE, as the content of thiol groups increased, the  $t_{\max}$  values decreased gradually from 45 s to 20 s, showing the increase of reactivity. It could be attributed to the high efficiency of thiol-vinyl ester reactions. Mechanism of thiol-vinyl ester photopolymerization is proposed in Figure 130. Upon irradiation, a photoinitiator (PI) generates free radicals, one of which abstracts a hydrogen atom from a thiol and forms a thiyl radical. This radical could propagate across the double bond of vinyl ester group and form a thioether linkage. The resultant carbon-centered radical can abstract a hydrogen atom from another thiol and regenerate the thiyl radical. It is important to note the reactivity difference between thiyl radicals and ethylene glycol units towards H-abstractions. In all, thiol-vinyl ester reactions are highly efficient.

### 3.2.3 2PP Microfabrication

Based on one-photon characterization of PEG-based oligomers, two-photon microfabrication was carried out in order to test the applicability of these materials for 2PP-hydrogel systems. For PEG (meth)acrylates, the 2PP trials were performed based on

homopolymerization due to the ineffectiveness of thiol-ene chemistry. For PEG vinyl esters, thiol-ene copolymerization was selected as the crosslinking strategy given that addition of thiols is supposed to increase reactivity. Besides, variations of these oligomers with the same pendant groups but with different molecular weight or molecular structures were also tested in order to modulate the reactivity and/or toxicity.

The 2PP experiments in this section were performed by Jan Torgersen (IMST) except the experiment of PEGDA-10k by Peter Gruber (IMST).

### **3.2.3.1 PEG Diacrylates**

It is well known that PEGDA is among the most reactive macromers for preparing hydrogels. However, one has to keep in mind that commercial PEGDA with low MW (e.g., 700 Da) is highly cytotoxic and often results in extremely long kinetic chains and high crosslinking density. However, for most biological applications, it is desirable to design cytocompatible hydrogels that provide a permissive environment. Interestingly, in a pioneering study by Nuttelman and Anseth,<sup>197</sup> PEG hydrogels formed by higher MW PEGDA (4.6 kDa) enabled photoencapsulation of human mesenchymal stem cells (hMSC) with high viability (> 95%). In a control experiment where hMSC cells were incubated with UV light and initiator only, cell viability was decreased to 85% due to the toxicity of free radicals. The authors attributed the cell viability difference to a probable protection mechanism of PEGDA gel networks.

With this information in mind, two types of PEGDA with different MW (700 Da, 10 kDa) were screened in this section. It is supposed that the high MW PEGDA is less reactive but also less cytotoxic than the low MW one.

#### **3.2.3.1.1 PEGDA-700**

At the initial stage of this study, PEGDA-700 formulations were tested using 2 wt% WSPI as photoinitiator and at varying water content (90, 80, 70, 60, 50 wt%) in M9 buffer. M9 is a standardized media for culturing *C. elegans*.<sup>205</sup> The 2PP fabrication was performed at prescribed writing speed and average laser power. After structuring, the

samples were soaked in M9 buffer for 2 h to remove residual PEGDA. Afterward, the samples were soaked in fresh M9 buffer for 24 h to reach an equilibrium water uptake.

As shown in Figure 131, influences of water content and average laser power on the gel structure were screened using a rod-shaped 2D-CAD model. At 90% water content, no gel structure could be observed, showing the low crosslinking efficiency at 10% macromer content. At lower water content (50–80 %), PEGDA hydrogels could be fabricated in good accordance with the rod model. At each of the formulations, the decrease of average laser power induced a decrease of rod width, showing the increase of gel crosslinking density.

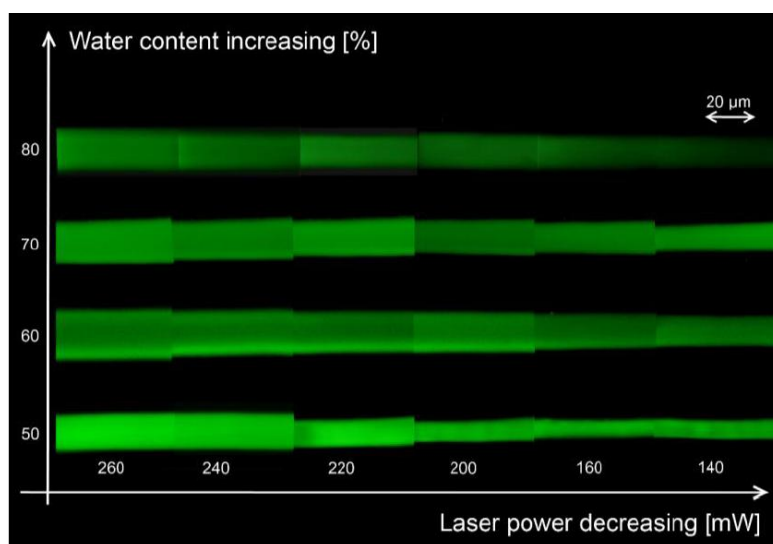


**Figure 131.** Influence of water content and average laser power on rod-shaped structures (visualized by LSM, writing speed: 10 mm/s)<sup>39</sup>

Based on 2D structuring, 3D microfabrication was later attempted using a CAD model (Figure 132,  $280 \times 280 \times 225 \mu\text{m}^3$ ) which has a complex geometry and defined porosity in 3D. The scaffold was devised according to previous work by Ovsianikov et al., which has proved the usefulness of the scaffold for 3D cell culture in tissue engineering.<sup>156</sup> To verify the processing window for this 3D model, 2PP structuring was performed using PEGDA formulations with 50% or 80% water content.



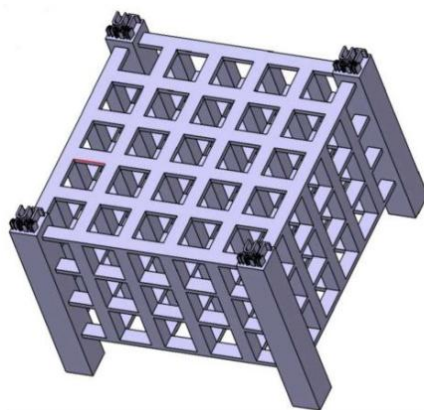


**Figure 132.** A CAD scaffold for 3D microfabrication of PEGDA-700 ( $280 \times 280 \times 225 \mu\text{m}^3$ )<sup>39</sup>

As shown in Figure 133, the speed-power array implies a processing window for a PEGDA-700 formulation with 50% water. On the bottom-right corner, when the writing speed was beyond 7 mm/s, no structure could be obtained. On the up-left corner, when the average power exceeded 220 mW, the energy dose was too high and caused damage to the gel networks. Defined structures could be obtained at 60 mW·1 mm/s, 100 mW·4 mm/s, 140 mW·7 mm/s, and 220 mW·10 mm/s, respectively. Beyond these thresholds (i.e., higher writing speed), structure defects were observed because the gel was too soft to withstand the developing process.

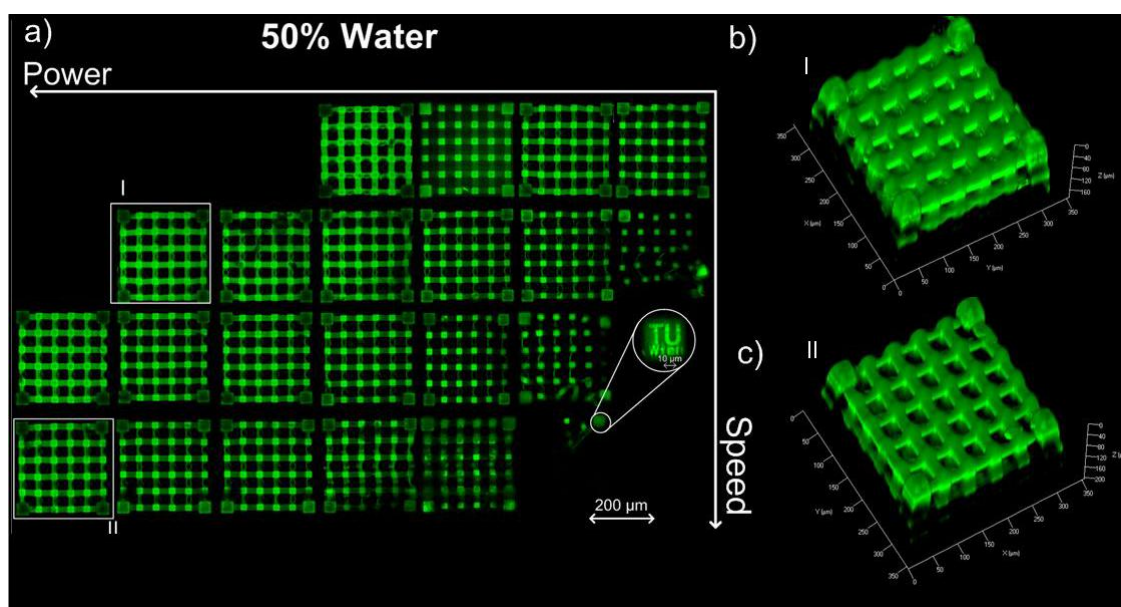


**Figure 133.** LSM images of the 3D gel scaffolds containing 50% water. a) speed-power array with average laser power (horizontal right-left: 60-300 mW, +40 mW per step) and writing speed (vertical top-down: 1-10 mm/s, +3 mm/s per step); b) z-stacked LSM image of scaffold-I; and c) z-stacked LSM image of scaffold-II<sup>39</sup>

The water content in a variety of soft tissues is over 50%. For instance, in articular cartilage the water content is approximately 80%. Therefore, to better design biomimetic hydrogels for tissue engineering applications, it is essential to investigate the 2PP feasibility at high water content (80%).

As shown in Figure 134, the speed-power array of a PEGDA formulation with 80% water indicated a much smaller processing window compared to the aforementioned formulation with lower water content (50%). This could be explained the decrease of crosslinking efficiency as a result of decreased double bond concentration. Defined structures could be obtained at 180 mW·1mm/s, 220 mW·4 mm/s, and 300 mW·7mm/s, respectively. Beyond these threshold parameters, the structures were poorly crosslinked and thus prone to deformation.

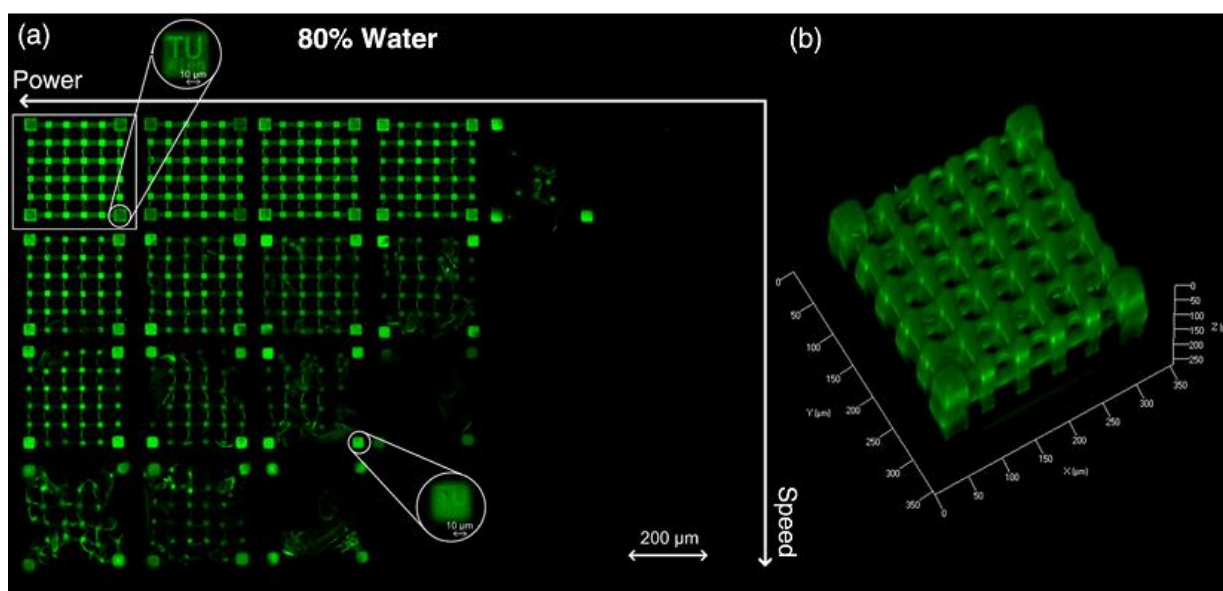


**Figure 134.** LSM images of the 3D gel scaffolds containing 80% water. a) speed-power array with average laser power (horizontal right-left: 100-300 mW, +40 mW per step) and writing speed (vertical top-down: 1-10 mm/s, +3 mm/s per step); b) z-stacked LSM image of the up-left scaffold<sup>39</sup>

### 3.2.3.1.2 PEGDA-10k

In order to optimize the cytocompatibility of PEGDA-700, PEGDA with higher MW (10 kDa) was also tested in this study. The samples were prepared by dissolving PEGDA-10k in photoinitiator stock solutions of P2CK (2.23 mM, in PBS).

At the initial experiment, a PEGDA-10k formulation with 80% water content was attempted. However, no structuring could be realized, presumably due to the limited reactivity of PEGDA-10k. In comparison with the results in last section, the double bond concentration of 20 % PEGDA-10k is no more than 10% of that of 20% PEGDA-700. When the macromer content was increased to 30%, the structuring was successful. As shown in Figure 135, a speed-power array indicated a broad processing window of 30% PEGDA-10k. Defined structures were obtained within an average power of 50-80 mW and in all writing speeds. However, structure defects were observed when the power exceeded 90 mW, presumably because the laser dose was too high and induced the break-down of gel network.

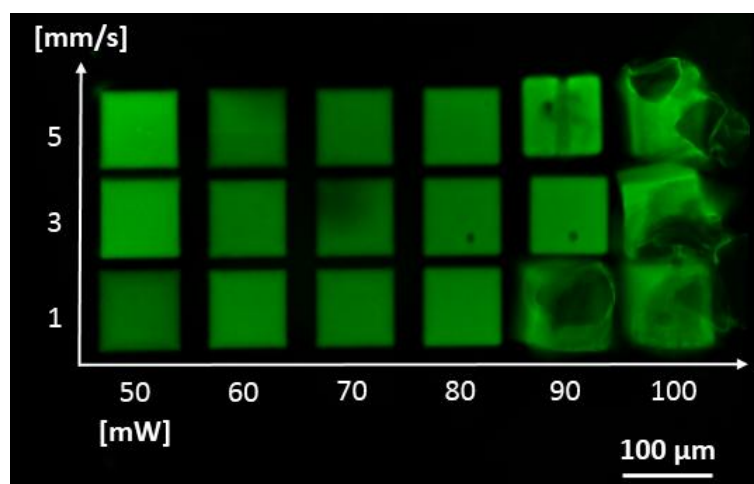


**Figure 135.** LSM images of a 2D speed-power array of PEGDA-10k containing 70% water with average laser power (horizontal left-right: 50-100 mW, +10 mW per step) and writing speed (vertical bottom-up: 1, 3, 5 mm/s)

In all, the 2PP structuring of PEGDA-700 and PEGDA-10k was successful. In particular, PEGDA-10k exhibited feasibility for 2PP structuring at a macromer content of 30%. Since alternative PEGDA with different MW (4.6 kDa) was also reported in literature, it is anticipated that PEGDA-4.6k may offer a better tradeoff between high reactivity (2PP processability) and low cytotoxicity. Nevertheless, regardless of MW long-term biocompatibility of PEGDA macromers may still arouse significant concern. Therefore, development of alternative hydrogel systems that circumvents acrylate chemistry and keeps high reactivity and cytocompatibility is worthy of additional research efforts.

### 3.2.3.2 PEG Dimethacrylates

In order to circumvent the toxicity issue of PEGDA, it is reasonable to evaluate the fabrication feasibility of the methacrylate analogue, PEG dimethacrylates (PEGDMA), which is supposed to be less cytotoxic. Particularly, two types of PEGDMA (PEG-600-DMA and PEG-1000-DMA) were selected in this study. Although both of these materials are water-soluble, preliminary 2PP structuring was not successful for formulations with 30% macromer content and 2% WSPI as photoinitiator. Given that reactivity of hydrogel formulations is not comparable to that of macromer alone, it is essential to test the 2PP feasibility of the macromer alone. The oil soluble initiator R1 was used instead in the following experiments.

#### 3.2.3.2.1 PEG-1000-DMA

The initial structuring test was performed using PEG-1000-DMA and 0.2% R1. Notably, due to high melting point this formulation became solid at room temperature and thus the processing was only possible after warming up the sample beyond 50 °C. As shown in Figure 136a, the speed-power array showed that this formulation was only processable at the lowest writing speed (10  $\mu\text{m/s}$ ). The change of laser power (70-100 mW) did not make a significant influence on the structure. However, after developing the sample in ethanol at 60 °C, the structures could not be observed, showing that the structure was too weak to withstand the developing procedure.

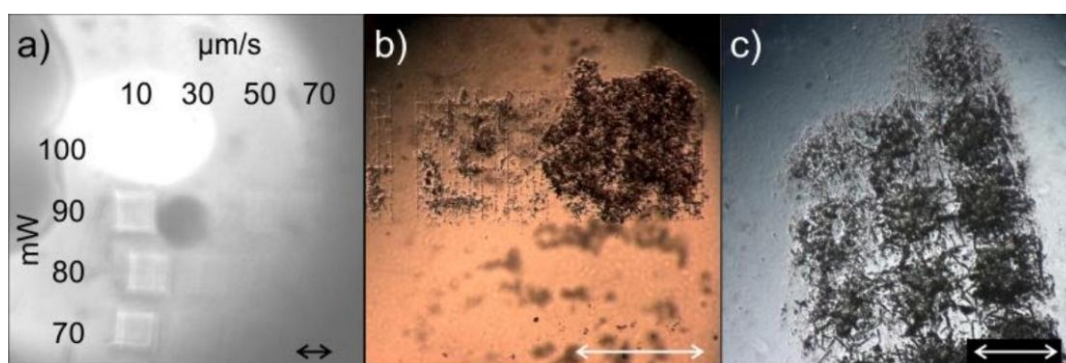


**Figure 136.** a) speed-power array of PEG-1000-DMA, online captured graph, 0.2 % R1; b) LM image (10 $\times$ ) of PEG-600-DMA structures, 0.2% B3FL; c) LM image (5 $\times$ ) of PEG-600-DMA structures, 0.2% R1; scale bars: 50  $\mu\text{m}$ <sup>206</sup>

### 3.2.3.2.2 PEG-600-DMA

In later experiments, PEG-600-DMA was screened with 0.2% two-photon initiator (either B3FL or R1). Although the formulations remained as liquid at room temperature, neither the structuring using B3FL (Figure 136b) nor R1 (Figure 136c) was feasible. The laser power was either too low to initiate polymerization, or too high to keep the polymer undamaged.

In order to optimize the reactivity, PEG-600-DMA was mixed with a glycerol dimethacrylates (90:10, w/w) and 0.5% R1. However, the 2PP structuring was not successful at any writing speed or laser power. Together, these negative results show that 2PP processing of PEGDMA macromers alone is challenging, not to mention the processing of PEGDMA hydrogels.

### 3.2.3.2.3 Formulation-3

In order to draw a general conclusion of the feasibility of methacrylates in 2PP, additional experiment was carried out using formulation-3 as the macromer and 0.5% R1 as photoinitiator. Formulation-3 is a composite formulation used in restorative dentistry. It is a 1:1:1 mixture of three commercial monomer/oligomers (Figure 137): bisphenol A-diglycerolate dimethacrylate (Bis-GMA), diurethane dimethacrylate (UDMA) and 1,10-decanediol dimethacrylate (D3MA).

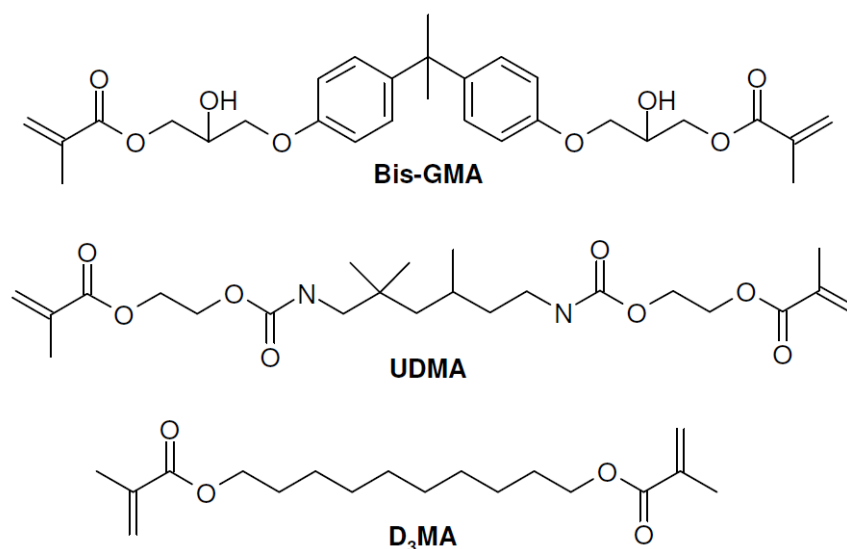


**Figure 137.** Chemical structures of the components in formulation-3

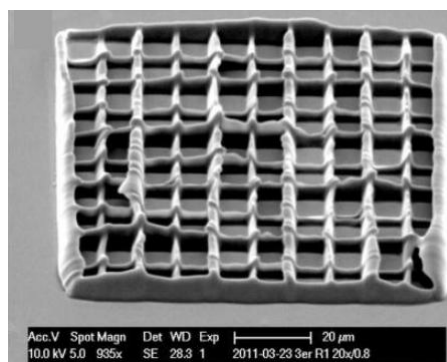


**Figure 138.** SEM image of the 2PP-fabricated lattice structure of formulation-3 (layer distance: 1  $\mu\text{m}$ , line distance: 5  $\mu\text{m}$ , speed: 300  $\mu\text{m/s}$ , power: 30 mW, 0.5% R1)<sup>206</sup>

As shown in Figure 138, a 3D construct of formulation-3 ( $100 \times 100 \times 30 \mu\text{m}^3$ ) was successfully built up by 2PP. The structure distortion indicated the shrinkage of the polymer networks and low crosslinking efficiency of formulation-3. This preliminary experiment showed that 2PP of methacrylates is feasible. Nevertheless, it is important to mention that formulation-3 is too hydrophobic to be used in hydrogel applications.

### 3.2.3.3 PEG Divinyl Esters

Given that PEG divinyl esters (PEGDVE) were successfully prepared and thiol-vinyl ester reactions exhibit high efficiency as demonstrated in Photo-DSC studies, the 2PP-fabrication feasibility of PEGDVE should be tested. Two types of PEGDVE (PEG-250-DVE and PEG-600-DVE) were screened in combination with either WPSI for water-based formulations, or R1 for non-water systems. PEG-250-VE was developed by Dr. Andreas Mautner during his thesis research. For thiol-ene copolymerization, ETTMP-1300 was added as the water-soluble macrothiol while TT was used as oil soluble macrothiol. It is important to mention that water solubility of PEG-250-VE and ETTMP-700 are not sufficient for preparing homogeneous solutions. To minimize the possibility of premature polymerization, 0.05 % pyrogallol was added as stabilizer.

#### 3.2.3.3.1 PEG-600-DVE

Initially, a water-based formulation containing 1% WPSI, 80% water, 13% PEG-600-DVE and 7% ETTMP-1300 ( $n_{\text{SH:ene}}=0.4$ ) was tested. However, the structuring was not possible even at the maximum laser power ( $\sim 200$  mW). In order to optimize the reactivity, another thiol-ene formulation containing 0.5% R1, 71% PEG-600-VE, 5.4%

DVA (of VE), 23.6% ETTMP-1300 ( $n_{\text{SH:-ene}}=0.2$ ) was prepared. In the absence of water, this formulation was still not processable, showing very limited reactivity of this formulation.

Alternatively, the trifunctional thiol (ETTMP-1300) was replaced with tetrathiol (TT) for the 2PP structuring with PEG-600-VE ( $n_{\text{SH:-ene}}=0.2$ ). Although initial online monitoring evidenced the formation of thin lattice structures at the scanned area, afterward the structures became dissolved by the surrounding formulation and finally disappeared. It is speculated that the double bond conversion was quite low and the crosslinking density of the structure was too weak to withstand the gravity of the surrounding materials.

### 3.2.3.3.2 PEG-250-DVE

Given that PEG-600-VE based formulations exhibited limited reactivity in preliminary experiments, PEG-250-VE was later attempted as the alternative material. While it is poorly water-soluble, the reactivity is supposed to be higher than that of PEG-600-DVE. Therefore, a thiol-ene formulation containing PEG-250-VE/TT ( $n_{\text{SH:-ene}}=0.2$ ), 0.4% R1, and 0.1% pyrogallol was prepared. From online monitoring, the structuring was in good accordance to the CAD model. The structures were later developed in ethanol and further analyzed by SEM.

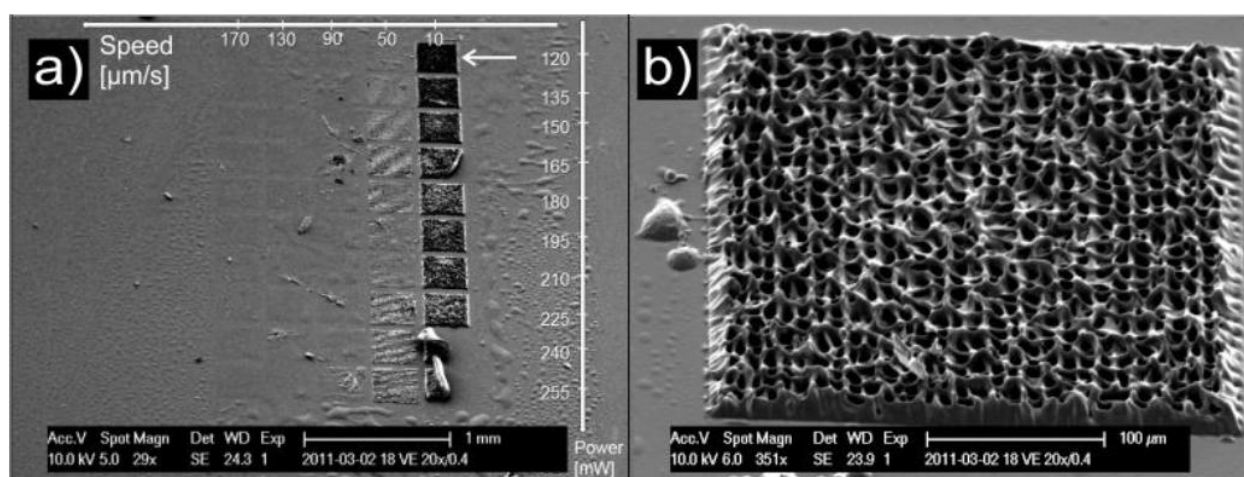


**Figure 139.** 2PP fabrication of a PEG-250-VE/TT formulation: a) SEM image of speed-power array and b) SEM image of one of the lattice structure fabricated at 10  $\mu\text{m/s}$  and 120 mW

The SEM picture (Figure 139a) of the speed-power array shows that the whole lattice-structures were only visible at the range with slowest writing speed (10  $\mu\text{m/s}$ ). Beyond this speed, only the contours of the unit structure were visible. In addition, structuring at

higher writing speeds was not accessible by increasing the laser power. Although one of the units (up-right) seems in best accordance to CAD, a closer look at this structure (Figure 139b) shows that the lattice deformed drastically after developing. The online-SEM variance of the structures indicates that the crosslinking efficiency of PEG-250-DVE/TT formulation was not sufficient and the formed structure was not strong enough to withstand the procedure.

### 3.2.3.3.3 DVA

As discussed in section 3.2.2.2, the reactivity of DVA is significantly higher than that of PEG-based divinyl esters due to the absence of abstractable hydrogens.<sup>159</sup> As such, the 2PP processability of DVA and DVA-based thiol-ene formulations should be investigated. In an initial trial, a DVA formulation was processed in the presence of 0.4% R1. As expected, the structuring was not visible through online monitoring. It is attributed to the very low crosslinking efficiency of DVA towards homopolymerization. It is very likely that the linear polyDVA is immediately dissolved by the surrounding DVA monomer.

In a later trial, a thiol-ene formulation containing DVA, TT ( $n_{\text{SH:-ene}}=0.2$ ), 0.4% R1 and 0.01% pyrogallol was processed according to a lattice-CAD model ( $300 \times 100 \times 20 \mu\text{m}^3$ ). It is supposed that the addition of a tetrathiol like TT would significantly increase the network crosslinking density.

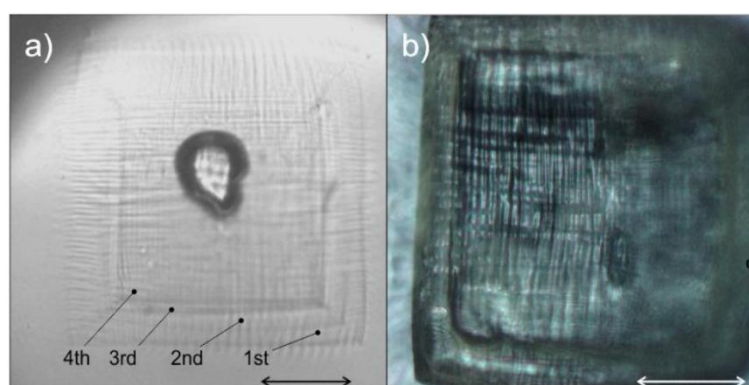


**Figure 140.** 2PP fabrication of a DVA/TT formulation: a) an online process observation showing the structured layers and b) the lattice-structure after development (line distance:  $5 \mu\text{m}$ ; layer distance:  $3.5 \mu\text{m}$ ; writing speed:  $10 \mu\text{m/s}$ ; power of  $100 \text{ mW}$ ; scale bars:  $30 \mu\text{m}$ )



As shown in Figure 140a, an online-graph was captured during the fabrication process. Although delicate polymer lines could be observed at the exposed area of each layer, the size shrinkage of the layer contour was also detected. I.e., at the 1<sup>st</sup> layer that is the closest to the cover slip, the size of the contour is much larger than the underneath layers that are more distant from the cover slip.

After the structuring, the sample was developed in ethanol and analyzed by a laser microscope. As shown in Figure 140b, the geometry-deformation (i.e., bending to the center) in the z-axis was observed. It is consistent with the online observation. To explain the underlined mechanism, one has to analyze the polymerization processes involved in thiol-ene polymerization of DVA and TT. It is accepted that thiol-vinyl ester reactions does not belong to the category of “ideal” thiol-ene reactions where homopolymerization is negligible. Instead, thiol-vinyl ester polymerizations should follow a mixed-mode mechanism. Once DVA is homopolymerized, the resultant polyDVA is supposed to be linear polymers that do not contribute to the crosslinking density and even cause stress defects. Although the use of TT could incorporate highly efficient chain-transfer reactions and build up a thiol-ene network, it is unclear that whether the crosslinking density of this network is sufficient to counteract the surrounding forces. The z-axis distortion is likely a combinatory consequence of: 1) weak mechanical strength of the network and 2) the gravity influence during 2PP fabrication.

To overcome the shape-distortion issue, optimizations on monomers and fabrication procedure are warranted. On one hand, it is reasonable to use alternative high MW macromers that are water-soluble and provide fast polymerization kinetics. On the other hand, it is critical to use cover slips that are surface-functionalized with “ene” or “thiol” groups to build up covalent bridges between the network and the cover slip.

Together, proof-of-concept 2PP of vinyl esters was established. While of PEGDVE exhibits very low efficiency towards homopolymerization, it is demonstrated that highly efficient thiol-vinyl ester reactions could increase the reactivity and 2PP-processibility of PEGDVE to a sufficient level. In comparison, PEGDA suffers from high cytotoxicity though it is highly reactive. Reactivity of PEGDMA is too low for 2PP and cannot be optimized by using thiol-ene chemistry, although it is less cytotoxic.



### 3.3 PVA-based Hydrogels

#### 3.3.1 Background

PVA are hydrophilic polymers originated from partial hydrolysis of poly (vinyl acetate). PVA-based hydrogels have been widely used in space filling and drug delivery systems because of their superior biocompatibility (FDA-approved). In addition, PVA hydrogels are uniquely stronger than most other synthetic hydrogels.<sup>21</sup>

#### Photopolymerizable PVA-derivatives

In the last decade, researchers have extensively explored PVA-based hydrogels formed by photopolymerization in a minimally invasive fashion. Anseth and co-workers have developed photopolymerizable PVA macromers with varying degree of degradable ester linkages and reactive acrylate groups.<sup>70</sup>

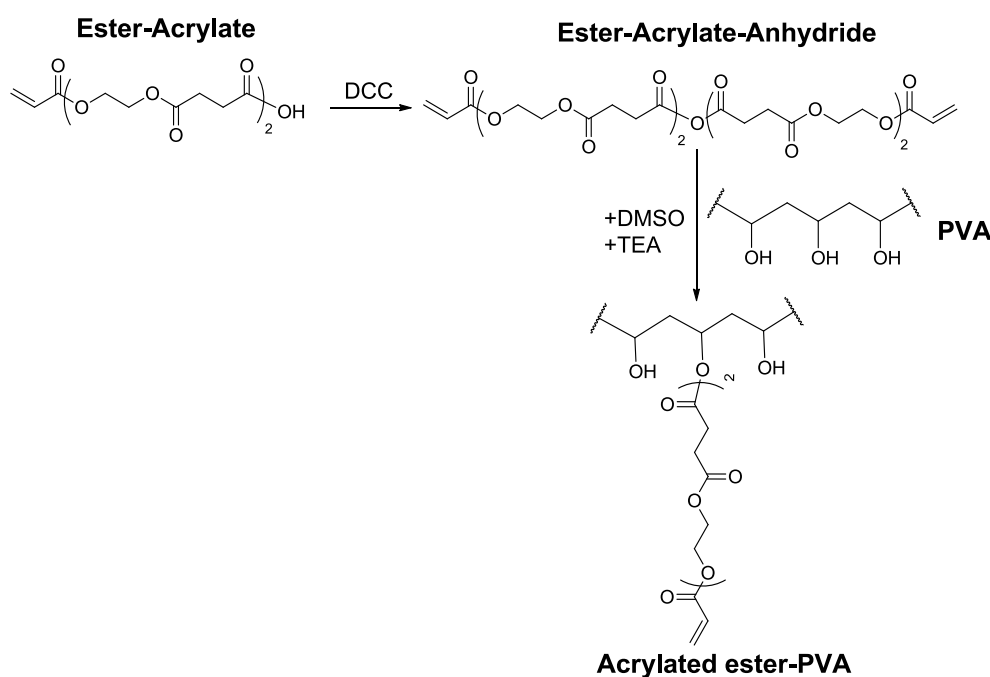


**Figure 141.** Synthetic scheme of acrylated ester-PVA

In this work, an acrylate terminated ester-anhydride was prepared and subsequently reacted with pendant hydroxyl groups of PVA to form the desired acrylated ester-PVA (Figure 141).

Synthetic hydrogels with tunable degradation profiles are important for most biodegradable scaffolds in tissue engineering. To this end, Martens et al. have copolymerized methacrylated PEG and acrylated PVA macromers that are hydrolytically degradable to produce hydrogels.<sup>207</sup> In this work, it was found that degradation rates of copolymerized PEG-PVA gel were faster than the rates of PEG gel, but slower than the rates of PVA gel.

Although PVA hydrogels are not cell-adhesive like most other neutral polymers, they can be rendered cell-adhesive by covalently conjugating biological molecules (e.g., RGD motif, fibronectin) to the pendant hydroxyl groups of PVA (Figure 142). For instance, Schmedlen et al. have prepared bioactive PVA hydrogels that were not only non-cytotoxic but also supported the attachment and spreading of fibroblasts.<sup>71</sup>

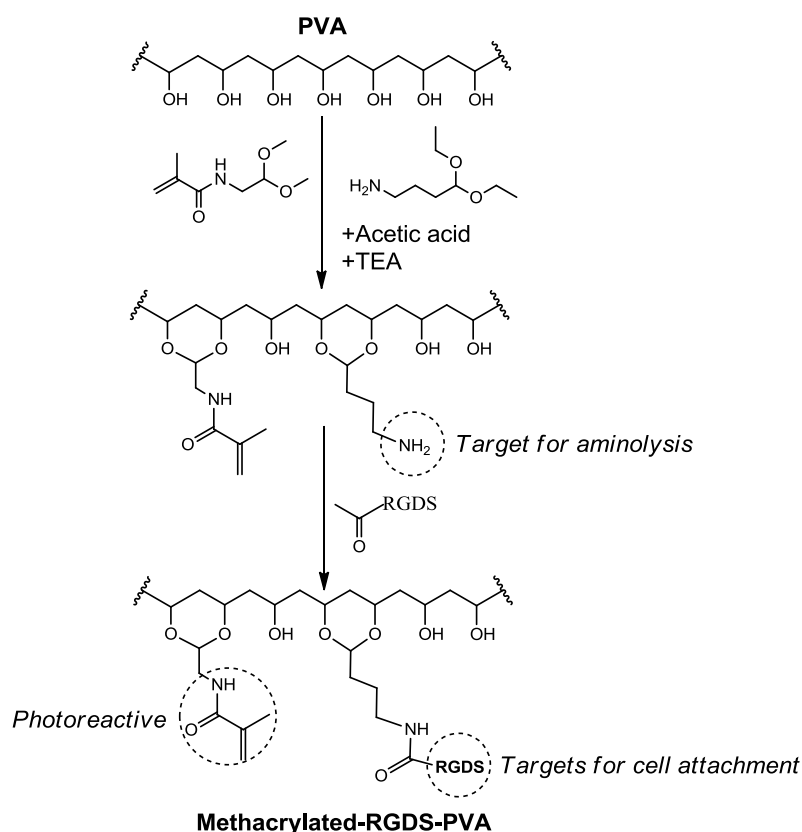


**Figure 142.** Synthetic scheme of methacrylated-RGDS-PVA

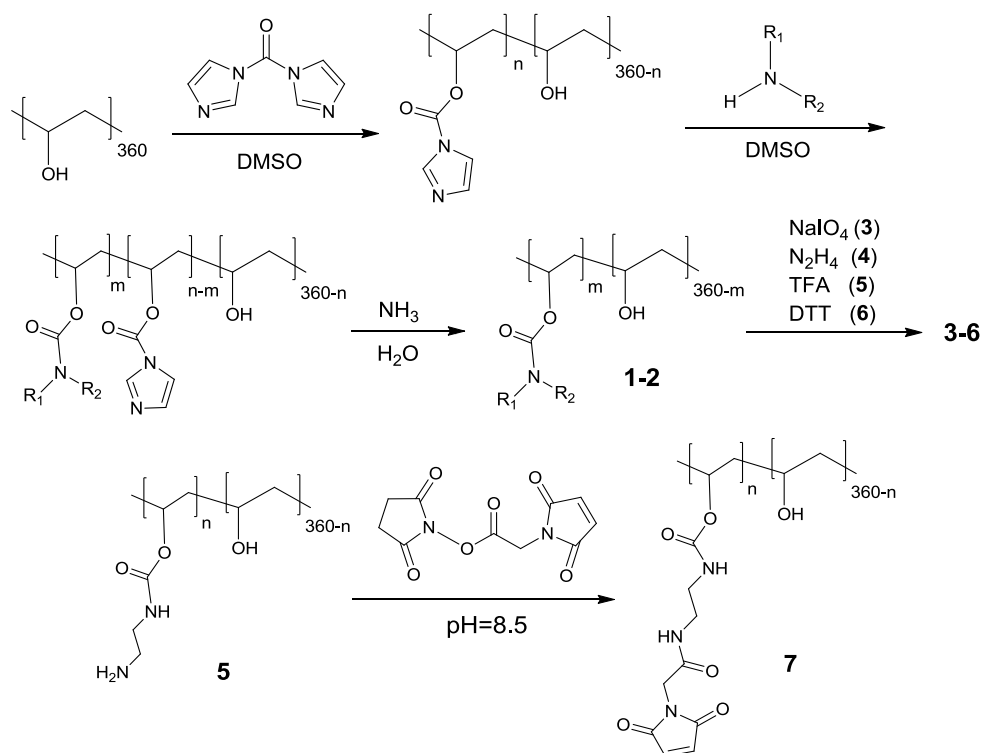
In this study, PVA was firstly modified with methacrylamide (for photocrosslinking) and amino groups (for RGD conjugation) via reaction of methacrylamidoacetaldehyde dimethyl acetal and aminobutyraldehyde diethyl acetal. Acetylated RGDS peptide was then immobilized on the modified PVA through an aminolysis reaction. It was found that

the extent to which these hydrogels can support cell attachment and spreading was dose-dependent on the immobilized RGDS. In another work, Nuttelman et al. have covalently attached fibronectin on the surface of preformed PVA (6 k) hydrogels through carbonyl diimidazol (CDI) chemistry.<sup>66</sup> The biofunctionalized PVA hydrogels drastically increased the rate of NIH3T3-fibroblast attachment and proliferation, and promoted 2D cell migration.

#### Clickable PVA-derivatives

Besides photopolymerizable PVA macromers, clickable PVA-derivatives have also been developed in the last decade. Notably, Ossipov and co-workers have developed a series of PVA derivatives for *in situ* formation of hydrogels at physiological conditions. These materials have orthogonal groups (Figure 143) including azide, alkyne, aldehyde, hydrazide, thiol, and maleimide. As mentioned in the introduction section, bio-orthogonal chemistry is leading a new fashion for various biological applications since these reactions provide superior specificity, high efficiency and quantitative yield in complex living systems. Comprehensive reviews related to bio-orthogonal (or click) chemistry could be found in literatures written by Carolyn Bertozzi<sup>46</sup> and Craig Hawker.<sup>47</sup>

As shown in Figure 143, a variety of clickable PVA-derivatives (**1-6**) could be developed by direct coupling of various nucleophilic functionalities to the hydroxyl groups of PVA through carbamate linkages. First, hydroxyl groups of PVA are activated with CDI groups. Second, CDI-activated PVA undergo nucleophilic substitution with the corresponding amines and form carbamate linkages. Third, the unreacted CDI groups are removed in ammonia, giving PVA-alkyne (**1**) and PVA-azide (**2**) as products and intermediates of **3-6**. To prepare PVA-aldehyde (**3**), the 3-amino-1,2-propanediol-modified PVA is further reacted with a 10-fold excess of NaIO<sub>4</sub> at 0 °C for 30 min and later purified by dialysis. To prepare PVA-hydrazide (**4**), glycine ethyl ester-modified PVA is further reacted with excessive hydrazine for another 24 h at room temperature and followed by dialysis purification. For PVA-amine (**5**), the Boc-protected intermediate is incubated with a mixture of trifluoroacetic acid (TFA) and water (95:5, v/v) for 1 h at room temperature and then purified by dialysis.



Compounds	Functionalities	R <sub>1</sub>	R <sub>2</sub>
1	alkyne	H	
2	azide	H	
3	aldehyde	H	
4	hydrazide	H	
5	amino	H	
6	thiol	H	
7	maleimide*	-	-

**Figure 143.** Schematic showing the synthesis of PVA-derivatives (\*indicating "7" was prepared by reacting "5" with 2-maleimidoacetic acid N-hydroxy succinimide ester, summarized from lit.<sup>49, 68, 69</sup>)

For thiolated PVA (6), the disulfide intermediate is mixed with reducing agent dithiothreitol (DTT) for disulfide cleavage and the resultant solution is further purified by

dialysis against dilute HCl (pH=3). On the other hand, PVA-maleimide (**7**) could be prepared by reacting PVA-amine (**5**) with 2-maleimidoacetic acid N-hydroxy succinimide ester at alkaline conditions (pH=8.5).

In one of these studies,<sup>68</sup> cytotoxicities of PVA-derivatives (macromer solution and gel extracts) were tested by MTT-assay using human dermal fibroblasts. The results showed that the toxic effects of the macromer solutions (0.1 wt%) and extractions out of gel pellets are not significant.<sup>68</sup> However, it is important to mention that the DS of these materials is generally around 1-5% and the water solubility of these compounds are quite limited. As a result, DMSO has to be used as the primary solvent for hydrogel preparation and removed after gelation by exchanging with water. The poor water solubility of these derivatives will definitely pose a challenge for potential clinical applications such as surgical sealants. Therefore, it is essential to devise alternative synthetic approaches for reaching a better tradeoff between appropriate DS and good water solubility.

### 3.3.2 Synthesis of PVA-Norbornene

In order to address the solubility limitation in reported PVA-derivatives, alternative approaches should be devised for the synthesis of photopolymerizable PVA-derivatives with good water solubility. Among various "ene" functionalities for thiol-ene photopolymerization, strain-promoted "norbornene" group is one of the most reactive "ene" functionalities.<sup>55</sup> Furthermore, Fairbanks and Anseth reported that 4-arm-PEG-norbornenes exhibited high reactivity and hydrogels formed by thiol/PEG-norbornene photopolymerization enabled access to *in situ* cell photoencapsulation.<sup>54</sup> Considering that PVA-norbornene remains unreported in literature, it is intriguing to incorporate highly reactive norbornene groups onto PVA backbones and utilize it for hydrogel applications.

As reported by Fairbanks et al.,<sup>54</sup> 4-arm-PEG-norbornene was prepared by reacting 5-norbornene-2-carboxylic acid with hydroxyl groups of 4-arm-PEG under the catalysis of DCC and DMAP in DCM. Although it seems reasonable to utilize a similar method (Figure 144a) to prepare PVA-norbornene, it is important to note the substrate variance between PEG and PVA in terms of water solubility. For instance, high MW PVA (22 kDa) often necessitates several hours of dissolution at high temperature (> 60 °C)

whereas high MW PEG (10 kDa) can be dissolved in several minutes. Thus, it is supposed that PVA-norbornene prepared by approach-(a) (Figure 144) still suffers from limited water solubility.

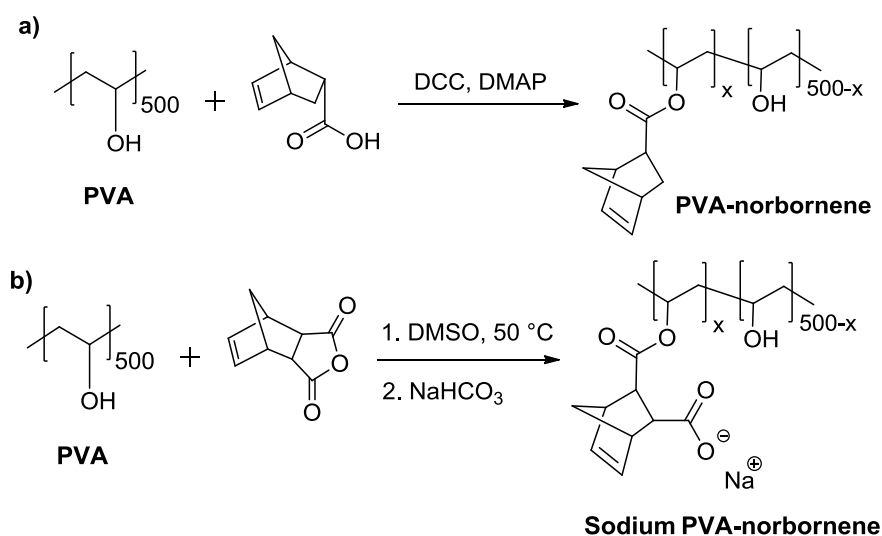


**Figure 144.** Proposed synthetic schemes of PVA-norbornene: reaction of PVA with **a)** 5-norbornene-2-carboxylic acid, and **b)** *cis*-5-norbornene-*endo*-2,3-dicarboxylic anhydride

In the master thesis of Daniel Bomze (IAS),<sup>208</sup> PVA-derivatives with pendant allyl groups were prepared by reacting allylsuccinic anhydride with hydroxyl groups of PVA. After ring-opening reaction, both allyl and carboxylate groups are incorporated into PVA backbone. Allyl groups can be utilized for thiol-ene polymerization while the carboxylate groups are advantageous for offering good water solubility once neutralized.

With this in mind, an adapted approach (Figure 144b) was devised for the synthesis of sodium PVA-norbornene. Specifically, PVA (22 kDa) was allowed to react with *cis*-5-norbornene-*endo*-2,3-dicarboxylic anhydride (NorA) under the catalysis of *p*-toluenesulfonic acid in anhydrous DMSO. After a 48 h reaction at 50 °C, the crude product was directly purified by dialysis against distilled water. After ~6 h ( $\times 2$  changes of water), it was supposed that most of the DMSO had been removed. The solution was further dialyzed against dilute NaHCO<sub>3</sub> solution (10 mM) to convert the products into the sodium salt form. The products were finally lyophilized.

To confirm the synthesis, the lyophilized PVA-norbornene was analyzed using proton NMR in comparison with unmodified PVA. As shown in Figure 145a, the spectrum of unmodified PVA represents two major peaks at 4.0 ppm and 1.6 ppm, which are



corresponding to the -CH- and methylene groups, respectively. The spectrum of PVA-norbornene (Figure 145b) shows new peaks at 6.2 ppm (s, 2H, -CH=CH-), 3.3 ppm (s, 2H, -C=C-CH-CH-), 3.1 ppm (s, 2H, -C=C-CH-CH-) and 1.3 ppm (s, 2H, -CH<sub>2</sub>-), respectively.

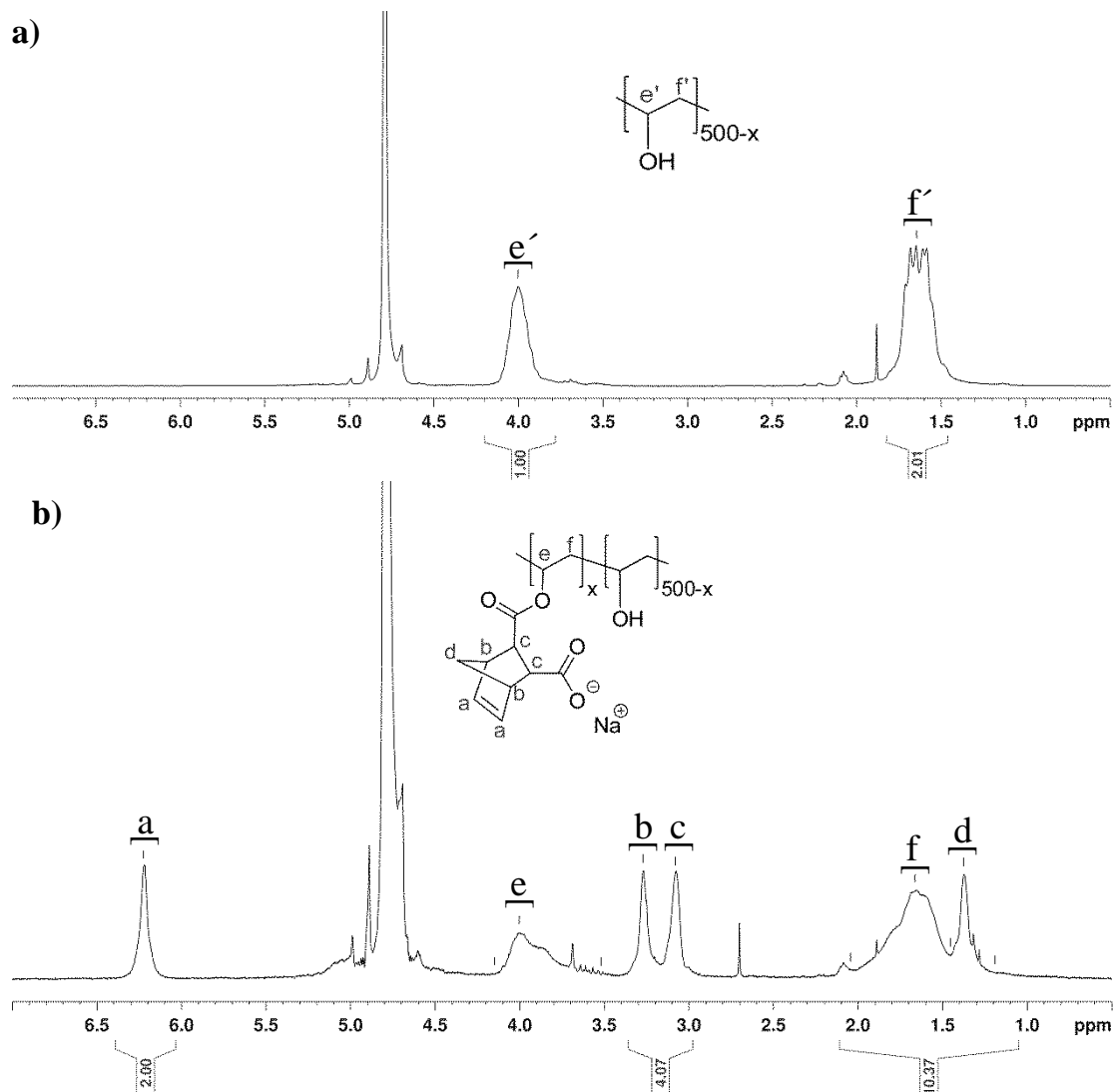


**Figure 145.** <sup>1</sup>H-NMR spectra of PVA (a) and PVA-norbornene (b) in D<sub>2</sub>O

The DS of PVA-norbornene was determined according to equation (4) & (5):

$$\frac{2x}{2 \times 500} = \frac{\iint a}{\iint f, d - \iint d} = \frac{2.00}{10.37 - 2.00} \quad (1)$$

$$DS = \frac{x}{500} \quad (2)$$

After calculation, a DS value of “0.24” was obtained, indicating the presence of ~24 norbornene groups per 100 PVA repeating units.

In order to test the feasibility of PVA-norbornene with tunable DS, further experiments were performed by changing either the reaction time or the stoichiometry. The synthesis was made possible under the assistance from Daniel Bomze and Viktoria Schwartz. As shown in Table 21, it was found that the DS could be adjusted within a wide range from 0.07, 0.19, 0.24 to 0.42. Three types of PVA-norbornene were used in further characterization: PVA-Norb-High (DS=0.43), PVA-Norb-Mid (DS=0.24), and PVA-Norb-Low (DS=0.07).

**Table 21.** Influence of reaction time and stoichiometry on DS (\*stoichiometry: the molar ratio between NorA and –OH groups of PVA)

Entry	Stoichiometry *	Reaction Time (h)	DS	PVA-Norb-X
1	1:10	24	0.07	Low
2	1:2	24	0.19	-
3	1:2	48	0.24	Mid
4	1:2	72	0.42	High

### 3.3.3 Characterization

#### 3.3.3.1 Cytotoxicity

Cytotoxicity of PVA-based macromers was evaluated by Presto-Blue assay using a L929-fibroblast cell line, as described in section 2.3.2.1. The experimental work was made possible with the assistance of Ms. Marica Markovic (IMST). At the initial stage, the toxic effects of PVA substrate at varying concentrations were screened in order to test whether the substrate alone would influence metabolic activity of L929. Since it was hard to prepare a 10% solution of PVA (22 kDa), the macromer solutions were tested at three concentrations: 5%, 1%, and 0.1%.

As shown in Figure 146, the results from Presto-blue assay proved that at all tested concentrations, the substrate alone did not induce significant toxicity on L929 cells. Even

at 5%, the concentrated macromer solutions nearly doubled the metabolic activity of L929. This might be explained as a mechano-transduction mechanism. It is well established that mammalian cells can convert mechanical stimuli into biochemical signals and consequently change their physiological processes.<sup>187</sup> In this experiment the medium viscosity is increased due to the presence of a high number of PVA macromers. Therefore, the cytoskeleton is possibly stressed and certain metabolic pathways may be activated.

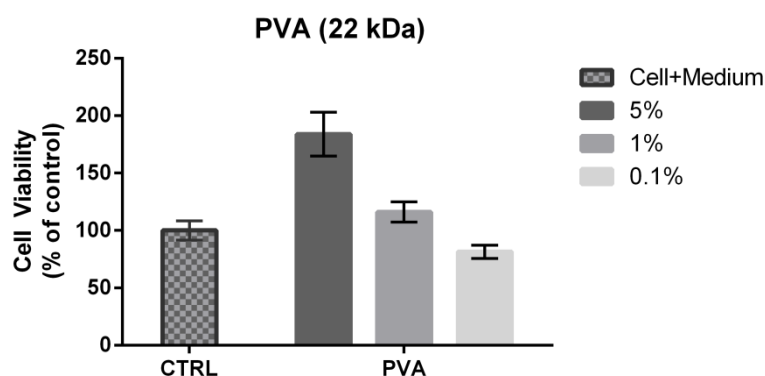


**Figure 146.** Cell viability of PVA solutions at varying concentrations (5, 1, 0.1 %)

Based on the preliminary toxicity results, PVA-norbornene with three different DS were tested using the same method. As shown in Figure 147, formulations of PVA-norbornene at 10% induced a significant decrease of metabolic activity of L929. This phenomenon is distinctive from that of 5% PVA as discussed in preliminary test.

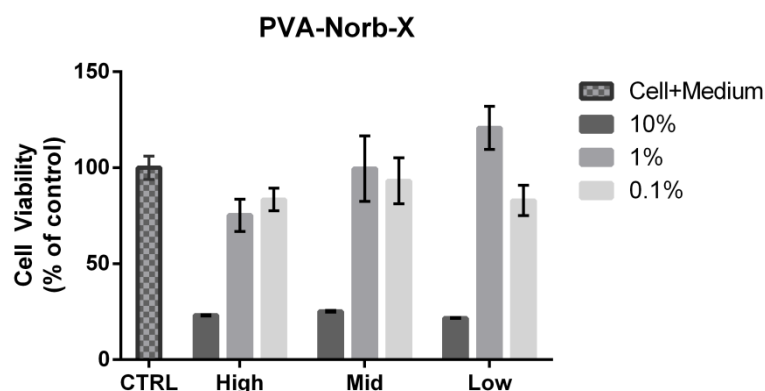


**Figure 147.** Cell viability of PVA-Norb-X solutions at varying concentrations (10, 1, 0.1 %)

The varying cellular response to different macromer solutions at high concentration suggests a different acting mechanism between unmodified and modified PVA. In particular, PVA substrates are neutral polymers whereas PVA-norbornenes are negatively

charged after modification. The charge effects may directly/indirectly give an influence on certain signaling pathways that are relevant to the metabolic activities of L929. As the macromer concentration decreases to 1% and 0.1%, the charge effects become insignificant and thus do not make a significant influence on metabolic activity of L929.

### 3.3.3.2 Photo-Rheometry

Photoreactivity of PVA-norbornene was analyzed using photo-rheometry as described in section 2.3.2.2. Specifically, PVA-Norb-Mid (DS=0.24) was tested in comparison with PEGDA-10k at 10% macromer content and 0.5 % I2959 in water. To verify the influence of thiol-ene chemistry, PVA-Norb-Mid were also investigated in combination with varying thiols (Figure 148): either DTT (dithiol) or PVA-SH (macrothiol, DS=0.1). PVA-SH was developed by Daniel Bomze in his master thesis.<sup>208</sup>

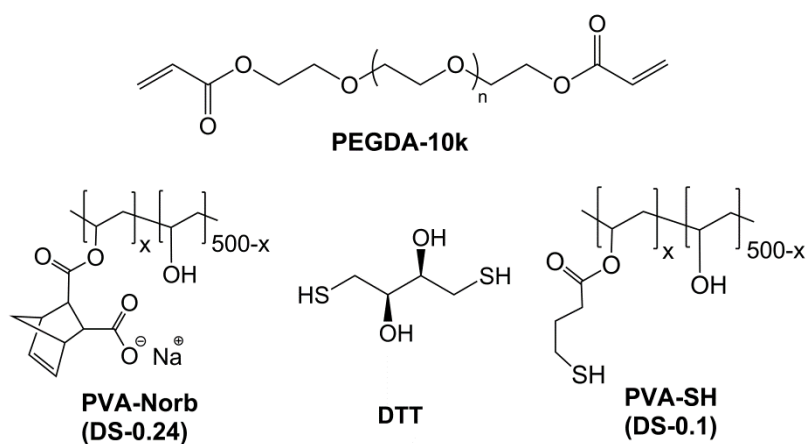


**Figure 148.** Chemical structures of materials used in photo-rheometry

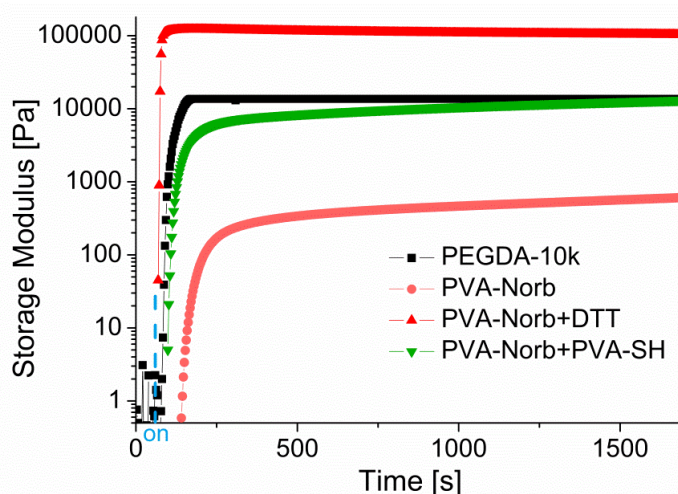


**Figure 149.** Photo-rheometry of formulation I-IV (60 s blank period, 10% macromer content, 0.5% I2959 in PBS,  $n_{\text{SH:norbornene}}=1$ ): plotted  $G'$ -curves during photopolymerization

As shown in Figure 149, after a blank period of 60 s, light-induced homopolymerization of PEGDA-10k (-■-) represents a rapid onset of  $G'$  (Entry-I, Table 22) with a plateau value of 14 kPa. The gel point (i.e.,  $G'/G''$  vicinity) of PEGDA-10k was defined as 21 s.

**Table 22.** Thiol to ene ratios, gel points,  $G'$  and  $G''$  values of formulations I-IV

Entry	macromer (10%)	$n_{\text{-SH:-ene}}$	Gel point (s)	$G'$ -plateau (kPa)	$G''$ -plateau (kPa)
I	PEGDA-10k	0:1	21	13.5	0.02
II	PVA-Norb	0:1	102	1.0	0.01
III	PVA-Norb/DTT	1:1	7	121.3	0.2
IV	PVA-Norb/PVA-SH	1:1	42	16.5	0.03

In 2009, Fairbanks et al. reported that the extent of homopolymerization of 4-arm-PEG-norbornene was negligible and the associated gel point was infinite.<sup>54</sup> To test whether homopolymerization of PVA-norbornene proceeds in the same fashion, 10% PVA-Norb-Mid solution was exposed to UV-irradiation for 30 min. Surprisingly, a  $G'$ -increase could be observed after an irradiation time of 84 s and the sample finally reaches a  $G'$ -plateau value of 1 kPa (Figure 149). Although the gel point (Entry-II, Table 22) was 102 s, the  $G'$ -increase indicates the presence of partial crosslinking. Since the propagation rate of norbornene functionality is supposed to be very low,<sup>55</sup> the norbornene-centered radicals may combine and form a crosslink. An intermolecular-crosslinking mechanism is proposed in Figure 150.

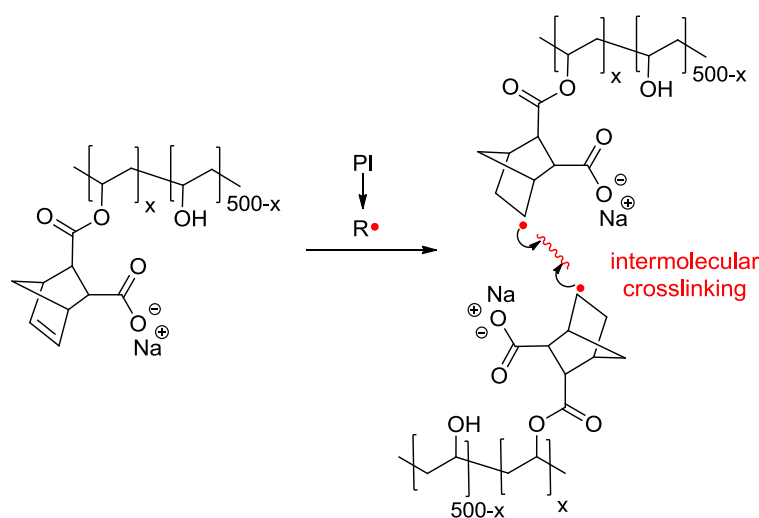


**Figure 150.** Proposed mechanism for the photocrosslinking of PVA-norbornene/I2959 solutions under UV-irradiation

### Influence of Thiol-ene Chemistry

To investigate the influence of thiols on the photoreactivity of PVA-norbornene, a water-soluble dithiol (DTT) was selected as the model crosslinker due to its efficacy demonstrated in section 2.3.2.3. Specifically, PVA-Norb was tested in combination with varying amounts of thiol groups (Table 23) at constant macromer content (10 %). It is hypothesized that the change of thiol to ene ratio could influence the physicochemical properties of the hydrogel networks.

As shown in Figure 151, the addition of DTT into PVA-norbornene solution ( $n_{\text{thiol:ene}}=0.2$ ) dramatically shifted the  $G'$ -plot to the left, indicating the significant increase of photoreactivity. In comparison with PVA-Norb (Figure 151, -■-), the gel point was shortened from 102 s to 10 s while the  $G'$ -plateau value increased from 1 kPa to 4 kPa. As the thiol to ene ratio increased from 0.2 to 0.4 and to 0.8, the gel point decreased to 10 s and 9 s, while the  $G'$ -plateau value gradually increased to 10 kPa and 43 kPa, respectively. When the thiol to ene ratio was 1:1, the gel point was 7 s and the  $G'$ -plateau value was 121 kPa.

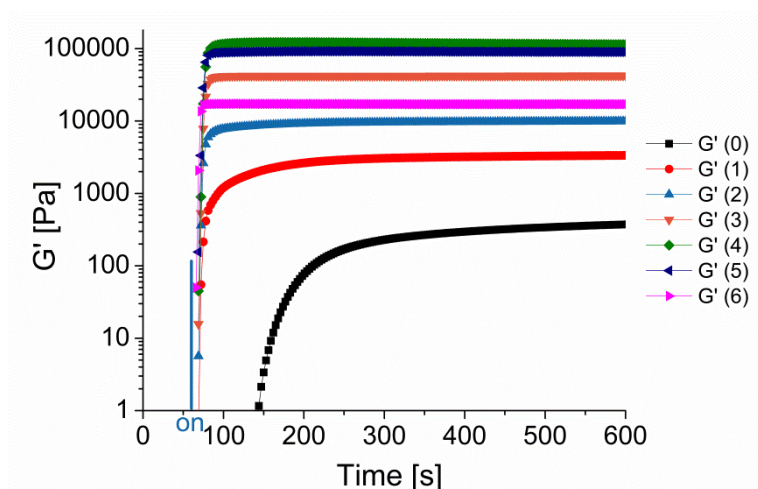


**Figure 151.** Influence of thiol to ene ratio on the  $G'$ -plots of formulation 0-6 (10% macromer and 0.5 % I2959 in water)

Interestingly, as the thiol to ene ratio further increased to 1.25 and to 2.5, the gel point was further shortened to 6 s and 3 s, respectively. This suggests that the photoreactivity was indeed increased due to the increase of thiol groups. However, the  $G'$ -plateau value decreased to 91 kPa and 17 kPa, respectively. This is attributed to the decreased crosslinking density when the thiol groups are in excess. In other words, although the norbornene groups are quickly consumed by DTT, a large amount of thiol groups remain

unreacted. The mono-substituted DTT does not contribute to the crosslinking density of gel networks. Given that a sufficient G'-plateau value is needed for 2PP microfabrication, the optimal thiol to ene ratio for PVA-Norb/DTT was defined as "1:1".

**Table 23.** Influence of thiol/ene ratio on gel points and G'-/G"-plateau values

Entry	Ratio -SH:Norb	Stoichiometric ratio	Gel points (s)	G'-plateau (kPa)	G"-plateau (kPa)
0	0:1	0	102	1.0	0.01
1	1:5	0.2	11	4.0	0.01
2	2:5	0.4	10	10.0	0.02
3	4:5	0.8	9	43.0	0.06
4	1:1	1	7	121.0	0.2
5	5:4	1.25	6	91.0	0.2
6	5:2	2.5	3	17.0	0.02

### PEGDA vs. PVA-Norb

Given that acrylate chemistry is termed as the most effective approach for hydrogel formation, it is intriguing to compare the efficiency of thiol-norbornene chemistry with conventional acrylate chemistry. As such, further analysis on the rheometry results of PEGDA-10k (I) and PVA-Norb/DTT (III) was carried out. For PVA-Norb/DTT, the gel point was as short as 9 s (21 s for I) and the G'-plateau value was 120 kPa (14 kPa for I). These data show that thiol-ene photopolymerized hydrogels exhibit a faster gelation and a higher crosslinking density in comparison with PEGDA gels. This is attributed to the extremely high efficiencies of thiol-norbornene reactions. These results are consistent with previous studies related to PEG-norbornene hydrogels.<sup>54</sup>

In order to quantitatively compare the reactivity differences, two important parameters (i.e., slope value and induction time) were further quantified by analyzing the G'-plots. The slope value corresponds to the maximum rate of polymerization. As shown in Figure 152b, PEGDA-10k has a slope value of ~700 while PVA-Norb/DTT has a slope value of 35000. These data quantitatively confirm that the polymerization rate of DTT-involved thiol-norbornene photopolymerization was significantly higher than that of

PEGDA-10k. Furthermore, the induction time of PEGDA-10k was  $\sim 20$ s while the thiol-ene sample took  $\sim 7$  seconds to initiate polymerization.

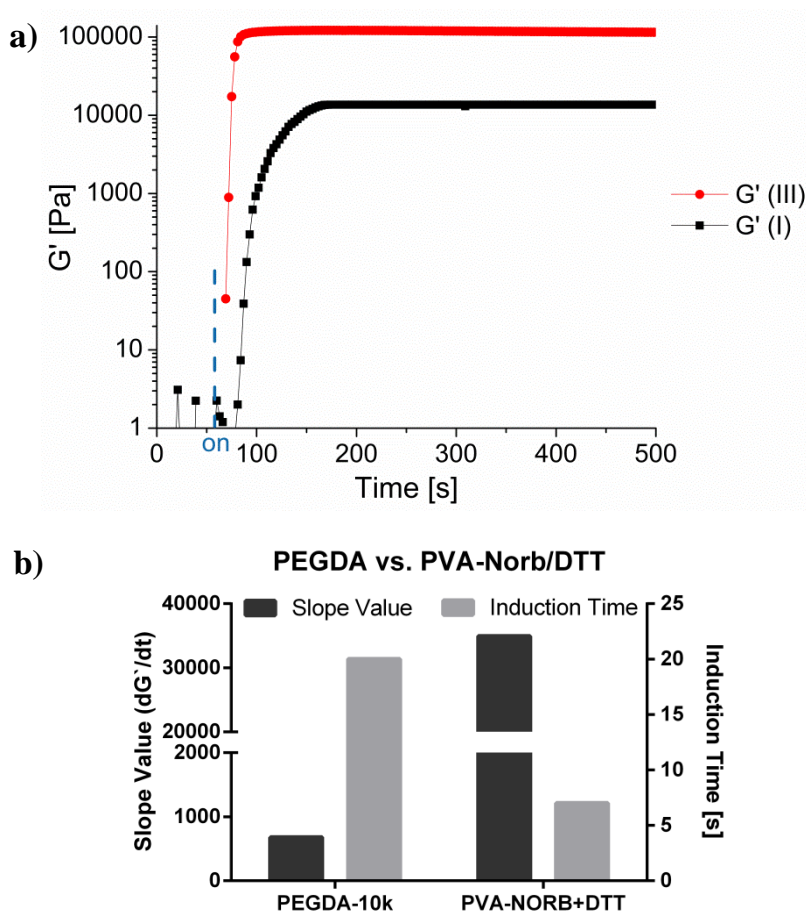


**Figure 152.** Comparative analysis on the rheometry curves of PEGDA-10k (I) and PVA-Norb-Mid/DTT (III): **a)** the  $G'$ -plots and **b)** comparison in slope values and induction time (60 s blank period, 10% macromer, 0.5 % I2959 in water,  $-\text{SH}:\text{-norbornene}=1$ )

### Influence of Thiol Type (DTT vs. PVA-SH)

Besides DTT, it is intriguing to explore the utility of a macrothiol (PVA-SH) for thiol-ene photopolymerization of PVA-Norb. A thiolated-PVA macromer (PVA-SH, 22 kDa, DS=0.1) was also screened as a macrothiol crosslinker. It is assumed that the size variance between DTT and PVA-SH would provide hydrogel networks with different mesh sizes and distinctive physical properties.

PVA-SH was mixed with PVA-Norb (IV) according to the DTT control (III), to reach a thiol to ene ratio of 1:1, a total macromer content of 10% and an initiator (I2959) concentration of 0.5 %. Notably, it was challenging to prepare a 20% solution of PVA-SH. To exclude the possibility of presence of disulfide bridges, TCEP was added a



reducing agent for disulfide cleavage. However, the addition of TCEP did not improve the solubility. As such, the dissolution challenge should be addressed to the poor water solubility of PVA-SH (DS=0.1) which has ~50 thiol groups per molecule.

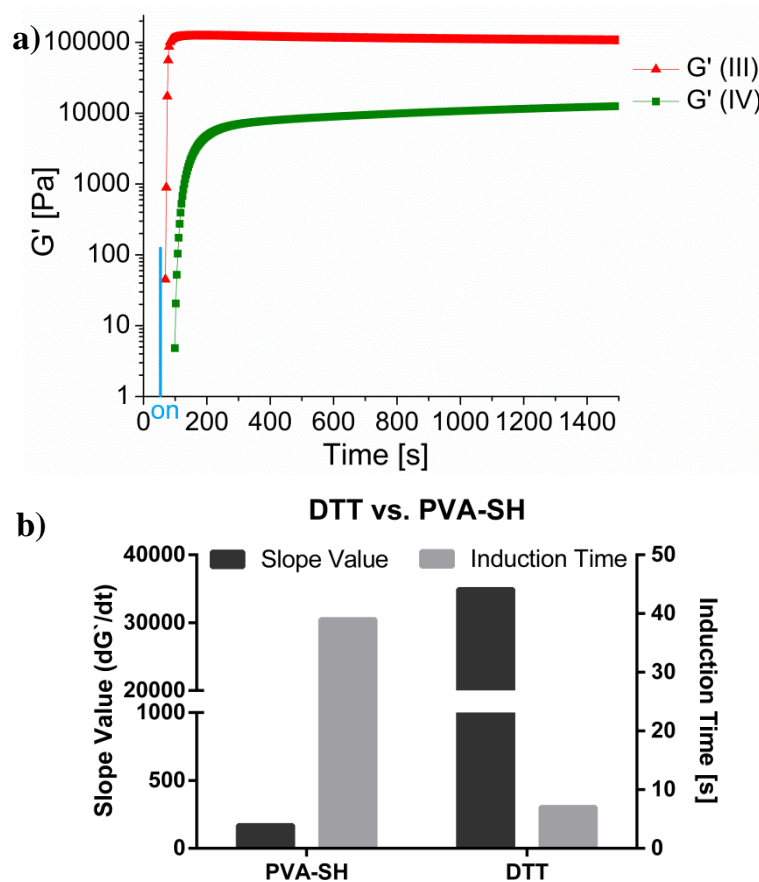


**Figure 153.** Comparative analysis on the rheometry curves of PVA-Norb-Mid/DTT (III) and PVA-Norb-Mid/PVA-SH (IV): **a)** the  $G'$ -plots and **b)** comparison in slope values and induction time (60 s blank period, 10% macromer, 0.5 % I2959 in water, -SH:-norbornene=1)

As shown in Figure 153a, the rheometry results show that the addition of PVA-SH indeed improved the reactivity of PVA-Norb, but exhibited much lower reactivity than the control formulation (III) containing DTT. The gel point of this formulation (IV) was 42 s (7s for III) while the  $G'$ -plateau value was only 16.5 kPa (121 kPa for III), showing the lower crosslinking efficiency. The low reactivity of formulation-IV is likely attributed to the decreased accessibility of  $-SH$  groups donated by the large crosslinker ‘‘PVA-SH’’ and the compromised efficiency of thiol-ene reactions. By contrast, the smaller crosslinker ‘‘DTT’’ may provide a much higher degree of accessible  $-SH$  groups and a higher reactivity.

As shown in Figure 153b, the lower crosslinking efficiency of PVA-SH than DTT is also evidenced by the slope value and induction time of respective formulation. The slope value of formulation-IV was  $\sim 170$  which is more than two orders of magnitude lower than that of formulation-III ( $\sim 35000$ ). Furthermore, the induction time was  $\sim 39$  s which is significantly longer than that of the DTT control ( $\sim 7$  s). Together, these results lead to a conclusion that DTT exhibits higher crosslinking efficiency than PVA-SH for preparing PVA-Norb hydrogels.

### Influence of Macromer Content

In order to test whether the mechanical properties of PVA-Norb gels could match various soft tissues, PVA-Norb/DTT formulations with varying macromer content but with constant thiol to ene ratio (1:1) were screened using photo-rheometry. In order to minimize the effects of initiator-dose, the molar ratio between I2959 and PVA-Norb was kept constant.

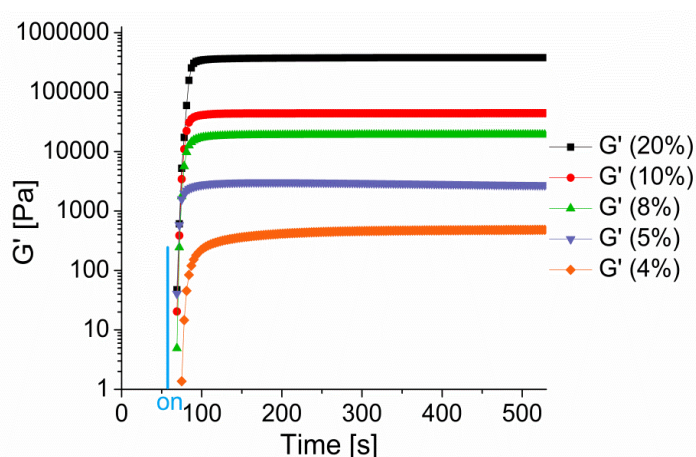


**Figure 154.** Influence of macromer content on G'-plots

As shown in Figure 154, by changing the macromer content the elastic moduli ( $G'$ ) of PVA-Norb gels are tunable within a wide range (400 Pa to 500 kPa). As the macromer content decreased from 20% to 4%, the gel point (Table 24) was delayed to varying degree, indicating the decreased reactivity as a result of lower concentration of reactive groups. The lower limitation of macromer content to form a gel was found to be 3%. Together, one can envisage that PVA-Norb/DTT gels can be utilized as photopolymerizable materials for mimicking various soft tissues.

**Table 24.** Influence of macromer content on gel points and G'/G"-plateau values

macromer (%)	n <sub>-SH:-ene</sub>	gel points (s)	G'-plateau (kPa)	G"-plateau (kPa)
20	1:1	6	380.0	6.8
10	1:1	6	44.3	0.07
8	1:1	9	19.3	0.02
5	1:1	9	3.0	0.006
4	1:1	15	0.5	0.003

### 3.3.4 2PP Microfabrication

Based on the one-photon rheometry studies, 2PP-feasibility of PVA-Norb was investigated in combination with DTT (n<sub>-SH:-ene</sub>=1), at a macromer content of 20% and a P2CK concentration of 2.23 mM. The processing window of this formulation was firstly evaluated based on a power-speed array of simplified 2D squares. The 2PP experiments in this section were performed by Peter Gruber (IMST).

As shown in Figure 155, the thiol-norbornene formulation exhibited a broad processing window for 2PP. It was processable at laser power (20-90 mW) and writing speeds (1-6 mm/s). Although at the right corner the gel structures seem disappeared, these structures were found outside of the prescribed area after development in PBS (data not shown). The full access to the gel structures indicates the high crosslinking efficiency of the tested formulation. The detachment was due to low affinity between the hydrogel network and the methacrylated cover slip. In other words, it is attributed to the low efficiency of methacrylate groups to be involved in thiol-norbornene reactions. Therefore, optimizations on the surface chemistry of cover slips are needed to fix 2PP-fabricated gel structures.

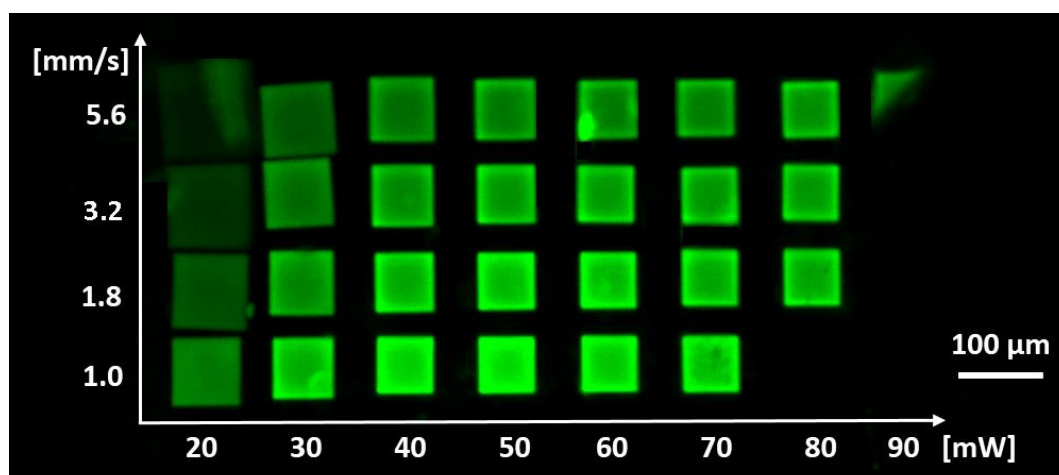


**Figure 155.** Speed-power array of a PVA-Norb/DTT formulation (20% PVA-Norb-Mid,  $n_{\text{SH-ene}}=1$ , 2.23 mM P2CK as initiator in PBS)

To better build up the interface-binding, sulfhydryl groups were immobilized on the cover slips by reacting the surface  $-\text{OH}$  groups with (3-mercaptopropyl)trimethoxysilane. It is anticipated that after treatment the surface  $-\text{SH}$  groups could efficiently participate in the thiol-norbornene polymerization and therefore contribute to a desirable interface-binding via thioether linkages. Based on this optimization, the detachment problem was finally circumvented in the following 2PP-experiments of PVA-Norb, as demonstrated in the master thesis of Daniel Bomze.<sup>208</sup>

Given that the primary target of this thesis research is to construct 3D hydrogel scaffolds for tissue engineering applications via 2PP, it is essential to investigate the feasibility of PVA-Norb for 2PP microfabrication of 3D hydrogels with complex geometries. As mentioned in section 1.5.5, rational design of hydrogel scaffolds with programmed microstructures is critical for many applications, such as long-term culture of hepatocytes for liver regeneration. As such, a 3D model (Figure 156) was devised as an interconnected, porous structure with relatively large sizes in x- (1.2 mm) and y- (1.0 mm). Specifically, this scaffold consists of three layers of packed cylinders arranged in a hexagonal geometry. Each cylinder has an outer (inner) diameter of 160 (120)  $\mu\text{m}$ , a spaced-distance of 150  $\mu\text{m}$  and a thickness of 50  $\mu\text{m}$ .

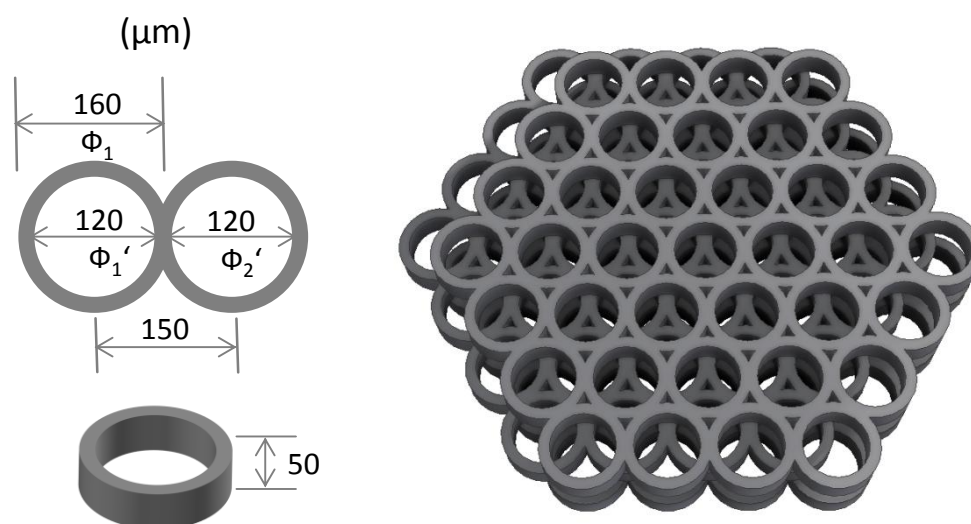


**Figure 156.** Schematic showing the scaffold model ( $1.5 \times 1.2 \times 0.15 \text{ mm}^3$ ) for 2PP fabrication of hydrogel constructs

To fabricate a scaffold with large sizes, high writing speed plays an important role in determining the processing time. Thus, the formulation was processed at a writing speed of 100 mm/s and an average power of 100 mW. Through online observation, vivid hydrogel structures were visible during 2PP, showing superior processability at selected conditions. Notably, similar performance had only been observed for a non-water based formulation consisting of highly reactive ETA and TTA.

After 2PP processing, however, it was found that the gel structure could not be developed into the prescribed shape. In other words, the “unpolymerized” materials outside of the exposed area were also crosslinked. There exist several probable explanations for this phenomenon. First, the 2PP-threshold of the thiol-norbornene formulation was too low to keep the 2PP probability only in the most focused area. Second, due to low threshold the radical diffusion during 2PP might enlarge the polymerization volume. Third, thiol-ene formulations are well-known for their poor storage stability. After 2PP fabrication, any remaining radical may induce further crosslinking of residual gel precursors.

To address this limitation, another hydrogel formulation containing 10-fold less photoinitiator (0.22 mM P2CK) was attempted. It is supposed that the decrease of initiator concentration may likely increase the polymerization threshold and keep the 2PP more localized. Unfortunately, it was found that the processability of this formulation

was very poor. Alternatively, a water-soluble stabilizer (pyrogallol) was added into the formulation (2.23 mM P2CK). On one hand, the presence of stabilizer is supposed to increase the polymerization threshold. On the other hand, the stabilizer should improve the storage stability of the formulation, scavenge residual radicals and keep left materials unpolymerized during development.

As shown in Figure 157, the LSM image of the hydrogel construct shows that 2PP processing of stabilized thiol-ene formulations was successful. Stable and delicate gel structures were produced in good accordance with the CAD model. The feature size of the structure was  $\sim 5 \mu\text{m}$ , which is superior to those of the GH-VE/BSA-SH constructs described in section 1.5.5. In addition, the high crosslinking efficiency of the stabilized thiol-ene formulation also enabled the access to hydrogels with high stiffness, which is often difficult to achieve in 2PP. Since gel stiffness could be further adjusted by changing the macromer content, these highly reactive synthetic hydrogels are promising materials for mimicking various soft tissues.

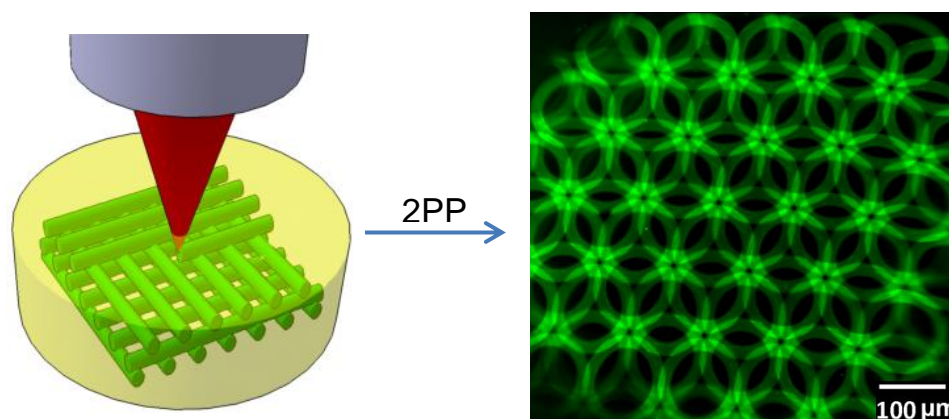


**Figure 157.** 2PP fabrication of a 3D hydrogel construct with complex geometry: schematic showing the 2PP fabrication (**left**) and z-stacked LSM image of the gel construct (**right**) formed with 20% PVA-Norb, 2.23 mM P2CK in PBS, 0.03 % pyrogallol, scanning speed of 100 mm/s, and average power of 100 mW

## 4 Two-photon Cell-Encapsulation

At the last stage of this thesis research, a novel concept termed “two-photon cell-encapsulation” was explored. The aim was to verify the feasibility of microencapsulation of living cells within hydrogel constructs by 2PP microfabrication.

### 4.1 Background

The origin of “cell-encapsulation” concept could date back to the 1930s when Vincenzo Bisceglie did the first attempt to encapsulate tumor cells in polymer membranes.<sup>209</sup> Human tumor cells were encapsulated in polymer membranes and the device was transplanted into pig. Surprisingly, the encapsulated tumor cells were not rejected by the immune system of pig and remained viable for a long period. Three decades later in 1964, T.M. Chang reported that ultra-thin polymer membranes could be used as microcapsules for immunoprotection of transplanted cells and the cell-encapsulation concept was established.<sup>210</sup> The polymeric, semi-permeable membranes allow for bidirectional diffusion of various molecules ( $O_2$ , nutrients, wastes...) that are essential for cell metabolism. Meanwhile, the semi-permeable nature of the microcapsules (Figure 158) prevents immune cells (e.g., macrophages) and/or antibodies from clearing out the encapsulated cells once taking them as foreign invaders. Importantly, the encapsulated cells can serve as a source for long-term, sustained release of therapeutic products (e.g., insulin) at the site of implantation. As such, cell-encapsulated microcapsules have been successfully applied in controlled drug delivery for treating diabetes, heart attack, cancer and other diseases.<sup>211</sup>

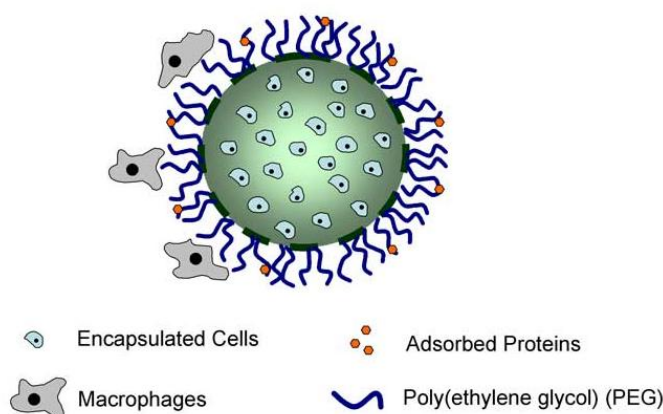


**Figure 158.** Schematics of the early concept of cell-encapsulation<sup>212</sup>

The primary task in tissue engineering is to develop effective strategies that repair and regenerate the damaged tissue as well as the lost function. The use of 3D biodegradable scaffolds has been accepted as a general strategy for cell growth and development of new tissues. Compared to traditional scaffolds that only provide structural support and passive cues, novel bioactive scaffolds that provide key biological cues to cells have shown great promise to guide cell growth and tissue development.<sup>23</sup> To do so, establishment of favorable cell-scaffold interactions are critical. Generally, there are two main approaches regarding how cells are integrated with biomaterial scaffolds. Cells can either be seeded onto prefabricated scaffolds with prescribed porosity and later adapt themselves to a new environment. Or cells could also be encapsulated within the scaffolding material and undergo the fabrication process. In the former approach, a variety of materials and even harsh solvents/procedures could be used as long as the final scaffold is not cytotoxic. In the latter approach, for cell-encapsulation both the materials and the fabrication process must be cytocompatible. As a result, there are few materials/formulations that meet the requirements of cell-encapsulation. ‘‘Everything is a double-edged sword’’. Since the encapsulation procedure is mild and cell-friendly, cell-encapsulation strategy is highly promising for clinical applications once integrated with injectable systems where cell/liquid precursor suspensions could be allocated in the area of tissue defect.

Due to high water content and tissue-like elasticity, hydrogels are ideal scaffolding materials for 3D cell culture and tissue regeneration. In 1990s, early research in tissue engineering has utilized naturally-derived hydrogels such as fibrin and alginate for cell-encapsulation and regeneration of soft tissues.<sup>213-215</sup> Notably, the gelation process and mechanical properties of these hydrogel systems are often difficult to control. To better control the gelation conditions for cell-encapsulation, photopolymerization appears to be the right approach that provides spatiotemporal control. Photopolymerizable hydrogel systems have been extensively explored by Bryant, Anseth, Elisseeff and their co-workers.<sup>23, 31, 62, 216</sup> By careful selection of hydrogel chemistry and irradiation conditions, mammalian cells such as chondrocytes were successfully photoencapsulated into PEGDA hydrogels with high viability.<sup>62</sup>

A typical procedure for cell-photoencapsulation is shown in Figure 159. Firstly, gel precursors such as PEGDA are mixed with water-soluble photoinitiator (PI, e.g. I2959).



Next, cells are suspended in this solution and later transferred to a mold. Upon exposure to UV light, cells are immobilized in the hydrogel networks. Finally, the cell-containing hydrogel constructs are transferred into a multi-well cell culture plate containing appropriate cell medium for further biological studies.

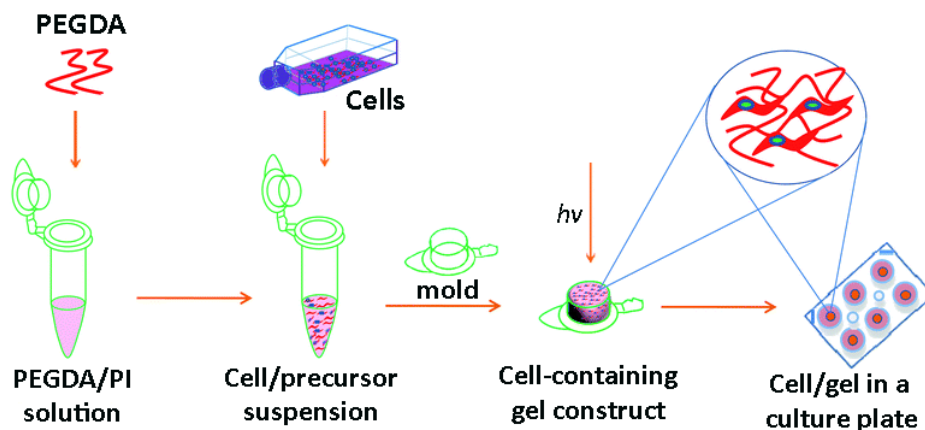


**Figure 159.** Schematics of UV-photoencapsulation of cells in hydrogels<sup>217</sup>

## 4.2 Two-photon Photo-encapsulation

While UV-based (one-photon) photoencapsulation has been established, laser-induced (two-photon) photoencapsulation of living cells at the  $\mu\text{m}$ -scale is largely unexplored. The typical wavelength of near-IR laser for 2PP is around 800 nm. At this wavelength most biological tissues are transparent, as demonstrated in the applications of multiphoton microscopy for tissue-imaging.<sup>113, 114</sup> Thus, it is anticipated that the use of 2PP technique (Figure 160) would provide more accurate control over the hydrogel-based cellular microenvironment. Precise manipulation of single-cell geometry and/or cell-cell contacts may offer invaluable insights to answer key biological questions and to better design a regenerative environment.

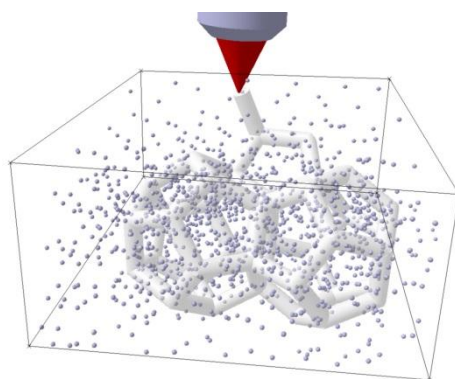


**Figure 160.** Illustration of cell photoencapsulation via 2PP technique (courtesy: A. Ovsianikov)

Although 2PP technique indeed permits 3D microfabrication of hydrogels with user-defined geometry, it is unknown whether the presence of laser irradiation, photoinitiator, and photo-activated chemical species would influence cell viability.

#### 4.2.1 Material Selection

In order to verify the feasibility of 2PP in the presence of living cells, a cytocompatible, photosensitive hydrogel formulation (Figure 161) was designed. It contains 20% methacrylated gelatin (gelMOD) as gel precursor, 0.1 % two-photon photoinitiators (G2CK and P2CK) and 80% DMEM as cell medium. Human osteosarcoma (MG63) cells were used in this study due to easy handling and high proliferation rate.

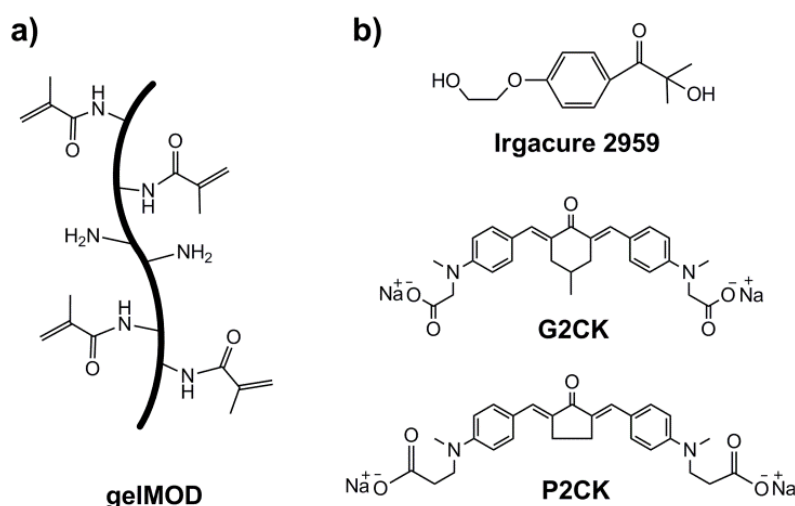


**Figure 161.** Chemical structures of materials used for photoencapsulation<sup>155</sup>

GelMOD was prepared by reacting methacrylic anhydride with the lysine units of high MW gelatin (50-100 kDa) as described in section 1.1. By <sup>1</sup>H-NMR analysis, the DS of gelMOD was found to be ~65%, indicating on average ~20 methacrylamide groups per gelMOD. Notably, this value is significantly higher than that of GH-MA (4.5 kDa) and thus gelMOD is supposed to be more reactive. GelMOD has enabled UV-based photoencapsulation of fibroblasts with high viability (~92%) as reported by Nicol et al.<sup>87</sup> In another study by Ovsianikov et al.,<sup>155</sup> gelMOD-based hydrogel scaffolds with well defined microstructures were produced by 2PP using I2959 as initiator and a green laser emitting at ~515 nm. It is noteworthy that the photophysical property of I2959 makes it inappropriate for 2PP settings (800 nm) in this study.

Two benzylidene cycloketone-based two-photon initiators (G2CK and P2CK) were prepared through Adol condensation as described in the PhD thesis of Zhiquan Li.<sup>218</sup> These photoinitiators have superior water solubility due to their “carboxylate-sodium salt” nature. More importantly, 2PA cross section values of G2CK and P2CK were 163 and 176 GM, respectively. These values are significantly higher than that of most reported initiators such as eosin yellow.<sup>168</sup> Besides, both G2CK and P2CK exhibit high initiating efficiency for 2PP processing of PEGDA-700-based hydrogels.<sup>37</sup> Exposure-toxicity of P2CK and/or G2CK was tested in DMEM solutions (1.83 mM) via MTT assay. As one classical initiator for photoencapsulation, I2959 was selected as the initiator control and tested in DMEM solution (1.83 mM). As shown in Figure 162, the toxicity results show that G2CK exhibited a certain degree of exposure-toxicity to MG63 cells while P2CK presented a similar toxicity profile as I2959.

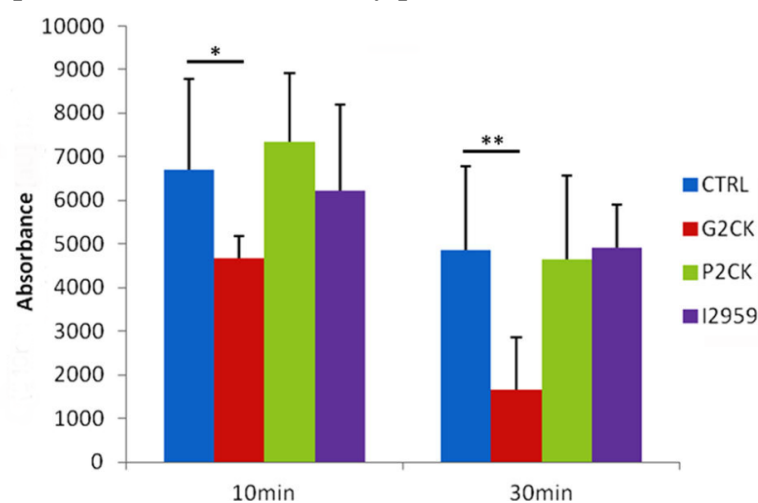


**Figure 162.** MTT assay results showing the metabolic activities of MG63 cells incubated with photoinitiator/DMEM solutions for 10 and 30 min<sup>155</sup> (\* $p < 0.05$ , \*\* $p < 0.01$ )

Prior to two-photon encapsulation, cytocompatibility of gelMOD formulations was further evaluated using an UV-based encapsulation procedure in which I2959 was used as the photoinitiator. It is important to note the thermo-reversible characteristic of gelMOD solution. It solidifies at room temperature and turns into a physical gel due to the formation of rigid triple helices. When the temperature is raised up to  $\sim 35$  °C, the conformation changes from a helix to a more flexible coil and consequently the gel is dissolved into a solution. As a result, preparation and transfer of the cell/gelMOD suspensions was carefully performed at 37 °C. The UV-encapsulation results show that a high level of cell viability ( $>90\%$ ) could be achieved using the selected procedure.

In addition, the gelation kinetics and physical properties of gelMOD gels were tested using photo-rheometry at 20% macromer content and 0.5 % I2959. The gel point of this formulation was  $\sim 28$  s and the  $G'$ -plateau value was  $\sim 77$  kPa. While one-photon rheometry measurement provides important indication of a hydrogel formation, this information cannot directly correlate with the properties of hydrogels formed by 2PP.

#### 4.2.2 2PP Processing

For 2PP cell-encapsulation, a ‘‘Yin-Yang’’-shaped 3D cylinder (Figure 163) was designed and used as the CAD model. The unique structural feature of ‘‘Yin-Yang’’ offers direct comparisons in cell viability between exposed area (Yang) and unexposed area (Yin). This would provide good indications for evaluating the cytocompatibility of 2PP processing conditions and/or the hydrogel formulation. In order to achieve optimal cytocompatibility, the formulation was composed of 20% gelMOD and 1.83 mM G2CK/P2CK in cell-laden DMEM, in which a cell density was set to  $\sim 10^7$  cells/mL. It is noteworthy that the 2PP processing was performed at room temperature. Under this condition, cells were physically entrapped within the precursor solution. After 2PP, the unpolymerized part was removed by developing the sample in DMEM at 37 °C.

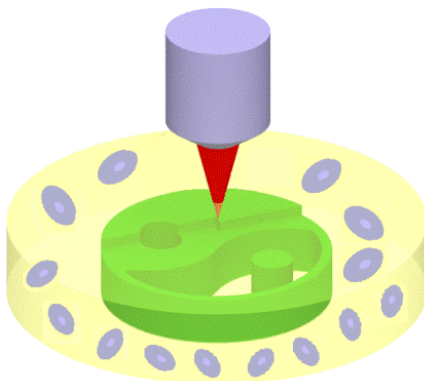


**Figure 163.** Schematics of laser-induced 2PP microfabrication of gel constructs in a cell suspension (yellow) using a Yin-Yang CAD-model (green, 400  $\mu\text{m}$  wide)

To evaluate cell viability, the cell-laden gel construct was further incubated with a PBS solution of live/dead staining reagents (propidium iodide/calcein-AM) for 20 min. After washing in PBS, fluorescently-labeled cells (green-live/red-dead) were visualized using a confocal laser microscope. Moreover, it was feasible to quantify the cell number by using software ‘‘Image J’’.

Figure 164 represents the live/dead staining images of the cell-laden gel construct including four “Yin-Yang” structures. As shown in Figure 164a, large number of cells outside of the laser-exposed area remained alive, showing the cytocompatibility of hydrogel formulation in the absence of laser irradiation. Although indeed there were certain red-stained cells, the cell viability in this region was quite high (~95%).

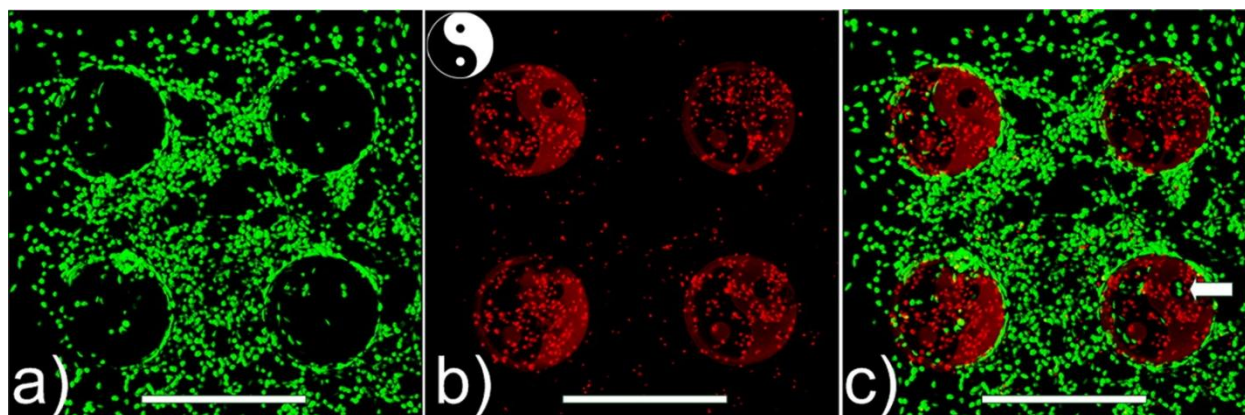


**Figure 164.** Live/dead staining images of the cell-laden gel construct including four “Yin-Yang” structures<sup>155</sup>: **a)** green-labeled (live) cells; **b)** red-labeled (dead) cells; and **c)** an overlay (**a+b**); scale bar: 500  $\mu\text{m}$

The red region in Figure 164b represents the contour of the “Yin-Yang” structure, yet most of cells inside the bulk region were stained red. Only a few cells located in the very vicinity to the bulk/void boundary were stained green (Figure 164c). In the void-region, a considerable number of cells were also red-stained, giving a rather low level of cell viability (~25 %). Together, these results indicate that the cell death inside the “Yin-Yang” structure is likely due to laser exposure and/or release of toxic species from activated PI.

Although previous studies have shown that cellular microenvironments could be noninvasively probed by modulating hydrogels through laser-induced photodegradation,<sup>138</sup> it is unclear whether laser-induced photochemical reactions during 2PP are similarly cytocompatible. To investigate the influence of laser irradiation, control experiments were carried out in the absence of PI. However, without PI the gel precursors cannot be polymerized and consequently cells are not encapsulated. To mimic the encapsulation condition, cell layers were firstly distributed on top of cover slip and covered with 20 % gelMOD/DMEM solution that excluded PI.

As shown in Figure 165a, a speed-power array was screened to verify the influence of different laser-processing conditions on cell viability. A cross pattern was created in the left-bottom corner to mark the extra-exposed region where maximum laser power was applied for a few seconds. The live/dead staining graph shows that cells in this region were substantially damaged and labeled with red. Thus, cells in this region could serve as negative-control for other cells in this experiment.

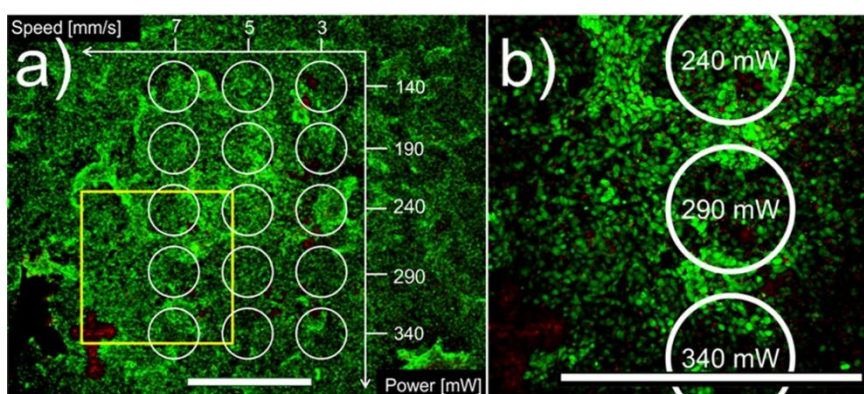


**Figure 165.** Live/dead staining graphs<sup>155</sup>: a) cells exposed to different laser-processing conditions (speed-power array) in the absence of PI; b) magnified view of the lower-left part of the array in a); scale bars: 1 mm

In other regions the sample was laser-scanned at varying speed and power according to a cylinder model (Figure 165a) that has a comparable size (width and thickness) to the ‘‘Yin-Yang’’ model. It was found that most cells in the scanned region were green-stained. Even in the area exposed with high laser power ( $\sim 300$  mW), cells remained viable after laser irradiation (Figure 165b). This control experiment leads to a conclusion that in the absence of PI, the laser-processing conditions used in 2PP encapsulation present negligible influences on cell viability.

### 4.2.3 Molecular Pathways to Cell Damage

In order to elucidate the molecular mechanisms of cell damage during 2PP encapsulation, it is essential to look into possible molecular pathways that generate cytotoxic species. In photodynamic therapies (PDT), a general principle is that the photosensitizer of choice should possess a long lifetime of triplet state to keep high efficiency of energy transfer between the excited photosensitizer and molecular oxygen, for generating singlet oxygen to kill tumor cells.<sup>219</sup> Previous studies related to UV-based photoencapsulation have demonstrated that I2959 can induce cytotoxic effects in a dose-dependent fashion.<sup>32</sup>

Bryant et al. reported that the appropriate concentration of I2959 for photoencapsulation is ~0.05 % (2.2 mM). Notably, I2959 is a Type-I PI, which undergoes Norrish-I cleavage upon UV irradiation and forms two free radicals. Generally, cleavable PIs have fairly short-lived triplet states to facilitate fast fragmentation. Therefore, it is supposed that the triplet quenching by molecular oxygen is negligible for I2959 in aqueous solutions.<sup>220</sup> Considering that I2959 has a limited ability to generate reactive oxygen species (ROS), the observed cellular damage in UV photoencapsulation should be addressed to free radicals from activated PI. It is well-known that free radicals can impose oxidative damage on several cellular components such as plasma membrane, proteins, and DNA.<sup>221</sup> As such, free radicals should be taken into account for analyzing the molecular pathways of cell damage in 2PP encapsulation.

Although the cytotoxic effects by one-photon-activated I2959 have been studied,<sup>32</sup> it is unknown that how two-photon-activated initiators (e.g., P2CK\*) induce cellular damage during 2PP encapsulation. To date, it is accepted that the initiating mechanism of 2PP involves charge-transfer reactions between the two-photon excited chromophore and the macromer (e.g., gelMOD), resulting in macromer radicals for subsequent polymerization (Figure 166).<sup>30, 222</sup> Although these macromer-based radicals are expected to be cytocompatible,<sup>87</sup> in the presence of oxygen the initiator-derived radicals might form peroxy radicals that possibly cause cellular damage.<sup>223</sup> By abstracting hydrogen atoms from unsaturated fatty acids, peroxy radicals have been generally thought to induce lipid peroxidation and related human diseases.<sup>224</sup>

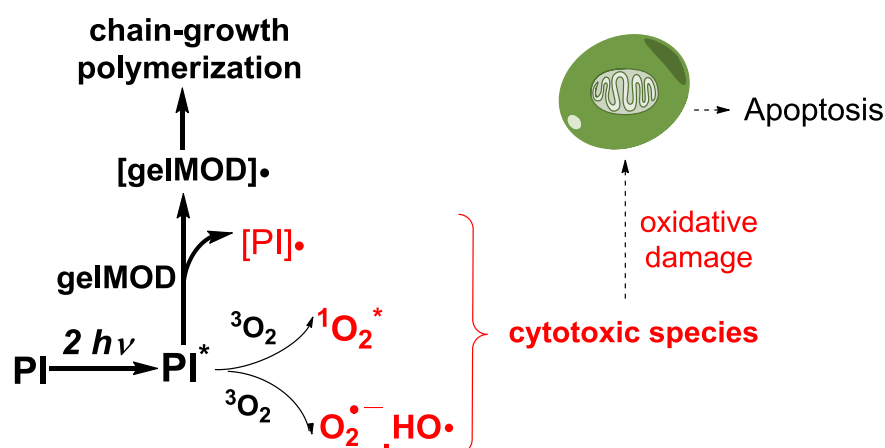


**Figure 166.** Proposed initiating mechanism of 2PP and molecular pathways for generating cytotoxic species during 2PP cell encapsulation

On the other hand, two-photon-excited PIs generally have a quite long triplet lifetime compared to cleavable one-photon initiators such as I2959. They can undergo two pathways to generate varying cytotoxic reactive oxygen species. First, it can transfer its energy to molecular oxygen (triplet) and form excited singlet oxygen ( $^1\text{O}_2^*$ ) which has proven effective for killing tumor cells in PDT.<sup>219</sup> Second, oxidative species such as superoxide anion ( $\text{O}_2^{\cdot-}$ ) could also be generated by electron transfer from the excited initiator to molecular oxygen. In addition, superoxide could further produce hydrogen peroxide and highly reactive hydroxyl radicals ( $\text{OH}^{\cdot}$ ). It is well established that all these species can cause detrimental damage to plasma membrane and mitochondria, leading to subsequent apoptosis.<sup>225</sup>

Together, both PI-derived free radicals and two-photon-induced ROS are supposed to be responsible for the observed cell damage during 2PP encapsulation. Nevertheless, further experiments are warranted to prove each of these assumptions. On one hand, radical scavengers such as Tempol,<sup>226</sup> may be utilized to clarify the role of PI-derived radicals. On the other hand, ROS-sensitive, fluorescent probes could help quantify the ROS content during 2PP encapsulation and the extent of ROS-induced cell damage.

#### 4.2.4 Cell Proliferation

In order to test the proliferative potential of cells that survived the encapsulation procedure, the viable MG63 cells caged within the voids of the ‘‘Yin-Yang’’ construct (right-bottom in Figure 164c) were allowed to proliferate for a longer period. After 3 weeks of cell culture, it was found that the voids area was filled with a large number of viable cells (Figure 167). Moreover, inside the small cylindrical void there were at least 8 viable cells, compared to 2 viable cells before proliferation (arrow oriented, Figure 164c).

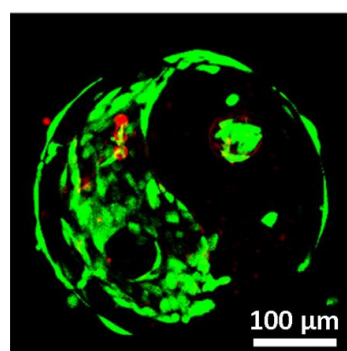


**Figure 167.** Proliferation of MG63 cells in the voids of the ‘‘Yin-Yang’’ gel construct after 3 weeks of cell culture<sup>155</sup>



In all, these evidences suggest that the encapsulated cells are able to proliferate within a 3D-confined region according to the structural design once they survive the encapsulation conditions.



# Experimental

## 1 Gelatin-based Hydrogels

### Preparation of starting material

In this study, a commercially available enzymatic gelatin hydrolysate (Sigma-Aldrich, G0262) was used as starting material. It has a molecular weight up to 6000 Da. Dialysis tubing with a cutoff value of 3.5 kDa was purchased from Carl-Roth (Germany). Specifically, a 25% solution of GH in deionized water was dialyzed against a 30-fold excess of deionized water for 24 h with several changes of water. To avoid bacterial contamination, penicillin-streptomycin was always added to a final concentration of 10 k units/L. After lyophilization, approximately 70% of the starting material was cut off.

### Characterization of starting material

To estimate the concentration of  $-\text{CH}_3$  groups in GH ( $\text{C}_{-\text{CH}_3}$ ),  $^1\text{H-NMR}$  ( $\text{D}_2\text{O}$ , 40 °C, 400 MHz) spectrum of GH with phenol as internal standard was measured (Figure 24). Phenol standard was recrystallized from petrol ether. For NMR experiments, recrystallized phenol (4.95 mg) and dialyzed GH (22.52 mg) was dissolved in  $\text{D}_2\text{O}$  (0.7 mL).

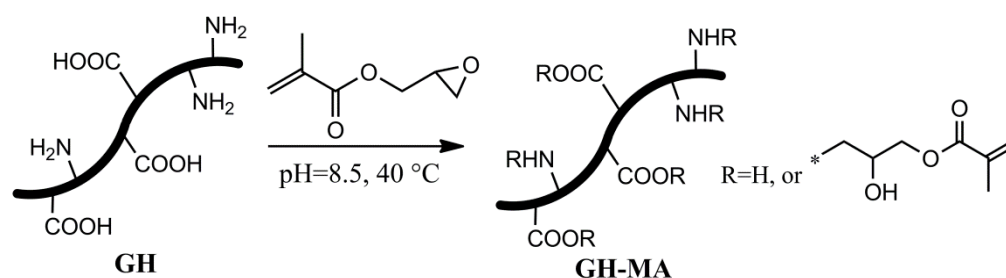
Calculation of methyl groups in gelatin is based on NMR values using the following equation:

$$\frac{m_{phenol}/mw_{phenol}}{m_{GH \times C-CH_3}} = \frac{\int H_{phenol}}{\int H_{-CH_3}} = \frac{2.24}{1} \quad \text{-----Equation 1}$$

The calculation provides a  $\text{C}_{-\text{CH}_3}$  value of 1.04 mmol/g. This value is used as reference for further DS quantification of other gelatin derivatives.

## 1.1 Synthesis of Gelatin Derivatives

### 1.1.1 Synthesis of GH-MA<sup>154</sup>



Reagents	MW (g/mol)	Density (g/mL)	mmol	g	mL	eq.
dialyzed GH	-	-	1.65*	1.0	-	1
glycidyl methacrylate	142	1.08	8.25	1.2	1.1	5
hydroquinone	110	-	0.02	0.002	-	0.01
diluted NaOH (pH 8.5)					50	

\* indicates the total amount of Asp, Glu, and Lys residues in gelatin according to literature<sup>151</sup>; the involvement of N-terminus and C-terminus could contribute additional groups ( $0.21 \text{ mmol/g} \times 2$ ), giving a total value of  $2.07 \text{ mmol/g}$ .

#### Procedure:

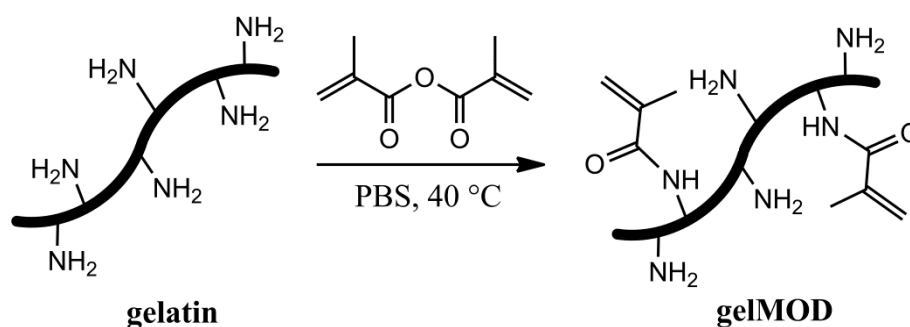
GH was firstly dissolved in deionized water. The pH value was adjusted to 8.5 by adding diluted NaOH (0.1 M). Then the mixture was heated up to  $40\text{ }^\circ\text{C}$  under stirring. To this solution, excessive glycidyl methacrylate (5 eq.) including inhibitor was added dropwise. The reaction was allowed to stir overnight at  $40\text{ }^\circ\text{C}$ . After reaction, the mixture was extracted with ethyl acetate ( $2 \times 20 \text{ mL}$ ) and the aqueous layer was dialyzed against deionized water for 24 h with several changes of water. The collected solution was evaporated to a desirable volume ( $<40 \text{ mL}$ ) and finally lyophilized.

Yield: 0.79 g (65 % of theory) of yellowish solid

$^1\text{H-NMR}$ ( $\text{D}_2\text{O}$ , $25\text{ }^\circ\text{C}$ ): $\delta$ (ppm)	6.2 (1H, s, $\text{HCH}=\text{C}$ )	Int = 0.60
	5.7 (1H, s, $\text{HCH}=\text{C}$ )	Int = 0.62
	1.9 (3H, s, $\text{CH}_3$ )	Int = 1.74
	0.9 ( $-\text{CH}_3$ reference)	Int = 1

corresponding to  $1.90 \text{ mmol/g}$  methacrylic groups

### 1.1.2 Synthesis of gelMOD<sup>86</sup>



Reagents	MW (g/mol)	Density (g/mL)	mmol	g	mL	eq.
Type-A gelatin	50-100 k	-	1.16*	3.0	-	1
methacrylic anhydride	154	1.04	11.6	1.8	1.7	10
hydroquinone	110	-	0.08	0.009	-	0.07
PBS					60	

\*indicating the amount of (hydroxyl)lysine residues in gelatin according to literature<sup>151</sup>

#### Procedure:

Type-A gelatin (Sigma, bloom strength: 300) was dissolved in PBS (pH 7.4) at 40 °C under vigorous stirring to provide a 5 % solution. After dissolution, excessive methacrylic anhydride (MA) including trace amount of inhibitor was added under vigorous stirring. After 6 h reaction at 40 °C, the reaction mixture was diluted with sodium bicarbonate solution (10 %) to neutralize the unreacted MA and/or methacrylic acid. The resultant solution was further purified in a dialysis tubing (Sigma, MW cut-off value: 12 kDa) against distilled water at 40 °C. After 24 h dialysis, the collected solution was lyophilized.

Yield: 2.75 g (92 % of theory) of white solid

<sup>1</sup> H-NMR (400 MHz, D <sub>2</sub> O, 40 °C): δ (ppm)	5.8 (1H, s, HCH=C)	Int = 0.07
	5.6 (1H, s, HCH=C)	Int = 0.07
	2.1 (3H, s, CH <sub>3</sub> )	overlapped
	1.1 (-CH <sub>3</sub> reference)	Int = 1.00

The DS of gelMOD was defined according to the following equation:

$$\text{DS (\%)} = 3.84 \times (I_{5.6\text{ppm}}/I_{1.1\text{ppm}}) \times (100/0.38)$$

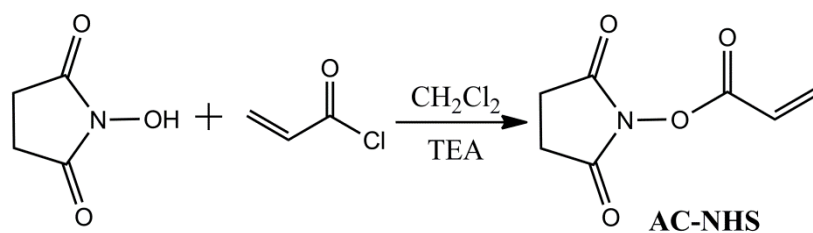
Where “3.84” mmol/g corresponds to the concentration of protons at 1.1 ppm; and “0.38” mmol/g corresponds to the lysine concentration.

The DS was calculated to be 70 %, corresponding to 70 methacrylamide groups per 100 lysines

By taking the average MW of gelMOD as 75 kDa, further calculation suggests that ~20 methacrylamide groups per gelMOD.

### 1.1.3 Synthesis of GH-AC

#### 1.1.3.1 Synthesis of AC-NHS<sup>157</sup>



Reagents	MW (g/mol)	Density (g/mL)	mmol	g	mL	eq.
acryloyl chloride	91	1.12	34.8	3.2	2.82	1
N-hydroxysuccinimide	115	-	34.8	1.2	-	1
triethylamine	101	0.73	38.2	3.9	5.33	1.1
CHCl <sub>3</sub>					30	

#### Procedure:

A diluted solution of acryloyl chloride in CH<sub>2</sub>Cl<sub>2</sub> (1:5, v/v) was added dropwise into a stirred solution of *N*-hydroxysuccinimide (1 equiv) and triethylamine (1.1 equiv) in CH<sub>2</sub>Cl<sub>2</sub> at 0 °C on an ice bath. The reaction mixture was allowed to stir for 3 h at 0 °C. Then it was washed with deionized water (2 × 15 mL) and dried over MgSO<sub>4</sub>. Finally, the product was recrystallized from a solution of ethyl acetate/hexane (1:1).

Yield: 4.29 g (73% of theory) of colorless crystals

TLC (Hexane:EE=1:1)

R<sub>f</sub>=0.54

m.p.:

64-66 °C (69 °C in lit.<sup>157</sup>)

<sup>1</sup>H-NMR (CDCl<sub>3</sub>): δ (ppm)

6.7 (1H, d, CHH=CH-C(=O)-)

6.3 (1H, q, CHH=CH-C(=O)-)

6.2 (1H, d, CHH=CH-C(=O)-)

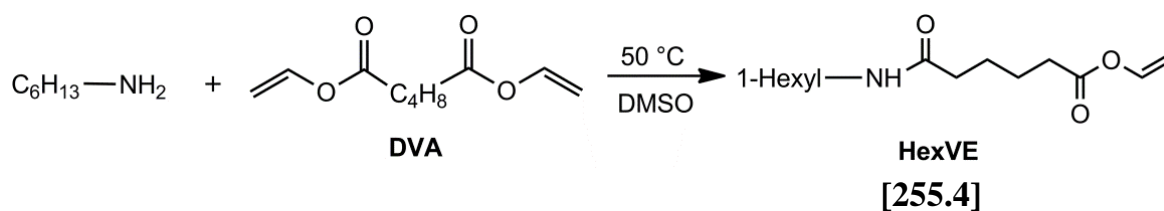
2.9 (4H, s, -CH<sub>2</sub>-CH<sub>2</sub>-)





## 1.1.4 Synthesis of GH-VE

### 1.1.4.1 Model reaction



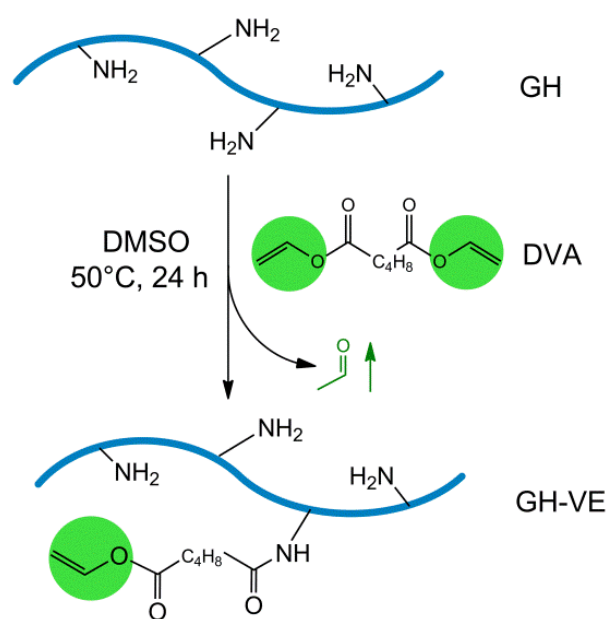
Reagents	MW (g/mol)	Density (g/mL)	mmol	g	mL	eq.
1-hexyl-amine	101	0.77	1	0.10	0.13	1
divinyldipate (DVA)	198	1.05	10	1.98	1.89	10
DMSO					20	

#### Procedure:

The model compound (1-hexyl-amine) was firstly dissolved in anhydrous DMSO. Then this solution was added dropwise into an excessive amount of DVA (10 eq.) at 50 °C under vigorous stirring. The reaction process was monitored hourly by GC-MS and <sup>1</sup>H-NMR. After 3 h reaction, GC-MS and <sup>1</sup>H-NMR analysis proved that characteristic signals (parent chromatogram peak with m/z: 102 and 55; methylene protons adjacent to -NH<sub>2</sub> with δ=2.65 ppm) had disappeared. The final product (vinyl 6-(hexylamino)-6-oxohexanoate, Hex-VE) was confirmed by the dominant signal in GC-MS analysis.

GC-MS (m/z): 256, 212, 184

### 1.1.4.2 Synthesis of GH-VE



Reagents	MW (g/mol)	Density (g/mL)	mmol	g	mL	eq.
dialyzed GH	-	-	0.38*	1.0	-	1
DVA	198	1.05	3.8	0.75	0.72	10
hydroquinone	110	-	0.08	0.008	-	0.2
DMSO					20	

\*indicates the amount of (hydroxyl)lysine residues in gelatin according to literature<sup>151</sup>; the involvement of amino group at N-terminus may provide additional -NH<sub>2</sub> groups (0.21 mmol/g), giving a total -NH<sub>2</sub> concentration of 0.59 mmol/g.

#### Procedure:

Dialyzed GH was firstly dissolved in anhydrous DMSO (10 mL) at 40 °C, to make a 10% solution. In a second flask, divinyladipate (DVA) and inhibitor were dissolved in anhydrous DMSO (10 mL) at 50 °C under vigorous stirring. To this flask, the GH/DMSO solution was added dropwise within 30 min. After 24h reaction at 50 °C, the dark brown solution was distilled under high-vacuum ( $1 \times 10^{-2}$  mbar, 40°C) to get rid of DMSO. Then the remaining slurry was dissolved in 50 mL deionized water and washed with ethyl acetate ( $3 \times 20$  mL). The aqueous layer was dialyzed for 48 h with several changes of deionized water. The collected solution was filtered, evaporated to a desirable volume (<40 mL) and finally lyophilized.

Yield: 0.70 g (66% of theory) of orange solid

$^1\text{H-NMR}$ ( $\text{D}_2\text{O}$ , 40 °C): $\delta$ (ppm)	7.4 (1H, dd, $\text{CH}_2=\text{CH-O}$ )	Int = 0.18
	5.2 (1H, dd, $\text{CH}_2=\text{CH-O}$ )	Int = 0.20
	4.8 (1H, dd, $\text{CH}_2=\text{CH-O}$ )	overlapped ( $\text{D}_2\text{O}$ )
	3.5 (1H, s, $-\text{NH-C(=O)-}$ )	Int = 0.10
	2.7 (2H, s, $\text{CH}_2=\text{CH-O-CH}_2-$ )	overlapped (GH)
	2.5 (2H, s, $-\text{CH}_2-\text{NH-C(=O)-}$ )	overlapped (GH)
	1.8 (4H, s, $-\text{CH}_2-\text{CH}_2-$ )	overlapped (GH)
	1.1 ( $\text{CH}_3$ reference)	Int = 1
	corresponding to 0.57 mmol/g vinyl ester groups	

To estimate the average number of VE groups per peptide chain, further calculation (Equation 2) was carried out based on the average molecular weight value of GH (4750 g/mol).

$$n_{VE} = \frac{C_{VE}}{1} = \frac{0.57 \text{ mmol/g}}{4,750 \text{ g/mmol}} \quad \text{-----Equation 2}$$

The number of vinyl ester groups per GH-VE ( $n_{VE}$ ) was calculated to be 2.7.

## 1.2 Characterization of Gelatin Derivatives

### 1.2.1 Photo-Rheometry

The rheometry setting is described in section **Methods**.

#### Preparation of gel precursor solutions

The precursor solutions consisted of varying GH derivatives and along with 0.5 % photoinitiator (I2959 in PBS), to provide a final macromer concentration of 25 wt%.

### 1.2.2 Cytotoxicity

The cytotoxicities of macromer solutions were evaluated via MTT assay. The human osteosarcoma cell line MG63 was cultured in DMEM containing 10 % fetal bovine serum (FBS). Macromer solutions of GH-VE and GH (1% and 0.1%) were prepared in DMEM. MG63 cells were then seeded in a 96-well tissue culture plate at a density of  $1 \times 10^4$  cells per well in 200  $\mu\text{L}$  of DMEM containing 10% FBS. After 24 h incubation (37 °C, 5%  $\text{CO}_2$ ), each of the macromer solutions were added to the cells. After 24 h incubation, cells were washed twice with sterile PBS before the addition of 120  $\mu\text{L}$  of MTT reagents. Then the cells were incubated at 37 °C for 4 h. The absorbance of the medium was measured at 540 nm using a microplate reader.

## 1.3 Preparation of Albumin Macrothiols

### 1.3.1 Preparation of BSA Macrothiols

Stock solutions of bovine serum albumin (BSA) were freshly prepared by dissolving BSA in phosphate buffered saline (PBS) to give a 30 % solution (w/w). Then varying amounts of the reducing agent tricarboxyethylphosphate (TCEP) were added to the BSA solution, to provide a 25 wt% solution with varying concentration of free cysteines. After 30 min incubation, the solution was dialyzed against PBS buffer under nitrogen protection for half a day with several changes of PBS. The sulfhydryl concentration was measured by Ellman's test (see section 1.3.2). After calculation, the final concentration of free cysteines was checked to be 11.35 mM (BSA-SH-3), 22.73 mM (BSA-SH-6), and 45.48 mM (BSA-SH-12), respectively.

**Table 1.3.1.** Detailed information concerning the reductive cleavage of BSA

Entry	Reduced disulfides per BSA	Accessible Cys per BSA	TCEP [mM]	C <sub>-SH</sub> [mM]
BSA-SH-3	1.0	3.0	3.79	11.35
BSA-SH-6	2.5	6.0	9.47	22.73
BSA-SH-12	5.5	12.0	20.83	45.48

Figure 1.3.1 represents the experimental observation showing the precipitation of BSA when TCEP was added 16 times relative to BSA amount.



**Figure 1.3.1.** Observation showing the precipitation of reduced BSA (left: 25% BSA-SH-12, right: 25% BSA-SH-16, pH 7.4, 23 °C)

### 1.3.2 Ellman's test

Quantification of the concentration of free cysteine was determined by the method of Ellman.<sup>164</sup> N-acetyl-L-cysteine (Acetyl-Cys) was used as the standard thiol-containing compound and a series of Acetyl-Cys stock solutions (625  $\mu$ M - 20 mM, n=8) were prepared in 0.1 M potassium phosphate buffer (pH 7.4). The stock solution of Ellman's reagent (5,5'-dithio-bis-(2-nitrobenzoic acid), DTNB) was prepared in the same buffer with a final concentration of 25 mM.

**Table 1.3.2.1** Preparation of the stock solution

Reagents	Stock concn. [mM]
N-acetyl-L-cysteine	200
DTNB solution	25

A working solution (1 mL) consists of 940  $\mu\text{L}$  of 0.1 M phosphate buffer, 50  $\mu\text{L}$  of 25 mM DTNB stock solution and 10  $\mu\text{L}$  of the standard Acetyl-Cys solution listed in Table 1.3.2.2. For the blank control, the sample was replaced with equivalent volume of buffer (i.e., 950  $\mu\text{L}$  buffer instead). After 60 min incubation, the samples were transferred to polystyrene cuvettes from which sample absorbance at 412 nm were recorded using a Perkin Elmer Lambda-35 UV-VIS spectrometer.

**Table 1.3.2.2.** Detailed information of working solutions for Ellman's Test

sample	$C_{\text{standard}}$ [mM]	$V_{\text{sample}}$ [ $\mu\text{L}$ ]	$V_{\text{buffer}}$ [ $\mu\text{L}$ ]	$V_{\text{DTNB}}$ [ $\mu\text{L}$ ]	$C_{\text{cuvette}}$ [mM]
1	0.625	10	940	50	0.00625
2	1.25	10	940	50	0.01250
3	2.5	10	940	50	0.025
4	5.0	10	940	50	0.050
5	7.5	10	940	50	0.075
6	10	10	940	50	0.10
7	15	10	940	50	0.15
8	20	10	940	50	0.20
blank	0	0	950	50	0

An extinction value of 2-nitro-5-thiobenzoate (TNB) was calculated from Beer-Lambert law after linear regression and used to correlate the thiol concentration of BSA-SH. The extinction coefficient of TNB at 412 nm (23  $^{\circ}\text{C}$ , pH=7.4) was calculated to be 11963  $\text{M}^{-1}\cdot\text{cm}^{-1}$ .

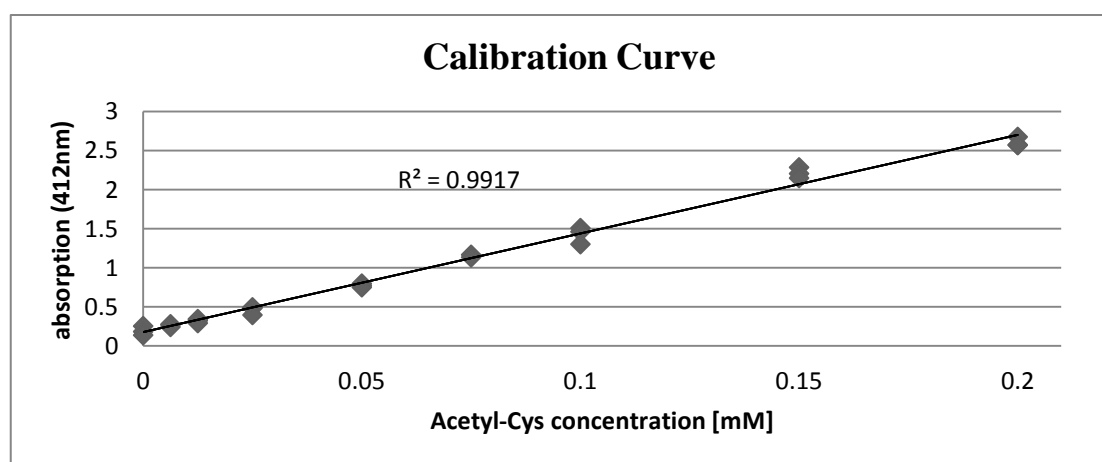


**Figure 1.3.2.** Calibration curve of standard 'thiol' compound (N-acetyl Cys) measured by Ellman's Test

## 1.4 Characterization of GH-VE/BSA-SH Hydrogels

### 1.4.1 Hydrogel Formation

The rheometry setting is as same as described in section 1.1.2, except using different gel precursors.

#### Preparation of gel precursor solutions

The precursor solutions consisted of GH-VE and BSA-SH along with 0.5 % photoinitiator (I2959 in PBS). Entry 0 contains 25 wt% GH-VE with no BSA-SH. Entries i-iii all contain 9 wt% GH-VE and 16 wt% BSA-SH where the latter has three different degrees of reduction such that n-SH: n-ene=0.1 (i), 0.2 (ii), and 0.4(iii)). To prevent premature radical-mediated thiol-ene polymerization, 500 ppm pyrogallol was added as stabilizer.

#### Preparation of hydrogel pellets

For swelling and cytotoxicity studies, hydrogel pellets were prepared in a multiwell PDMS chamber (well diameter: 6 mm). Two hundred microliters of macromer solution was pipetted between two glass coverslips separated by a PDMS spacer with a thickness of 1.5 mm and then exposed to UV light (20 mW/cm<sup>2</sup>) for 600 s. Pellets were detached from the slides and washed twice with sterile PBS.

### 1.4.2 Swelling Test

For swelling analysis, hydrogel pellets were prepared as in section 1.5.1 and allowed to swell in PBS (pH 7.4) for 24 h at room temperature. The wet pellets were weighed to determine the equilibrium swollen mass (**Ms**) and then lyophilized to obtain the dry weight (**Md**). The equilibrium mass swelling ratio was calculated as **Ms/Md**. The experiments were repeated in triplicate to provide an average value with the standard deviation indicated by an error bar.

### **1.4.3 Hydrogel Toxicity**

For toxicity tests, hydrogel pellets were prepared as in section 1.4.1 and incubated in DMEM so that macromer concentration was 1%. Then the pellets toxicity was measured by MTT assay as described in 1.2.2, except using pellet extracts.

### **1.4.4 Cell Adhesion**

For cell adhesion studies, hydrogel pellets were prepared in a similar approach as mentioned in section 1.5.2. Pellets were transferred to a 24-well plate and covered with MG 63 suspension ( $5 \times 10^6$  cells per well). After 24 h incubation (37 °C, 5% CO<sub>2</sub>), supernatants were removed and samples were washed twice with PBS. Cells were stained using a LIVE/DEAD kit (Invitrogen). Fluorescence was visualized using an epifluorescence microscope (Leica DMI6000B).

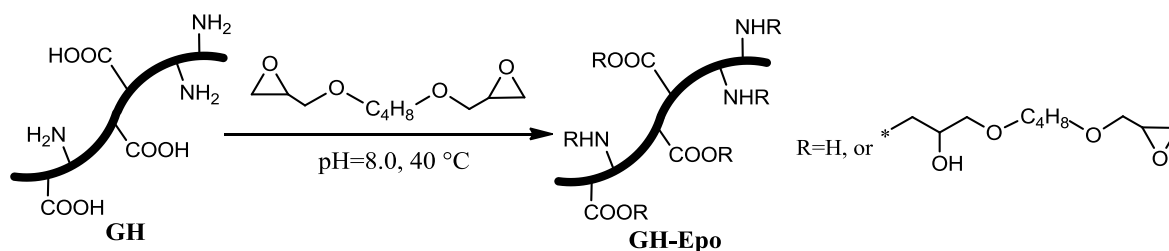
## **1.5 2PP Microfabrication**

Hydrogel precursor solutions were prepared as in section 1.5.2, except using 0.5 % two – photon initiator (WSPI). A Ti:sapphire laser system (HighQ Femtotrain 800 nm, 80 fs pulse duration, 75 MHz repetition rate) was used for 2PP microfabrication of hydrogels. Detailed information about the 2PP experimental setup and CAD-model design is available in **Methods**.



## 1.6 Attempts to Increase Crosslinking Density

### 1.6.1 Synthesis of GH-Epo



Reagents	MW (g/mol)	Density (g/mL)	mmol	g	mL	eq.
dialyzed GH	-	-	10.4*	5.0	-	1
1,4-butanediol diglycidyl ether	202	1.10	104	21	19	10
potassium phosphate buffer (0.1 M, pH=8.0)					80	

\*indicates the total amount of Asp, Glu, and Lys residues in gelatin according to literature<sup>151</sup>; the involvement of N-/C-terminus could contribute additional groups (0.21 mmol/g  $\times$  2), giving a total value of 2.07 mmol/g.

#### Procedure:

GH was firstly dissolved in 0.1 M potassium phosphate buffer (pH=8.0) to form a 5 % solution. Then the mixture was heated up to 40 °C and added dropwise into a 10-fold excess of 1,4-butanediol diglycidyl ether. The reaction was allowed to stir overnight at 40 °C. After reaction, the mixture was directly dialyzed against deionized water for 24 h with several changes of water. The collected solution was evaporated to a desirable volume (< 40 mL) and finally lyophilized.

Yield: 2.95 g (55 % of theory) of yellowish solid

<sup>1</sup> H-NMR (D <sub>2</sub> O, 25 °C): $\delta$ (ppm)	3.5 (8H, m, 2 $\times$ OCH <sub>2</sub> )
	2.9 (1H, m, CH <sub>2</sub> (O)CH)
	2.7 (2H, m, CH <sub>2</sub> (O)CH)
	1.6 (4H, m, OCH <sub>2</sub> CH <sub>2</sub> CH <sub>2</sub> CH <sub>2</sub> O)

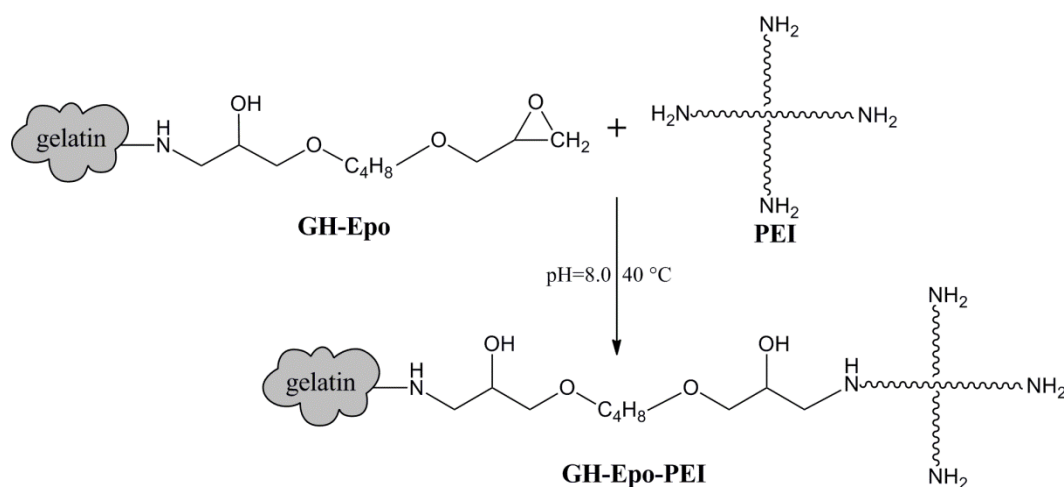
### Epoxy Titration

The titration experiments were performed in triplicate. GH-Epo was firstly dissolved in deionized water. To this solution, 2 drops of phenolphthalein was added as pH indicator. Afterward, 3 mL of 1.5 M sodium thiosulfate solution was added to initiate the reaction. The reaction was stirred at room temperature for 1 h. As the reaction proceeded, a color change from colorless to pink could be observed, indicating the formation of  $-OH$  ions. Then, the stirring solution was titrated with 4 mM HCl until the point when pink color disappeared. Detailed information regarding the procedure and the results are listed below:

NO.	GH-Epo [mg]	Consumed HCl [mL]	Consumed [mmol]	[mmol/g]	DS [epoxy/GH-Epo]
1 <sup>st</sup>	35.1	4.8	0.0192	0.547	2.60
2 <sup>nd</sup>	29.6	3.9	0.0156	0.527	2.50
3 <sup>rd</sup>	32.8	4.2	0.0168	0.512	2.43

The average concentration of epoxy groups was calculated as  $0.529 \pm 0.017$  mmol/g, corresponding to 2.5 epoxy groups per macromer.

### 1.6.2 Synthesis of GH-Epo-PEI



Reagents	MW (g/mol)	Density (g/mL)	mmol	g	mL	eq.
GH-Epo	-	-	1.59*	3.0	-	1
PEI	800	-	15.9	12.7	-	10
potassium phosphate buffer (0.1 M, pH=8.0)					60	

\*indicating the amount of epoxy groups

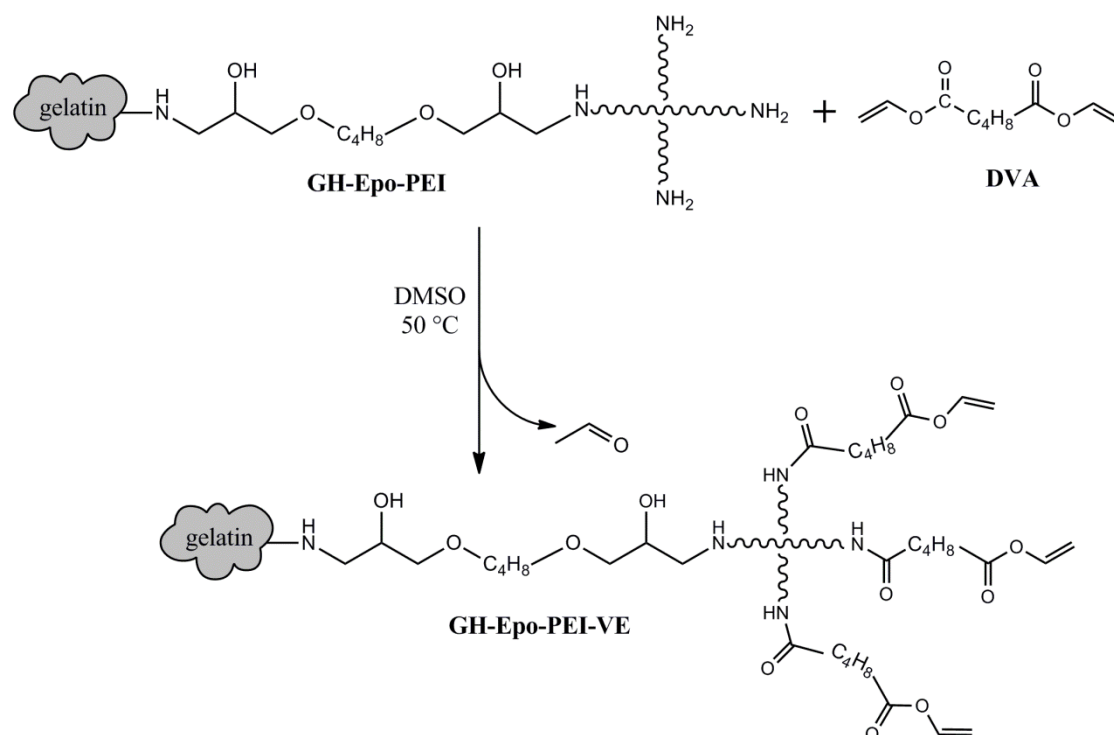
#### Procedure:

GH-Epo was firstly dissolved in potassium phosphate buffer (0.1 M, pH=8.0) to form a 5% solution. Then the mixture was heated up to 40 °C and added dropwise into a 10-fold excess of PEI. The reaction was allowed to stir overnight at 40 °C. After reaction, the mixture was directly dialyzed against deionized water for 1 week with several changes of water. The collected solution was evaporated to a desirable volume (< 60 mL) and finally lyophilized.

Yield: 1.69 g (47.7 % of theory) of yellowish oil

$^1\text{H-NMR}$ ( $\text{D}_2\text{O}$ , 25 °C): $\delta$ (ppm)	3.5 (8H, m, $2 \times \text{OCH}_2$ )
	2.4 - 3.0 (4 H, m, $12 \times \text{N-CH}_2\text{-CH}_2\text{-N}$ )
	1.6 (4H, m, $\text{OCH}_2\text{CH}_2\text{CH}_2\text{CH}_2\text{O}$ )

### 1.6.3 Synthesis of GH-Epo-PEI-VE



Reagents	MW (g/mol)	Density (g/mL)	mmol	g	mL	eq.
GH-Epo-PEI	-	-	2.1*	1.2	-	1
DVA	198	1.05	21.0	4.2	4.0	10
hydroquinone	110	-	0.08	0.008	-	0.2
abs. DMSO					40	

\*this value is ~4 times of the amount of epoxy groups, by assuming that one -NH<sub>2</sub> group of PEI (~5 in total) reacts with one epoxy group.

#### Procedure:

GH-Epo-PEI was firstly dissolved in DMSO (28 mL) at 40 °C, to make a 5% solution. In a second flask, DVA and inhibitor were dissolved in DMSO (12 mL) at 50 °C under vigorous stirring. To this flask, the GH-Epo-PEI/DMSO solution was added dropwise within 45 min. After 24h reaction at 50 °C, the dark brown solution was distilled under high-vacuum ( $1 \times 10^{-2}$  mbar, 40°C) to remove DMSO. Then the remaining slurry was dissolved in 80 mL deionized water and washed with ethyl acetate ( $3 \times 40$  mL). The aqueous layer was dialyzed for 48 h with several changes of deionized water. The collected solution was filtered, evaporated and finally lyophilized.

Yield: 0.82 g (59% of theory) of light yellowish solid

$^1\text{H-NMR}$ ( $\text{D}_2\text{O}$ , 25 °C): $\delta$ (ppm)	7.4 (1H, dd, $\text{CH}_2=\text{CH-O}$ )	Int = 0.17
	5.0 (1H, dd, $\text{CH}_2=\text{CH-O}$ )	overlapped ( $\text{D}_2\text{O}$ )
	4.8 (1H, dd, $\text{CH}_2=\text{CH-O}$ )	overlapped ( $\text{D}_2\text{O}$ )
	0.9 ( $-\text{CH}_3$ reference)	Int = 1
	corresponding to 0.54 mmol/g vinyl ester groups	

The number of vinyl ester groups per peptide ( $n_{VE}$ ) was calculated to be 2.5.



## 2 Hyaluronan-based Hydrogels

### 2.2 Synthesis of HA-derivatives

#### 2.2.1 Preparation of Low MW HA

Procedure:

HA substrates were prepared through acidic degradation of high molecular weight HA. Specifically, high molecular weight HA (sodium salt, 1.3 MDa, 5.0 g) was dissolved in deionized water to give a 0.5 % solution. The pH value of solution was decreased to 1.0 by the addition of concentrated HCl. From then on, the acidic degradation was performed at 60 °C with constant stirring speed for 24 h. After that, the pH value of the solution was readjusted to 7.0 by the addition of 1 N NaOH before transferring the solution to dialysis tubing (MW cut-off, 3.5 kDa), and these solution were dialyzed against deionized water for 48 h. Finally, the solution was lyophilized at -51°C and 0.01 mbar.

Yield: 3.1 g (62% of theory) of colorless solid

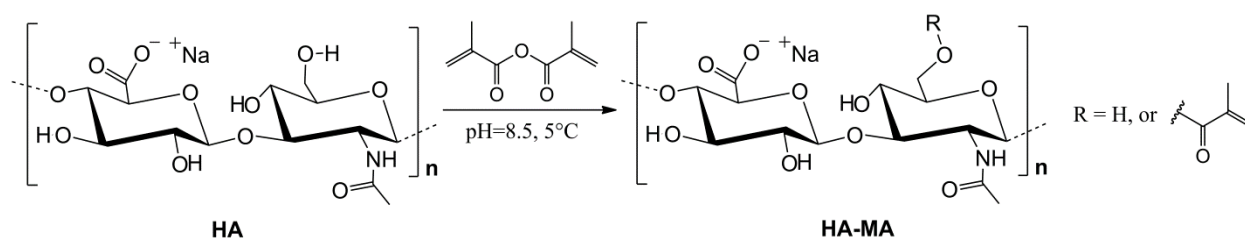
<sup>1</sup> H-NMR (D <sub>2</sub> O): δ (ppm)	3.1-4.1 (12H, m)	Int = 12.16
	2.0 (3H, s, acetyl)	Int = 3.00

The DS of HA derivatives were determined using <sup>1</sup>H-NMR by calculating the ratio of the peak area of respective proton (e.g., a methacrylic proton) relative to peak area of the acetyl group of HA at 2.0 ppm.

GPC: M <sub>w</sub> :	18.2 kDa
M <sub>n</sub> :	11.4 kDa
PDI:	1.6

For GPC analysis, the eluent was 50 mM NaCl solution/acetonitrile 80:20 (v/v), and the flow rate was 0.3 or 0.5 mL/min. The GPC system was calibrated with standard PEG samples provided by American Polymer Standards Corporation.

### 2.2.2 Synthesis of Hyaluronate Methacrylates (HA-MA)



Reagents	MW (g/mol)	Density (g/mL)	mmol	g	mL	eq.
HA (sodium salt)	11.4	-	0.75*	0.3	-	1
methacrylic anhydride	154	1.04	7.5	1.15	1.11	10
diluted NaOH (pH=8.5)					60	

\* indicating the molar amount of HA repeating unit (401 g/mol)

Procedure:

HA-MA was synthesized by reacting HA with methacrylic anhydride (MA) as reported in literature.<sup>96, 227</sup> HA was firstly dissolved in deionized water at 5°C under a cooling bath. To this solution, MA was added dropwise under vigorous stirring. The reaction media was maintained at pH~8.5 by dropwise addition of 1 N NaOH for 3 h, followed by overnight reaction at 5 °C. The mixture was filtered and the filtrate was neutralized with NaHCO<sub>3</sub>. The solution was dialyzed against deionized water for 24 h with several changes of water. The collected solution was evaporated to a desirable volume (<40 mL) and finally lyophilized.

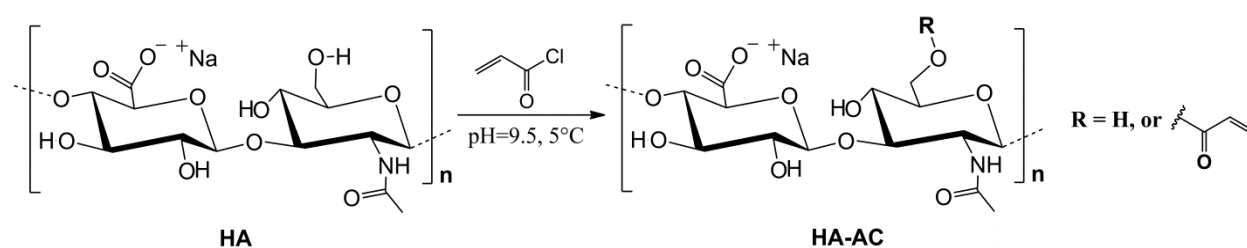
Yield: 0.28 g (80% of theory) of white solid

<sup>1</sup> H-NMR (D <sub>2</sub> O): δ (ppm)	5.6 (1H, s, CH <sub>2</sub> =C)	Int = 0.56
	5.3 (1H, s, CH <sub>2</sub> =C)	Int = 0.58
	2.0 (3H, s, acetyl)	Int = 3.00
	1.9 (3H, s, CH <sub>2</sub> =C)	Int = 1.81

DS: 0.57 (57 MA groups per 100 HA units)



### 2.2.3 Synthesis of Hyaluronate Acrylates (HA-AC)



Reagents	MW (g/mol)	Density (g/mL)	mmol	g	mL	eq.
HA (sodium salt)	-	-	0.75	0.3	-	1
acryloyl chloride	91	1.12	22.4	2.04	1.82	30
diluted NaOH (pH=9.5)					60	
dichloromethane					60	

Procedure:

HA-AC was synthesized according to a procedure described by Novozyme.<sup>175</sup> HA was dissolved in deionized water and this solution was cooled down to 5 °C under a cooling bath. Then, drops of 0.3 N NaOH was added till reaching a pH value of 9.5. A mixture of excessive acryloyl chloride and dichloromethane was prepared in a dropping funnel. This solution was added into the HA solution dropwise for 1 hour. During addition, pH value was maintained at 8.0-9.5 by dropwise addition of 1N NaOH. After the addition was complete, the reaction was allowed to stir for 1 hour at 5 °C. Then the reaction mixture was filtered and the filtrate was neutralized with NaHCO<sub>3</sub>. The solution was dialyzed against deionized water for 24 h with several changes of water. The collected solution was evaporated to a desirable volume (<40 mL) and finally lyophilized.

Yield: 0.29 g (85 % of theory) of white solid

<sup>1</sup>H-NMR (D<sub>2</sub>O): δ (ppm)

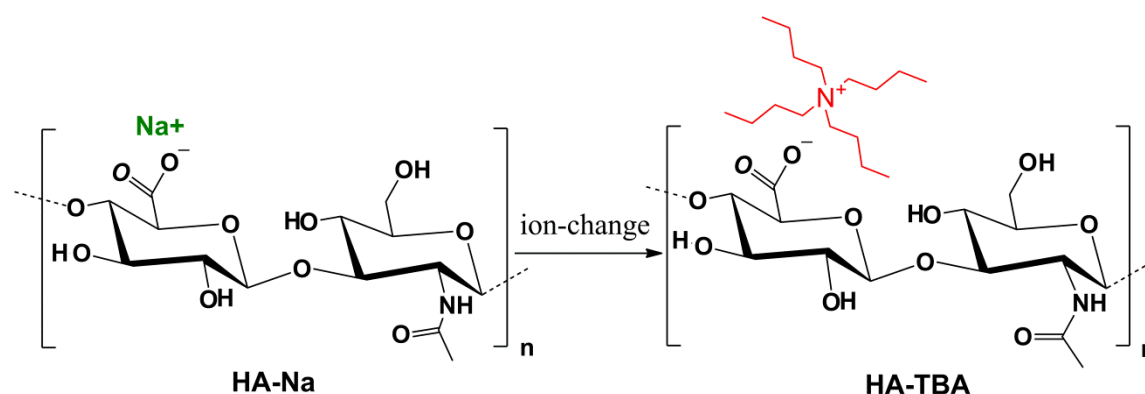
5.9-6.6 (3H, m, CH<sub>2</sub>=CH) Int = 1.47

2.0 (3H, s, acetyl) Int = 3.00

DS: 0.49 (49 AC groups per 100 HA units)

## 2.2.4 Synthesis of Hyaluronate Vinyl esters (HA-VE)

### 2.2.4.1 Preparation of Tetrabutylammonium Salt of HA (HA-TBA)



Reagents	MW (g/mol)	Density (g/mL)	mmol	g	mL	eq.
HA (sodium salt)	-	-	2.49	1.0	-	1
TBA-OH	259	-	-	-	-	-
Amberlite® IR120 (H <sup>+</sup> )				3.0	-	
deionized water					100	

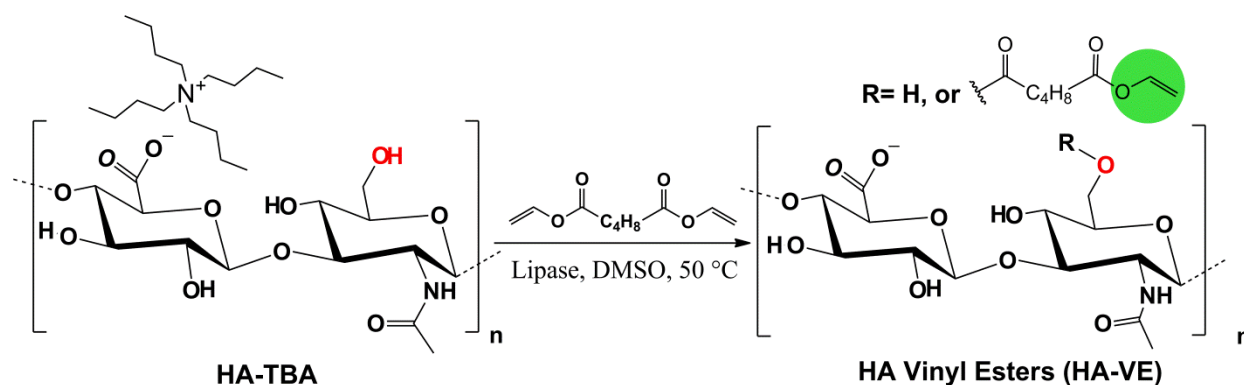
#### Procedure:

HA-TBA was prepared using an adapted protocol from literature.<sup>97</sup> The sodium salt of HA was dissolved in deionized water to give a 1 % solution. Then, highly acidic ion-exchange resin (Amberlite® IR120, H<sup>+</sup> form) was added and the resultant slurry was stirred for 4 h. After that, the slurry was filtrated to remove the resin. The acidic solution was neutralized by the addition of 20 % tetrabutylammonium hydroxide solution (TBA-OH) to pH 7.01-7.06, forming a HA-TBA solution. The solution was directly lyophilized (-51°C, 0.02 mbar).

Yield: 1.54 g (99.5% % of theory) of white solid

<sup>1</sup> H-NMR (D <sub>2</sub> O): δ (ppm)	3.3 (8H, m, 4 × -CH <sub>2</sub> -N <sup>+</sup> )	Int = 8.90
	2.0 (3H, s, acetyl)	Int = 3.00
	1.6 (8H, m, 4 × -CH <sub>2</sub> C-N <sup>+</sup> )	Int = 8.93
	1.3 (8H, m, 4 × -CH <sub>2</sub> -CH <sub>3</sub> )	Int = 9.24
	0.9 (12H, m, 4 × -CH <sub>3</sub> )	Int = 13.50

### 2.2.4.2 Synthesis of HA-VE



Reagents	MW (g/mol)	Density (g/mL)	mmol	g	mL	eq.
HA-TBA	-	-	1.6	1.0	-	1
DVA	198	-	1.6 (4.8)	0.32 (0.96)	-	1 (3)
CAL-B lipase				0.1	-	
hydroquinone	110	-	0.08	0.008	-	0.05
DMSO					100	

Procedure:

HA-VEs with varying DS were synthesized using lipase-catalyzed transesterification. To investigate the influence of reaction time and stoichiometry on DS, the synthesis was carried out in two flasks in parallel: flask-**A**, 1 eq. DVA; flask-**B**, 3 eq. DVA. From each flask, specific amount of the reaction mixture was taken out for workup at prescribed time points (24 h, 48 h, 72 h or 96 h).

HA-TBA was firstly dissolved in anhydrous DMSO to form a 1 % solution. Lipase CAL-B (Sigma,  $\geq 10$  U/mg) and hydroquinone was added into another flask containing either equivalent (**A**) or 3-fold DVA (**B**) at 50°C. To this solution, the HA-TBA solution was added dropwise within 1 h. The reactions were maintained for 24 h, 48 h, 72 h, or 96h, respectively. After reaction, the mixture was firstly distilled under high vacuum to remove DMSO. Then the slurry was diluted with deionized water by 10 times (v/v) and extracted with dichloromethane to remove excessive DVA. The extracted solution was further dialyzed against 100 mM NaCl (24 h) and deionized water for two days. The solution was lyophilized to yield HA-VE (brown solid) as the final product, giving a final yield (> 80%) of starting material.

---

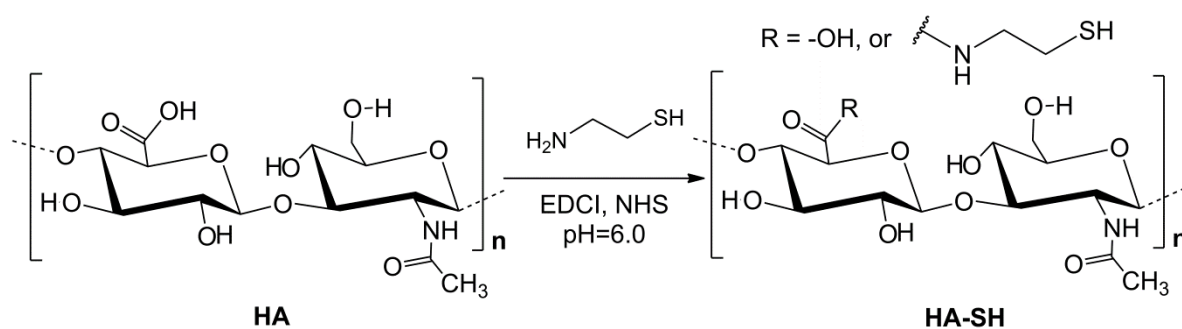
$^1\text{H-NMR (D}_2\text{O): } \delta$ (ppm)	7.2 (1H, q, COCH=CH <sub>2</sub> )
	4.9 (1H, d, COC=CH <sub>2</sub> )
	4.6-4.7 (1H, d, COC=CH <sub>2</sub> )
	2.5 (4H, s, 2 × CH <sub>2</sub> -C(=O)-)
	2.0 (3H, s, acetyl)
	1.7 (4H, s, 2 × C <sub>H2</sub> -CH <sub>2</sub> -C(=O)-)

The DS of HA-VEs were determined using  $^1\text{H-NMR}$  by calculating the ratio of the integrated vinyl protons at 7.20 ppm relative to that of the acetyl protons at 2.0 ppm. Depending on the reaction condition, the DS of HA-VE is listed below:

Entry	Stoichiometry *	Reaction Time (h)	DS
1	1:1	24	0.13
2	1:1	48	0.21
3	1:1	72	0.34
4	3:1	24	0.33
5	3:1	48	0.71
6	3:1	72	1.04
7	3:1	96	1.25

---

### 2.2.5 Synthesis of Thiolated Hyaluronate (HA-SH)



Reagents	MW (g/mol)	Density (g/mL)	mmol	g	mL	eq.
HA (sodium salt)	-	-	2.49*	1.0	-	1
cysteamine hydrochloride	114	-	7.47	0.85	-	3
1-ethyl-3-(3-dimethyl amino propyl)carbodiimide (EDCI)	192	-	12.45	2.39	-	5
N-hydroxysuccinimide (NHS)	115	-	12.45	1.43		5
dilute HCl (pH 6.0)					250	

\*indicating the molar amount of -COOH groups in HA

#### Procedure:

The sodium salt of HA was dissolved in deionized water to give a 1 % solution. After that, the slurry was filtrated to remove the resin. The pH value of the resultant solution was decreased to 5.5 by adding 0.1 M HCl. Afterwards, coupling reagents (EDCI and NHS) were added giving final concentrations at 50 mM. Then the pH was further tuned to 5.5 by the addition of 0.1 M NaOH. The obtained solution was stirred for 30 min. To this solution, cysteamine hydrochloride was added and the pH was increased to 6.0. After 24 h reaction at room temperature, the reaction mixture was dialyzed against 10 mM NaCl solution (three times) and later against distilled water (twice). Finally, the collected solutions were lyophilized at -49 °C and 0.02 mbar.

Yield: 1.04 g (92% of theory) of colorless solid

$^1\text{H-NMR}$ ( $\text{D}_2\text{O}$ ): $\delta$ (ppm)	2.9 (m, 2H, -NH- <u>CH</u> <sub>2</sub> -)	Int=0.67
	2.4-2.8 (m, 2H, - <u>CH</u> <sub>2</sub> -SH)	Int=0.65
	2.0 (s, 3H, acetyl)	Int=3.00

DS: 0.33

corresponding to 33 sulfhydryl groups per 100 HA units.

## **2.3 Characterization of HA-derivatives**

### **2.3.1 HA-VE Hydrogels**

#### **2.3.1.1 Photopolymerization**

Hydrogel Preparation: Gel precursors were firstly mixed with photoinitiator stock solution (0.5% I2959 in PBS), achieving a final macromer concentration of 2.5, 5 and 10%, respectively. Hydrogel pellets were prepared in a multiwell PDMS chamber (well diameter: 6 mm). Two hundred microliters of macromer solution was pipetted between two glass coverslips separated by a 1.5 mm spacer and then exposed to UV light (20 mW/cm<sup>2</sup>) for 900 s (450 s each side). Pellets were detached from the slides and washed twice with sterile PBS.

#### **2.3.1.2 Influence of DS on Photoreactivity**

HA-VE macromers with three different DS (0.13, 0.19, 0.53) were screened using photo-rheometry according to a generic protocol: 50  $\mu$ L sample, 15 mW cm<sup>2</sup>, 10 Hz, 10 %strain, 50  $\mu$ m thickness. The formulations consisted of 10 wt% macromer and 0.5 % I2959 in PBS.

#### **2.3.1.3 Influence of Macromer Content on Gel Stiffness**

A series of HA-VE formulations with varying macromer content (4, 5, 6, 7, 10 %) were prepared by serial dilution of 10 % HA-VE solution with PBS. To minimize the effects of initiator, the molar ratio between HA-VE (DS-0.13) and I2959 was kept constant. The formulations were screened using photo-rheometry according to a generic protocol as described in section 2.3.1.2.

#### **2.3.1.4 Temporal Control**

To prove that photopolymerization of HA-VE is under temporal control, photo-rheometry measurement of a HA-VE (DS-0.13) formulation including 10 % macromer and 0.5 I2959, was performed according to customized protocol where the UV-light was switched off for 80s at 100s and again at 260s. The other rheometry settings were identical as described in section 2.3.1.2.

### 2.3.1.5 Degradation

To monitor the enzymatic degradation process, an adapted procedure was applied.<sup>54</sup> Specifically, work solutions containing 10 % HA-VE (DS=0.54) and 0.5 % I2959 in PBS were prepared and stored on ice-bath. Varying amounts of hyaluronidase were added into the macromer solutions giving final concentrations (10, 30, 60 mg/mL, respectively). The mixed macromer/enzyme solutions were transferred to the thermo-controlled glass plate which was set at 5 °C. Then the rheometer system adapted the solution to a 50 µm thickness. The solutions were photopolymerized *in situ* for 10 mins. Finally, the plate temperature was increased to 37 °C to activate the enzyme and initiate the enzymatic degradation.

## 2.3.2 Comparative Characterization

### 2.3.2.1 Cytotoxicity

The cytotoxicities of four macromer solutions (HA, HA-AC, HA-MA, HA-VE) were evaluated by a cell metabolic activity assay using a Presto-Blue agent (Life Technologies). A mouse fibroblast cell line (L929, Sigma) was cultured in high glucose Dulbecco's Modified Eagle's Medium (DMEM, Lonza) including L-glutamine, which was further supplemented with 10% fetal bovine serum (Sigma) and 1% Penicillin-Streptomycin (Sigma). Macromers were dissolved in DMEM at 10% (HA only), 1% and 0.1%. L929 cells were seeded in a 96-well tissue culture plate at a density of  $1 \times 10^4$  cells per well in 100 µL of growth medium and left to attach to the plate in the incubator (37 °C, 5% CO<sub>2</sub>) over night. After 24 h, the medium was removed and 100 µL of each freshly prepared macromer solutions were added to the cells. After 24 h incubation, macromer solutions were carefully removed and 100 µL of Presto-Blue/DMEM solution (1:10, v/v) was added. After 30 minutes of incubation at 37 °C, the fluorescence of the samples was recorded at 560 nm (excitation) and 590 nm (emission) using a microplate reader (Synergy H1, BioTek). Obtained signals were compared with fluorescence of Presto-Blue in wells without cells (blank sample – no metabolic activity of the cells) and DMSO control (negative control – dead cells without metabolic activity) and with wells in which the cells were not treated with investigated substances (positive control – 100 % of cell metabolic activity).

### 2.3.2.2 Photoreactivity

Photoreactivity of HA macromers with different functionalities (AC, MA, VE) were compared using photo-rheometry. Each of the macromer was dissolved in 0.5 % I2959/PBS stock solution to give a final macromer concentration of 10 %. The photo-rheometry measurements were performed according to a generic protocol as described in section 2.3.1.2. The slope value of plotted  $G'$  values were generated from a linear regression of the  $G'$  plots from 60 s to 200 s while the induction time was defined as the point when  $G'$  value surpassed 5 Pa.

### 2.3.2.3 Influence of Thiol-ene Chemistry

A series of HA-VE/DTT formulations were prepared by mixing 20 % HA-VE stock solution with DTT solutions (1:1, v/v) containing different amount of DTT. After mixing, the macromer and initiator content was set to 10 % and 0.5 %, respectively; while the thiol/ene ratio was set to 0, 0.2, 0.4, 0.6, 1, respectively. These formulations were screened using photo-rheometry according to a generic protocol as described in section 2.3.1.2.

### 2.3.2.4 Swelling Test

For swelling test, HA-VE gel pellets were prepared as described in section 2.3.1.1. The determination of swelling ratio of HA gel pellets were performed using the same protocol as described in section 1.4.2.

### 2.3.2.5 AFM Modulus Test

Gel elastic moduli were analyzed using an atomic force microscopy (AFM-NanoWizard 3, JPK Instruments, Berlin). A detailed explanation of the principle of AFM Nanoindentation could be found in **Methods**.

Prior to test, gel samples were UV-polymerized as aforementioned, except on top of methacrylated cover slips and then soaked in Milli-Q H<sub>2</sub>O for 24 h. These hydrated samples were probed using a pyramidal-tipped cantilever (MSNL, Veeco Instruments, Plainview, NY). Prior to each AFM measurement, the spring constant of each cantilever



was measured according to a general method,<sup>228</sup> with average values of  $\sim 10$  pN/nm. The force-indentation curves of each sample were recorded with a tip velocity of  $2 \mu\text{m/s}$  and a trigger force of  $\sim 300$  pN. Young's modulus values were calculated from the force curves according to a Hertz model (JPK software). Poisson's ratio of the gel samples was assumed as 0.5.

## 2.4 2PP Microfabrication

Gel precursor solutions were prepared as above except using a water-soluble two-photon initiator (P2CK, 2.23 mM) which was donated by Dr. Zhiqian Li (IAS). A detailed procedure for the synthesis of P2CK could be found in literature.<sup>37</sup> One hundred microliters of the precursor solution was pipetted between two glass cover slips separated by a 0.5 mm spacer. In order to fix gel structures, the bottom cover slip was pre-functionalized with methacrylate groups according to a generic protocol.<sup>229</sup>

A Ti:sapphire laser system (HighQ Femtotrain 800 nm, 80 fs pulse duration, 75 MHz repetition rate) was used for 2PP microfabrication of hydrogels. Detailed information about the 2PP experimental setup is available in a previous report of our group.<sup>230</sup> After 2PP processing, the sample was developed in PBS to remove the unpolymerized materials. After 2 h, the gel construct was visualized by a confocal laser scanning microscope (Zeiss LSM 700).

## 2.5 Engineering Cell Adhesion

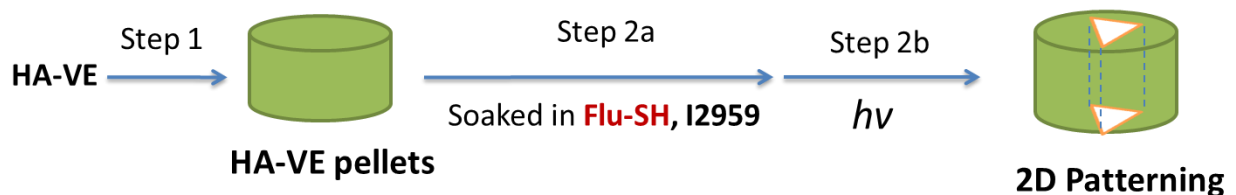
### 2.5.1 Preliminary Cell Top-seeding

For cell top-seeding, HA-VE gel pellets were prepared as described in section 2.3.1.1. The subsequent top-seeding of MG63 cells onto HA-VE gels was as same as described in section 1.4.4.

### 2.5.2 A Photopatterning Approach

### 2.5.3 Model One-photon Patterning

Model UV photopatterning was carried out based on a multi-step procedure as described below. First, 10 % HA-VE (DS-0.53) precursor solutions containing 0.5 % I2959 was transferred into a multi-well PDMS mold (each well: 6 mm diameter, 1.5 mm thickness). The samples were exposed to UV-light ( $30 \text{ mW cm}^{-2}$ ) for 450 s (225 s each side), forming partially crosslinked gel pellets.

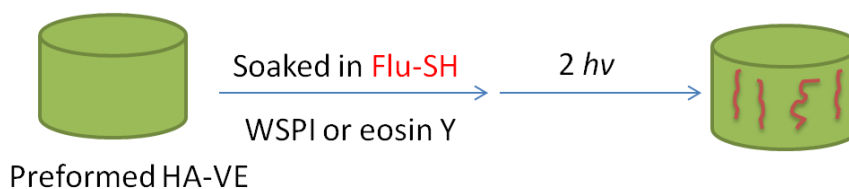


Second, the gel pellets were soaked in a solution containing thiolated fluorescein (Flu-SH, 1 mg/ml) and 0.1 % I2959 for 2 h. Afterward, the pellets were transferred on top of cover slips for photopatterning. Photomasks were self-prepared by laser printing (Canon-C2380) of ‘TU Wien’ logos with varying sizes on a transparent paper (Canon-CLT500-A4). Then, the photomask with appropriate size (~5 mm) was put on top of the gel pellet. The top of this set-up was exposed to UV light ( $30 \text{ mW cm}^{-2}$ ) for 120 s.

After photopatterning, the gel pellets was soaked in PBS for 4 h to remove unconjugated Flu-SH. The patterned pellets were subsequently visualized using a fluorescent microscope (Zeiss Axiovert 200, Biophysiscs lab).

### 2.5.4 Model Two-photon Patterning

Model two-photon photopatterning was performed via a similar protocol as model UV patterning except using WSPI or eosin Yellow as two-photon initiator in the patterning step and ultrafast NIR laser (800 nm) as light source.



For two-photon patterning, the laser was allowed to scan the gel pellet according to a simplified CAD-model consisting of a series of squares that are spaced from each other with a gap of 1  $\mu\text{m}$ .

After photopatterning, the gel pellets were developed in PBS for 4 h to remove unreacted Flu-SH and/or photoinitiator. Then the patterned pellet was analyzed using a confocal laser scanning microscope (Zeiss LSM 700).

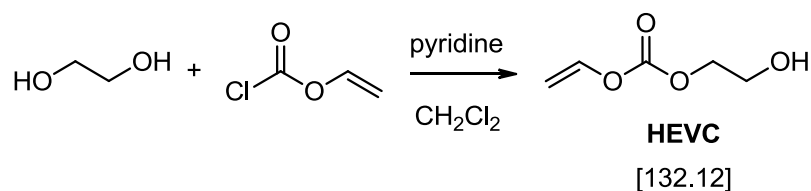


### 3 Synthetic Hydrogels

#### 3.1 Vinyl Carbonates/Carbamates-based Hydrogels

##### 3.1.1 Synthesis

##### 3.1.1.1 Synthesis of Hydroxyethyl Vinyl Carbonate



Reagents	MW (g/mol)	Density (g/mL)	mmol	g	mL	eq.
ethylene glycol	62	1.11	96.7	6.00	-	1
vinyl chloroformate	107	1.17	9.67	1.03	0.9	0.1
pyridine	79	0.98	9.67	0.76	0.8	0.1
DCM					20	

##### Procedure:

A solution of ethylene glycol and anhydrous pyridine in DCM was cooled with an ice bath under stirring and then purged with argon. Vinyl chloroformate was diluted with 5 mL DCM and this solution was added dropwise to the stirred solution over a period of 30 min. After addition, the mixture was allowed to react for 4 h at room temperature.

The reaction mixture was extracted with 1N HCl (10 mL) and the DCM layer was extracted with deionized water (2 x 10 mL). Afterwards, a saturated NaCl solution (40 mL) was added to the aqueous layer. This solution was re-extracted with DCM (3 x 15 mL). The combined organic layer were dried with sodium sulfate, filtered and the solvent was evaporated. The crude product was purified by kugelrohr distillation (60 °C/2 mbar).

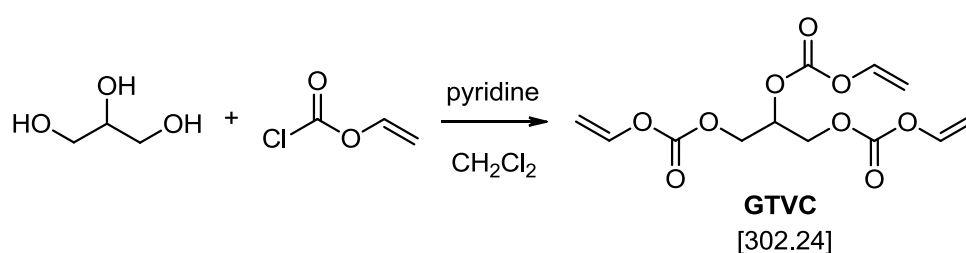
Yield: 0.83 g (65 % of theory) of a colorless liquid

TLC (PE:EE = 3:1)

R<sub>f</sub> = 0.42

$^1\text{H-NMR}$ ( $\text{CDCl}_3$ ): $\delta$ (ppm):	7.05 (1H, dd, $J = 13.9$ Hz, $J = 6.1$ Hz, $\text{H}_2\text{C}=\underline{\text{C}}\text{H-O}$ ); 4.91 (1H, dd, $J = 13.9$ Hz; $J = 2.1$ Hz, $\underline{\text{H}}_2\text{C}=\text{CH-O}$ <i>trans</i> ); 4.58 (1H, dd, $J = 6.1$ Hz, $J = 2.1$ Hz, $\underline{\text{H}}_2\text{C}=\text{CH-O}$ , <i>cis</i> ); 4.31(2H, t, $\text{O-CH}_2$ ); 3.85 (2H, t, $\text{HO-CH}_2$ )
$^{13}\text{C-NMR}$ ( $\text{CDCl}_3$ ): $\delta$ (ppm):	152.8, 142.6, 98.0, 69.8, 60.4
GC-MS ( $m/z$ ):	114.96, 88.97, 70.03, 62.98, 57.02

### 3.1.1.2 Synthesis of Glycerol Trivinyl Carbonate



Reagents	MW (g/mol)	Density (g/mL)	mmol	g	mL	eq.
glycerol	92	1.26	4.22	0.77	-	1
vinyl chloroformate	107	1.17	12.65	1.35	1.2	3
pyridine	79	0.98	12.65	1.02	1.1	3
DCM					10	

#### Procedure:

The glycerol trivinyl carbonate (**GTVC**) was synthesized according to a generic procedure described by Heller.<sup>176</sup> A solution of glycerol and pyridine in DCM was cooled down with an ice bath, stirred and purged with argon. To this solution, vinyl chloroformate was added dropwise over a period of 20 min. After addition, the reaction was stirred for 10 h at room temperature.

The reaction mixture was extracted with 1N HCl (10 mL) and the DCM layer was washed with deionized water (2 x 10 mL). The combined organic layers were dried with sodium sulfate, filtered and the solvent was evaporated. The crude product was purified by column chromatography (PE:EE = 5:1).

Yield: 0.8 g (63 % of theory) of a colorless liquid

TLC (PE:EE = 3:1)

$R_f = 0.65$

$^1\text{H-NMR}$  ( $\text{CDCl}_3$ ):  $\delta$  (ppm):

7.04 (3H, dd,  $J = 12.8$  Hz,  $J = 6.2$  Hz,  $\text{H}_2\text{C}=\text{CH}-\text{O}$ );  
5.21 (1H, m, CH), 4.94 (3H, dd,  $J = 12.8$  Hz;  
 $J = 2.5$  Hz,  $\text{H}_2\text{C}=\text{CH}-\text{O}$  *trans*); 4.57 (3H, dd,  
 $J = 6.2$  Hz,  $J = 2.5$  Hz,  $\text{H}_2\text{C}=\text{CH}-\text{O}$  *cis*); 4.45 (4H,  
m,  $\text{CH}_2$ )

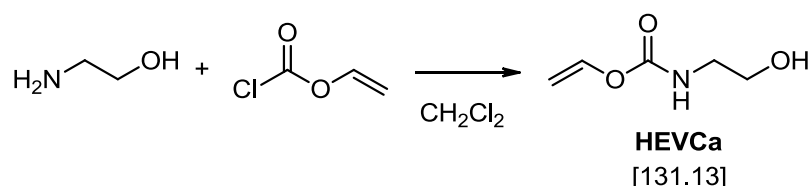
$^{13}\text{C-NMR}$  ( $\text{CDCl}_3$ ):  $\delta$  (ppm):

151.6, 151.2, 141.8, 98.0, 97.9, 72.2, 64.7

GC-MS ( $m/z$ ):

319.61, 214.83, 205.88

### 3.1.1.3 Synthesis of Hydroxyethyl Vinyl Carbamate



Reagents	MW (g/mol)	Density (g/mL)	mmol	g	mL	eq.
ethanol amine	61	1.01	6.9	0.42	-	1
vinyl chloroformate	107	1.17	3.45	0.37	0.3	0.5
DCM					10	

#### Procedure:

The 2-hydroxyethyl vinyl carbamate (**HEVCa**) was synthesized according to literature.<sup>194</sup> A stirred solution of ethanol amine (2 equiv) in DCM was cooled down with an ice bath and purged with argon. To this solution, vinyl chloroformate (1 equiv) was added dropwise over a period of 20 min. After addition the reaction was allowed to warm up to room temperature and stirred for 6 h.

After reaction, the white precipitate (i.e., ethanol amine hydrochloride) was filtered off. Then the filtrate was dried over sodium sulfate, filtered, and the solvent was evaporated. The crude product was purified by kugelrohr distillation.

Yield: 0.31 g (71% of theory, 72% of lit.<sup>194</sup>) of a colorless liquid

B.P.: 87 °C at 0.02 mbar (lit<sup>194</sup>: 125 °C at  $8.9 \times 10^{-1}$  Torr)

TLC (PE:EE = 1:1)

$R_f = 0.34$

<sup>1</sup>H-NMR (CDCl<sub>3</sub>):  $\delta$  (ppm):

7.09 (dd, 1H, J = 14.1 Hz, J = 5.9 Hz, CH<sub>2</sub>=CH-O), 5.83 (s, 1H, -NH-), 4.68 (dd, 1H, J = 13.8 Hz, J = 1.4 Hz, CH<sub>2</sub>=CHO *trans*), 4.37 (dd, 1H, J = 6.4 Hz, J = 1.5 Hz, C H<sub>2</sub>=CH-O *cis*), 3.64 (t, 2H, HOCH<sub>2</sub>CH<sub>2</sub>), 3.47 (s, 1H, -OH), 3.28 (t, 2H, HOCH<sub>2</sub>CH<sub>2</sub>)

<sup>13</sup>C-NMR (CDCl<sub>3</sub>):  $\delta$  (ppm):

151.8, 141.9, 95.4, 64.2, 43.2



### **3.1.2 Characterization**

#### **3.1.2.1 Cytotoxicity**

Cytotoxicity test in this section was performed according to a generic protocol for MTT assay as described in section 1.2.2.

#### **3.1.2.2 Photo-DSC**

Photo-DSC measurements were carried out according to a generic method described in **Methods**. The formulations were prepared by mixing the respective monomer or oligomer with 5 % I2959.

#### **3.1.2.3 Proof-of-Concept 2PP**

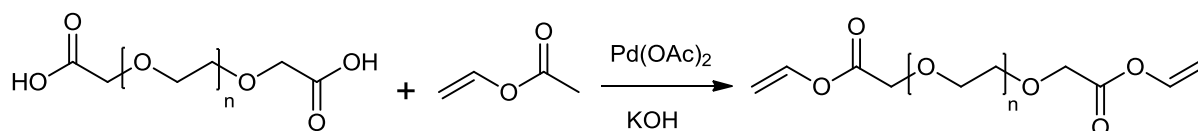
For 2PP test of vinyl carbonates, GTVC was mixed with 1 wt% two-photon initiator (B3FL). The formulation was structured using a M3DL device with an average power of 75 mW, a writing speed of 100  $\mu\text{m/s}$ , and a 20 $\times$  NA 0.8 objective. The size of the lattice structure was set to 300  $\times$  300  $\times$  20  $\mu\text{m}$  (layer distance of 5  $\mu\text{m}$ ).

After 2PP structuring, the sample was developed in ethanol to remove unpolymerized material. The structure was later analyzed by phase-contrast laser scanning microscope.

## 3.2 PEG-based Hydrogels

### 3.2.1 Synthesis

#### 3.2.1.1 Synthesis of PEG-600-DVE



Reagents	MW (g/mol)	Density (g/mL)	mmol	g	mL	eq.
PEG-600-diacetic acid	600	1.11	35.0	21.0	-	1
vinyl acetate	86	0.93	1750	150.7	161	50
Pd(OAc) <sub>2</sub>	224		4.2	0.94	-	0.12
KOH	56		3.5	0.20	-	0.10

#### Procedure:

The PEG-600-diacid was firstly dissolved in vinyl acetate under vigorous stirring. To this solution, the Pd(OAc)<sub>2</sub> catalyst and powdered potassium hydroxide were added under argon atmosphere. The reaction mixture was heated to 60°C for 48 h under argon atmosphere. After reaction, the mixture was allowed to cool down to room temperature and filtered with Kieselgel. The filtrate was washed with saturated NaHCO<sub>3</sub> solution (2 x 25 mL). The organic layer was further washed with brine (1 x 25 mL), dried over Na<sub>2</sub>SO<sub>4</sub>, filtered and concentrated. The crude product was finally dried by high vacuum. Purification by column chromatography was not successful.

Yield: 10.7 g (47 % of theory) of yellowish oil

TLC (CHCl<sub>3</sub> : MeOH = 12:1)

R<sub>f</sub> = 0.6

<sup>1</sup>H-NMR (CDCl<sub>3</sub>): δ (ppm):

7.20 (2H, dd, J = 13.9 Hz, J = 6.3 Hz, -O(CH)=CH<sub>2</sub>); 4.90 (2H, dd, J = 13.9 Hz, J = 1.7 Hz, H<sub>2</sub>C=C *trans*); 4.60 (2H, dd, J = 6.3 Hz, H<sub>2</sub>C=C *cis*); 4.18 (4H, s, -CH<sub>2</sub>-); 3.80-3.44 (53H, m, -O-CH<sub>2</sub>-CH<sub>2</sub>-)

For PEG-600-DVE, two unsaturated protons should correspond to 48 ethylene glycol protons; while for mono-substituted products, one unsaturated proton should correspond to 48 ethylene glycol protons. Purity of the crude product was defined with the aid of Eq. (1) and (2) and NMR integration.

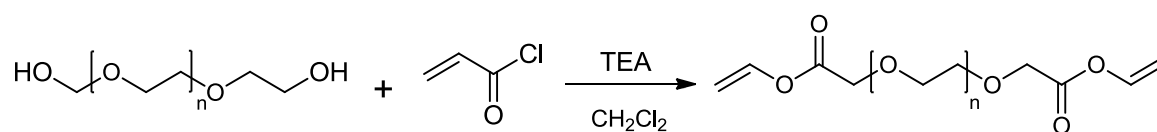
$$x + y = 1 \quad \text{Equation (1)}$$

$$\frac{2x + y}{48 \times (x + y)} = \frac{2}{53} \quad \text{Equation (2)}$$

Where “x” stands for the fraction of di-substituted product and “y” stands for the fraction of mono-substituted one, respectively.

After calculation, the fraction value of “x” was 0.81. The product was used for characterization without further purification.

### 3.2.1.2 Synthesis of PEGDA (10 k)



Reagents	MW (g/mol)	Density (g/mL)	mmol	g	mL	eq.
PEG-10k	10000	1.11	0.3	3	-	1
acryloyl chloride	91	1.12	1.5	0.14	0.12	5
triethylamine	101	0.73	1.2	0.12	0.16	4
abs. CH <sub>2</sub> Cl <sub>2</sub>					32	

#### Procedure:

PEG (10 kDa) was firstly dried through azeotropic distillation with toluene at ambient pressure. The dried PEG-10k was dissolved in methylene chloride. Triethylamine (TEA) was added to the flask and bubbled with argon for 10 min. In a second flask, excessive acryloyl chloride (5 eq.) was dissolved in 2 mL methylene chloride. This solution was transferred into a syringe and added dropwise into the first flask which was pre-cooled on ice. The mixture was stirred for overnight under argon. The crude product was

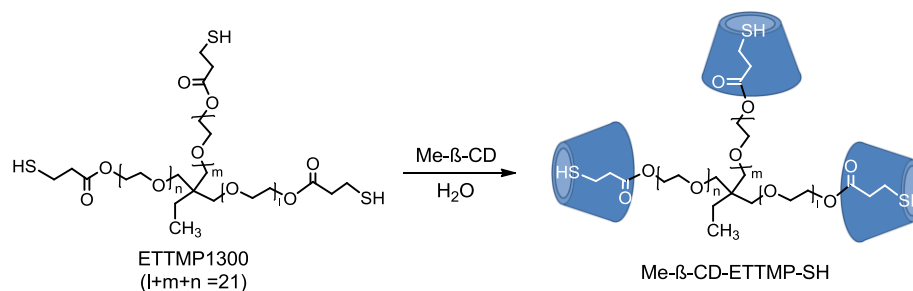
concentrated under reduced pressure, filtered, precipitated in cold ethyl ether, filtered and dried in a desiccator overnight. The dry product was further purified by dialysis against distilled water for 24 h and finally lyophilized.

Yield: 2.25 g (75 % of theory) of a white solid

$^1\text{H-NMR}$  ( $\text{CDCl}_3$ ):  $\delta$  (ppm): 6.40 (2H, m,  $\text{CH}_2=\text{CH}$ -), 6.20 (2H, m,  $\text{CH}_2=\text{CH}$  *trans*), 5.80 (2H, m,  $\text{CH}_2=\text{CH}$  *cis*), 3.80-3.30 ( $280 \times 4$  H, s,  $-\text{CH}_2-\text{CH}_2-$ )

### 3.2.1.3 Synthesis of Water-soluble Thiols

#### 3.2.1.4 Preparation of Macrothiols by Inclusion Complexation



Reagents	MW (g/mol)	Density (g/mL)	mmol	g	mL	eq.
methyl-beta-cyclodextrin	1310		1.26	1.65	-	1
ETTMP-1300	1300		0.77	1.0*	-	0.6
dist. $\text{H}_2\text{O}$				-	6	

\*indicating the max. amount to form a transparent solution after complexation

Procedure:

To prepare the inclusion complex, methyl-beta-cyclodextrin ( $\text{M}\beta\text{CD}$ ) was firstly dissolved in distilled water to form a 22 wt% solution. Subsequently, varying amounts of macrothiol ETTMP-1300 was added to aliquoted  $\text{M}\beta\text{CD}$  solution. The solution was incubated for 10 h under stirring at room temperature. After complexation, the max. solubility of ETTMP-1300 was determined by the concentration at which there was no turbidity in resultant solutions. The max. solubility was found to be ~12 wt%.

For hydrogel formation, distilled water was replaced with equal amount of photoinitiator stock solution (0.5 wt% I2959 in PBS).

### **3.2.2 Characterization**

#### **3.2.2.1 Cytotoxicity**

Cytotoxicity test in this section was performed according to a generic protocol for MTT assay as described in section 1.2.2.

#### **3.2.2.2 Photo-DSC**

Photo-DSC measurements were carried out according to a generic method described in **Methods**. The PEG-based formulations were prepared by mixing the respective oligomer with 1 wt% I2959.

### **3.2.3 2PP Microfabrication**

#### **3.2.3.1 PEGDA**

##### **3.2.3.1.1 PEGDA-700**

Varying amounts of PEGDA-700 (Sigma) was mixed with 1 wt% WSPI stock solution to provide hydrogel precursor solutions with macromer content from 50 wt% to 90 wt%. These formulations were processed using a M3DL 2PP-device:

writing speed: 1-10 mm/s

average power: 60-300 mW

objective: 20× NA 0.4

rod-like structure:  $15 \times 140 \times 21 \mu\text{m}^3$  (layer distance: 3.5/0.8  $\mu\text{m}$ )

3D woodpile structure:  $280 \times 280 \times 225 \mu\text{m}^3$  (layer distance: 3.5/0.8  $\mu\text{m}$ )

After 2PP structuring, the hydrogel structures were analyzed using LSM 700.

### **3.2.3.1.2 PEGDA-10k**

The 2PP structuring of PEGDA-10k was carried out using a similar protocol in section 3.2.3.1.1, except using 0.1 wt% P2CK as photoinitiator, 30 % PEGDA-10k as macromer, and Mipro-2PP device.

writing speed: 1-5 mm/s

average power: 50-100 Mw

### **3.2.3.2 PEGDMA**

#### **3.2.3.2.1 PEG-1000-DMA**

The 2PP structuring of PEG-1000-DMA was carried out using a similar protocol in section 3.2.3.1.1, except using 0.2 wt% R1 as photoinitiator.

writing speed: 10  $\mu\text{m/s}$

average power: 70-100 mW

objective: 20 $\times$  NA 0.8

lattice structure:  $50 \times 50 \times 40 \mu\text{m}^3$

#### **3.2.3.2.2 PEG-600-DMA**

The 2PP structuring of PEG-600-DMA was carried out using a similar protocol in section 3.2.3.2.1, except using 0.5 wt% R1 as photoinitiator and 10 wt% glycerol dimethacrylates as crosslinker.

#### **3.2.3.2.3 Formulation-3**

The 2PP structuring of formulation-3 was carried out as described in section 3.2.3.2.1, except using 0.5 wt% R1 as photoinitiator.

writing speed: 300  $\mu\text{m/s}$

average power: 30 mW

objective: 20 $\times$  NA 0.8

lattice structure:  $100 \times 100 \times 30 \mu\text{m}^3$

### 3.2.3.3 PEG Divinylesters

#### 3.2.3.3.1 PEG-600-DVE

The 2PP structuring of PEG-600-DVE was performed as described in section 3.2.3.2.1, except using tetrathiol (TT,  $n_{\text{SH}}:n_{\text{ene}}=0.2$ ) for thiol-ene copolymerization.

#### 3.2.3.3.2 PEG-250-DVE

The 2PP structuring of PEG-250-DVE was performed as described in section 3.2.3.3.1, except using PEG-250-DVE/TT formulation ( $n_{\text{SH}}:n_{\text{ene}}=0.2$ ) for thiol-ene copolymerization.

writing speed: 120-300  $\mu\text{m/s}$

average power: 10-250 mW

objective: 20 $\times$  NA 0.4

#### 3.2.3.3.3 DVA

The 2PP structuring of DVA was performed as described in section 3.2.3.3.1, except using DVA/TT formulation ( $n_{\text{SH}}:n_{\text{ene}}=0.2$ ), 0.4 % R1, and 0.01 % pyrogallol as stabilizer.

writing speed: 10  $\mu\text{m/s}$

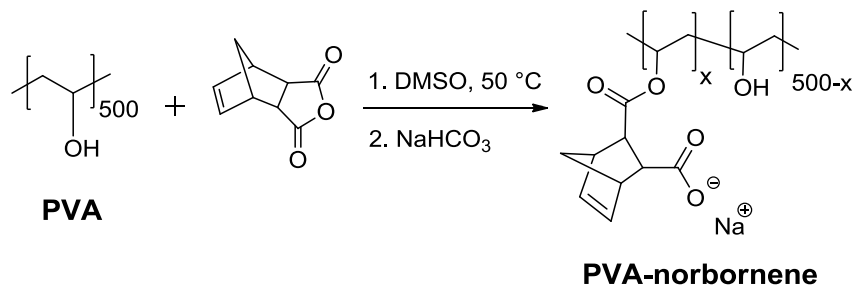
average power: 100 mW

objective: 20 $\times$  NA 0.4

lattice structure:  $300 \times 100 \times 20 \mu\text{m}^3$  (line/layer distance: 5/3.5  $\mu\text{m}$ )

### 3.3 PVA-based Hydrogels

#### 3.3.2 Synthesis of PVA-Norbornene



Reagents	MW (g/mol)	Density (g/mL)	mmol	g	mL	eq.
PVA (22 k)	22000		18*	0.8	-	1
<i>cis</i> -5-norbornene- <i>endo</i> -2,3-dicarboxylic anhydride	164		1.8(9)	0.16(1.0)	-	0.1(0.5)
<i>p</i> -toluenesulfonic acid	172	1.28	0.06	0.01	-	0.003
abs. DMSO				-	30	

\*indicating the molar amount of –OH groups in PVA

#### Procedure:

In a three-neck flask, PVA and *p*-toluenesulfonic acid (*p*-TsOH) were dissolved in anhydrous DMSO (25 mL) at 60 °C for 2 h under vigorous stirring. In a second flask, appropriate amount of *cis*-5-norbornene-*endo*-2,3-dicarboxylic anhydride (0.1/0.5 eq.) was dissolved in anhydrous DMSO (5 mL) under argon atmosphere. This solution was added dropwise to the first flask containing PVA. The reaction was maintained at 50 °C for 24, 48, and 72 h, respectively.

After reaction, the crude product was directly purified by dialysis against distilled water. After ~6 h of dialysis (×2 changes of water), it was supposed that most of the DMSO had been removed. The solution was further dialyzed against dilute NaHCO<sub>3</sub> solution (10 mM) to convert the products into the sodium salt form. After lyophilization, colorless solids were obtained with a general yield of ~95% of theory.

<sup>1</sup>H-NMR (D<sub>2</sub>O): δ (ppm): 6.2 (2H, s, -CH=CH-), 3.3 (2H, s, -C=C-CH-CH-), 3.1 (2H, s, -C=C-CH-CH-), 1.3 (2H, s, -CH<sub>2</sub>-)



The DS of PVA-norbornene was determined by calculating the relative integral ratio from NMR spectrum, as described in section 3.3.2. Depending on stoichiometry and reaction time, the DS of PVA-Norbornene was calculated and listed below.

Entry	Stoichiometry *	Reaction Time (h)	DS
1	1:10	24	0.07
2	1:2	24	0.19
3	1:2	48	0.24
4	1:2	72	0.42

### 3.3.3 Characterization

#### 3.3.3.1 Cytotoxicity

Cytotoxicity of PVA and PVA-Norb macromer solutions were tested using Presto-blue assay as described in section 2.3.2.1.

#### 3.3.3.2 Photo-Rheometry

Photoreactivity of PVA-norbornene macromers were analyzed in comparison with PEGDA-10k using photo-rheometry. Each of the macromer in formulation I-IV was dissolved in 0.5 % I2959 stock solution to give a final macromer concentration of 10 %. The photo-rheometry measurements were performed according to a generic protocol as described in section 2.3.1.2.

Entry	macromer (10%)	$n_{\text{-SH:-ene}}$
I	PEGDA-10k	0:1
II	PVA-Norb	0:1
III	PVA-Norb/DTT	1:1
IV	PVA-Norb/PVA-SH	1:1

The slope value of plotted  $G'$  values were generated from a linear regression of the  $G'$  plots from 60 s to 200 s while the induction time was defined as the point when  $G'$  value surpassed 5 Pa.

To Investigate the thiol to ene ratio on photoreactivity, a series of PVA-Norb/DTT formulations were prepared by mixing 20 % PVA-Norb stock solution with DTT solutions (1:1, v/v) containing different amount of DTT. After mixing, the macromer and initiator content was set to 10 % and 0.5 %, respectively; while the thiol/ene ratio was set to 0, 0.2, 0.4, 0.8, 1, 1.25 and 2.5, respectively. These formulations were screened using photo-rheometry according to a generic protocol as described in section 2.3.1.2.

### **3.3.4 2PP Microfabrication**

The 2PP structuring of PVA-Norb was carried out using a Mipro-2PP device. The formulation consisted of 20 % PVA-Norb (DS-0.24), DTT (-SH:-ene=1), 2.23 mM P2CK, and 0.01 % pyrogallol.

writing speed: 1-100 mm/s

average power: 20-100 mW

objective: 20× NA 0.8

cylinder structure size: 1.5×1.2×0.15 mm<sup>3</sup>

The hydrogel structure was developed in PBS and visualized using LSM-700.

## 4 Two-photon Cell-Encapsulation

### MTT Assay

Cytotoxicity of photoinitiator solutions (2.23 mM) against MG63 cells were tested according to a generic protocol for MTT assay as described in section 1.2.2.

### Hydrogel Formulations for Cell-encapsulation

The hydrogel formulations were prepared by dissolving gelMOD in respective stock solution of PI/PBS solutions at 37 degree.

Items	name	Conc.
gel precursor	gelMOD	20 %
nutrients	DMEM	80 %
PI (single-photon)	I2959	1.8 mM
PI (two-photon)	G2CK/P2CK	1.8 mM

### Two-photon Cell-Encapsulation & 2PP Processing

The detailed procedure on cell-encapsulation and 2PP processing could be found in a published paper by Ovsianikov et al.<sup>155</sup>

### Live/dead Staining

To evaluate cell viability, the cell-laden gel construct was further incubated with a PBS solution of live/dead staining reagents (propidium iodide/calcein-AM) for 20 min. After washing in PBS, fluorescently-labeled cells (green-live/red-dead) were visualized using a confocal laser microscope (Zeiss LSM 700). The cell number was quantified by using software ‘‘Image J’’.

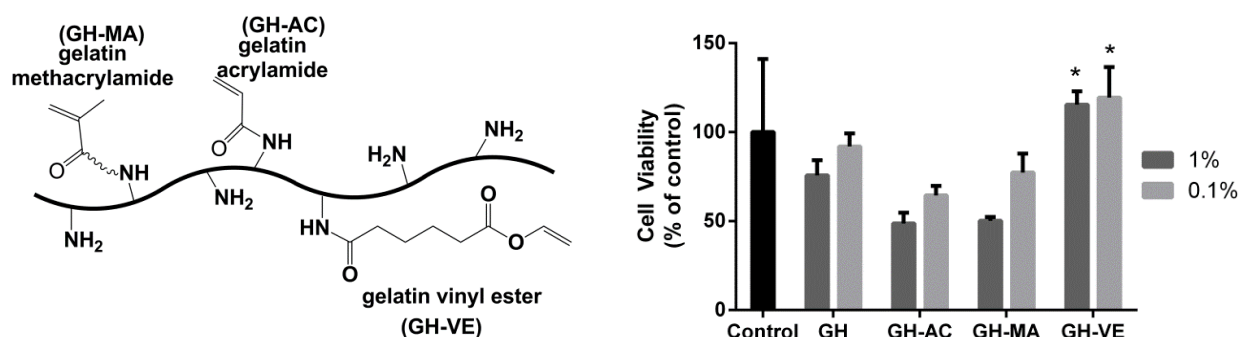


## Conclusion

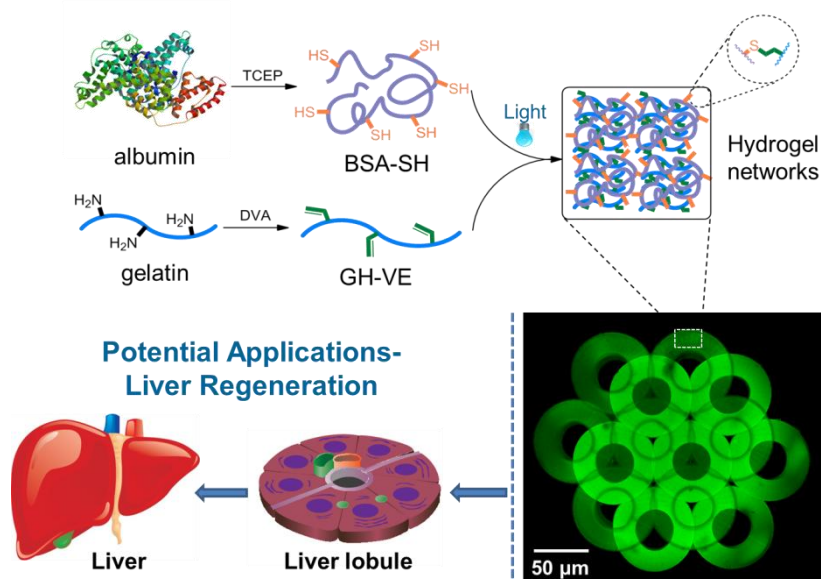
Research in tissue engineering and regenerative medicine asks for experimental tools to precisely recapitulate the native ECM environment that is a complex hydrogel network. Two-photon polymerization (2PP) allows user-defined microfabrication of ECM-mimetic hydrogels with complex geometry. Development of highly reactive and cytocompatible hydrogel precursors is essential to utilize 2PP as a biofabrication technique. In the present work, a series of novel cytocompatible hydrogel precursors (natural or synthetic origin) have been developed for 2PP microfabrication of artificial ECM gels.

### Gelatin-based Hydrogels

The first chapter of this thesis is focused on the preparation and characterization of gelatin-derivatives with different vinyl groups. The first naturally-derived gel precursor with pendant low-cytotoxic vinyl ester moieties, GH-VE, was successfully prepared and compared with the gelatin acrylate (GH-AC) and gelatin methacrylate (GH-MA). Notably, MTT assay showed that GH-VE presented significantly lower cytotoxicity than those of GH-AC and GH-MA.

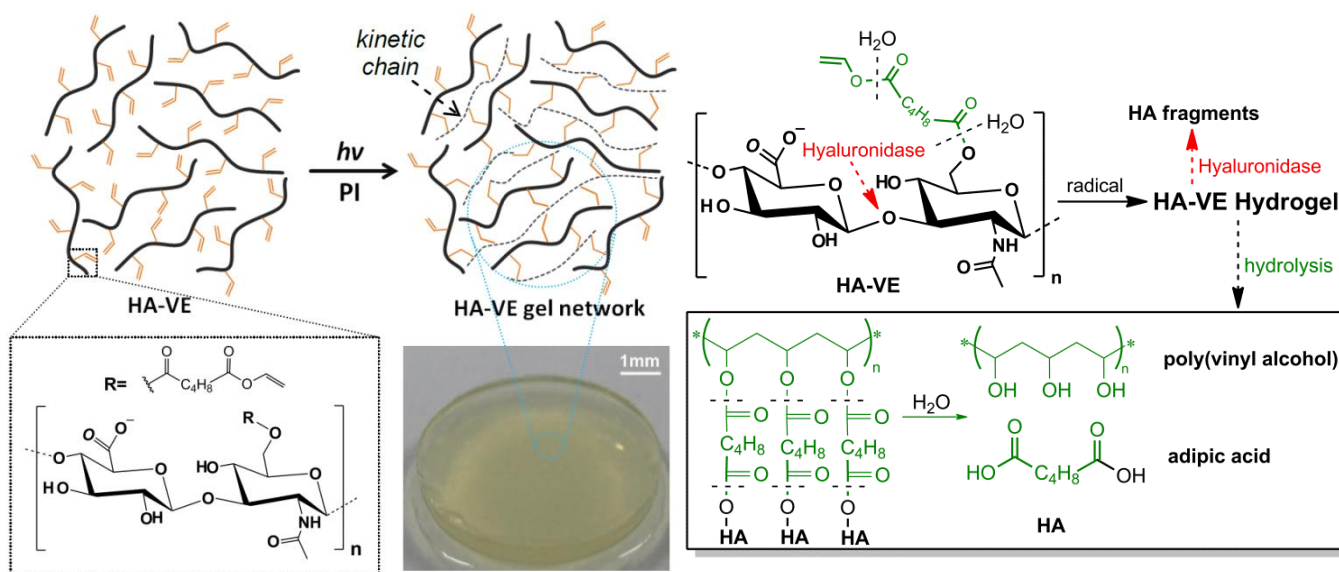


Since GH-VE exhibited a rather low photoreactivity towards homopolymerization, naturally-derived macrothiols were utilized to improve its reactivity. Specifically, BSA macrothiols (BSA-SH) with varying amount of cysteines were prepared through reductive cleavage and these cysteine moieties were used for thiol-ene copolymerization with GH-VE. It was found that the thiol to ene ratio played an important role in determining the photoreactivity, gelation kinetics, gel modulus, and swelling ratio. Based on the highly efficient thiol-VE reactions, GH-VE/BSA-SH formulations enabled 2PP lithography of 3D tissue-mimetic hydrogel structures at high writing speed (50 mm/s). It was also found that cell attachment on these protein gels was dependent on the relative ratio between two macromers since gelatin favors cell adhesion while albumin resists.

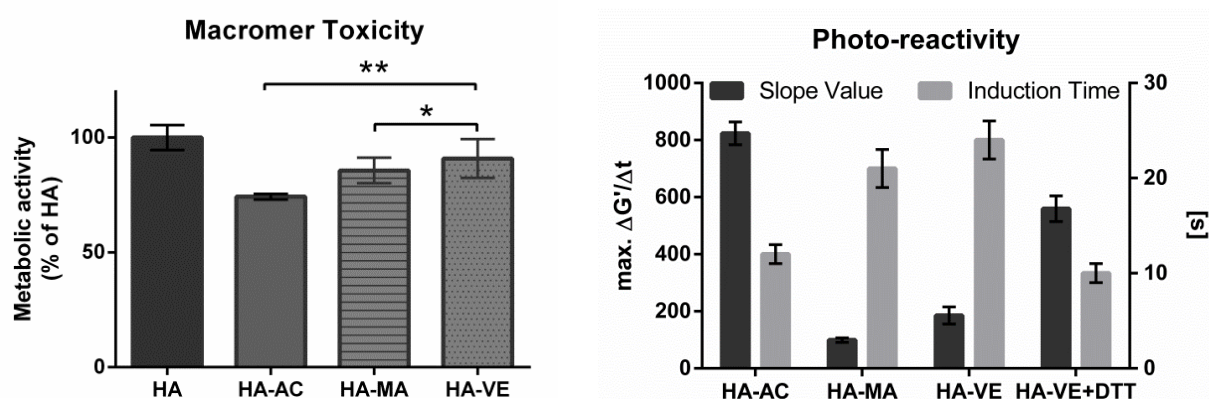


### Hyaluronan-based Hydrogels

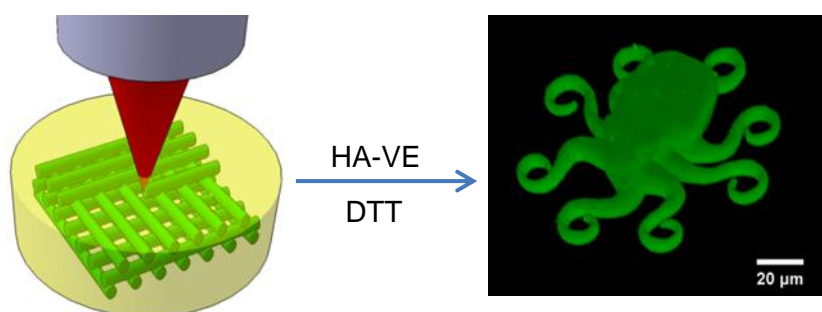
The second chapter of this thesis was focused on the preparation and characterization of photopolymerizable gel precursors based on hyaluronan (HA), which is a major ECM component. Hyaluronan vinyl esters (HA-VE), a novel hydrogel precursor, was prepared through lipase-catalyzed transesterification reactions. By carefully controlling the reaction conditions, HA-VE with tunable DS were accessible. In comparison with GH-VE, HA-VE has more reactive sites and improved photoreactivity. It is feasible to control the gel properties by either controlling the macromer DS or macromer content.



In addition, HA-VE were systematically compared with (meth)acrylated-HA analogues from varying aspects. Presto-Blue assay proved that HA-VE was significantly less cytotoxic than HA-AC and HA-MA analogues. Furthermore, HA-VE gels provide non-cytotoxic degradation products: PVA, adipic acid, and HA fragments. Since the reactivity of HA-VE towards homopolymerization was not sufficient for 2PP, dithiolthretol (DTT) was used as a dithiol crosslinker to boost the reactivity. Photo-rheometry studies showed that the photoreactivity of HA-VE/DTT formulations were significantly higher than that of HA-VE control. Fast gelation and high crosslinking efficiency was demonstrated in HA-VE/DTT formulations.



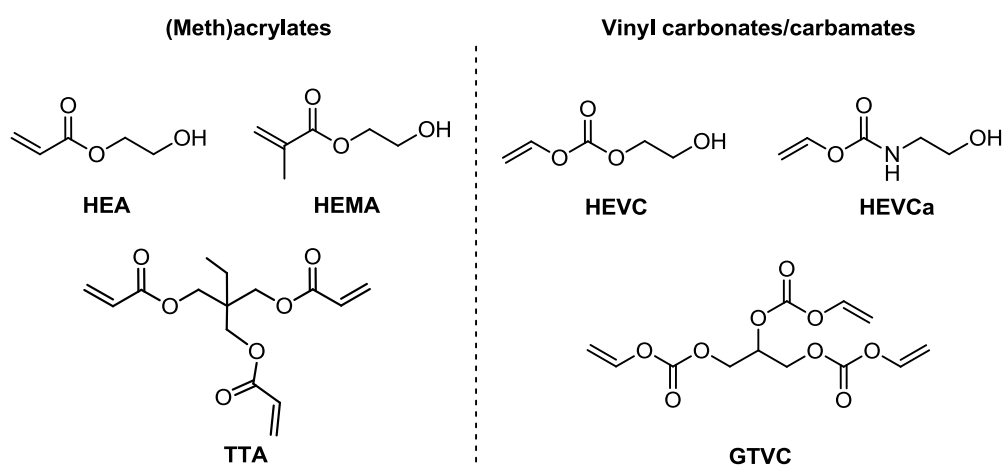
Using two-photon thiol-ene lithography, a 3D HA-VE gel construct was directly printed with  $\mu\text{m}$ -scale accuracy. Although HA-VE gels are not cell adhesive, model photopatterning work has laid the foundation for further work using RGD peptides. In all, the HA-VE hydrogel system is biocompatible, biodegradable and processable in 2PP, making it highly promising for potential applications in tissue regeneration.



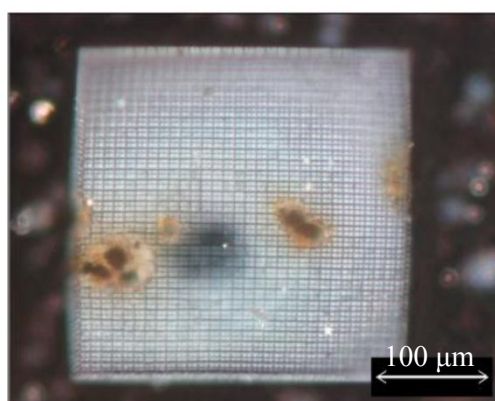
### Synthetic Hydrogels

The third chapter of this thesis was centered on the development of synthetic hydrogel systems for 2PP microfabrication. The attempts in this chapter could be further divided into three sub-parts: HEMA-, PEG-, and PVA-based hydrogels.

Considering that vinyl carbonates/carbamates-based monomers exhibit low cytotoxicity while giving PVA-based degradation products, 2-hydroxyethyl vinyl carbonate (HEVC) and 2-hydroxyethyl vinyl carbamate (HEVCa) were prepared and compared to HEA and HEMA. Photo-DSC results proved that the reactivity of these monomers are lower than HEA, but higher than HEMA. Cytotoxicity results showed that HEVCa was significantly less toxic than HEMA.



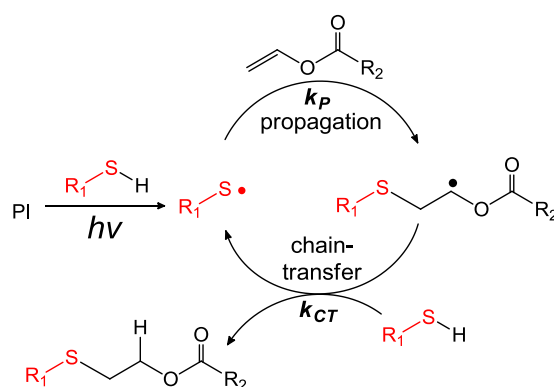
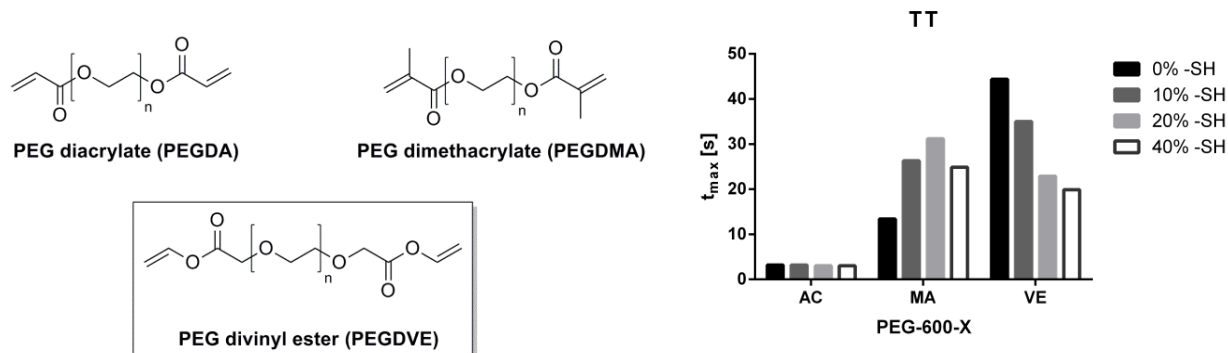
In order to increase crosslinking density, a vinyl carbonates-based crosslinker, glycerol trivinyl carbonates (GTVC), was prepared and compared to a benchmark crosslinker-TTA. Cytotoxicity test proved that GTVC was much less cytotoxic than TTA. Photo-DSC measurements showed that the photoreactivity and crosslinking efficiency of GTVC was comparable to that of TTA. Although GTVC suffers from poor water-solubility, proof-of-concept 2PP fabrication of 3D vinyl carbonates-based scaffolds was demonstrated in a non-water formulation of GTVC.



PEG-based hydrogels was explored in this thesis by introducing a novel hydrogel precursor-PEG divinyl esters (PEGDVE). PEGDVE was characterized in comparison with its (meth)acrylate analogues with a focus on cytotoxicity and photoreactivity. While homopolymerization of PEGDVE exhibited very low efficiency, Photo-DSC results demonstrated that highly efficient thiol-vinyl ester reactions could significantly increase



the reactivity of PEGDVE. The underlined mechanism could be addressed to the highly efficient chain transfer reactions. Proof-of-concept 2PP of PEGDVE was demonstrated in a non-water based formulation. In comparison, the lower toxic PEGDMA could neither be directly processed by 2PP nor optimized by using thiol-ene chemistry.



In order to increase the number of reactive groups for further improvement of photoreactivity, PVA-based hydrogels were explored in this thesis. A novel hydrogel precursor, PVA-norbornene (PVA-Norb), was prepared with tunable degree of substitution. Cytotoxicity test of these macromers confirmed that they present negligible toxicity on L929 fibroblasts.

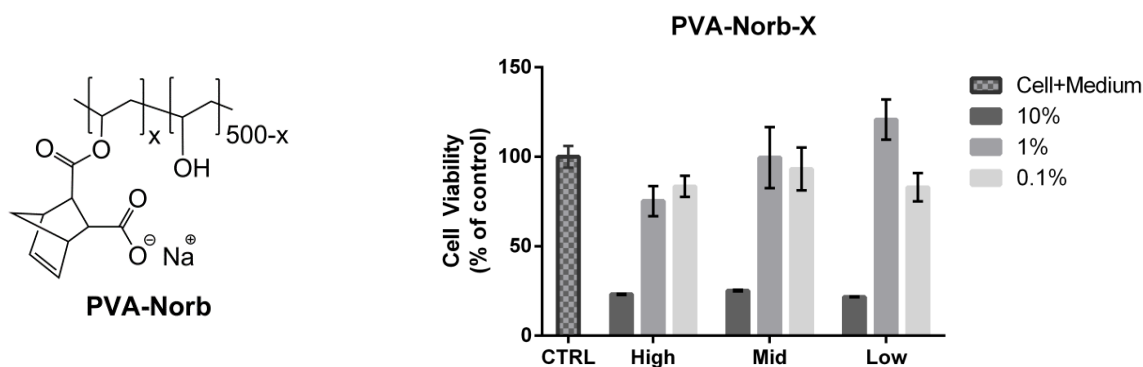
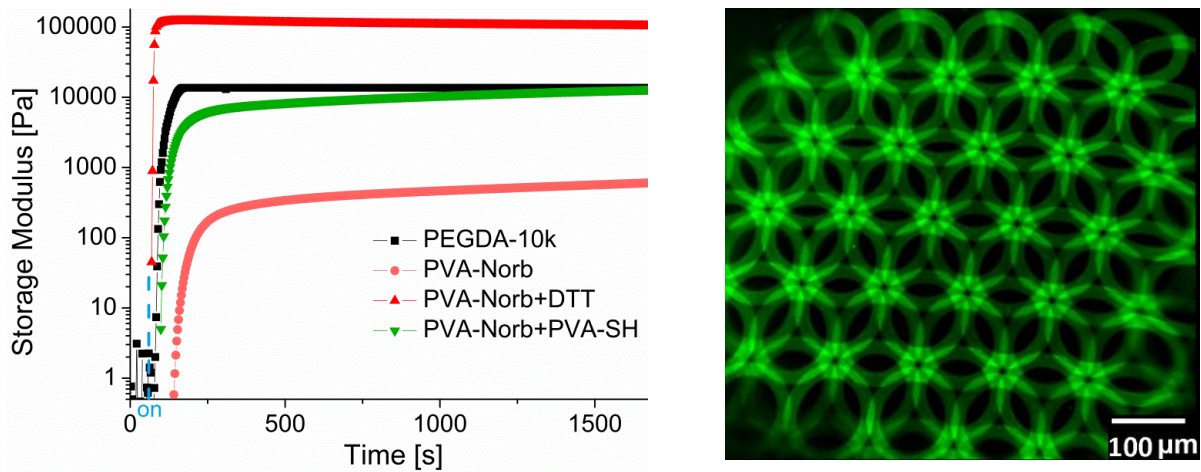


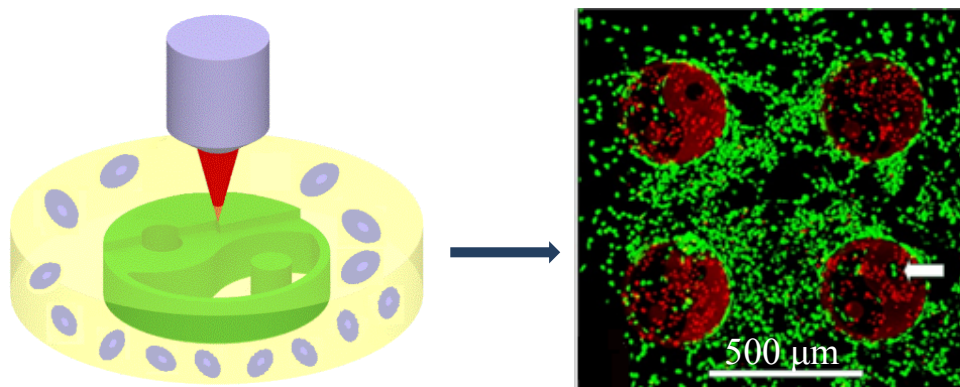
Photo-rheometry results proved that the reactivity of PVA-Norb/DTT formulations was dependent on the thiol to ene ratio. The optimal formulation ( $n_{\text{-SH}}:n_{\text{-ene}}=1:1$ ) exhibited

extraordinarily higher reactivity than a control formulation of PEGDA-10k. The physical properties of PVA-Norb/DTT gels could be precisely controlled in a physiological-relevant range from 500 Pa to 400 kPa. The robustness of thiol-norbornene chemistry provided the access to two-photon thiol-ene lithography at high writing speed (100 mm/s), providing 3D hydrogel constructs with complex architectures at  $\mu\text{m}$ -scale accuracy.

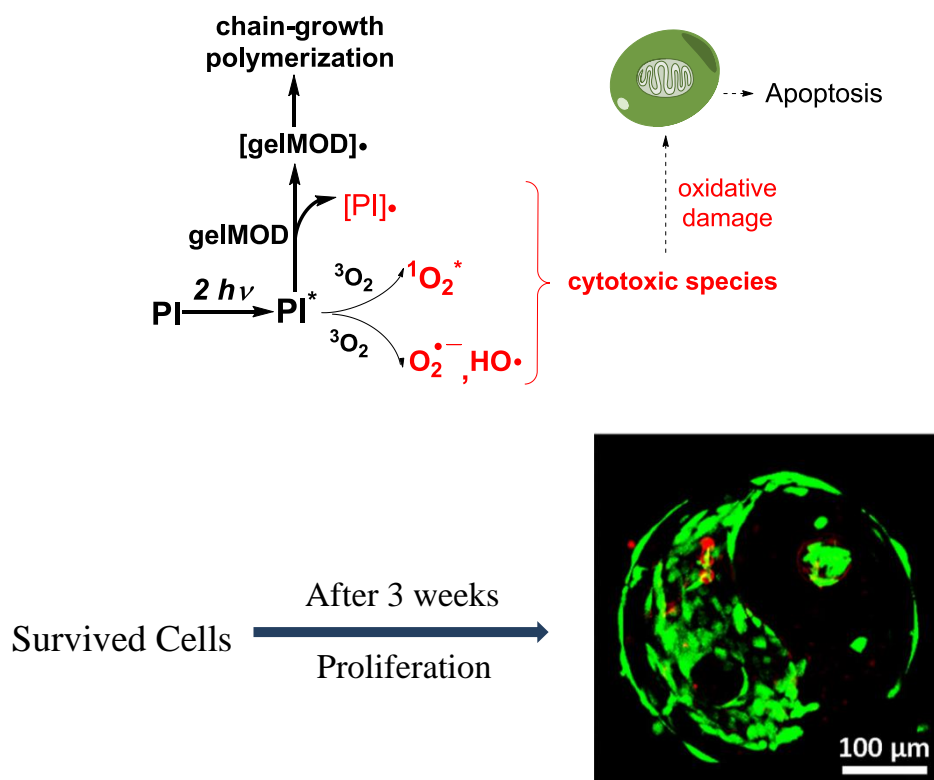


### Two-photon Cell-Encapsulation

In the last chapter of this thesis, a novel concept termed “Two-photon Cell-Encapsulation” was explored. The aim was to verify the feasibility of microencapsulation of living cells within hydrogel constructs by 2PP microfabrication. A cytocompatible hydrogel formulation consisting of gelMOD and highly efficient water-soluble initiator (P2CK) was utilized for two-photon encapsulation of MG63 cells using a Yin-Yang structure model.



After photoencapsulation, it was found that most of the cells located in the area exposed to laser irradiation were dead and only a very limited number of cells in the void area remained viable. Control experiments were performed to test the laser-induced cell death in the absence of photoinitiator. These results confirmed that laser irradiation did not cause significant cell death when photoinitiators were absent. Proposed molecular mechanisms to cell damage during 2PP encapsulation could be addressed into two aspects: photoinitiator-derived free-radicals and reactive oxygen species (ROS).



In order to test the proliferative potential of cells that have survived the encapsulation procedure, the viable cells caged within the cylindrical-voids area were allowed to proliferate for a longer period. After 3 weeks of cell culture, it was found that the voids area was filled with a large number of viable cells.

## Outlook

In summary, progressive integration of hydrogel chemistry, photopolymerization and varying AMT techniques has enabled the creation of 3D bioactive hydrogels for specific applications. It is critical to mention that tissue engineering of complex tissues or organs is still a big challenge. However, this challenge may be addressed from different aspects in the next stage of engineering evolution.

From the material point of view, water-soluble photoinitiators continue to be the key element of photolithography-based AMT. Besides water solubility, appropriate absorption wavelength (>350 nm) and high initiating efficiency will be a golden standard for the design of next generation of photoinitiators. Furthermore, cytotoxicity of photoinitiators and especially photo-induced cellular damage due to reactive oxygen species (ROS) poses a big challenge for AMT hydrogel fabrication in the presence of cells. This problem might be circumvented by incorporating ROS scavengers into the hydrogel formulation.

In addition, the selection of optimum gel precursor (natural or synthetic origin) remains the top concern of most researchers. Synthetic polymers are advantageous for most AMT techniques because of cost-efficacy and controllable property. But the use of synthetic polymers often necessitates the incorporation of bioactive motifs to foster favorable cell-material interactions. In comparison, the performance of naturally-derived polymers largely depends on the number of polymerizable groups which is further related to both the substrate chemistry and modification strategy. However, naturally-derived polymers often provide superior cytocompatibility. On the other hand, cytocompatibility of gel precursors and gel formation chemistry has gained increasing attention in recent years since whether cells can survive the hydrogel fabrication process is a critical standard. It is anticipated that the toxicity issue related to acrylate chemistry can finally be circumvented by using alternative vinyl ester chemistry since vinyl esters are much less irritant while providing PVA (FDA-approved) as the degradation products. Besides, gel formation chemistry has been extended to bio-orthogonal reactions where light-triggered click reactions hold the most promise. In particular, radical-mediated thiol-ene reactions

---

represent a number of advantages for potential integration with AMT hydrogel platforms, including spatiotemporal control, robust kinetics and mild reaction conditions.

It is well established that varying photolithography-based AMT techniques allow the fabrication of hydrogel scaffolds with appropriate macrostructure (porosity) and micro-scale patterns of biochemical, mechanical and gradient properties. But it is important to note that each of the reviewed AMT techniques may have pros and cons. For instance, DLP appears to be a promising technique for layer-by-layer assembly of a large 3D hydrogel construct whereas currently it is unable to achieve feature sizes below 30  $\mu\text{m}$ . In contrast, 2PP seems to be the most promising technique to engineer hydrogels with (sub) cellular features. However, a major challenge related to 2PP is the long processing time required to fabricate a hydrogel construct with clinically-relevant sizes. The processing time can be shortened either by increasing the setup scanning speed or by improving the robustness of gel formation chemistry.

In the future, the fusion of rationally-designed hydrogel precursors, robust gel formation chemistry and optimized AMT platforms would help researchers to better understand cell-cell and cell-matrix interactions. The knowledge can be exploited for engineering complex tissues and designing therapeutic strategies for regenerative medicine.

## Abbreviations

2D.....	two-dimensional
2PA.....	two-photon absorption
2PI.....	two-photon photoinitiator
2PP.....	two-photon-induced polymerization
3D.....	three-dimensional
3PA.....	three-photon absorption
AC.....	acrylate
AFM.....	atomic force microscopy
AMT.....	additive manufacturing technology
ATR.....	attenuated total reflexion
BSA.....	bovine serum albumin
b.p.....	boiling point
CAD.....	computer aided design
CAL-B.....	lipase acrylic resin from <i>Candida antarctica</i>
DBC.....	double bond conversion
$\delta$ .....	chemical shift (NMR)
DCM.....	dichloromethane
DLP.....	digital light processing
DMEM.....	Dulbecco's Modification of Eagle's Medium
DMSO.....	dimethylsulfoxide
DS.....	degree of substitution
DTT.....	dithiothretol
DVA.....	divinyl adipate
ECM.....	extracellular matrix
EDCI.....	1-Ethyl-3-(3-dimethylaminopropyl)carbodiimide hydrochloride
EE.....	ethyl acetate
FDA.....	United States Food and Drug Administration
G'.....	elastic modulus
G''.....	loss modulus
G2CK.....	sodium 2,2'-((((1E,1'E)-(5-methyl-2-oxocyclohexane-1,3-diylidene) bis (methanylylidene)) bis(4,1-phenylene))bis (methylazanediy))diacetate

---

GC	gas chromatography
GelMOD	gelatin methacrylamide
GH	gelatin hydrolysate
GM	Göppert-Mayer (SI unit) $1 \text{ GM}^{\circ} = 10^{-50} \text{ cm}^4 \text{ s photon}^{-1} \text{ molecule}$
GMA	glycidyl methacrylate
HA	hyaluronic acid
Hase	hyaluronidase
HEA	2-hydroxyethyl acrylate
HEMA	2-hydroxyethyl methacrylate
IR	infrared
Irg(acure) 2959	(2-hydroxyethoxy)-2-methylpropiophenone
Irg(acure) 819	Bis(2,4,6-trimethyl benzoyl)phenyl phosphine oxide
LAP	Lithium phenyl-2,4,6-trimethylbenzoylphosphinate
LC <sub>50</sub>	Lethal Concentration-50%: concentration required to induce half death
LSM	laser scanning microscopy
M	$\text{mol L}^{-1}$
M <sub>n</sub>	number average molecular weight
m.p.	melting point
MA	methacrylate
MAA	methacrylic acid
MALDI-TOF	Matrix-Assisted Laser Desorption/Ionization Time of Flight
MS	mass spectroscopy
MTT	3-(4,5-dimethylthiazol-2-yl)-2,5-diphenyltetrazolium bromide
MW	molecular weight
mW	milliwatt
NHS	N-Hydroxysuccinimide
NMR	nuclear magnetic resonance
o-NB	ortho-nitrobenzylether
P2CK	sodium 3,3'-((((1E,1'E)-(2-oxocyclopentane-1,3-diyldiene) bis (methanylylidene))bis(4,1-phenylene))bis(methylazanediy)) dipropanoate
PBS	phosphate buffered saline
PCL	poly( $\epsilon$ -caprolactone)
PDI	polydispersity index

---

PE	petroleum ether
PEG	poly(ethylene glycol)
PI	photoinitiator
PLA	poly(lactic acid)
PVA	poly(vinyl alcohol)
Photo-DSC	Photo-Differential Scanning Calorimetry
R1	4,4'-((2,5-dimethoxy-1,4-phenylene)di-(1E)-2,1-ethenediyl) bis[N,N-dibutylbenzenamine]
R <sub>f</sub>	retention factor
R <sub>p</sub>	rate of polymerization
RGD	arginine-glycine-asparaginic acid
ROS	reactive oxygen species
SD	standard deviation
SEM	scanning electron microscope
TBA	tetrabutylammonium
TCEP	tris(2-carboxyethyl)phosphine
TEA	triethylamine
TLC	thin layer chromatography
t <sub>max</sub>	time to reach the maximum heat of polymerization
TT	pentaerythritol tetrakis (3-mercaptopropionate)
TTA	trimethylolpropane triacrylate
UDMA	2-methyl-acrylic acid 2-{2,2,4-trimethyl-6-[2-(2-methyl-acryloyloxy) -ethoxycarbonylamino]-ethylcarbamoyloxy}-ethyl ester
UV	ultraviolet
UV/Vis	ultraviolet/visible
VE	vinyl ester
VC	vinyl carbonate
VCa	vinyl carbamate
WSPI	1,4-bis(4'-(N,N-bis(6''-(N,N,N-trimethylammonium)hexyl)amino)-styryl)- 2,5-dimethoxybenzene tetraiodide



## Materials and Methods

### Materials

**Reagents and solvents** were all used as received unless otherwise mentioned. Purification was performed according to <<Purification of Laboratory Chemicals-4<sup>th</sup> Edition>> by Perrin *et al.*.

Commercial name and purchase information related to the major chemicals in this study are listed below:

Commerical Names	Product No.
Gelatin hydrolysate enzymatic	Sigma G0262
Bovine serum albumin (Fraction V)	Sigma 05470
D,L-dithiolthretol	Sigma 43819
Tris(2-carboxyethyl)phosphine hydrochloride (0.5 M sol.)	Sigma 646547
5-(3-Carboxy-4-nitrophenyl)disulfanyl-2-nitrobenzoic acid (DTNB)	Sigma D8130
Hyaluronic acid sodium salt from <i>Streptococcus equi</i> (1.5-1.8 MDa)	Sigma 53747
Hyaluronidase Type I-S	Sigma H3506
Lipase resin from <i>Candida antarctica</i>	Sigma L4777
Divinyl adipate	TCI A1188
Poly(vinyl alcohol) (22 kDa)	Merck
<i>Cis-endo-5-Norbornene-2,3-dicarboxylic anhydride</i>	Sigma 247634

Low MW hyaluronic acid (Na<sup>+</sup>, miniHA, M<sub>n</sub> ≈ 7 kDa) was kindly donated by Bloomage Freda Biopharm Company (P.R. China). Irgacure 2959 (I2959) was donated by BASF (Germany) and used as photoinitiator for UV photopolymerization. Two-photon initiators were prepared in the IAS by Niklas Pucher (R1, WSPI) and Zhiquan Li (P2CK, G2CK).

Dulbecco's modified eagle medium (DMEM) was purchased from VWR Austria. L929 fibroblast cells were purchased from Sigma-Aldrich while the MG63 cells were donated by LBI-Trauma (Vienna).

To prepare 1 L of **PBS buffer** (1x) use:

	g	mL
KH <sub>2</sub> PO <sub>4</sub>	0.24	-
Na <sub>2</sub> HPO <sub>4</sub>	1.44	-
NaCl	8.00	-
KCl	0.20	-
dist. H <sub>2</sub> O	1L	

For 1 L of **M9 Buffer** (1x) use:

	g	mL
KH <sub>2</sub> PO <sub>4</sub>	3.00	-
Na <sub>2</sub> HPO <sub>4</sub>	6.00	-
NaCl	5.00	-
MgSO <sub>4</sub> (1M)	-	1.0
dist. H <sub>2</sub> O		1L

The aliquoted solutions were finally autoclaved for 20 min.

For **thin layer chromatography** (TLC) aluminum foils, coated with silicagel 60 F254 (Merck) were used.

For **column and flash column chromatography**, silicagel 60, from the distributor VWR Austria was applied.

Preparation and analysis of photosensitive compounds and formulations was conducted in a **yellow light lab**. This laboratory was placed in a window-less room to avoid admittance of day-light.

## Methods

**Photo-differential scanning calorimetry (Photo-DSC)** experiments were done on Netzsch DSC 204 F1 Phoenix using filtered UV-light (280 – 500 nm) from a double light guide (EXFO Omnicure 2001) attached to the top of the DSC unit. The light intensity at the tip of the light guide surface was determined to be  $3000 \text{ mW cm}^{-2}$ . All experiments were performed under nitrogen atmosphere ( $20 \text{ mL min}^{-1}$ ). The principle of Photo-DSC (Figure 168) is based on measurement of the different heat flux between a sample pan filled with a monomer/initiator formulation and a reference pan. Due to heat generation in UV-photopolymerization, the sample pan warms by far more than the reference pan.

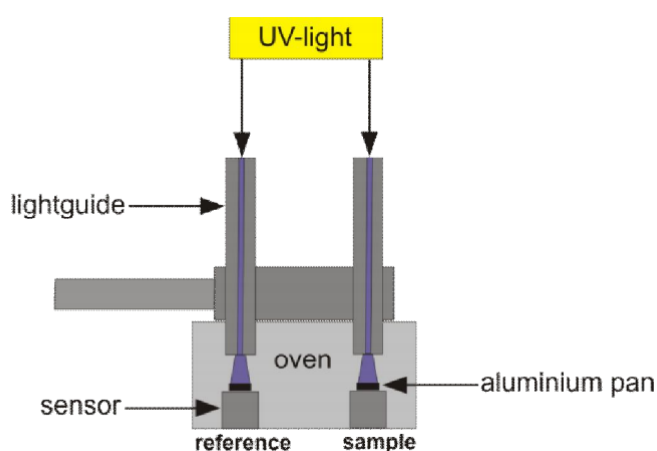


**Figure 168.** Schematic showing the assembly-principle of Photo-DSC

A typical Photo-DSC measurement provides a plotted curve as depicted in Figure 169. By evaluation of the curve, one can define the time to reach the maximum polymerization heat flux ( $t_{\text{max}}$ ), the double bond conversion (**DBC**) and the rate of polymerization ( $R_p$ ).

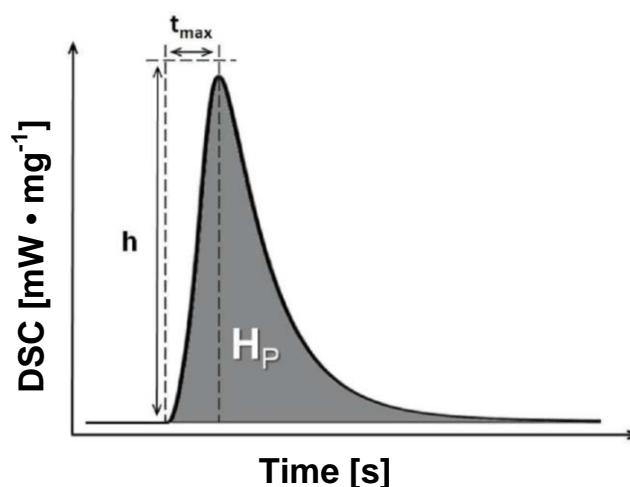


**Figure 169.** Schematic of a Photo-DSC plot

The value of  $t_{\max}$  can be easily determined using computer software. By comparing the value of the area under the peak ( $\Delta H_p$ ) and the theoretical heat of polymerization of the monomer ( $\Delta H_{0,p}$ ) which is known from literature, the double bond conversion (DBC) can be calculated with the help of equation (3) and (4):

$$DBC = \frac{\Delta H_p}{\Delta H_{0,p}} \quad (3)$$

$\Delta H_p$ .....	heat of polymerization (area)	$[J \cdot g^{-1}]$
$\Delta H_{0,p}$ .....	theoretical heat of polymerization of the formulation	$[J \cdot mol^{-1}]$

$$\Delta H_{0,p} = \Delta H_{0,DB} \sum \frac{w_i}{M_i} x_i \quad (4)$$

$\Delta H_{0,DB}$ .....	theoretical heat of polymerization of the double bond	$[J \cdot g^{-1}]$
w .....	weight fraction of the monomer	[ ]
M .....	molecular weight of the monomer	$[g \cdot mol^{-1}]$
x .....	number of double bonds	[ ]

Based on the height of the peak (h) at  $t_{\max}$ , the rate of polymerization ( $R_p$ ) can be calculated according to equation (5):

$$R_p = \frac{h \times \rho}{\Delta H_{0,p}} \quad (5)$$

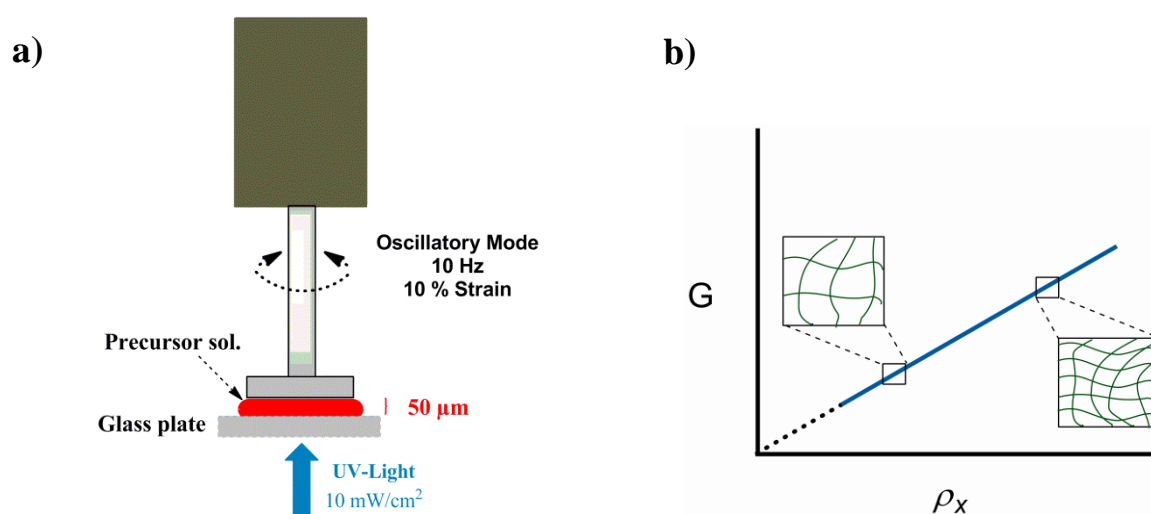
$R_p$ .....	rate of polymerization	$[mol \cdot L^{-1} \cdot s^{-1}]$
h .....	specific heat flow at maximum	$[mW \cdot mg^{-1}]$
$\rho$ .....	density of the monomer	$[g \cdot L^{-1}]$

Depending on the type of vinyl group, the theoretical heat of polymerization varies one from another. The values of the different vinyl groups are listed in Table 25.

**Table 25.** Theoretical heat of polymerization (double bond)

monomer	$\Delta H_{0,P}$ [kJ·mol <sup>-1</sup> ]
vinyl ester	87.8 <sup>176</sup>
vinyl carbonate	89.5 <sup>176</sup>
vinyl carbamate	89.8 <sup>176</sup>
acrylate	80.0 <sup>231</sup>
methacrylate	60.0 <sup>231</sup>

**Photo-rheometry** were performed on a modular photo-rheometer (Anton Paar MCR-301) using filtered UV-light (320 – 500 nm) from a light guide (Omniculture S2000) attached to the bottom of the glass plate (Figure 170a). Specifically, plate-to-plate oscillatory photo-rheometry was applied for real-time monitoring of the curing kinetics of hydrogel formulations during photopolymerization. Light intensity at the plate surface was  $\sim 10 \text{ mW}\cdot\text{cm}^{-2}$  as determined with an Ocean Optics USB 2000+ spectrometer. This method monitors the moduli change during the liquid-to-solid transition of photocurable hydrogel formulations. For hydrogels, the principle (Figure 170b) is that the measured bulk modulus correlates with degree of polymerization and the ultimate modulus reflects the gel crosslinking density ( $\rho_x$ ). Both elastic modulus ( $G'$ ) and loss modulus ( $G''$ ) of the samples could be monitored as a function of irradiation time. Gel point was determined in the vicinity of the  $G'$  and  $G''$  crossover.

**Figure 170.** Schematics showing the photo-rheometer setup (a) and the method principle (b)

Typically, after a 60 s blank period, filtered UV light was triggered to irradiate the samples. The measurements were made in oscillatory mode, at 25 °C, 10% strain, 10 Hz and 50  $\mu\text{m}$  gap thickness. The data points were collected in every 3 s. Strain and frequency sweeps were always performed before and after polymerization to verify the linear response regime.

For hydrogel degradation studies, the same rheometer was applied in combination with an adapted procedure. Specifically, precursor solutions containing macromer and photoinitiator were firstly prepared and stored on ice-bath. Appropriate amounts of enzyme were added into these solutions to give prescribed concentrations. Next, the mixed macromer/enzyme solutions were transferred to the thermo-controlled glass plate which was set at 5 °C. Then the rheometer system adapted the solution to a 50  $\mu\text{m}$  thickness. The solutions were photopolymerized *in situ* for 10 min at 5 °C. Finally, the plate temperature was increased to 37 °C to activate the enzyme and initiate the enzymatic degradation. The data points were collected in every 100 s.

**Fourier transformed-infrared (FT-IR) spectra** were measured with an ATR-arrangement using a Biorad FTS-135 IR-device.

General  $^1\text{H-NMR}$  (200 MHz, 25 °C) were measured with a BRUKER AC-E-200 FT-NMR- spectrometer, while specific spectra (400 MHz) were measured at elevated temperature (40 °C) with a BRUKER AC-E-400 FT-NMR-spectrometer. The chemical shift is displayed in ppm (s = sigulett, d = duplet, t = triplett, q = quartett, quin = quintet, m = multipllett). Deutero-chloroform ( $\text{CDCl}_3$ ) and Deutero-water ( $\text{D}_2\text{O}$ ) from the company Eurisotop were used as solvents. The grade of deuteration was at least 99.5%.

**UV-Vis spectroscopy** was measured using a Perkin Elmer Lamda 35 spectrometer and disposable PMMA-made cuvettes (VWR K1960). The parameters are listed below:

Layer thickness: 1 cm

Wavelength Range: 600 – 300 nm

Scan Speed: 480 nm  $\text{s}^{-1}$

Lamp Change: 350 nm

**Melting points** were determined with a “Zeiss Axioskop” microscope equipped with a heating device from Leitz. Melting points are not corrected.

**HPLC** measurements were carried out on a reversed-phase HP-1100 HPLC system with a DAD-detector. All separations were carried out on a Waters Xterra MS C<sub>18</sub> column, particle size 5 μm, 150 x 3.9 mm<sup>2</sup> ID. A linear gradient with flow 0.8 mL/min was formed from 97% water to 97% acetonitrile (MeCN) over a period of 30 min.

**GC runs** were performed on a HP5890 Series II Gas Chromatograph with flame ionization detector with the following temperature method (injection volume: 1 μL): 1 min at 60°C, 15°C/min until 180°C.

**GC-MS runs** were performed on a Thermo Scientific GC-MS DSQ II using a BGB 5 column (L = 30 m, d = 0.32 mm, 1.0 μm film, achiral) with the following temperature method (injection volume: 1 μL): 2 min at 80°C, 20°C/min until 280°C, 2 min at 280°C. MS spectra were recorded using EI ionization (70 eV) and a quadrupole analyzer.

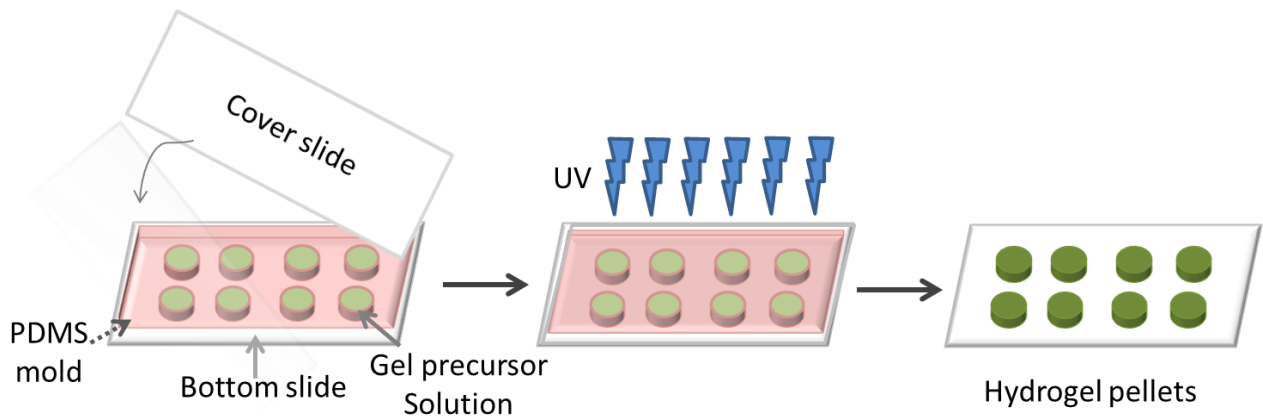
**GPC measurements** were carried out on a Viscotek GPCmax VE2001 equipped with a Waters Ultrahydrogel<sup>TM</sup> 250 and 1000 column equipped with a Viscotek VE3580 RI detector. Samples were eluted with 0.05 M sodium sulfate in 80 % water, 20 % acetonitrile. Polyethyleneglycol standards were used for calibration.

**MALDI-TOF** mass spectrometry was performed on a Micromass TofSpec 2E Time-of-Flight Mass Spectrometer by Prof. Robert Saf at TU Graz. The instrument is equipped with a nitrogen laser (337 nm wavelength, operated at a frequency of 5 Hz), and a time lag focusing unit. Ions were generated by irradiation just above the threshold laser power. Positive ion spectra were recorded in reflectron mode applying an accelerating voltage of 20 kV and externally calibrated with a suitable mixture of poly(ethyleneglycol)s (PEG). The spectra of 100-150 shots were averaged. Analysis of data was done with MassLynx-Software V4.1 (Micromass/Waters, Manchester, UK). Samples were dissolved in 1% TFA (c = 0.1 and 0.01 mg/mL, respectively), 2, 5-dihydroxybenzoic acid (2, 5-DHB) and α-cyano-4-hydroxycinnamic acid (CHCA) were used as matrix (c = 10 mg/mL in acetonitrile: 1% TFA = 70:30 (v/v)). Generally, solutions were mixed in the cap of a

microtube in the ratio of 1  $\mu\text{L}$ : 10  $\mu\text{L}$ . 0.5  $\mu\text{L}$  of the resulting mixture were spotted onto the target and allowed to air dry.

**UV-curing** was performed with a UV lamp from the company UV-Technik Meyer with a special dysprosium UV lamp (UVH 2022 DY-0, 380V, 2.2kW, irradiation power 1kW, UV-A: 59  $\text{mW}/\text{cm}^2$ , UV-B: 25  $\text{mW}/\text{cm}^2$ , UV-C: 3  $\text{mW}/\text{cm}^2$ , Vis: 45  $\text{mW}/\text{cm}^2$ )

**Hydrogel pellets** were prepared using a customized protocol as described in the graph below. The pellets were made in a multi-well PDMS chamber with a thickness of 1.5 mm (well diameter: 6 mm). Two hundred microliters of macromer solution was pipetted between two glass coverslips separated by the PDMS mold and then exposed to UV light ( $\sim 20 \text{ mW}/\text{cm}^2$ ) for 900 s (450 s each side). To avoid heat-induced water loss, the sandwich sample was placed on top of an ice-bath. After a 5 min development in distilled water, the pellets were detached from the slides.



**Mass swelling ratio** of hydrogels was measured using a generic protocol.<sup>232</sup> hydrogel pellets were prepared as aforementioned and allowed to swell in PBS for 24 h at room temperature. The wet pellets were weighed to determine the equilibrium swollen mass ( $M_s$ ) and then lyophilized to obtain the dry weight ( $M_d$ ). The equilibrium mass swelling ratio ( $Q_m$ ) was calculated as  $M_s/M_d$ .

**AFM Nanoindentation** experiments were done on a atomic force microscopy (AFM-NanoWizard 3, JPK Instruments, Berlin) by Dr. Birgit Plochbirger at the Biophysics group of TU Vienna. Prior to test, gel samples were UV-polymerized as aforementioned, except on top of methacrylated cover slips and then soaked in Milli-Q  $\text{H}_2\text{O}$  for 24 h.



These hydrated samples were probed using a pyramidal-tipped cantilever (MSNL, Veeco Instruments, Plainview, NY). Prior to each AFM measurement, the spring constant of each cantilever was measured according to a general method,<sup>228</sup> with average values of  $\sim 10$  pN/nm. The force-indentation curves of each sample were recorded with a tip velocity of  $2 \mu\text{m/s}$  and a trigger force of  $\sim 300$  pN. Young's modulus values were calculated from the force curves according to a Hertz model (JPK software). Poisson's ratio of the gel samples was assumed as 0.5.

An example of a force-indentation curve recorded from a hydrogel sample is shown in Figure 171. For indentations, at the beginning the cantilever was not in contact with the hydrogel. As the cantilever pyramidal tip contacted the hydrogel, the force recorded by the cantilever started to increase, exhibiting a non-linear relationship with the indentation, caused by an increase of the contact area as the triangular/pyramidal tip indented the sample. By fitting the part of the force-indentation curve where the tip was in contact with the hydrogel with the triangular indenter model the Young's modulus ( $E$ ) as a function of position on the gel surface was estimated.

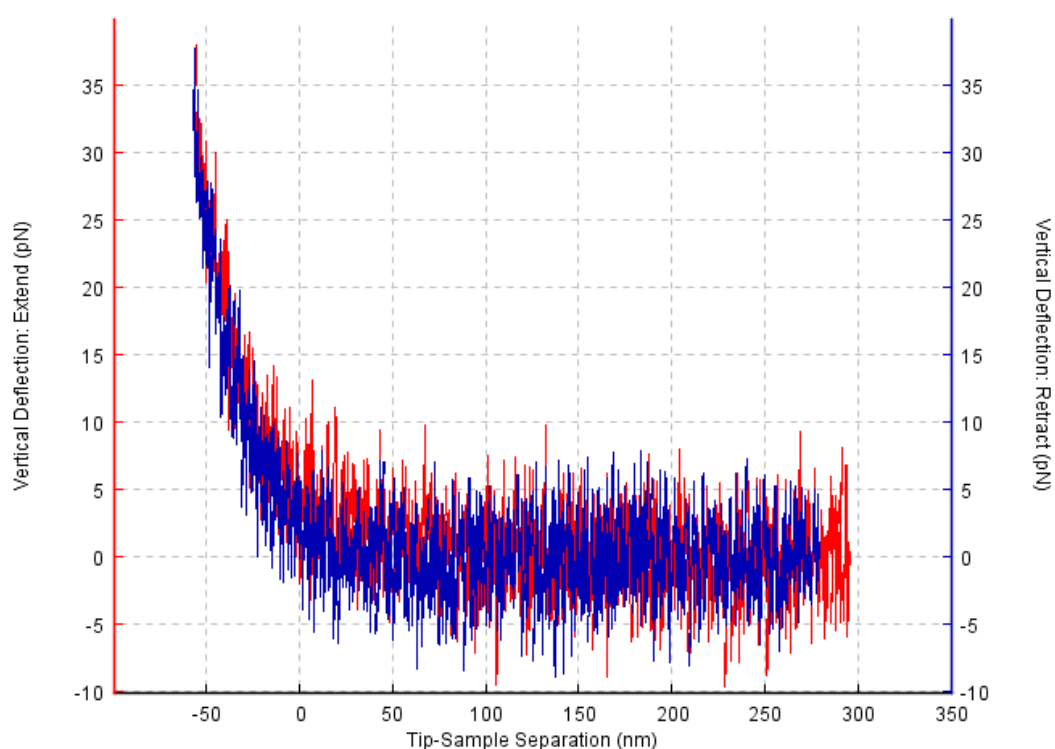
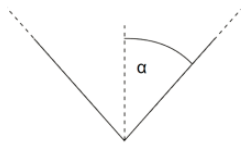


**Figure 171.** An exemplary force curve of a hydrogel (spring constant of cantilever: 10 pN/nm; tip velocity:  $1 \mu\text{m/s}$ ; set trigger force: 35 pN)

For **AFM data analysis**, each indentation generates a force-indentation ( $F$ - $\delta$ ) curve to be saved and analyzed with JPK software. First the calibration of the vertical-deflection was done using JPK software. For that the sensitivity and the tips spring constant were taken to calibrate the vertical deflection. The baseline was subtracted and data not showing a flat curve during the tip approach was discarded, since this would suggest an unwanted surface tip interaction. Next the tip-sample distance was calculated using tip bending and height signal. The curves were corrected for cantilever bending. In general, according to the Hertz model of a sphere indenting an elastic half-space, the Young's modulus  $E$  is directly proportional to the force  $F$  and inversely proportional to the  $3/2$  power of the deformation  $\delta$ :

$$F = \frac{E}{1-\nu^2} \frac{4\sqrt{R_C}}{3} \delta^{3/2}$$

Here, the AFM tip is approximated as a cone indenter with a certain contact circle on a cantilever deflected by a force  $F$ . All force data points are incremented by a constant so they are all positive, subsequently raised to the  $1/2$  power, and then plotted in a  $F^{1/2}$ - $\delta$  curve. For a conical indenter, the Young's modulus  $E$  is directly proportional to the force  $F$  and inversely proportional to the  $1/2$  power of the deformation  $\delta$ :



$$F = \frac{E}{1-\nu^2} \frac{2\tan\alpha}{\pi} \delta^2 \quad a = \frac{2\tan\alpha}{\pi} \delta$$

where  $F$  is the load distributed over the contact area,  $R_C$  is the radius of tip curvature,  $E$  is the Young's Modulus,  $\nu$  is the Poisson ratio of the surface,  $\delta$  is the deformation of the sample (indentation – tip sample separation), and  $E$  is the Young's modulus of the sample.

In general, the cone angles from the manufactures are defined differently for silicon and for silicon nitride tips. In the data processing software of JPK, there is the possibility to choose which angel is defined. The geometry is selected in the data processing software using the tip shape selection. For all the different model, the data curve is fitted using a least squares fit with the Levenberg-Marquardt algorithm. The contact point, baseline and Young's modulus values are all fitted simultaneously.

**Two-photon microfabrication** was performed on two structuring devices by Jan Torgersen and Peter Gruber (IMST). Specifically, a micro-3D structuring device (M3DL) was used for 2PP processing in section 3.1 and 3.2. Alternatively, a novel processing system (Mipro) was used in Chapter 1, 2, and 4 as well as in section 3.3.

### Two-photon processing System-M3DL<sup>206</sup>

The micro-3D structuring device-M3DL (Laser Zentrum Hannover) was equipped with a Ti:sapphire laser (High Q) system (repetition rate: 73 MHz; output wavelength: 810 nm; laser power: 225 mW; pulse duration: 100 fs). After passing through an acusto-optic modulator (AOM), the laser beams were diffracted, leaving the first-order waves for 2PP. The input laser intensity could be adjusted using a  $\lambda/2$  waveplate in combination with a polarization-dependent beam-splitter. The laser beam was focused into the samples through microscope objectives with different magnifications (20x NA = 0.4, 100x NA = 1.35, 63x NA = 0.75, Carl Zeiss). The obtained laser intensity can be measured with a power meter after the objective. Accurate movement of the selected objective in X- and Y-dimensions was realized by two high-precision air-bearing axes (Aerotech). Another air-bearing axis fixed with the sample was responsible for the movement in Z-dimension.

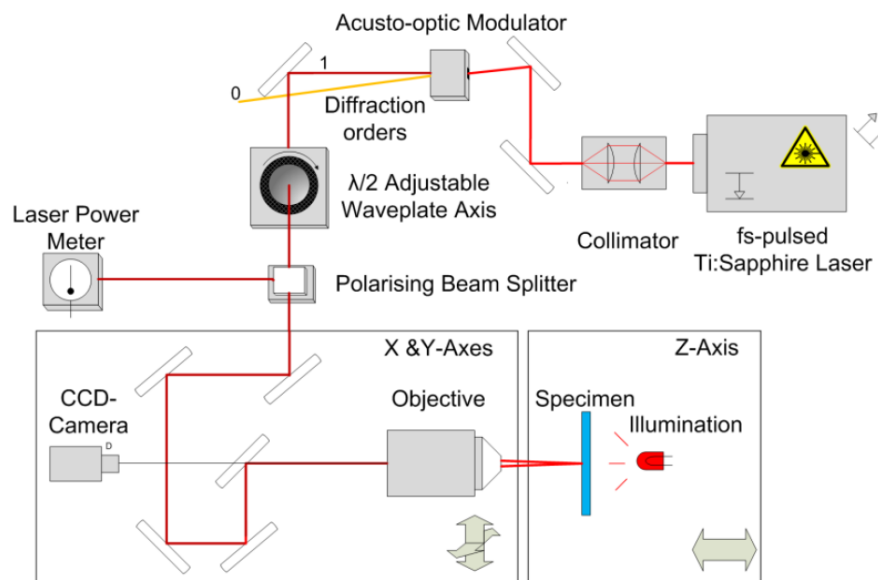


**Figure 172.** Schematic showing the setup of M3DL<sup>206</sup>

The mirror system guaranteed that movements in X- and Y- was always parallel to the direction of the laser beam, allowing that the guidance of the beam was stable throughout the process. For online observation, a camera was positioned along the laser beam and

allowed to focus on the excitation spot through the same objective for focusing the laser. Mounting the axes on a hard-stone frame allowed appropriate damping of noises and vibrations. The whole setup was placed on an optical table which was equipped with an air-friction damping to further minimize vibrations. To control the processing, all of the axes and the laser power meter were plugged into an electronic device, which could process the commands given by the control computer. A red-LED lamp was applied to illuminate the sample to avoid premature polymerization.

### Two-photon processing System-Mipro<sup>206</sup>

In order to increase writing speed, a novel structuring system Mipro (Figure 173) was designed by Jan Torgersen and Peter Gruber(IMST).

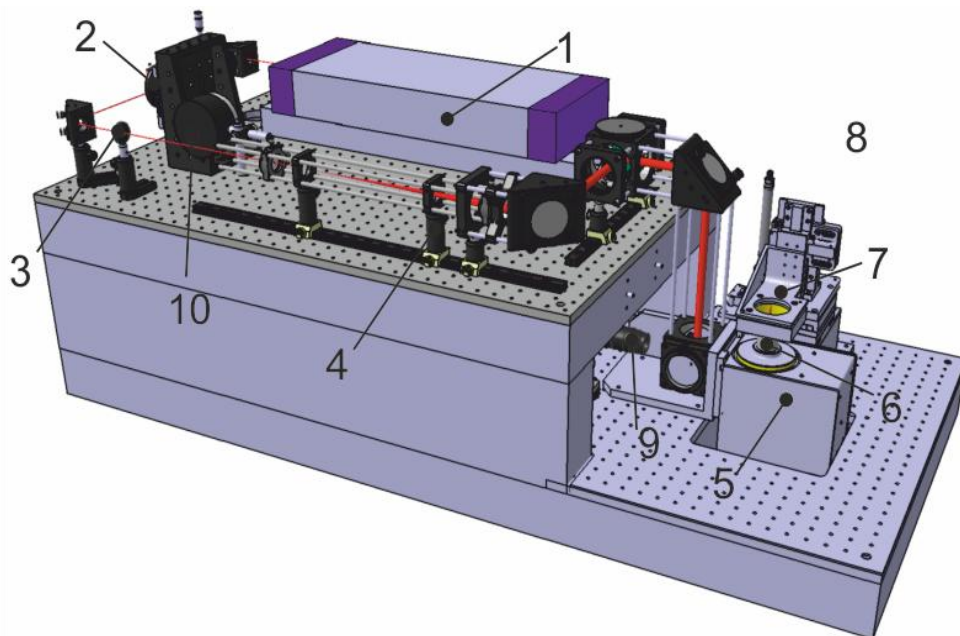


**Figure 173.** CAD illustration of the Mipro setup: (1) Laser, (2) AOM, (3) Pinhole, (4) Beam expander, (5) Galvanoscanner, (6) Microscope objective, (7) Specimen clamp, (8) X/Y/Z translation axes, (9) CCD camera, and (10) Laser power meter<sup>206</sup>

In this new setup, the laser beam (1) passed through the AOM (2) leaving the first-order of diffraction for two-photon structuring. The beam could be switched and controlled in pre-defined intensity by applying waves of different amplitudes inside the crystal. The use of a pinhole (3) prevented other beam orders from propagation in the setup. After passing through the pinhole, the diameter of the beam was expanded six times to its initial size diameter (1.8 mm). The galvanoscanner (5) deflected the beam before focusing it with a microscope objective (6). To create 3D structures, the rotating mirrors

of the galcanoscanner traced the focal point inside the formulation. A clamp (7) carrying with the formulation container was mounted to a linear XYZ axes system. The axes from the old setup (8) were adapted and used to position the specimen clamp for creating the third order of dimension (Z-) and to increase the limited field of view of the objective. For online observation, a CCD camera (9) was integrated. The whole setup was mounted on the old setup's hard stone frame for damping considerations. The laser power was measured using a power meter behind the AOM (10).

Compared to the M3DL setup, the new setup used fewer mirrors and lenses, reduced distortions of the pulse width, and ensured high beam quality when focused into the photosensitive formulations. Further information on the setup design could be found in the dissertation of Jan Torgersen.

### 2PP Structuring

The samples for 2PP structuring were prepared by casting a liquid formulation between two microscope slides (1, 3) that were separated by Tixo strips (2), as shown in Figure 174.

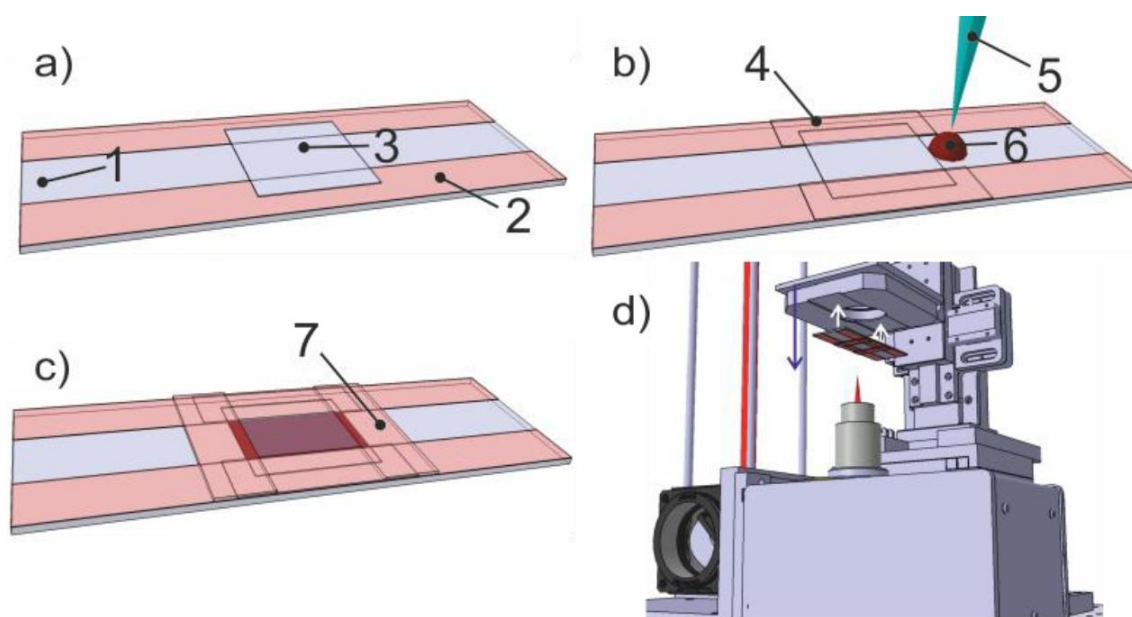


**Figure 174.** Schematics of sample preparation prior to 2PP structuring: **a)** placement of strip spacers and coverslip on a glass slide, **b)** fixation of the coverslip and pipetting formulation liquid to the area adjacent to the building volume, **c)** sealing of the building volume, **d)** specimen loading onto the clamp on the axes system

A general procedure to prepare the specimen for 2PP structuring is described below:

- First, a coverslip **(3)** ( $18 \times 18 \times 0.17 \text{ mm}^3$ ) was placed on top of a custom-made glass slide **(1)** containing two pieces of adhesive Tixo-strips **(2)** in parallel, leaving a thickness of  $\sim 120 \text{ }\mu\text{m}$ . To better fix the structures on the specimen, the bottom glass slide **(1)** was pre-functionalized with methacrylate groups via sol-gel chemistry according to literature.<sup>229</sup>
- Second, another two pieces of adhesive Tixo-strips **(4)** were attached on the coverslip for fixation. The building area is roughly  $18 \times 10 \times 0.12 \text{ mm}^3$  and the corresponding required amount of formulation was approximately  $20 \text{ }\mu\text{L}$ .
- Third,  $30 \text{ }\mu\text{l}$  of liquid formulation was pipetted to the glass slide adjacent to the building area via a Eppendorf-Pipette tip **(5)**. The liquid drop **(6)** was allowed to fill in the void area between the glass slide and the coverslip. When the building volume was completely occupied, the excessive liquid was removed.
- Fourth, two additional pieces of Tixo-strips **(7)** were attached on either side of the coverslip in order to seal the formulation in the building volume. This step was particularly important for hydrogel formulations due to water loss during 2PP processing.
- Finally, the prepared specimen was fixed by the designated clamp on the XYZ axes system.

The focused laser was allowed to scan the sample inside the building volume according to the CAD model, finally leaving an embedded 3D structure. After 2PP processing, the unpolymerized material was removed by developing the specimen in appropriate solvents: ethanol for non-water formulations and PBS for hydrogels.

Feature size, structural integrity and geometric fidelity of the resultant structures were analyzed by different microscopes: SEM (JEOL JSM-5600 or FEI Philips XL 30) for non-water systems and laser scanning microscopy (LSM 700, Carl-Zeiss) for hydrogels.

**Cytotoxicity** tests and **cell culture** were done through collaboration with three research groups:

- 1) **MTT assay**<sup>\*</sup> and **cell adhesion** of gelatin-based hydrogels using MG63 cells were performed by Mr. Severin Mühleder at the Ludwig Boltzmann Institute of Traumatology.
- 2) **Presto-Blue assay**<sup>\*\*</sup> of HA- and PVA-based hydrogels using L929 cells were done by Ms. Marica Markovic (IMST) at TU Vienna.
- 3) **MTT assay**<sup>\*\*\*</sup> of vinyl carbonate/carbamate-based monomers and thiols using osteoblasts were done by Mag. Barbara Kapeller at the Medical University of Vienna. Further experimental details are given in respective sections.

### **MTT Assay**<sup>\*</sup>

For gelatin-based hydrogels, cytotoxicities of macromer solutions and/or hydrogel extracts were evaluated via MTT assay. The human osteosarcoma cell line MG63 (LBI Trauma) was cultured in Dulbecco's Modified Eagles Medium (DMEM) containing 10% fetal bovine serum (FBS). Macromer solutions with three concentrations (10%, 1% and 0.1%) were prepared in DMEM. For hydrogel extracts, the pellets were incubated with appropriate amount of DMEM for 12 h so that the macromer concentration was 1%. MG63 cells were then seeded in a 96-well plate at a density of  $1 \times 10^4$  cells per well in 200  $\mu\text{L}$  of DMEM containing 10% FBS. After 24 h incubation (37 °C, 5%  $\text{CO}_2$ ), 200  $\mu\text{L}$  of the respective macromer or extract solutions were added to the cells ( $n > 3$ ). After 24 h incubation, cells were washed twice with sterile PBS before the addition of 120  $\mu\text{L}$  of MTT reagents (5 mg/mL in PBS). Then the cells were incubated at 37 °C for 4 h. The formazan crystal was dissolved in DMSO and the absorbance of the medium was measured at 540 nm using a microplate reader.

### **Cell Adhesion**

For cell adhesion studies, hydrogel pellets were prepared in a similar approach as mentioned before. Pellets were transferred to a 24-well plate and covered with MG63 suspension ( $5 \times 10^6$  cells per well). After 24 h incubation (37 °C, 5%  $\text{CO}_2$ ), supernatants were removed and the pellets were washed twice with PBS. Cells were stained using a LIVE/DEAD kit (Invitrogen). Fluorescence was visualized using an epifluorescence microscope (Leica DMI6000B).

**Presto-Blue Assay\*\***

Cytotoxicities of HA- and PVA-based macromers were evaluated by a cell metabolic activity assay using a Presto-Blue agent (Life Tech.). A mouse fibroblast cell line (L929, Sigma) was cultured in high glucose DMEM (Lonza) including L-glutamine, which was further supplemented with 10% FBS and 1% Penicillin-Streptomycin (Sigma). Macromers were dissolved in DMEM to reach final concentrations of 10%, 1% and 0.1%. Cells were seeded in a 96-well plate at a density of  $1 \times 10^4$  cells per well in 100  $\mu$ L of growth medium and incubated overnight (37 °C, 5% CO<sub>2</sub>). After 24 h, the medium was removed and 100  $\mu$ L of each macromer solutions were added to the cells (n=3). Cells that were not treated with the macromers were set as positive control while cells treated with DMSO were set as negative control. After 24 h incubation, macromer solutions were carefully removed and 100  $\mu$ L of Presto-Blue/DMEM solution (1:10, v/v) was added. After 30 minutes of incubation at 37 °C, the fluorescence of the samples was recorded at 560 nm (excitation) and 590 nm (emission) using a microplate reader (Synergy H1, BioTek). Obtained signals were compared with fluorescence of Presto-Blue in wells without cells (blank sample – no metabolic activity of the cells), wells of negative control and wells of positive control (100 % metabolic activity).

**MTT Assay\*\*\***

Stock solutions of the monomers, thiols, and photoinitiators were prepared in DMSO to give a final concentration of 1M. Each solution was diluted with DMEM containing 10 % FBS, 100 U/ml Penicillin, and 100  $\mu$ g/ml Streptomycin (Invitrogen), to give solutions with 7 concentrations (10, 5, 2.5, 1.25, 0.63, 0.31, and 0.16 mM). Osteoblast cells (MC3T3-E1) were cultured in 100  $\mu$ L DMEM Medium supplemented with 10% FBS, 100 U/ml Penicillin, and 100  $\mu$ g/ml Streptomycin. Cells were seeded in 96-well plates at a density of  $6.4 \times 10^3$  cells/well and allowed for settlement for 24 h in humidified air (95% relative humidity) with 5% CO<sub>2</sub> at 37°C. After 24 h, the cells were treated with 100  $\mu$ L of the samples with different concentrations for 5 days in triplicates. Cells were treated with 1% DMSO-solution (Negative control) and/or PBS (Positive control). After incubation, 50  $\mu$ L of the MTT reagent were added and the cells were incubated for 4 h at 37°C. The absorbance intensity was measured for absorption at 570 nm with a reference wavelength of 650 nm and compared to untreated cells (cell+DMEM). The results represent the mean value with standard deviations of triplicate assays.



---

**References**

- (1) Palakkan, A. A.; Hay, D. C.; P, R. A.; T, V. K.; Ross, J. A. "*Liver tissue engineering and cell sources: issues and challenges*"; *Liver international : official journal of the International Association for the Study of the Liver* 2013, 33 (5), 666-76.
- (2) Perico, N.; Remuzzi, G. "*Xenotransplantation: problems and prospects*"; *Nephrology, dialysis, transplantation : official publication of the European Dialysis and Transplant Association - European Renal Association* 1997, 12 Suppl 1, 59-64.
- (3) Stock, U. A.; Vacanti, J. P. "*Tissue engineering: current state and prospects*"; *Annual review of medicine* 2001, 52, 443-51.
- (4) Raghunath, J.; Rollo, J.; Sales, K. M.; Butler, P. E.; Seifalian, A. M. "*Biomaterials and scaffold design: key to tissue-engineering cartilage*"; *Biotechnology and applied biochemistry* 2007, 46 (Pt 2), 73-84.
- (5) Ratner, B. D.; Bryant, S. J. "*Biomaterials: Where we have been and where we are going*"; *Annual review of biomedical engineering* 2004, 6, 41-75.
- (6) Hofmann, D.; Entrialgo-Castano, M.; Kratz, K.; Lendlein, A. "*Knowledge-based approach towards hydrolytic degradation of polymer-based biomaterials*"; *Advanced materials* 2009, 21 (32-33), 3237-45.
- (7) Kohn, J.; Welsh, W. J.; Knight, D. "*A new approach to the rationale discovery of polymeric biomaterials*"; *Biomaterials* 2007, 28 (29), 4171-7.
- (8) Herrmann, J. B.; Kelly, R. J.; Higgins, G. A. "*Polyglycolic acid sutures: Laboratory and clinical evaluation of a new absorbable suture material*"; *Archives of Surgery* 1970, 100 (4), 486-490.
- (9) Gilding, D. K.; Reed, A. M. "*Biodegradable polymers for use in surgery—polyglycolic/poly(lactic acid) homo- and copolymers: I*"; *Polymer* 1979, 20 (12), 1459-1464.
- (10) Ignatius, A. A.; Claes, L. E. "*In vitro biocompatibility of bioresorbable polymers: poly(L, DL-lactide) and poly(L-lactide-co-glycolide)*"; *Biomaterials* 1996, 17 (8), 831-9.
- (11) Ikada, Y. "*Challenges in tissue engineering*"; *Journal of the Royal Society, Interface / the Royal Society* 2006, 3 (10), 589-601.
- (12) Ramakrishna, S.; Mayer, J.; Wintermantel, E.; Leong, K. W. "*Biomedical applications of polymer-composite materials: a review*"; *Compos Sci Technol* 2001, 61 (9), 1189-1224.
- (13) Lu, S. X.; Anseth, K. S. "*Release behavior of high molecular weight solutes from poly(ethylene glycol)-based degradable networks*"; *Macromolecules* 2000, 33 (7), 2509-2515.
- (14) Cushing, M. C.; Anseth, K. S. "*Hydrogel Cell Cultures*"; *Science* 2007, 316 (5828), 1133-1134.
- (15) Discher, D. E.; Mooney, D. J.; Zandstra, P. W. "*Growth factors, matrices, and forces combine and control stem cells*"; *Science* 2009, 324 (5935), 1673-7.
- (16) Discher, D. E.; Janmey, P.; Wang, Y. L. "*Tissue cells feel and respond to the stiffness of their substrate*"; *Science* 2005, 310 (5751), 1139-1143.
- (17) West, J. L. "*Protein-patterned hydrogels: Customized cell microenvironments*"; *Nature materials* 2011, 10 (10), 727-729.

- (18) Lutolf, M. P.; Blau, H. M. "*Artificial Stem Cell Niches*"; *Advanced materials* 2009, 21 (32-33), 3255-3268.
- (19) Hunt, N. C.; Grover, L. M. "*Cell encapsulation using biopolymer gels for regenerative medicine*"; *Biotechnology letters* 2010, 32 (6), 733-42.
- (20) Cellesi, F.; Tirelli, N.; Hubbell, J. A. "*Materials for cell encapsulation via a new tandem approach combining reverse thermal gelation and covalent crosslinking*"; *Macromolecular Chemistry and Physics* 2002, 203 (10-11), 1466-1472.
- (21) Drury, J. L.; Mooney, D. J. "*Hydrogels for tissue engineering: scaffold design variables and applications*"; *Biomaterials* 2003, 24 (24), 4337-51.
- (22) Nguyen, K. T.; West, J. L. "*Photopolymerizable hydrogels for tissue engineering applications*"; *Biomaterials* 2002, 23 (22), 4307-14.
- (23) Nicodemus, G. D.; Bryant, S. J. "*Cell encapsulation in biodegradable hydrogels for tissue engineering applications*"; *Tissue Eng Part B Rev* 2008, 14 (2), 149-65.
- (24) Liska, R.; Schwager, F.; Maier, C.; Cano-Vives, R.; Stampfl, J. "*Water-soluble photopolymers for rapid prototyping of cellular materials*"; *J Appl Polym Sci* 2005, 97 (6), 2286-2298.
- (25) Zorlutuna, P.; Jeong, J. H.; Kong, H.; Bashir, R. "*Stereolithography-Based Hydrogel Microenvironments to Examine Cellular Interactions*"; *Advanced Functional Materials* 2011, 21 (19), 3642-3651.
- (26) Bryant, S. J.; Cuy, J. L.; Hauch, K. D.; Ratner, B. D. "*Photo-patterning of porous hydrogels for tissue engineering*"; *Biomaterials* 2007, 28 (19), 2978-2986.
- (27) Bryant, S. J.; Davis-Arehart, K. A.; Luo, N.; Shoemaker, R. K.; Arthur, J. A.; Anseth, K. S. "*Synthesis and Characterization of Photopolymerized Multifunctional Hydrogels: Water-Soluble Poly(Vinyl Alcohol) and Chondroitin Sulfate Macromers for Chondrocyte Encapsulation*"; *Macromolecules* 2004, 37 (18), 6726-6733.
- (28) Hahn, M. S.; Miller, J. S.; West, J. L. "*Three-Dimensional Biochemical and Biomechanical Patterning of Hydrogels for Guiding Cell Behavior*"; *Advanced materials* 2006, 18 (20), 2679-2684.
- (29) Ullrich, G.; Burtscher, P.; Salz, U.; Moszner, N.; Liska, R. "*Phenylglycine derivatives as coinitiators for the radical photopolymerization of acidic aqueous formulations*"; *Journal of Polymer Science Part A: Polymer Chemistry* 2006, 44 (1), 115-125.
- (30) Lu, Y.; Hasegawa, F.; Goto, T.; Ohkuma, S.; Fukuhara, S.; Kawazu, Y.; Totani, K.; Yamashita, T.; Watanabe, T. "*Highly sensitive measurement in two-photon absorption cross section and investigation of the mechanism of two-photon-induced polymerization*"; *Journal of Luminescence* 2004, 110 (1-2), 1-10.
- (31) Williams, C. G.; Malik, A. N.; Kim, T. K.; Manson, P. N.; Elisseff, J. H. "*Variable cytocompatibility of six cell lines with photoinitiators used for polymerizing hydrogels and cell encapsulation*"; *Biomaterials* 2005, 26 (11), 1211-1218.
- (32) Bryant SJ; Nuttelman CR; KS., A. "*Cytocompatibility of UV and visible light photoinitiating systems on cultured NIH/3T3 fibroblasts in vitro*"; *Journal of Biomaterials Science, Polymer Edition* 2000, 11 (5), 439-457.
- (33) Sawhney, A. S.; Pathak, C. P.; Hubbell, J. A. "*Interfacial photopolymerization of poly(ethylene glycol)-based hydrogels upon alginate-poly(l-lysine) microcapsules for enhanced biocompatibility*"; *Biomaterials* 1993, 14 (13), 1008-16.

- (34) CS Bahney, T. L., CW Hsu, M Bottlang, JL West, B Johnstone "Visible light photoinitiation of mesenchymal stem cell-laden bioresponsive hydrogels"; *European Cells and Materials* 2011, 22, 43-55.
- (35) Orellana, B.; Rufs, A. M.; Encinas, M. V.; Previtali, C. M.; Bertolotti, S. "The Photoinitiation Mechanism of Vinyl Polymerization by Riboflavin/Triethanolamine in Aqueous Medium"; *Macromolecules* 1999, 32 (20), 6570-6573.
- (36) Woo, H. Y.; Liu, B.; Kohler, B.; Korystov, D.; Mikhailovsky, A.; Bazan, G. C. "Solvent effects on the two-photon absorption of distyrylbenzene chromophores"; *Journal of the American Chemical Society* 2005, 127 (42), 14721-9.
- (37) Li, Z.; Torgersen, J.; Ajami, A.; Muhleder, S.; Qin, X.; Husinsky, W.; Holnthoner, W.; Ovsianikov, A.; Stampfl, J.; Liska, R. "Initiation efficiency and cytotoxicity of novel water soluble two-photon photoinitiators for direct 3D microfabrication of hydrogels"; *RSC Advances* 2013, 3 (36), 15939-15946.
- (38) Fairbanks, B. D.; Schwartz, M. P.; Bowman, C. N.; Anseth, K. S. "Photoinitiated polymerization of PEG-diacrylate with lithium phenyl-2,4,6-trimethylbenzoylphosphinate: polymerization rate and cytocompatibility"; *Biomaterials* 2009, 30 (35), 6702-6707.
- (39) Torgersen, J.; Ovsianikov, A.; Mironov, V.; Pucher, N.; Qin, X.; Li, Z.; Cicha, K.; Machacek, T.; Liska, R.; Jantsch, V.; Stampfl, J. "Photo-sensitive hydrogels for three-dimensional laser microfabrication in the presence of whole organisms"; *Journal of biomedical optics* 2012, 17 (10), 105008.
- (40) Rice, J. J.; Martino, M. M.; De Laporte, L.; Tortelli, F.; Briquez, P. S.; Hubbell, J. A. "Engineering the regenerative microenvironment with biomaterials"; *Advanced healthcare materials* 2013, 2 (1), 57-71.
- (41) Husar, B.; Liska, R. "Vinyl carbonates, vinyl carbamates, and related monomers: synthesis, polymerization, and application"; *Chemical Society reviews* 2012, 41 (6), 2395-2405.
- (42) Moszner, N.; Hirt, T. "New polymer-chemical developments in clinical dental polymer materials: Enamel-dentin adhesives and restorative composites"; *Journal of Polymer Science Part A: Polymer Chemistry* 2012, 50 (21), 4369-4402.
- (43) Heller, C.; Schwentenwein, M.; Russmueller, G.; Varga, F.; Stampfl, J.; Liska, R. "Vinyl esters: Low cytotoxicity monomers for the fabrication of biocompatible 3D scaffolds by lithography based additive manufacturing"; *Journal of Polymer Science Part A: Polymer Chemistry* 2009, 47 (24), 6941-6954.
- (44) Lee, T. Y.; Kaung, W.; Jönsson, E. S.; Lowery, K.; Guymon, C. A.; Hoyle, C. E. "Synthesis and photopolymerization of novel multifunctional vinyl esters"; *Journal of Polymer Science Part A: Polymer Chemistry* 2004, 42 (17), 4424-4436.
- (45) Esfandiari, P. Dissertation, Vienna University of Technology, 2011.
- (46) Sletten, E. M.; Bertozzi, C. R. "Bioorthogonal Chemistry: Fishing for Selectivity in a Sea of Functionality"; *Angewandte Chemie International Edition* 2009, 48 (38), 6974-6998.
- (47) Iha, R. K.; Wooley, K. L.; Nystrom, A. M.; Burke, D. J.; Kade, M. J.; Hawker, C. J. "Applications of orthogonal "click" chemistries in the synthesis of functional soft materials"; *Chemical reviews* 2009, 109 (11), 5620-86.
- (48) Malkoch, M.; Vestberg, R.; Gupta, N.; Mespouille, L.; Dubois, P.; Mason, A. F.; Hedrick, J. L.; Liao, Q.; Frank, C. W.; Kingsbury, K.; Hawker, C. J. "Synthesis of

- well-defined hydrogel networks using Click chemistry*"; Chem Commun 2006, 0 (26), 2774-2776.
- (49) Ossipov, D. A.; Hilborn, J. n. "*Poly(vinyl alcohol)-Based Hydrogels Formed by Click Chemistry*"; Macromolecules 2006, 39 (5), 1709-1718.
- (50) Crescenzi, V.; Cornelio, L.; Di Meo, C.; Nardecchia, S.; Lamanna, R. "*Novel Hydrogels via Click Chemistry: Synthesis and Potential Biomedical Applications*"; Biomacromolecules 2007, 8 (6), 1844-1850.
- (51) Adzima, B. J.; Tao, Y.; Kloxin, C. J.; DeForest, C. A.; Anseth, K. S.; Bowman, C. N. "*Spatial and temporal control of the alkyne-azide cycloaddition by photoinitiated Cu(II) reduction*"; Nat Chem 2011, 3 (3), 256-259.
- (52) Alge, D. L.; Azagarsamy, M. A.; Donohue, D. F.; Anseth, K. S. "*Synthetically Tractable Click Hydrogels for Three-Dimensional Cell Culture Formed Using Tetrazine-Norbornene Chemistry*"; Biomacromolecules 2013.
- (53) Grover, G. N.; Lam, J.; Nguyen, T. H.; Segura, T.; Maynard, H. D. "*Biocompatible Hydrogels by Oxime Click Chemistry*"; Biomacromolecules 2012.
- (54) Fairbanks, B. D.; Schwartz, M. P.; Halevi, A. E.; Nuttelman, C. R.; Bowman, C. N.; Anseth, K. S. "*A Versatile Synthetic Extracellular Matrix Mimic via Thiol-Norbornene Photopolymerization*"; Advanced materials 2009, 21 (48), 5005-5010.
- (55) Hoyle, C. E.; Bowman, C. N. "*Thiol-ene click chemistry*"; Angewandte Chemie 2010, 49 (9), 1540-73.
- (56) Hoyle, C. E.; Lee, T. Y.; Roper, T. "*Thiol-enes: Chemistry of the past with promise for the future*"; Journal of Polymer Science Part A: Polymer Chemistry 2004, 42 (21), 5301-5338.
- (57) Kirschner, C. M.; Brennan, A. B. "*Bio-Inspired Antifouling Strategies*"; Annual Review of Materials Research, Vol 42 2012, 42, 211-229.
- (58) Kirschner, C. M.; Anseth, K. S. "*Hydrogels in healthcare: From static to dynamic material microenvironments*"; Acta Materialia 61 (3), 931-944.
- (59) Weber, L. M.; Lopez, C. G.; Anseth, K. S. "*Effects of PEG hydrogel crosslinking density on protein diffusion and encapsulated islet survival and function*"; J Biomed Mater Res A 2009, 90 (3), 720-9.
- (60) Roberts, J. J.; Bryant, S. J. "*Comparison of photopolymerizable thiol-ene PEG and acrylate-based PEG hydrogels for cartilage development*"; Biomaterials 2013.
- (61) Sawhney, A. S.; Pathak, C. P.; Hubbell, J. A. "*Bioerodible hydrogels based on photopolymerized poly(ethylene glycol)-co-poly(.alpha.-hydroxy acid) diacrylate macromers*"; Macromolecules 1993, 26 (4), 581-587.
- (62) Bryant, S. J.; Bender, R. J.; Durand, K. L.; Anseth, K. S. "*Encapsulating chondrocytes in degrading PEG hydrogels with high modulus: engineering gel structural changes to facilitate cartilaginous tissue production*"; Biotechnology and bioengineering 2004, 86 (7), 747-55.
- (63) Metters, A. T.; Anseth, K. S.; Bowman, C. N. "*Fundamental studies of a novel, biodegradable PEG-b-PLA hydrogel*"; Polymer 2000, 41 (11), 3993-4004.
- (64) McCall, J. D.; Anseth, K. S. "*Thiol-ene photopolymerizations provide a facile method to encapsulate proteins and maintain their bioactivity*"; Biomacromolecules 2012, 13 (8), 2410-7.
- (65) Cascone, M. G.; Laus, M.; Ricci, D.; Sbarbati Del Guerra, R. "*Evaluation of poly(vinyl alcohol) hydrogels as a component of hybrid artificial tissues*"; Journal of Materials Science: Materials in Medicine 1995, 6 (2), 71-75.

- (66) Nuttelman, C. R.; Mortisen, D. J.; Henry, S. M.; Anseth, K. S. "*Attachment of fibronectin to poly(vinyl alcohol) hydrogels promotes NIH3T3 cell adhesion, proliferation, and migration*"; *Journal of biomedical materials research* 2001, 57 (2), 217-23.
- (67) Orienti; Trere, R.; Zecchi, V. "*Hydrogels formed by cross-linked polyvinylalcohol as colon-specific drug delivery systems*"; *Drug Dev Ind Pharm* 2001, 27 (8), 877-84.
- (68) Ossipov, D. A.; Piskounova, S.; Hilborn, J. n. "*Poly(vinyl alcohol) Cross-Linkers for in Vivo Injectable Hydrogels*"; *Macromolecules* 2008, 41 (11), 3971-3982.
- (69) Ossipov, D. A.; Brännvall, K.; Forsberg-Nilsson, K.; Hilborn, J. "*Formation of the first injectable poly(vinyl alcohol) hydrogel by mixing of functional PVA precursors*"; *J Appl Polym Sci* 2007, 106 (1), 60-70.
- (70) Martens, P.; Holland, T.; Anseth, K. S. "*Synthesis and characterization of degradable hydrogels formed from acrylate modified poly(vinyl alcohol) macromers*"; *Polymer* 2002, 43 (23), 6093-6100.
- (71) Schmedlen, R. H.; Masters, K. S.; West, J. L. "*Photocrosslinkable polyvinyl alcohol hydrogels that can be modified with cell adhesion peptides for use in tissue engineering*"; *Biomaterials* 2002, 23 (22), 4325-32.
- (72) Thomas H, B. "*The role of ECM proteins and protein fragments in guiding cell behavior in regenerative medicine*"; *Biomaterials* 32 (18), 4211-4214.
- (73) Jeon, O.; Bouhadir, K. H.; Mansour, J. M.; Alsberg, E. "*Photocrosslinked alginate hydrogels with tunable biodegradation rates and mechanical properties*"; *Biomaterials* 2009, 30 (14), 2724-2734.
- (74) Kong, H. J.; Smith, M. K.; Mooney, D. J. "*Designing alginate hydrogels to maintain viability of immobilized cells*"; *Biomaterials* 2003, 24 (22), 4023-9.
- (75) Lee, K. Y.; Rowley, J. A.; Eiselt, P.; Moy, E. M.; Bouhadir, K. H.; Mooney, D. J. "*Controlling mechanical and swelling properties of alginate hydrogels independently by cross-linker type and cross-linking density*"; *Macromolecules* 2000, 33 (11), 4291-4294.
- (76) Garcia-Fuentes, M.; Alonso, M. J. "*Chitosan-based drug nanocarriers: Where do we stand?*"; *Journal of Controlled Release* 2012, 161 (2), 496-504.
- (77) Kim, Y. K.; Jiang, H. L.; Choi, Y. J.; Park, I. K.; Cho, M. H.; Cho, C. S., Polymeric Nanoparticles of Chitosan Derivatives as DNA and siRNA Carriers. in *Chitosan for Biomaterials I*, Jayakumar, R.; Prabakaran, M.; Muzzarelli, R. A. A., Eds. Springer Berlin Heidelberg: 2011; Vol. 243, pp 1-21.
- (78) Abrahams, J. M.; Chen, W. Modified chitosan for vascular embolization. US20070031468A1, 2007.
- (79) Shoulders, M. D.; Raines, R. T. "*Collagen structure and stability*"; *Annu Rev Biochem* 2009, 78, 929-58.
- (80) Leitinger, B.; Hohenester, E. "*Mammalian collagen receptors*"; *Matrix Biology* 2007, 26 (3), 146-155.
- (81) Schoof, H.; Apel, J.; Heschel, I.; Rau, G. "*Control of pore structure and size in freeze-dried collagen sponges*"; *Journal of biomedical materials research* 2001, 58 (4), 352-357.
- (82) Lee, C. R.; Grodzinsky, A. J.; Spector, M. "*The effects of cross-linking of collagen-glycosaminoglycan scaffolds on compressive stiffness, chondrocyte-mediated contraction, proliferation and biosynthesis*"; *Biomaterials* 2001, 22 (23), 3145-3154.

- (83) Park, S.-N.; Park, J.-C.; Kim, H. O.; Song, M. J.; Suh, H. "Characterization of porous collagen/hyaluronic acid scaffold modified by 1-ethyl-3-(3-dimethylaminopropyl)carbodiimide cross-linking"; *Biomaterials* 2002, 23 (4), 1205-1212.
- (84) oYoung, S.; Wong, M.; Tabata, Y.; Mikos, A. G. "Gelatin as a delivery vehicle for the controlled release of bioactive molecules"; *Journal of Controlled Release* 2005, 109 (1-3), 256-274.
- (85) Holland, T. A.; Tabata, Y.; Mikos, A. G. "Dual growth factor delivery from degradable oligo(poly(ethylene glycol) fumarate) hydrogel scaffolds for cartilage tissue engineering"; *Journal of Controlled Release* 2005, 101 (1-3), 111-125.
- (86) Van den Bulcke, A. I.; Bogdanov, B.; De Rooze, N.; Schacht, E. H.; Cornelissen, M.; Berghmans, H. "Structural and rheological properties of methacrylamide modified gelatin hydrogels"; *Biomacromolecules* 2000, 1 (1), 31-38.
- (87) Nichol, J. W.; Koshy, S. T.; Bae, H.; Hwang, C. M.; Yamanlar, S.; Khademhosseini, A. "Cell-laden microengineered gelatin methacrylate hydrogels"; *Biomaterials* 2010, 31 (21), 5536-44.
- (88) Fraser, J. R. E.; Laurent, T. C.; Laurent, U. B. G. "Hyaluronan: its nature, distribution, functions and turnover"; *Journal of Internal Medicine* 1997, 242 (1), 27-33.
- (89) Liu, Y.; Ahmad, S.; Shu, X. Z.; Sanders, R. K.; Kopesec, S. A.; Prestwich, G. D. "Accelerated repair of cortical bone defects using a synthetic extracellular matrix to deliver human demineralized bone matrix"; *Journal of Orthopaedic Research* 2006, 24 (7), 1454-1462.
- (90) Duflo, S.; Thibeault, S. L.; Li, W. H.; Shu, X. Z.; Prestwich, G. D. "Vocal fold tissue repair in vivo using a synthetic extracellular matrix"; *Tissue Eng* 2006, 12 (8), 2171-2180.
- (91) Shu, X. Z.; Liu, Y. C.; Luo, Y.; Roberts, M. C.; Prestwich, G. D. "Disulfide cross-linked hyaluronan hydrogels"; *Biomacromolecules* 2002, 3 (6), 1304-1311.
- (92) Burdick, J. A.; Prestwich, G. D. "Hyaluronic acid hydrogels for biomedical applications"; *Advanced materials* 2011, 23 (12), 41-56.
- (93) Zheng Shu, X.; Liu, Y.; Palumbo, F. S.; Luo, Y.; Prestwich, G. D. "In situ crosslinkable hyaluronan hydrogels for tissue engineering"; *Biomaterials* 2004, 25 (7-8), 1339-1348.
- (94) Smeds, K. A.; Pfister-Serres, A.; Miki, D.; Dastgheib, K.; Inoue, M.; Hatchell, D. L.; Grinstaff, M. W. "Photocrosslinkable polysaccharides for in situ hydrogel formation"; *Journal of biomedical materials research* 2001, 54 (1), 115-21.
- (95) Baier Leach, J.; Bivens, K. A.; Patrick, C. W., Jr.; Schmidt, C. E. "Photocrosslinked hyaluronic acid hydrogels: natural, biodegradable tissue engineering scaffolds"; *Biotechnology and bioengineering* 2003, 82 (5), 578-89.
- (96) Khademhosseini, A.; Eng, G.; Yeh, J.; Fukuda, J.; Blumling, J.; Langer, R.; Burdick, J. A. "Micromolding of photocrosslinkable hyaluronic acid for cell encapsulation and entrapment"; *Journal of Biomedical Materials Research Part A* 2006, 79A (3), 522-532.
- (97) Khetan, S.; Katz, J. S.; Burdick, J. A. "Sequential crosslinking to control cellular spreading in 3-dimensional hydrogels"; *Soft Matter* 2009, 5 (8), 1601-1606.
- (98) Brauker, J. H.; Carr-Brendel, V. E.; Martinson, L. A.; Crudele, J.; Johnston, W. D.; Johnson, R. C. "Neovascularization of synthetic membranes directed by membrane

- microarchitecture*"; Journal of biomedical materials research 1995, 29 (12), 1517-1524.
- (99) Chirila, T. V. "An overview of the development of artificial corneas with porous skirts and the use of PHEMA for such an application"; Biomaterials 2001, 22 (24), 3311-3317.
- (100) Billiet, T.; Vandenhoute, M.; Schelfhout, J.; Van Vlierberghe, S.; Dubruel, P. "A review of trends and limitations in hydrogel-rapid prototyping for tissue engineering"; Biomaterials 2012, 33 (26), 6020-6041.
- (101) Liu, V.; Bhatia, S. "Three-Dimensional Photopatterning of Hydrogels Containing Living Cells"; Biomedical microdevices 2002, 4 (4), 257-266.
- (102) Tsang, V. L.; Chen, A. A.; Cho, L. M.; Jadin, K. D.; Sah, R. L.; DeLong, S.; West, J. L.; Bhatia, S. N. "Fabrication of 3D hepatic tissues by additive photopatterning of cellular hydrogels"; The FASEB Journal 2007, 21 (3), 790-801.
- (103) Marklein, R. A.; Burdick, J. A. "Spatially controlled hydrogel mechanics to modulate stem cell interactions"; Soft Matter 2010, 6 (1), 136-143.
- (104) Nemir, S.; Hayenga, H. N.; West, J. L. "PEGDA Hydrogels With Patterned Elasticity: Novel Tools for the Study of Cell Response to Substrate Rigidity"; Biotechnology and bioengineering 2010, 105 (3), 636-644.
- (105) Seidi, A.; Ramalingam, M.; Elloumi-Hannachi, I.; Ostrovidov, S.; Khademhosseini, A. "Gradient biomaterials for soft-to-hard interface tissue engineering"; Acta Biomater 2011, 7 (4), 1441-51.
- (106) Du, Y.; Shim, J.; Vidula, M.; Hancock, M. J.; Lo, E.; Chung, B. G.; Borenstein, J. T.; Khabiry, M.; Cropek, D. M.; Khademhosseini, A. "Rapid generation of spatially and temporally controllable long-range concentration gradients in a microfluidic device"; Lab on a chip 2009, 9 (6), 761-7.
- (107) Khetan, S.; Burdick, J. A. "Patterning network structure to spatially control cellular remodeling and stem cell fate within 3-dimensional hydrogels"; Biomaterials 2010, 31 (32), 8228-8234.
- (108) Lu, Y.; Mapili, G.; Suhali, G.; Chen, S.; Roy, K. "A digital micro-mirror device-based system for the microfabrication of complex, spatially patterned tissue engineering scaffolds"; Journal of Biomedical Materials Research Part A 2006, 77A (2), 396-405.
- (109) Luo, Y.; Shoichet, M. S. "A photolabile hydrogel for guided three-dimensional cell growth and migration"; Nature materials 2004, 3 (4), 249-253.
- (110) Andrade, C. D.; Yanez, C. O.; Rodriguez, L.; Belfield, K. D. "A series of fluorene-based two-photon absorbing molecules: synthesis, linear and nonlinear characterization, and bioimaging"; J Org Chem 2010, 75 (12), 3975-82.
- (111) Kasko, A. M.; Wong, D. Y. "Two-photon lithography in the future of cell-based therapeutics and regenerative medicine: a review of techniques for hydrogel patterning and controlled release"; Future Med Chem 2010, 2 (11), 1669-80.
- (112) Deshayes, S.; Kasko, A. M. "Polymeric biomaterials with engineered degradation"; Journal of Polymer Science Part A: Polymer Chemistry 2013, 51 (17):3531-3566.
- (113) Zipfel, W. R.; Williams, R. M.; Christie, R.; Nikitin, A. Y.; Hyman, B. T.; Webb, W. W. "Live tissue intrinsic emission microscopy using multiphoton-excited native fluorescence and second harmonic generation"; Proceedings of the National Academy of Sciences of the United States of America 2003, 100 (12), 7075-80.

- (114) Zipfel, W. R.; Williams, R. M.; Webb, W. W. "*Nonlinear magic: multiphoton microscopy in the biosciences*"; *Nature biotechnology* 2003, 21 (11), 1369-77.
- (115) LaFratta, C. N.; Fourkas, J. T.; Baldacchini, T.; Farrer, R. A. "*Multiphoton fabrication*"; *Angewandte Chemie* 2007, 46 (33), 6238-58.
- (116) Xu, C.; Williams, R. M.; Zipfel, W.; Webb, W. W. "*Multiphoton excitation cross-sections of molecular fluorophores*"; *Bioimaging* 1996, 4 (3), 198-207.
- (117) Denk, W.; Strickler, J. H.; Webb, W. W. "*Two-photon laser scanning fluorescence microscopy*"; *Science* 1990, 248 (4951), 73-6.
- (118) Lee, K.-S.; Kim, R. H.; Yang, D.-Y.; Park, S. H. "*Advances in 3D nano/microfabrication using two-photon initiated polymerization*"; *Prog Polym Sci* 2008, 33 (6), 631-681.
- (119) Claeysens, F.; Hasan, E. A.; Gaidukeviciute, A.; Achilleos, D. S.; Ranella, A.; Reinhardt, C.; Ovsianikov, A.; Xiao, S.; Fotakis, C.; Vamvakaki, M.; Chichkov, B. N.; Farsari, M. "*Three-Dimensional Biodegradable Structures Fabricated by Two-Photon Polymerization*"; *Langmuir : the ACS journal of surfaces and colloids* 2009, 25 (5), 3219-3223.
- (120) Ovsianikov, A.; Gruene, M.; Pflaum, M.; Koch, L.; Maiorana, F.; Wilhelmi, M.; Haverich, A.; Chichkov, B. "*Laser printing of cells into 3D scaffolds*"; *Biofabrication* 2010, 2 (1), 014104.
- (121) Ovsianikov, A.; Malinauskas, M.; Schlie, S.; Chichkov, B.; Gittard, S.; Narayan, R.; Lobler, M.; Sternberg, K.; Schmitz, K. P.; Haverich, A. "*Three-dimensional laser micro- and nano-structuring of acrylated poly(ethylene glycol) materials and evaluation of their cytotoxicity for tissue engineering applications*"; *Acta Biomater* 2011, 7 (3), 967-74.
- (122) Jhaveri, S. J.; McMullen, J. D.; Sijbesma, R.; Tan, L. S.; Zipfel, W.; Ober, C. K. "*Direct Three-Dimensional Microfabrication of Hydrogels via Two-Photon Lithography in Aqueous Solution*"; *Chem Mater* 2009, 21 (10), 2003-2006.
- (123) Watanabe, T.; Akiyama, M.; Totani, K.; Kuebler, S. M.; Stellacci, F.; Wenseleers, W.; Braun, K.; Marder, S. R.; Perry, J. W. "*Photoresponsive hydrogel microstructure fabricated by two-photon initiated polymerization*"; *Advanced Functional Materials* 2002, 12 (9), 611-614.
- (124) Atala, A.; Kasper, F. K.; Mikos, A. G. "*Engineering Complex Tissues*"; *Science translational medicine* 2012, 4 (160), 160rv12.
- (125) Mikos, A. G.; Herring, S. W.; Ochareon, P.; Elisseeff, J.; Lu, H. H.; Kandel, R.; Schoen, F. J.; Toner, M.; Mooney, D.; Atala, A.; Van Dyke, M. E.; Kaplan, D.; Vunjak-Novakovic, G. "*Engineering complex tissues*"; *Tissue Eng* 2006, 12 (12), 3307-39.
- (126) Dvir, T.; Timko, B. P.; Kohane, D. S.; Langer, R. "*Nanotechnological strategies for engineering complex tissues*"; *Nat Nanotechnol* 2011, 6 (1), 13-22.
- (127) Tsang, V. L.; Bhatia, S. N. "*Three-dimensional tissue fabrication*"; *Adv Drug Deliv Rev* 2004, 56 (11), 1635-47.
- (128) Griffith, L. G.; Swartz, M. A. "*Capturing complex 3D tissue physiology in vitro*"; *Nature reviews. Molecular cell biology* 2006, 7 (3), 211-24.
- (129) Tibbitt, M. W.; Anseth, K. S. "*Dynamic microenvironments: the fourth dimension*"; *Science translational medicine* 2012, 4 (160), 160ps24.
- (130) Tibbitt, M. W.; Anseth, K. S. "*Hydrogels as extracellular matrix mimics for 3D cell culture*"; *Biotechnology and bioengineering* 2009, 103 (4), 655-63.



- (131)Chen, C. S.; Mrksich, M.; Huang, S.; Whitesides, G. M.; Ingber, D. E. "*Geometric Control of Cell Life and Death*"; *Science* 1997, 276 (5317), 1425-1428.
- (132)Massia, S. P.; Hubbell, J. A. "*An RGD spacing of 440 nm is sufficient for integrin alpha V beta 3-mediated fibroblast spreading and 140 nm for focal contact and stress fiber formation*"; *The Journal of cell biology* 1991, 114 (5), 1089-100.
- (133)Ovsianikov, A.; Deiwick, A.; Van Vlierberghe, S.; Dubruel, P.; Mol`ller, L.; Dra`lger, G.; Chichkov, B. "*Laser Fabrication of Three-Dimensional CAD Scaffolds from Photosensitive Gelatin for Applications in Tissue Engineering*"; *Biomacromolecules* 2011, 12 (4), 851-858.
- (134)Ovsianikov, A.; Mironov, V.; Stampfl, J.; Liska, R. "*Engineering 3D cell-culture matrices: multiphoton processing technologies for biological & tissue engineering applications*"; *Expert review of medical devices* 2012, 1-21.
- (135)Hsieh, T. M.; Benjamin Ng, C. W.; Narayanan, K.; Wan, A. C. A.; Ying, J. Y. "*Three-dimensional microstructured tissue scaffolds fabricated by two-photon laser scanning photolithography*"; *Biomaterials* 2010, 31 (30), 7648-7652.
- (136)Wu, S. H.; Serbin, J.; Gu, M. "*Two-photon polymerisation for three-dimensional micro-fabrication*"; *J Photoch Photobio A* 2006, 181 (1), 1-11.
- (137)Perry, J. W.; Cumpston, B. H.; Ananthavel, S. P.; Barlow, S.; Dyer, D. L.; Ehrlich, J. E.; Erskine, L. L.; Heikal, A. A.; Kuebler, S. M.; Lee, I. Y. S.; McCord-Maughon, D.; Qin, J. Q.; Rockel, H.; Rumi, M.; Wu, X. L.; Marder, S. R. "*Two-photon polymerization initiators for three-dimensional optical data storage and microfabrication*"; *Nature* 1999, 398 (6722), 51-54.
- (138)Kloxin, A. M.; Kasko, A. M.; Salinas, C. N.; Anseth, K. S. "*Photodegradable Hydrogels for Dynamic Tuning of Physical and Chemical Properties*"; *Science* 2009, 324 (5923), 59-63.
- (139)Pelliccioli, A. P.; Wirz, J. "*Photoremovable protecting groups: reaction mechanisms and applications*"; *Photochemical & Photobiological Sciences* 2002, 1 (7), 441-458.
- (140)Berg, A.; Wyrwa, R.; Weisser, J.; Weiss, T.; Schade, R.; Hildebrand, G.; Liefelth, K.; Schneider, B.; Ellinger, R.; Schnabelrauch, M. "*Synthesis of Photopolymerizable Hydrophilic Macromers and Evaluation of Their Applicability as Reactive Resin Components for the Fabrication of Three-Dimensionally Structured Hydrogel Matrices by 2-Photon-Polymerization*"; *Advanced Engineering Materials* 2011, 13 (9), B274-B284.
- (141)Nguyen, D. H.; Stapleton, S. C.; Yang, M. T.; Cha, S. S.; Choi, C. K.; Galie, P. A.; Chen, C. S. "*Biomimetic model to reconstitute angiogenic sprouting morphogenesis in vitro*"; *Proceedings of the National Academy of Sciences of the United States of America* 2013, 110 (17), 6712-7.
- (142)Bae, H.; Puranik, A. S.; Gauvin, R.; Edalat, F.; Carrillo-Conde, B.; Peppas, N. A.; Khademhosseini, A. "*Building Vascular Networks*"; *Science translational medicine* 2012, 4 (160), 160ps23.
- (143)Saik, J. E.; McHale, M. K.; West, J. L. "*Biofunctional materials for directing vascular development*"; *Curr Vasc Pharmacol* 2012, 10 (3), 331-41.
- (144)Silva, A. K. A.; Richard, C.; Bessodes, M.; Scherman, D.; Merten, O.-W. "*Growth Factor Delivery Approaches in Hydrogels*"; *Biomacromolecules* 2008, 10 (1), 9-18.
- (145)Hahn, M. S.; Miller, J. S.; West, J. L. "*Laser Scanning Lithography for Surface Micropatterning on Hydrogels*"; *Advanced materials* 2005, 17 (24), 2939-2942.

- (146)Wylie, R. G.; Ahsan, S.; Aizawa, Y.; Maxwell, K. L.; Morshead, C. M.; Shoichet, M. S. "*Spatially controlled simultaneous patterning of multiple growth factors in three-dimensional hydrogels*"; *Nature materials* 2011, 10 (10), 799-806.
- (147)West, J. L. "*Protein-patterned hydrogels: Customized cell microenvironments*"; *Nat Mater* 10 (10), 727-9.
- (148)Ovsianikov, A.; Li, Z.; Torgersen, J.; Stampfl, J.; Liska, R. "*Selective Functionalization of 3D Matrices Via Multiphoton Grafting and Subsequent Click Chemistry*"; *Advanced Functional Materials* 2012, 22 (16), 3429-3433.
- (149)Li, Z.; Ajami, A.; Stankevičius, E.; Husinsky, W.; Račiukaitis, G.; Stampfl, J.; Liska, R.; Ovsianikov, A. "*3D photografting with aromatic azides: A comparison between three-photon and two-photon case*"; *Optical Materials* 2013, 35 (10), 1846-1851.
- (150)Li, Z.; Stankevicius, E.; Ajami, A.; Raciukaitis, G.; Husinsky, W.; Ovsianikov, A.; Stampfl, J.; Liska, R. "*3D alkyne-azide cycloaddition: spatiotemporally controlled by combination of aryl azide photochemistry and two-photon grafting*"; *Chem Commun (Camb)* 2013, 49 (69), 7635-7.
- (151)Koepff, P.; Braeumer, K.; Babel, W. Water-resistant biodegradable crosslinked materials from polysaccharides and polypeptides. DE4210334A1, 1993.
- (152)Zorlutuna, P.; Annabi, N.; Camci-Unal, G.; Nikkhah, M.; Cha, J. M.; Nichol, J. W.; Manbachi, A.; Bae, H.; Chen, S.; Khademhosseini, A. "*Microfabricated Biomaterials for Engineering 3D Tissues*"; *Advanced materials* 2012, 24 (14), 1782-1804.
- (153)Shin, S. R.; Aghaei-Ghareh-Bolagh, B.; Dang, T. T.; Topkaya, S. N.; Gao, X.; Yang, S. Y.; Jung, S. M.; Oh, J. H.; Dokmeci, M. R.; Tang, X. S.; Khademhosseini, A. "*Cell-laden Microengineered and Mechanically Tunable Hybrid Hydrogels of Gelatin and Graphene Oxide*"; *Advanced materials* 2013.
- (154)Schuster, M.; Turecek, C.; Weigel, G.; Saf, R.; Stampfl, J.; Varga, F.; Liska, R. "*Gelatin-based photopolymers for bone replacement materials*"; *Journal of Polymer Science Part A: Polymer Chemistry* 2009, 47 (24), 7078-7089.
- (155)Ovsianikov, A.; Muhleder, S.; Torgersen, J.; Li, Z.; Qin, X. H.; Van Vlierberghe, S.; Dubruel, P.; Holthoner, W.; Redl, H.; Liska, R.; Stampfl, J. "*Laser photofabrication of cell-containing hydrogel constructs*"; *Langmuir : the ACS journal of surfaces and colloids* 2014, 30 (13), 3787-94.
- (156)Ovsianikov, A.; Deiwick, A.; Van Vlierberghe, S.; Dubruel, P.; Moller, L.; Drager, G.; Chichkov, B. "*Laser fabrication of three-dimensional CAD scaffolds from photosensitive gelatin for applications in tissue engineering*"; *Biomacromolecules* 2011, 12 (4), 851-8.
- (157)Mammen, M.; Dahmann, G.; Whitesides, G. M. "*Effective Inhibitors of Hemagglutination by Influenza Virus Synthesized from Polymers Having Active Ester Groups. Insight into Mechanism of Inhibition*"; *Journal of Medicinal Chemistry* 1995, 38 (21), 4179-4190.
- (158)Mautner, A.; Qin, X.; Kapeller, B.; Russmueller, G.; Koch, T.; Stampfl, J.; Liska, R. "*Efficient curing of vinyl carbonates by thiol-ene polymerization*"; *Macromolecular rapid communications* 2012, 33 (23), 2046-52.
- (159)Mautner, A.; Qin, X.; Wutzel, H.; Ligon, S. C.; Kapeller, B.; Moser, D.; Russmueller, G.; Stampfl, J.; Liska, R. "*Thiol-ene photopolymerization for efficient*

- curing of vinyl esters*"; Journal of Polymer Science Part A: Polymer Chemistry 2013, 51 (1), 203-212.
- (160) Tsai, D. H.; Delrio, F. W.; Keene, A. M.; Tyner, K. M.; Maccuspie, R. I.; Cho, T. J.; Zachariah, M. R.; Hackley, V. A. "*Adsorption and Conformation of Serum Albumin Protein on Gold Nanoparticles Investigated Using Dimensional Measurements and in Situ Spectroscopic Methods*"; Langmuir : the ACS journal of surfaces and colloids 2011, 27 (6), 2464-2477.
- (161) Gilbert, H. F., Molecular and Cellular Aspects of Thiol–Disulfide Exchange. in *Advances in Enzymology and Related Areas of Molecular Biology*, John Wiley & Sons, Inc.: 2006; pp 69-172.
- (162) Cleland, W. W. "*Dithiothreitol, a New Protective Reagent for Sh Groups*"; Biochemistry 1964, 3, 480-2.
- (163) Burns, J. A.; Butler, J. C.; Moran, J.; Whitesides, G. M. "*Selective reduction of disulfides by tris(2-carboxyethyl)phosphine*"; The Journal of Organic Chemistry 1991, 56 (8), 2648-2650.
- (164) Ellman, G. L. "*Tissue sulfhydryl groups*"; Archives of biochemistry and biophysics 1959, 82 (1), 70-7.
- (165) Wu, Y.; Chakraborty, S.; Gropeanu, R. A.; Wilhelmi, J.; Xu, Y.; Er, K. S.; Kuan, S. L.; Koynov, K.; Chan, Y.; Weil, T. "*pH-Responsive Quantum Dots via an Albumin Polymer Surface Coating*"; Journal of the American Chemical Society 2010, 132 (14), 5012-5014.
- (166) Slaughter, B. V.; Khurshid, S. S.; Fisher, O. Z.; Khademhosseini, A.; Peppas, N. A. "*Hydrogels in regenerative medicine*"; Advanced materials 2009, 21 (32-33), 3307-29.
- (167) Murphy, M. C.; Howell, N. K. "*Functional properties of native and positively and negatively charged modified bovine serum albumin*"; Journal of the Science of Food and Agriculture 1991, 55 (3), 489-492.
- (168) Campagnola, P. J.; Delguidice, D. M.; Epling, G. A.; Hoffacker, K. D.; Howell, A. R.; Pitts, J. D.; Goodman, S. L. "*3-dimensional submicron polymerization of acrylamide by multiphoton excitation of xanthene dyes*"; Macromolecules 2000, 33 (5), 1511-1513.
- (169) Rumi, M.; Ehrlich, J. E.; Heikal, A. A.; Perry, J. W.; Barlow, S.; Hu, Z.; McCord-Maughon, D.; Parker, T. C.; Röckel, H.; Thayumanavan, S.; Marder, S. R.; Beljonne, D.; Brédas, J.-L. "*Structure–Property Relationships for Two-Photon Absorbing Chromophores: Bis-Donor Diphenylpolyene and Bis(styryl)benzene Derivatives*"; Journal of the American Chemical Society 2000, 122 (39), 9500-9510.
- (170) Woo, H. Y.; Hong, J. W.; Liu, B.; Mikhailovsky, A.; Korystov, D.; Bazan, G. C. "*Water-soluble [2.2]paracyclophane chromophores with large two-photon action cross sections*"; Journal of the American Chemical Society 2005, 127 (3), 820-1.
- (171) Li, Z.; Pucher, N.; Cicha, K.; Torgersen, J.; Ligon, S. C.; Ajami, A.; Husinsky, W.; Rosspeintner, A.; Vauthey, E.; Naumov, S.; Scherzer, T.; Stampfl, J.; Liska, R. "*A Straightforward Synthesis and Structure–Activity Relationship of Highly Efficient Initiators for Two-Photon Polymerization*"; Macromolecules 2013, 46 (2), 352-361.
- (172) Tesoro, G. "*Epoxy resins-chemistry and technology, 2nd Edition, Clayton A. May, Ed., Marcel Dekker, New York, 1988, 1,288 pp. Price: \$195.00*"; Journal of Polymer Science Part C: Polymer Letters 1988, 26 (12), 539-539.

- (173) Lungwitz, U.; Breunig, M.; Blunk, T.; Gopferich, A. "Polyethylenimine-based non-viral gene delivery systems"; *European journal of pharmaceutics and biopharmaceutics : official journal of Arbeitsgemeinschaft für Pharmazeutische Verfahrenstechnik e.V* 2005, 60 (2), 247-66.
- (174) Kowitsch, A.; Yang, Y.; Ma, N.; Kuntsche, J.; Mader, K.; Groth, T. "Bioactivity of immobilized hyaluronic acid derivatives regarding protein adsorption and cell adhesion"; *Biotechnology and applied biochemistry* 2011, 58 (5), 376-89.
- (175) Gross, R. A.; Kumar, V. Manufacture of acrylated hyaluronic acid. WO2007106738A2, 2007.
- (176) Heller, C. *Biocompatible and Biodegradable Photopolymers by Additive Manufacturing: From Synthesis to In-Vivo Studies*. Dissertation, Vienna University of Technology, 2010.
- (177) Wang, N.; Chen, Z. C.; Lu, D. S.; Lin, X. F. "Controllable selective synthesis of a polymerizable prodrug of cytarabine by enzymatic and chemical methods"; *Bioorg Med Chem Lett* 2005, 15 (18), 4064-7.
- (178) Dai, S.; Xue, L.; Zinn, M.; Li, Z. "Enzyme-catalyzed polycondensation of polyester macrodiols with divinyl adipate: a green method for the preparation of thermoplastic block copolyesters"; *Biomacromolecules* 2009, 10 (12), 3176-81.
- (179) Uyama, H.; Kobayashi, S. "Enzymatic synthesis of polyesters via polycondensation"; *Enzyme-Catalyzed Synthesis of Polymers* 2006, 194, 133-158.
- (180) Kuo, J. W.; Swann, D. A.; Prestwich, G. D. "Chemical Modification of Hyaluronic-Acid by Carbodiimides"; *Bioconjugate Chemistry* 1991, 2 (4), 232-241.
- (181) Kafedjiiski, K.; Jetti, R. K. R.; Föger, F.; Hoyer, H.; Werle, M.; Hoffer, M.; Bernkop-Schnürch, A. "Synthesis and in vitro evaluation of thiolated hyaluronic acid for mucoadhesive drug delivery"; *International Journal of Pharmaceutics* 2007, 343 (1-2), 48-58.
- (182) Kloxin, A. M.; Kloxin, C. J.; Bowman, C. N.; Anseth, K. S. "Mechanical Properties of Cellularly Responsive Hydrogels and Their Experimental Determination"; *Advanced materials* 2010, 22 (31), 3484-3494.
- (183) Elisseff, J.; Anseth, K.; Sims, D.; McIntosh, W.; Randolph, M.; Langer, R. "Transdermal photopolymerization for minimally invasive implantation"; *Proceedings of the National Academy of Sciences* 1999, 96 (6), 3104-3107.
- (184) Heller, C.; Schwentenwein, M.; Russmüller, G.; Koch, T.; Moser, D.; Schopper, C.; Varga, F.; Stampfl, J.; Liska, R. "Vinylcarbonates and vinylcarbamates: Biocompatible monomers for radical photopolymerization"; *Journal of Polymer Science Part A: Polymer Chemistry* 2011, 49 (3), 650-661.
- (185) Kennedy, G. L., Jr. "Toxicity of adipic acid"; *Drug and chemical toxicology* 2002, 25 (2), 191-202.
- (186) Takahashi, A.; Suzuki, Y.; Suhara, T.; Omichi, K.; Shimizu, A.; Hasegawa, K.; Kokudo, N.; Ohta, S.; Ito, T. "In situ cross-linkable hydrogel of hyaluronan produced via copper-free click chemistry"; *Biomacromolecules* 2013, 14 (10), 3581-8.
- (187) Schoen, I.; Pruitt, B. L.; Vogel, V. "The Yin-Yang of Rigidity Sensing: How Forces and Mechanical Properties Regulate the Cellular Response to Materials"; *Annual Review of Materials Research* 2013, 43 (1), 589-618.
- (188) Trappmann, B.; Gautrot, J. E.; Connelly, J. T.; Strange, D. G.; Li, Y.; Oyen, M. L.; Cohen Stuart, M. A.; Boehm, H.; Li, B.; Vogel, V.; Spatz, J. P.; Watt, F. M.; Huck,

- W. T. "*Extracellular-matrix tethering regulates stem-cell fate*"; *Nature materials* 2012, 11 (7), 642-9.
- (189) Vogel, V.; Sheetz, M. "*Local force and geometry sensing regulate cell functions*"; *Nature reviews. Molecular cell biology* 2006, 7 (4), 265-75.
- (190) Hersel, U.; Dahmen, C.; Kessler, H. "*RGD modified polymers: biomaterials for stimulated cell adhesion and beyond*"; *Biomaterials* 2003, 24 (24), 4385-415.
- (191) Andrews, L. S.; Clary, J. J. "*Review of the toxicity of multifunctional acrylates*"; *Journal of Toxicology and Environmental Health* 1986, 19 (2), 149-164.
- (192) Liska, R.; Stampfl, J.; Varga, F.; Gruber, H.; Baudis, S.; Heller, C.; Schuster, M.; Bergmeister, H.; Weigel, G.; Dworak, C. Composition that can be cured by polymerization for the production of biodegradable, biocompatible, cross-linkable polymers on the basis of polyvinyl alcohol. WO2009065162A2, 2009.
- (193) Montheard, J.-P.; Chatzopoulos, M.; Chappard, D. "*2-Hydroxyethyl Methacrylate (HEMA): Chemical Properties and Applications in Biomedical Fields*"; *Journal of Macromolecular Science, Part C* 1992, 32 (1), 1-34.
- (194) Bambury, R. E.; Seelye, D. E. Preparation of vinyl carbonate and vinyl carbamate copolymers for contact lenses. EP396364A2, 1990.
- (195) Freidig, A.; Hofhuis, M.; Van Holstijn, I.; Hermens, J. "*Glutathione depletion in rat hepatocytes: a mixture toxicity study with alpha, beta-unsaturated esters*"; *Xenobiotica; the fate of foreign compounds in biological systems* 2001, 31 (5), 295-307.
- (196) Gautam, R.; Singh, R. D.; Sharma, V. P.; Siddhartha, R.; Chand, P.; Kumar, R. "*Biocompatibility of polymethylmethacrylate resins used in dentistry*"; *Journal of biomedical materials research. Part B, Applied biomaterials* 2012, 100 (5), 1444-1450.
- (197) Nuttelman, C. R.; Tripodi, M. C.; Anseth, K. S. "*In vitro osteogenic differentiation of human mesenchymal stem cells photoencapsulated in PEG hydrogels*"; *Journal of Biomedical Materials Research Part A* 2004, 68A (4), 773-782.
- (198) Jian, Y.; He, Y.; Sun, Y. K.; Yang, H. T.; Yang, W. T.; Nie, J. "*Thiol-epoxy/thiol-acrylate hybrid materials synthesized by photopolymerization*"; *J Mater Chem C* 2013, 1 (29), 4481-4489.
- (199) Faugeras, P.-A.; Boëns, B.; Elchinger, P.-H.; Brouillette, F.; Montplaisir, D.; Zerrouki, R.; Lucas, R. "*When Cyclodextrins Meet Click Chemistry*"; *European Journal of Organic Chemistry* 2012, 2012 (22), 4087-4105.
- (200) Rodal, S. K.; Skretting, G.; Garred, O.; Vilhardt, F.; van Deurs, B.; Sandvig, K. "*Extraction of cholesterol with methyl-beta-cyclodextrin perturbs formation of clathrin-coated endocytic vesicles*"; *Mol Biol Cell* 1999, 10 (4), 961-74.
- (201) Mautner, A. *Development of low cytotoxic Photopolymers*. Dissertation, Vienna University of Technology, 2012.
- (202) Held, K. D.; Melder, D. C. "*Toxicity of the sulfhydryl-containing radioprotector dithiothreitol*"; *Radiation research* 1987, 112 (3), 544-54.
- (203) Cramer, N. B.; Bowman, C. N. "*Kinetics of thiol-ene and thiol-acrylate photopolymerizations with real-time fourier transform infrared*"; *Journal of Polymer Science Part A: Polymer Chemistry* 2001, 39 (19), 3311-3319.
- (204) Lecamp, L.; Houllier, F.; Youssef, B.; Bunel, C. "*Photoinitiated cross-linking of a thiol-methacrylate system*"; *Polymer* 2001, 42 (7), 2727-2736.

- (205) Stiernagle, T. "*Maintenance of C. elegans*"; WormBook : the online review of C. elegans biology 2006, 1-11.
- (206) Torgersen, J. *Novel biocompatible materials for in vivo two-photon polymerisation*. Dissertation, Vienna University of Technology, 2013.
- (207) Martens, P. J.; Bryant, S. J.; Anseth, K. S. "*Tailoring the degradation of hydrogels formed from multivinyl poly(ethylene glycol) and poly(vinyl alcohol) macromers for cartilage tissue engineering*"; Biomacromolecules 2003, 4 (2), 283-92.
- (208) Bomze, D. *Modication of Poly(vinyl alcohol) for Two Photon Polymerisation via Thiol-Ene Chemistry*. Master Thesis, Vienna University of Technology, 2013.
- (209) Bisceglie, V. "*Über die antineoplastische Immunität*"; Z Krebs-forsch 1934, 40 (1), 141-158.
- (210) Chang, T. M. S. "*Semipermeable Microcapsules*"; Science 1964, 146 (3643), 524-525.
- (211) Murua, A.; Portero, A.; Orive, G.; Hernández, R. M.; de Castro, M.; Pedraz, J. L. "*Cell microencapsulation technology: Towards clinical application*"; Journal of Controlled Release 2008, 132 (2), 76-83.
- (212) Orive, G.; Hernandez, R. M.; Gascon, A. R.; Calafiore, R.; Chang, T. M.; De Vos, P.; Hortelano, G.; Hunkeler, D.; Lacik, I.; Shapiro, A. M.; Pedraz, J. L. "*Cell encapsulation: promise and progress*"; Nature medicine 2003, 9 (1), 104-7.
- (213) Sims, C. D.; Butler, P. E.; Cao, Y. L.; Casanova, R.; Randolph, M. A.; Black, A.; Vacanti, C. A.; Yaremchuk, M. J. "*Tissue engineered neocartilage using plasma derived polymer substrates and chondrocytes*"; Plastic and reconstructive surgery 1998, 101 (6), 1580-5.
- (214) Perka, C.; Spitzer, R. S.; Lindenhayn, K.; Sittinger, M.; Schultz, O. "*Matrix-mixed culture: new methodology for chondrocyte culture and preparation of cartilage transplants*"; Journal of biomedical materials research 2000, 49 (3), 305-11.
- (215) Mikos, A. G.; Papadaki, M. G.; Kouvroukoglou, S.; Ishaug, S. L.; Thomson, R. C. "*Mini-review: Islet transplantation to create a bioartificial pancreas*"; Biotechnology and bioengineering 1994, 43 (7), 673-7.
- (216) Bryant, S. J.; Nuttelman, C. R.; Anseth, K. S. "*Cytocompatibility of UV and visible light photoinitiating systems on cultured NIH/3T3 fibroblasts in vitro*"; Journal of biomaterials science. Polymer edition 2000, 11 (5), 439-57.
- (217) Singh, A.; Elisseff, J. "*Biomaterials for stem cell differentiation*"; Journal of Materials Chemistry 2010, 20 (40), 8832-8847.
- (218) Li, Z. *Novel Organic Materials for Multi-photon Photopolymerization and Photografting*. Dissertation, Vienna University of Technology, 2013.
- (219) Castano, A. P.; Demidova, T. N.; Hamblin, M. R. "*Mechanisms in photodynamic therapy: part one—photosensitizers, photochemistry and cellular localization*"; Photodiagnosis and Photodynamic Therapy 2004, 1 (4), 279-293.
- (220) Maillard, B.; Ingold, K. U.; Scaiano, J. C. "*Rate Constants for the Reactions of Free-Radicals with Oxygen in Solution*"; Journal of the American Chemical Society 1983, 105 (15), 5095-5099.
- (221) Lin, C.-C.; Sawicki, S. M.; Metters, A. T. "*Free-Radical-Mediated Protein Inactivation and Recovery during Protein Photoencapsulation*"; Biomacromolecules 2007, 9 (1), 75-83.
- (222) Cumpston, B. H.; Ananthavel, S. P.; Barlow, S.; Dyer, D. L.; Ehrlich, J. E.; Erskine, L. L.; Heikal, A. A.; Kuebler, S. M.; Lee, I. Y. S.; McCord-Maughon, D.; Qin, J.;

- Rockel, H.; Rumi, M.; Wu, X.-L.; Marder, S. R.; Perry, J. W. "*Two-photon polymerization initiators for three-dimensional optical data storage and microfabrication*"; *Nature* 1999, 398 (6722), 51-54.
- (223) Vonsonntag, C.; Schuchmann, H. P. "*The Elucidation of Peroxyl Radical Reactions in Aqueous-Solution with the Help of Radiation-Chemical Methods*"; *Angew Chem Int Edit* 1991, 30 (10), 1229-1253.
- (224) Porter, N. A.; Lehman, L. S.; Weber, B. A.; Smith, K. J. "*Unified mechanism for polyunsaturated fatty acid autoxidation. Competition of peroxy radical hydrogen atom abstraction, .beta.-scission, and cyclization*"; *Journal of the American Chemical Society* 1981, 103 (21), 6447-6455.
- (225) Winterbourn, C. C. "*Reconciling the chemistry and biology of reactive oxygen species*"; *Nature chemical biology* 2008, 4 (5), 278-86.
- (226) Chatterjee, P. K.; Cuzzocrea, S.; Brown, P. A.; Zacharowski, K.; Stewart, K. N.; Mota-Filipe, H.; Thiernemann, C. "*Tempol, a membrane-permeable radical scavenger, reduces oxidant stress-mediated renal dysfunction and injury in the rat*"; *Kidney Int* 2000, 58 (2), 658-73.
- (227) Khetan, S.; Guvendiren, M.; Legant, W. R.; Cohen, D. M.; Chen, C. S.; Burdick, J. A. "*Degradation-mediated cellular traction directs stem cell fate in covalently crosslinked three-dimensional hydrogels*"; *Nature materials* 2013, 12 (5), 458-65.
- (228) Hutter, J. L.; Bechhoefer, J. "*Calibration of Atomic-Force Microscope Tips*"; *Rev Sci Instrum* 1993, 64 (7), 1868-1873.
- (229) Goss, C. A.; Charych, D. H.; Majda, M. "*Application of (3-mercaptopropyl)trimethoxysilane as a molecular adhesive in the fabrication of vapor-deposited gold electrodes on glass substrates*"; *Anal Chem* 1991, 63 (1), 85-88.
- (230) Qin, X.-H.; Torgersen, J.; Saf, R.; Mühleder, S.; Pucher, N.; Ligon, S. C.; Holnthoner, W.; Redl, H.; Ovsianikov, A.; Stampfl, J.; Liska, R. "*Three-dimensional microfabrication of protein hydrogels via two-photon-excited thiol-vinyl ester photopolymerization*"; *Journal of Polymer Science Part A: Polymer Chemistry* 2013, 51 (22), 4799-4810.
- (231) Brandrup, J.; Immergut, E. H. "*Polymer Handbook*". 3rd ed.; Wiley: USA, 1989.
- (232) Burdick, J. A.; Chung, C.; Jia, X.; Randolph, M. A.; Langer, R. "*Controlled degradation and mechanical behavior of photopolymerized hyaluronic acid networks*"; *Biomacromolecules* 2005, 6 (1), 386-91.